UNIVERSITY OF CALIFORNIA
RIVERSIDE

Full Genome Characterization of Two Citrus Viruses: A Genomic, Phylogenetic,
Diagnostic and Virus-Host Interaction Study

A Dissertation submitted in partial satisfaction
of the requirements for the degree of

Doctor of Philosophy

in

Plant Pathology

by

Shih-hua Tan

September 2019

Dissertation Committee:
       Dr. Georgios Vidalakis, Chairperson
       Dr. Gregor Blaha
       Dr. Wenbo Ma

The Dissertation of Shih-hua Tan is approved:

_____

_____

_____

Committee Chairperson

University of California, Riverside

ACKNOWLEDGEMENTS

This dissertation would not have been finished without the help from so many people. First and foremost, I would like to thank my advisor, Dr. Georgios Vidalakis, for his dedicated support, guidance and encouragement. Under his mentorship, I have grown greatly from a graduate student to an independent scientist. I feel so fortunate to become his student at UC Riverside.

I would also like to extend my gratitude to my dissertation committee members, Dr. Gregor Blaha and Dr. Wenbo Ma, for their guidance and fully supports in completion of my dissertation. I thank the professors serving on my qualifying exam committee, Dr. Michael Coffey, Dr. Caroline Roper, Dr. James Ng, Dr. Wenbo Ma, and Dr. Carol Lovatt.

People from Vidalakis lab had provided enormous help to make my research projects possible. I am indebted to Greg Greer and Rock Christiano for the help with countless greenhouse experiments as well as sample collection. I am so grateful to work with Dr. Fatima Osman, Dr. Sohrab Bodaghi and Tyler Dang who taught, trained and assisted me on extensive experiments and projects. I would like to thank Dr. Deborah Pagliaccia, Dr. Irene Lavagi, Carolyn Anderson, Roya Campos, and Alexandra Syed who made my Ph.D. life much easier. I would like to show my gratefulness to all the staffs and students currently and previously work in Vidalakis lab, Amy Huang, Sarah Hammado, Brandon Ramirez, Sophia Kamenidou, Tavia Rucker, Shurooq Abu-Hajar, Ning Chen, Xingyu Chen, Adilene Gomez, Ramon Serna, Brittany Nguyen, Noora Siddiqui, Emily Dang, German Torres-Contreras, Iman Mimou, Isaac Menchaca, Bailey Van Zanten, Silvia

iv

DEDICATION

This dissertation is dedicated to my parents, Mei-chu Fan and Chien-pin Tan, my husband, Roy, and my brother, Shih-wei Tan.

ABSTRACT OF THE DISSERTATION

Full Genome Characterization of Two Citrus Viruses: A Genomic, Phylogenetic,
Diagnostic and Virus-Host Interaction Study

by

Shih-hua Tan

Doctor of Philosophy, Graduate Program in Plant Pathology
University of California, Riverside, September 2019
Dr. Georgios Vidalakis, Chairperson

The full genome of citrus tatter leaf virus (CTLV) and citrus vein enation virus
(CVEV) preserved at Citrus Clonal Protection Program were characterized through next
generation sequencing. The sequence analysis showed that CTLV is a strain of *Apple stem
grooving virus*, a type species belongs to *Capillovirus*, *Betaflexiviridae*, based on its
genome structure and sequence identity. The phylogenetic analysis highlighted that CTLV
is originated from Asia where the virus spillover to different plant species and then
introduced to USA in a variety introduction. On the other hand, CVEV is a relatively newly
characterized Enamovirus belongs to *Luteoviridae* family. High sequence identities were
found among isolates from different geographic locations. Phylogenetic analysis displayed
that the isolates from Spain, Korea and Japan were clustered together while Australia and
USA isolates were in another. A China isolate stands by itself suggested that it has its own
niche in evolution process. Through genome-wise analysis, detection assays of CTLV and
CVEV were designed at the most conserve area instead of focus only on a certain gene and

validated with different parameters including specificity, sensitivity, transferability and robustness by using multiple virus isolates. The virus-host interactions were also characterized by identifying the viral suppressors of RNA silencing (VSRs) in *Nicotiana benthamiana*. Both viruses have two VSRs. CTLV uses movement protein as a VSR to interact with double-stranded RNA (dsRNA) and presumably prevent dsRNA to be processed by the Dicer proteins. Meanwhile, CVEV P0 suppresses host antiviral RNA silencing by mimicking host F-box proteins, forming E3 ubiquitin ligase complex with host components and further guiding Argonautes, the core unit of RNA-induced silencing complex, to their degradation. Both CTLV coat protein and CVEV open reading frame 3 are also VSRs, especially in the systemic tissue, and use indirect mechanisms to suppress host antiviral RNA silencing. In summary, the present dissertation provides in-depth information of CTLV and CVEV in different aspects including genomic, phylogenetic, diagnostic and virus-host interaction. These studies lead to the development of detection assays and provide information to disease management strategies which can be applied to the high-value germplasm program and the citrus industry around the world.

TABLE OF CONTENTS

LIST OF FIGURES

examined for local infiltrated tissue. Number represents the intensity of signal compared to empty vector. U6 were used as loading control. (CMV-2b: cucumber mosaic virus 2b; CLBV-MP: citrus leaf blotch virus movement protein; CVEV: citrus vein enation virus; ORF3: open reading frame 3; ORF5: open reading frame 5; WB: western blot)

Figure 4.3. Relative expression analysis of *GFP* mRNA for silencing suppression co-infiltration assay with (a) local and infiltrated leaf tissue collected at 5 dpi and (b) systemic tissue collected at 14 dpi. (Significance level α=0.05) (CMV-2b: cucumber mosaic virus 2b; CLBV-MP: citrus leaf blotch virus movement protein; CVEV: citrus vein enation virus; ORF3: open reading frame 3; ORF5: open reading frame 5)

Figure 4.4. Potato virus X assay to test P0 and open reading frame 3 encoded by citrus vein enation virus on the suppression of siRNA-mediated host immunity in *N benthamiana* plants. (a) Leaf symptoms. (b) Relative expression analysis by PVX CP RT-qPCR (Significance level α=0.05). (c) Leaf symptoms of frameshifting mutations of P0 and open reading frame 3. (PVX: potato virus x; CLBV-MP: citrus leaf blotch virus movement protein; CVEV: citrus vein enation virus; ORF3: open reading frame 3; fs: frameshifting mutation)

Figure 4.5. RNA silencing suppression co-infiltration assay of citrus vein enation virus P0 and its deletions. (a) Western blot analysis to confirm protein expression. (b) Local silencing suppression observed under UV light at 5 dpi. (c) Relative expression level analysis of *GFP* mRNA level in local tissue by *GFP* RT-qPCR (Significance level α=0.05). (d) Systemic silencing suppression observed under UV light at 14 dpi. (e) Relative expression level analysis of *GFP* mRNA level in systemic tissue by *GFP* RT-qPCR (Significance level α=0.05). (CVEV: citrus vein enation virus; WB: western blot)

Figure 4.6. RNA silencing suppression co-infiltration assay of citrus vein enation virus P0, $P0^{L52A,P53A,L56A}$ and $P0^{\Delta36-83}$. (a) Western blot analysis to confirm protein expression. (b) Local and systemic silencing suppression observed under UV light at 5 and 14 dpi, respectively. Relative expression level analysis of *GFP* mRNA level (c) in local tissue and (d) in systemic tissue by *GFP* RT-qPCR (Significance level α=0.05). (CVEV: citrus vein enation virus; WB: western blot)

Figure 4.7. RNA silencing suppression co-infiltration assay of citrus vein enation virus open reading frame 3 and its deletions. (a) Western blot analysis to confirm protein expression. (b) Systemic silencing suppression observed under UV light at 14 dpi. (c) Relative expression level analysis of *GFP* mRNA level in systemic tissue by *GFP* RT-qPCR (Significance level α=0.05). (CVEV: citrus vein enation virus; ORF3: open reading frame 3; WB: western blot)

Figure 4.8. Western blot analysis of **c**o-immunoprecipitation of cMyc-AtSKP1 with CVEV-P0-FLAG. The immune-precipitated proteins were examined by western blot analysis. (IP: immunoprecipitation; WB: western blot)

LIST OF TABLES

CHAPTER 2

CHAPTER 3

CHAPTER 4

GENERAL INTRODUCTION

Citrus contain essential nutrients including vitamin C and other important elements needed in human diet. These nutrients help human body to maintain physical functions and protect against life-threatening diseases and conditions (Spreen 2010). Other than its nutrients, citrus also contributes economically to the production region which are distributed globally in tropical and sub-tropical countries. According to the annual report from the United States Department of Agriculture (USDA)- National Agricultural Statistic Service (NASS), citrus production in 2017-2018 totaled 6.13 million tons, and was valued at $3.28 billion within the United States (USDA-NASS 2018). The prime climate and soil conditions in California make it perfect for citrus growth and commercial production. Currently, the state of California becomes one of the top producers accounted for 61% of the total citrus utilized production in 2017-2018, while Florida totaled 34%, and Texas, Arizona and other states combined produced the remaining 5% (USDA-NASS 2018). Citrus industry contributed substantially to California's economy in 2016-2017, with the total impact valued at $7.12 billion (Babcock 2018). However, there are many factors and threats to this industry including but not limited to labors, policies, weather, water, and diseases which may affect the production and more broadly the state's economy.

As a Ph.D. student with plant pathology major and works under Dr. Georgios Vidalakis at the Citrus Clonal Protection Program (CCPP), our focus is to understand the insights of each pathogen and further develop the prevention and management strategies. Through this dissertation, two citrus viruses, citrus tatter leaf virus (CTLV) and citrus vein

enation virus (CVEV), were fully characterized in a comprehensive study of genomic, phylogenetic, diagnostic and virus-host interaction.

The dissertation is separated into two sections which part A is focused on full genome characterization and detection assay development and part B is mainly for identification and characterization of viral suppressors of RNA silencing. Each part has two chapters for CTLV and CVEV, respectively. Each chapter is fully developed into Abstract, Introduction, Materials and Methods, Results, Discussion, References, Figures and Tables.

References

Babcock, B. 2018. Economic impact of California's citrus industry. Pages 36-39, Citrograph.

Spreen, T. H. 2010. The World Citrus Industry. Soil, Plant Growth and Crop Production.

USDA-NASS. 2018. Agricultural Statistics 2018. United States Department of Agriculture- National Agricultural Statistics Service.

PART A- Full Genome Characterization and Detection Assay Development of Citrus tatter leaf virus and Citrus vein enation virus

CHAPTER 1: Citrus tatter leaf virus Full Genome Characterization and Development of a Detection Assay

Abstract

Citrus tatter leaf virus (CTLV) threatens citrus production worldwide because it induces bud-union crease on the commercially important Citrange (*Poncirus trifoliata* × *Citrus sinensis*) rootstocks. However, little is known about its genomic diversity and how such diversity may influence virus detection. In this study, full-length genome sequences of 12 CTLV isolates from different geographical areas, intercepted and maintained for the past 60 years at the Citrus Clonal Protection Program (CCPP), University of California, Riverside, were characterized using next generation sequencing. Genome structure and sequence for all CTLV isolates were similar to *Apple stem grooving virus* (ASGV), the type species of *Capillovirus* genus of the *Betaflexiviridae* family. Phylogenetic analysis highlighted CTLV's point of origin in Asia, the virus spillover to different plant species and the bottleneck event of its introduction in the United States of America (USA). A reverse transcription quantitative polymerase chain reaction assay was designed at the most conserved genome area between the coat protein and the 3'-untranslated region (UTR), as identified by the full genome analysis. The assay was validated with different parameters (e.g. specificity, sensitivity, transferability and robustness) using multiple CTLV isolates from various citrus growing regions and it was compared with other published assays. This study proposes that in the era of powerful affordable sequencing platforms the presented

4

approach of systematic full-genome sequence analysis of multiple virus isolates, and not only a small genome area of a small number of isolates, becomes a guideline for the design and validation of molecular virus detection assays, especially for use in high value germplasm programs.

Introduction

Citrus tatter leaf virus (CTLV), a *Capillovirus* belonging to the family *Betaflexiviridae*, is considered to be a strain of *Apple stem grooving virus* (ASGV) (Magome et al. 1997; Tatineni et al. 2009). CTLV is readily transmitted mechanically and no natural vectors have been yet identified (Tatineni et al. 2009). CTLV was first discovered in Chico, California, USA (Garnsey 1970; Wallace and Drake 1962) in latent infected Meyer lemon trees (*Citrus Limon* (L.) Burm.f. hyb.), a cultivar imported around 1908 from Asia into the country. CTLV is endemic to China (Roistacher 1991; Zhang and Liang 1988) and it has been found in Taiwan (Nishio et al. 1982; Roistacher 1991; Su and Cheon 1984), Japan (Inouye et al. 1979; Miyakawa 1980; Miyakawa and Matsui 1976; Miyakawa and Tsuji 1988; Yoshikawa et al. 1993), Australia (Broadbent et al. 1994; Fraser and Broadbent 1979), South Africa (da Graca 1977) and in the USA; in California (Wallace and Drake 1962), Florida (Garnsey 1964, 1970; Tatineni et al. 2009) and Texas (da Graca and Sharia 1996; Herron and Skaria 2000).

Although CTLV was first discovered in citrus, it has been reported to infect a wide range of herbaceous hosts, many of which remain symptomless (Inouye et al. 1979). Most CTLV infected commercial citrus varieties also remain asymptomatic except when CTLV infected budwood is propagated onto trifoliate orange (*Poncirus trifoliata* (L.) Raf.) or trifoliate hybrid citrange (*P. trifoliata* X *C. sinensis*) rootstocks (Garnsey and Jones 1968; Tatineni et al. 2009). The resulting citrus trees are stunted, display chlorotic leaves, and show bud union incompatibility, leading to the ultimate decline of the tree (Calavan et al. 1963; Miyakawa and Matsui 1976). This poses a serious problem because trifoliate and trifoliate hybrid rootstocks are widely used in all citrus producing areas of the world for their tolerance to citrus tristeza virus and *Phytophthora* species in addition to many other desirable horticultural characteristics (e.g. freeze tolerance, good yield and fruit quality) (Moreno et al. 2008; Roose 2014; Roose et al. 2015).

The numerous asymptomatic citrus and non-citrus hosts in combination with the destructive potential of the virus for trees propagated on commercially important rootstocks make CTLV a serious threat to the citrus industry (Calavan et al. 1963; Cowell et al. 2017; Garnsey 1964; Garnsey and Jones 1968). Reliable pathogen detection assays for the production, maintenance, and distribution of pathogen-tested propagative materials by citrus germplasm and certification programs are the basis for any successful mitigation effort against viral threats, including CTLV (Bostock et al. 2014; Hailstones et al. 2000; Navarro 1986; Osman et al. 2015; Smith et al. 1992; Vidalakis et al. 2014). Bioindicators for indexing of CTLV such as *C. excelsa,* and Rusk citrange, displaying symptoms of deformed young leaves under controlled greenhouse conditions, provide a reliable

diagnostic tool (Roistacher 1991). ASGV antiserum was used both in enzyme-linked immunosorbent assay (ELISA) and in immunocapture RT-PCR for CTLV detection (Hilf 2008). A series of conventional reverse-transcription polymerase chain reaction (RT-PCR) based methods were developed for CTLV including two-step multiplex assays (Hyun et al. 2017; Roy et al. 2005) and a one-step RT-PCR assay with a semi-nested variation (Hailstones et al. 2000). More recently, reverse transcription quantitative PCR (RT-qPCR) assays were developed for CTLV detection using SYBR® Green (Liu et al. 2011) and florescent probe platforms (Cowell et al. 2017).

At the time that Liu et al. published their assay in 2011, there were only four full-genome CTLV sequences deposited in the GenBank (Liu et al. 2011). Similarly, Cowell et al. (2017) reported that the RT-qPCR assay was designed based on seven full-genome sequences available at the time in the GenBank (Cowell et al. 2017). Today a total of 12 full-genome sequences are available in the GenBank (Ohira et al. 1995; Song et al. 2015; Tatineni et al. 2009). Due to the limited number of CTLV full-genome sequences, very little is known about the phylogenetic relationship and the genomic diversity of the virus and how such diversity may influence its detection by PCR. Next generation sequencing (NGS) technologies combined with bioinformatics have proven to be powerful tools for the assembly of full-genome virus sequences (Kehoe et al. 2014; Radford et al. 2012; Villamor et al. 2019) and the guidelines for the design and validation of real-time qPCR assays are well established (Broeders et al. 2014; Bustin et al. 2009). The purpose of this study was to characterize CTLV and further develop a robust CTLV RT-qPCR detection

7

assay based on the systematic analysis of newly generated full-length genome data from multiple virus isolates maintained for the past 60 years at the CCPP.

Materials and Methods

Virus isolates and RNA extraction for full-length genome sequencing.

Twelve CTLV isolates from various citrus varieties introductions, originating from different geographical locations, were intercepted and maintained *in planta* under quarantine at the CCPP disease collection between 1958 and 2014 (Table 1.1). Sweet orange (*C. sinensis* (L.) Osbeck) seedlings were graft-inoculated with the different CTLV isolates and total RNA was extracted from phloem-rich bark tissues of matured vegetative flush (i.e. one-year-old budwood) using TRIzol® reagent (Invitrogen, Carlsbad, California, USA) per manufacturer's instructions. The purity and concentration of the RNA were tested using a Nanodrop spectrophotometer and Agilent 2100 Bioanalyzer per manufacturer's instructions.

NGS library preparation and bioinformatics.

CTLV RNA libraries were constructed using 4μg of total RNA with TruSeq Stranded mRNA Library Prep Kit (Illumina, San Diego, California, USA) per manufacturer's instructions. The RNA libraries were sequenced on an Illumina HiSeq 2500

instrument with high-output mode and single-end 50 or 100 base pairs (bp) at SeqMatic LLC (Fremont, California, USA). All sequencing data was generated by SeqMatic using an Illumina Genome Analyzer IIx and filtered through the default parameters of the Illumina QC pipeline and demultiplexed. The files were uploaded onto the VirFind bioinformatics server and mapped to the reference genome by Bowtie 2, followed by outputting mapped and unmapped contig sequences (Ho and Tzanetakis 2014). Unmapped sequences were *de novo* assembled by Trinity (Ho and Tzanetakis 2014). Assembled contigs were analyzed through BLASTn with an E-value cutoff of 10^{-2} against all virus sequences in GenBank and generated outputs of reads and report for virus sequences.

Rapid amplification of cDNA ends of viral RNA.

The 5' and 3' end sequences were obtained via rapid amplification of cDNA ends (RACEs). The 5' end sequence of each CTLV isolate was confirmed using FirstChoice® RLM-RACE Kit (Thermo Fisher Scientific, Carlsbad, California, USA). As per manufacturer's instructions, first-strand cDNA was synthesized and followed by nested PCR with the primer sets listed in Table 1.2. To confirm the 3' end sequence of each CTLV isolate, first-strand cDNA was synthesized using SuperScript® II transcriptase (Thermo Fisher Scientific, Carlsbad, California, USA) with oligo dT 16mer and then performed PCR using Platinum® Taq DNA Polymerase High Fidelity Kit (Thermo Fisher Scientific, Carlsbad, California, USA) with the oligo dT 16mer and a CTLV specific primer (Table 1.2). The PCR product that contained either the 5' or 3' end was ligated into pGEM®-T

Easy Vector Systems (Promega, Madison, Wisconsin, USA) per manufacturer's instructions and sequenced using both T7 (5'-TAATACGACTCACTATAGGG-3') and SP6 (5'-ATTTAGGTGACACTATAG-3') primers. Together with the contigs containing CTLV sequences from NGS, the sequence data were then analyzed and assembled as consensus full-length genome, using Vector NTI Advance™11 software (Thermo Fisher Scientific, Carlsbad, California, USA).

Phylogenetic and genomic identity analysis of full-length virus sequences.

Phylogenetic analysis was performed using the Molecular Evolutionary Genetics Analysis tool (MEGA v. 7.0.21) (Tamura et al. 2013). ClustalW was used to align the 12 newly generated CTLV full-length cDNA sequences with the capilloviruses: CTLV, ASGV, pear black necrotic leaf spot virus (PBNLSV; a strain of ASGV), and cherry virus A (CVA) for which full genome sequences were available in GenBank (Table 1.3). Phylogenetic topologies were reconstructed using three different methods: neighbor-joining, maximum likelihood and minimum evolution and tested with 1,000 bootstrap replicates. All phylogenetic methods gave similar results and the neighbor-joining tree was presented in this study. Nucleotide (nt) percentage of sequence identities were calculated for CTLV full genome and specific regions using the pairwise sequence identity and similarity in a web-based analyzing program (http://imed.med.ucm.es/Tools/sias.html).

Citrus sample processing and RNA extraction for RT-qPCR detection of CTLV.

To account for the possible uneven distribution of the virus within a plant, budwood samples from four to six different branches around the tree canopy were randomly collected and combined in a single sample. Samples from the citrus trees' phloem-rich bark of matured budwood (approximately 12 to 18 months old) were collected and processed by freeze-drying and grinding as described by Osman et al. (2017). Total RNA was extracted from the ground sample using MagMAX^{TM} Express-96 (Thermo Fisher Scientific, Carlsbad, California, USA) along with a modified protocol of the 5X MagMax^{TM}-96 Viral RNA Isolation Kit optimized for citrus tissues (Osman et al. 2017). Total RNA was eluted in 100 µl elution buffer and used as template for RT-qPCR.

RT-qPCR assay design.

For the specific detection of CTLV in citrus tissues, an RT-qPCR assay was designed based on sequence conservation alignment of a total 28 full genome sequences: 23 sequences of CTLV, (12 generated in this study and 11 from the GenBank) and five GenBank sequences of ASGV isolated from citrus (*Citrus sp.*) and kumquat (*Fortunella sp.*), a citrus relative (Figure 1.1). Primers and probe were designed using the Primer Express™ software (Thermo Fisher Scientific, Carlsbad, California, USA) and following the guidelines for designing RT-qPCR assays a 58 °C optimum melting temperature for primers and a 10 °C increase for qPCR probes was used to prevent the formation of primer

dimers (Table 1.4). The fluorophore used for the CTLV probe was 6-carboxyfluorescein FAM and the 3' quencher was Black Hole Quencher (BHQ). The homology of the primers and qPCR probe was confirmed by a BLASTn search against the GenBank database.

The RT-qPCR reaction (12 µl total volume) was performed using the AgPath-ID^{TM} One-Step RT-PCR Kit (Thermo Fisher Scientific, Carlsbad, California, USA) with 2.65 µL water, 6.25 µL 2X RT buffer, 0.6 µL primer probe mix (417 nM for primers and 83 nM for probe as final concentrations), 0.5 µL 25X RT mix and 2 µL of RNA for each reaction. The cycling conditions were 45 °C for 10 minutes, 95 °C for 10 minutes during the first cycle, followed by 40 cycles of 95 °C for 15 seconds and 60 °C for 45 seconds. Samples were analyzed using Applied Biosystems™ 7900HT Fast Real-Time PCR System and Applied Biosystems™ QuantStudio 12K Flex Real-Time PCR System (Thermo Fisher Scientific, Carlsbad, California, USA). Fluorescent signals were collected during the amplification cycle and the quantitative cycle (Cq) was calculated and exported with a threshold of 0.2 and a baseline of 3 - 15 for the targets of interest. The Cq was calculated by the qPCR machine using an algorithm with a set range of cycles at which the first detectable significant increase in fluorescence occurs. RNA and reaction integrity were assessed using the qPCR assay targeting cytochrome oxidase (COX) gene in the citrus genome as the internal control (Osman et al. 2015).

RT-qPCR assay validation.

The newly designed CTLV RT-qPCR assay was validated using applicable parameters proposed in the "Guidelines for validation of qualitative real-time PCR methods" (Broeders et al. 2014). Applicability, practicability and transferability were evaluated by deploying the assay at two different laboratories, University of California (UC) Riverside- CCPP and UC Davis- Real-Time PCR Research & Diagnostic Core Facility. The robustness of the assay was evaluated with deviation in annealing temperatures (± 2 ^{o}C), reaction volumes (± 2 μL), and different qPCR instruments (CFX96 Real-Time PCR Detection System, Bio-Rad, Hercules, California, USA), and master mixes (iTaq™ Universal Probes One-Step Kit, Bio-Rad, Hercules, California, USA) to optimize the assay.

The specificity of the assay was evaluated both *in silico* and experimentally, using a variety of citrus samples with known CTLV infection status from broad geographical origins and isolation times. All virus isolates exotic to California were received as nucleic acids under the auspices of the USDA Animal and Plant Health Inspection Service (APHIS)- Plant Protection and Quarantine (PPQ) permits P526P-18-04608 and P526P-18-04609. Cross-reactivity was assessed using RNA of different non-inoculated citrus species and varieties and RNA from citrus inoculated with other non-targeted graft-transmissible pathogens of citrus.

The sensitivity (absolute limit of detection, LOD_6) and quantification of the amount of CTLV in samples was calculated by generating an absolute standard curve to determine

13

the starting number of copies. More specifically, amplicons for CTLV were obtained for each primer set (i.e. F1, 2, and 3 with R) and individually cloned into plasmids (Eurofins MWG Operon, Huntsville, Alabama, USA) (Table 1.4). The extracted plasmid DNA was linearized using *Hind*III enzyme, to increase the efficiency of dilutions. Serial 10-fold dilution of plasmids carrying a known copy number of CTLV inserts were made to construct a DNA standard curve. The standard curves for CTLV were run in singleplex RT-qPCR setting utilizing 6-carboxyfluorescein FAM fluorophores. Reactions were performed in triplicate to establish the linear response between the Cq values and the log of known copy numbers. The copy numbers for each sample were previously calculated as described (Leutenegger 2001). The slope of the standard curve and the coefficient of determination (R^2) were calculated using linear regression (Rasmussen 2001). Amplification efficiency (E) was calculated with the formula $E = 10^{(-1/\text{slope})} - 1$ (Pfaffl 2004; Svec et al. 2015).

Comparison of CTLV RT-qPCR detection assay with previously published assays.

The newly developed CTLV detection assay was compared to two recently the published RT-qPCR assays. Twenty-two samples from different CTLV isolates and 25 CTLV known negative samples were tested with the SYBR® Green-based RT-qPCR assay by Liu et al. (2011), and the probe-based RT-qPCR assay by Cowell et al. (2017) following the protocols described in each study. Based on the principal that a well performing diagnostic test correctly identifies the diseased individuals in a population, a series of

statistical measurements, as reviewed by Bewick et al. (2004), were used to compare the performance of the three RT-qPCR CTLV detection assays. An assay is performing well when sensitivity (Sn) = true positives / (true positives + false negatives) and specificity (Sp) = true negatives / (true negatives + false positives) approach 100%. High positive likelihood ratio (LR^+) = sensitivity / (1-specificity) and low (close to zero) negative likelihood ratio (LR^-) = (1-sensitivity) / specificity also indicate a well performing diagnostic test. Finally, Youden's index (J) = sensitivity + specificity − 1, can attain the maximum value of 1, when the diagnostic test is perfect and the minimum value of zero, when the test has no diagnostic value (Bewick et al. 2004).

Results

Full-length sequences of 12 CTLV isolates via NGS and RACEs.

Full-length viral genome sequences of 12 CTLV isolates were obtained by RNA-Seq and the average total reads generated was 27,158,037 which covered 74% to 100% of the viral genome. The full-length cDNA sequences were deposited in GenBank with accession numbers MH108975-MH108986 (Table 1.1). Excluding the poly (A) tail, the 12 CTLV complete sequences ranged from 6,494 to 6,497 nucleotides (nt) long. Sequence analysis showed the CTLV genome was similar to other capilloviruses, including ASGV and PBNLSV, with two overlapping open reading frames (ORFs) (Figure 1.2). ORF1 (37 - 6,354 nt) encoded a 2,105 amino acid (aa) polypeptide, a putative polyprotein around

242-kDa containing methyltransferase-like, papain-like protease, helicase-like, RdRp-like domains, and a coat protein (CP) region (Figure 1.2). The CP region encoded a 27-kDa protein which was located at the carboxyl-terminal end of the ORF1 polyprotein (5,641 - 6,354 nt) and was identified based on sequence identity of ASGV CP deposited in GenBank (NC001749) (Yoshikawa et al. 1992). Two variable regions previously described in ORF1 were also identified (Figure 1.2) (Magome et al. 1997; Tatineni et al. 2009). ORF2 (4,788 - 5,750 nt) was nested in ORF1 and encoded a 36-kDa protein which belongs to the 30-kDa cell-to-cell movement protein (MP) superfamily (Figure 1.2).

Phylogenetic and genomic identity analysis of CTLV full-length sequences.

Using three different methods, phylogenetic trees were generated with the available full-length nucleotide sequences of capilloviruses. All three methods generated similar topologies. The neighbor-joining unrooted tree identified four distinct clusters (I - IV) within two well supported clades (A and B) (bootstrap 99%) (Figure 1.3). Clusters I and II (bootstrap 100%), in clade A, contained CTLV isolates originating from Japan and China along with ASGV isolates from citrus and non-citrus hosts originated from the same geographic locations (Figure 1.3 and Table 1.3). Only one of the 12 CTLV isolates from this study (CTLV-IPPN122) was present in clade A (cluster I). This isolate was intercepted by the CCPP in a satsuma citrus introduction from China (Figure 1.3 and Table 1.3).

The nucleotide sequence identities among the isolates of cluster I ranged within 83.23 - 93.02% including a 100% identity between ASGV-241KP and ASGV-P-209, both isolated from apple in Japan (Figure 1.3, Table 1.3 and 1.5). Sequence identities in cluster II ranged within 94.04 - 98.47%. Notably, in clade A (clusters I and II), some virus isolates derived from apple (I: ASGV-241KP, and -P-209 and II: ASGV-Li-23), had the highest sequence identities with isolates from lily (II: CTLV-L, 98.47%), citrus (I: CTLV-ASGV-2-HJY, 92.36% and -MTH, 91.07% and II: ASGV-FKSS2, 94.70% and -N297, 94.04%) and citrus relatives (I: ASGV-Nagami, 92.96%) (Figure 1.3, Table 1.3 and 1.5). In addition, in cluster I, the isolates ASGV-Nagami from Japan in kumquat (citrus relative, *Fortunella margarita* (Lour.) Swing.) and CTLV-ASGV-2-HJY from China in pummelo (*C. maxima* (Burm.) Merrill) had the highest sequence identity (93.02%) (Figure 1.3, Table 1.3 and 1.5).

Clusters III and IV (bootstrap 34%), in clade B, contained 11 of the 12 isolates from this study (Figure 1.3). In cluster III, three isolates intercepted by the CCPP in citrus introductions from China (i.e. CTLV-TL112, -TL113 and -TL114) grouped with seven CTLV isolates from China and Taiwan, one ASGV citrus isolate from Japan and three ASGV isolates from non-citrus hosts (i.e. apple and actinidia) from China, India and Germany (Figure 1.3). The nucleotide sequence identities among the isolates of cluster III ranged within 81.49 - 99.43% including a 100% identity between CTLV-Ponkan8 and CTLV-Pk both isolated from Ponkan mandarin (*C. reticulata* Blanco) in Taiwan (Figure 1.3, Table 1.3 and 1.5).

The apple virus isolates in clade B (cluster III) (III: ASGV-AC and ASGVp12) had sequence identities with a virus isolate from actinidia (III: ASGV-Ac) and 22 isolates from citrus and citrus relatives (cluster III and IV) with range of 81.42 - 82.68% (Figure 1.3, Table 1.3 and 1.5). This was in contrast to the high levels of sequence identity observed between apple isolates and lily, citrus and citrus relatives in clade A (91.07 - 98.47%).

Cluster IV included 11 virus citrus isolates from Japan, China, and the USA. Eight CTLV isolates from this study grouped with two isolates from USA and China and one ASGV citrus isolate from Japan (Figure 1.3). The nucleotide sequence identities among the isolates of cluster IV ranged within 81.78 - 99.95% including 100% identity of the CTLV-ML and CTLV-TL111 isolated from Meyer lemon in Florida and CTLV-TL110 isolated from satsuma mandarin (*C. unshiu* (Macf.) Marc.) in California. Meanwhile, CTLV-TL103 which was isolated from pummelo in Japan showed 99.95% identity with CTLV-ML, CTLV-TL110, and CTLV-TL111 (Figure 1.3, Table 1.3 and 1.5).

Cluster IV contained two subgroups (bootstrap 100%) (Figure 1.3). The first subgroup contained five CTLV isolates from Meyer Lemon associated with the 1958 introduction of the virus into USA (CTLV-ML, -TL111, -TL101, -TL100 and -TL102). The sequence identities of these isolates ranged within 97.99 - 98.98% including identical isolates, CTLV-ML and CTLV-TL111, from Florida (Figure 1.3, Table 1.3 and 1.5). The California isolates (CTLV-TL101 and -TL102) had 98.56% identity. The isolate from Texas (CTLV-TL100) had 98.52 and 98.98% sequence identity to the isolates from Florida (CTLV-ML and -TL111) and California (CTLV-TL101), respectively (Figure 1.3, Table

1.3 and 1.5). The sequence identity of the Meyer Lemon isolates from Florida (CTLV-ML and -TL111) and California (CTLV-TL101 and -TL102) ranged within 97.99 - 98.70% (Figure 1.3, Table 1.3 and 1.5). The second subgroup contained three citrus virus isolates from China (CTLV-TL104) and Japan (CTLV-TL115 and ASGV-Kiyomi) with sequence identities ranged from 95.73 to 98.70% within themselves (Figure 1.3, Table 1.3 and 1.5). One China isolate (CTLV-ASGV-1-HJY) stood alone (bootstrap 44%) and had sequence identity of 81.78 - 82.81% with all other isolates in cluster IV (Figure 1.3, Table 1.3 and 1.5).

Genomic analysis for CTLV RT-qPCR assay design.

To analyze the sequence diversity of specific genomic regions, the CTLV genome was divided into three sections: the 5'-UTR and partial polyprotein excluding CP (1 - 5,640 nt), CP and 3'-UTR (5,641 - 6,495 nt), and MP (4,788 - 5,750 nt) (Table 1.6). The two previously identified variable regions (VRI and VRII) were also analyzed (Magome et al. 1997; Tatineni et al. 2009).

Sequence identity analysis of the 28 available full genome sequences of the CTLV and ASGV citrus isolates (developed in this study and available in GenBank) showed that VRI was the most diverse region of the virus genome with 111 variable nucleotide sites among the 117 of the region. In addition, the nucleotide diversity of the VRII was equivalent to that of MP (variable sites 35.08 and 32.81%, respectively) since VRII and

MP are essentially covering overlapping areas of the virus genome (Figure 1.2 and Table 1.6).

The CP and 3'-UTR (5,641 - 6,495 nt) was identified as the most conserved region. The percentage of variable nucleotide sites was the lowest (23.63%) and the minimum nucleotide sequence identity was the highest (89.60%) in the virus genome (Table 1.6). Further analysis revealed that nucleotide sites 6,241 - 6,440 were the most conserved within the CP and 3'-UTR (Table 1.7). Therefore, the newly developed RT-qPCR assay was designed to target this 200 nt region (Figure 1.1, 1.2 and Table 1.4).

CTLV RT-qPCR assay validation.

The applicability, practicability and transferability of this assay was validated by two independent laboratories with consistent reproducible results (Table 1.8a). The assay was also proven to be robust since different annealing temperatures, reaction volumes, qPCR instruments, and master mixes had a minor effect on the Cq values and did not affect the classification of samples as positive or negative (Table 1.9). The specificity of the assay was determined *in silico* by analyzing the sequence of amplicons from different samples followed by a BLASTn search that recognized the amplicon sequences associated only with CTLV. Additionally, the specificity of the assay was evaluated qualitatively with the correct classification (false negative and positive rate 0%) of 112 known CTLV positive and negative samples (Table 1.8a, 1.10, 1.11 and 1.12). More specifically, the assay

detected the virus in 39 known CTLV positive samples from various geographic locations (Table 1.8a and 1.10) and did not cross-react with 43 known CTLV negative samples of non-inoculated citrus varieties (Table 1.11) and a series of 30 non-targeted graft-transmissible citrus pathogens (Table 1.12). When samples were tested with 10-fold serial dilutions (run in triplicate), the sensitivity of the CTLV RT-qPCR showed a linear dynamic range from 10^5 copies to < 10 copies per µl which indicates the detection assay reached the level of LOD_6 with R^2 equal to 0.9999 and 100.4% as its efficiency (Figure 1.4). The mean of viral load was 6.37 x 10^4 copies of CTLV per µl of infected sample extraction measured by the newly designed CTLV RT-qPCR assay.

Comparison with published CTLV detection assays.

The SYBR® Green-based RT-qPCR assay developed by Liu et al. (2011) was able to detect CTLV in all 22 samples with the expected melting temperature for the amplicon (81.5 - 82.0 °C) and its performance measurements (Sn, Sp, LR^+, LR^- and J) were optimum and equal to those of the CTLV assay developed in this study (Table 1.8b). The Cq values of the Liu assay were consistently higher than the ones produced from the assay developed in the study (Table 1.8b).

The TaqMan® probe-based RT-qPCR assay designed by Cowell et al. (Cowell et al. 2017) detected CTLV in 15 samples with eight samples having lower Cq values than the assay developed in this study. However, Cowell et al. was unable to detect CTLV in

seven samples of three different isolates (LR$^-$ = 0.32) and its performance measurements Sn and J were not optimum (Table 1.8b).

Discussion

This study presented a systematic approach using the most current technologies for the development and analysis of genomic virus information for the development and validation of a diagnostic assay for CTLV that threatens citrus production worldwide (Calavan et al. 1963; Garnsey and Jones 1968; Tatineni et al. 2009).

The data obtained via NGS was *de novo* assembled onto 74% to 100% of the complete CTLV genome which demonstrated the strength of this technology to characterize the virus genome sequence. With RACE sequence data from each isolate, the full-length sequences were assembled in relatively short time compared to traditional sequencing methods. This allowed for a more comprehensive genome analysis of the CTLV not limited by the available sequences of a small number of virus isolates or parts of the virus genome (Magome et al. 1997; Tatineni et al. 2009).

The full genome sequence analysis of 28 CTLV and ASGV citrus and citrus relative isolates, developed in this study and from GenBank, confirmed the previously reported size, structure and variable regions in the virus genome (Magome et al. 1997; Tatineni et al. 2009). Data presented in this study also supported the current taxonomic classification of CTLV as a strain of the ASGV in the *Capillovirus* genus of the *Betaflexiviridae* family

since the analysis of multiple full genome sequences of CTLV and ASGV did not meet the species demarcation criteria (less than 72% nucleotide identity or 80% amino acid identity between their CP or polymerase genes) (Table 1.13 and 1.14) (King et al. 2011).

The phylogenetic analysis of the 41 ASGV isolates, revealed four interesting evolutionary and distribution patterns for the virus. First, Asia was highlighted as the point of origin of the virus since countries such as China, Taiwan and Japan were represented in multiple clusters of all phylogenetic clades. Such finding indicated that the origin and diversity of CTLV coincided with the origin of the citrus host. Second, the bottleneck event of the introduction of the virus in the USA with the citrus variety Meyer Lemon was reflected in cluster IV (first subgroup) in clade B and the high sequence identity (98.52-100%) among the isolates from Texas, Florida, and California. Third, high sequence identities among virus isolates from various citrus producing countries around the world demonstrated the impact of the human activities in the distribution of the virus and the importance of clean stock programs such as CCPP (Gergerich et al. 2015). For example, the CTLV-TL115 isolate was intercepted in an illegal citrus introduction in California (second subgroup, cluster IV, clade B) (Polek 2000; Yokomi et al. 2017) and it was different from the previously identified isolates of the virus in the state. In addition, the CTLV-IPPN122, -104, -112, -113, and -114 isolates were presented in different variety introductions, separated in time (1987 and 2014), from the original Meyer lemon introduction back in 1900s and even though they all originated in China, these isolates clustered in three different phylogenetic clusters (I, III, and IV) in agreement with the principal of high diversity in virus sequences at the area of origin (Holmes 2009; Moya et

23

al. 2004; Worobey and Holmes 1999). Last but not least, two ASGV spillover events were captured in clade A where ASGV isolates from apple had the highest sequence similarities (91.07-98.47%) with virus isolates from lily, citrus and citrus relatives (Geoghegan et al. 2017; Geoghegan and Holmes 2017; Olival et al. 2017; Parrish et al. 2008; Woolhouse et al. 2005). No spillover event was captured in clade B since sequence identities of apple isolates with actinidia, citrus and citrus relatives was low (81.42 - 82.68%). Clade B most likely represented the establishment of ASGV in citrus and citrus relatives after its spillover from other species. The spillover events presented here provided some insight to the CTLV ancestry questions for citrus, kumquat, lily and apple presented by Hilf 2008 (Hilf 2008).

Since the genetic variation within the targeted virus population can lead to false negative RT-qPCR results, for the design of the CTLV detection assay, we aimed to locate the most conserved region on the virus genome beyond the traditional approaches that focus on individual genes presumed conserved due to their function (Weber and Bujarski 2015). The newly developed detection assay was further validated according to the guidelines for validation of qualitative real-time PCR methods and its performance was assessed with statistical measurements (Bewick et al. 2004; Kralik and Ricchi 2017). We showed that the most conserved CTLV genome region was not confined in a single gene, but it spanned the region between the CP gene and 3'-UTR, thus it was targeted for the RT-qPCR assay design. The conserved nature of the CTLV CP could be a result of its function in virion assembly (Weber and Bujarski 2015). For the 3'-UTR of CTLV, the high identity among isolates indicates that it may play an important role in CTLV replication and/or translation (Burrell et al. 2017).

Compared to published CTLV qPCR assays that were designed on limited or single isolate sequences, the assay in this study performed better (e.g. Youden's index) and detected a diverse range of CTLV isolates from different geographic locations, citrus varieties, and isolation times, because it was designed using a high number of virus sequences (Cowell et al. 2017; Liu et al. 2011; Roy et al. 2005). These results agree with Roussel et al. (Roussel et al. 2005) who reported, that the RT-qPCR designed for prune dwarf virus (PDV) failed to detect many virus isolates because the assay was designed from very few published PDV sequences in the GenBank. In addition, the sensitivity and specificity of this assay was improved by using MGB probes (Kutyavin et al. 2000; Mingxiao et al. 2013), designed from the multiple sequence alignment, that targeted the identified conserved genomic region between the CP gene and 3'-UTR. Furthermore, measuring the intra and inter assay variations confirmed the reproducibility and repeatability of the developed RT-qPCR assay. Finally, measuring viral loads and performing reactions under variable conditions showed that the newly developed RT-qPCR is robust and can detect minimal quantities of the CTLV.

Next generation sequencing (NGS) technologies combined with bioinformatics analysis have proven to be powerful tools in identifying and characterizing novel sequences of pathogens, in studying disease occurrence, genome variability, and phylogeny (Kehoe et al. 2014; Radford et al. 2012; Villamor et al. 2019). Using NGS technologies within a well-defined qPCR design, development and validation protocol (Broeders et al. 2014; Bustin et al. 2009) is that qPCR assays can be regularly updated as more target pathogen

genomes are sequenced, therefore, increasing the value of the assay in preventing virus outbreaks and managing virus spread and induced disease.

We propose that in the era of powerful affordable sequencing platforms the presented approach of full-genome sequence analysis of multiple virus isolates, and not only a small genome region of a small number of virus sequences, becomes a guideline for the design and comprehensive validation of qPCR-based virus detection assays especially for use in high value germplasm programs (Bostock et al. 2014; Navarro 1986; Vidalakis et al. 2014). Although the academic urgency for scientific publications is understandable, specifically in the case of diagnostics that affect international trade, quarantines and regulatory decisions that affect the livelihoods of thousands of people, we urge the research community to dedicate the necessary resources and time for the appropriate design and validation of pathogen detection assays. We hope that this study offers a valuable case study for such consideration.

References

Bewick, V., Cheek, L., and Ball, J. 2004. Statistics review 13: receiver operating characteristic curves. Critical care (London, England) 8:508-512.

Bostock, R. M., Thomas, C., Hoenisch, R., Golino, D. A., and Vidalakis, G. 2014. Excluding Pests and Pathogens: Plant health: How diagnostic networks and interagency partnerships protect plant systems from pests and pathogens. California Agriculture 68:117-124.

Broadbent, P., Dephoff, C. M., and Gilkeson, C. 1994. Detection of citrus tatter leaf virus in Australia. Australasian Plant Pathology 23:20-24.

Broeders, S., Huber, I., Grohmann, L., Berben, G., Taverniers, I., Mazzara, M., Roosens, N., and Morisset, D. 2014. Guidelines for validation of qualitative real-time PCR methods. Trends in Food Science & Technology 37:115-126.

Burrell, C. J., Howard, C. R., and Murphy, F. A. 2017. Chapter 4 - Virus Replication. Pages 39-55 in: Fenner and White's Medical Virology (Fifth Edition). C. J. Burrell, C. R. Howard and F. A. Murphy, eds. Academic Press, London.

Bustin, S. A., Benes, V., Garson, J. A., Hellemans, J., Huggett, J., Kubista, M., Mueller, R., Nolan, T., Pfaffl, M. W., and Shipley, G. L. 2009. The MIQE guidelines: minimum information for publication of quantitative real-time PCR experiments. Clinical chemistry 55:611-622.

Calavan, E. C., Christiansen, D. W., and Roistacher, C. N. 1963. Symptoms associated with tatter-leaf virus infection of Troyer citrange rootstocks. Plant Disease Reporter 47:971-975.

Cowell, S. J., Harper, S. J., and Dawson, W. O. 2017. A real-time RT-qPCR assay for the detection of Citrus tatter leaf virus. J Virol Methods 244:29-31.

da Graca, J. V. 1977. Citrus tatter leaf virus in South African Meyer lemon. Citrus and sub-tropical fruit journal.

da Graca, J. V., and Sharia, M. 1996. Citrus Tatter Leaf Virus in the Rio Grande Valley of South Texas. Pages 198-200 in: Proceedings of 13th Conference of International Organization of Citrus Virologists.

Fraser, L. R., and Broadbent, P. 1979. Virus and related diseases of citrus in New South Wales. Dept. of Agriculture New South Wales.

Garnsey, S. M. 1964. Detection of tatter leaf virus of citrus in Florida. Florida State Horticultural Society 77:106-109.

Garnsey, S. M. 1970. Viruses in Florida's Meyer lemon trees and their effects on other citrus. Florida State Horticultural Society 83:66-71.

Garnsey, S. M., and Jones, J. W. 1968. Relationship of symptoms to the presence of tatter-leaf virus in several citrus hosts. Pages 206-212 in: Proceedings of 4th Conference of International Organization of Citrus Virologists.

Geoghegan, J. L., and Holmes, E. C. 2017. Predicting virus emergence amid evolutionary noise. Open Biol 7.

Geoghegan, J. L., Duchêne, S., and Holmes, E. C. 2017. Comparative analysis estimates the relative frequencies of co-divergence and cross-species transmission within viral families. PLOS Pathogens 13:e1006215.

Gergerich, R. C., Welliver, R. A., Gettys, S., Osterbauer, N. K., Kamenidou, S., Martin, R. R., Golino, D. A., Eastwell, K., Fuchs, M., Vidalakis, G., and Tzanetakis, I. E. 2015. Safeguarding Fruit Crops in the Age of Agricultural Globalization. Plant Disease 99:176-187.

Hailstones, D. L., Bryant, K. L., Broadbent, P., and Zhou, C. 2000. Detection of Citrus tatter leaf virus with reverse transcription- polymerase chain reaction (RT-PCR). Australasian Plant Pathology 29:240-248.

Herron, C. M., and Skaria, M. 2000. Further Studies on Citrus Tatter Leaf Virus in Texas. Pages 185-194 in: Proceedings of 14th Conference of International Organization of Citrus Virologists.

Hilf, M. E. 2008. An Immunocapture RT-PCR Procedure Using Apple stem grooving virus Antibodies Facilitates Analysis of Citrus tatter leaf virus from the Original Meyer Lemon Host. Plant Disease 92:746-750.

Ho, T., and Tzanetakis, I. E. 2014. Development of a virus detection and discovery pipeline using next generation sequencing. Virology 471-473:54-60.

Holmes, E. C. 2009. The Evolutionary Genetics of Emerging Viruses. Annual Review of Ecology, Evolution, and Systematics 40:353-372.

Hyun, J. W., Hwang, R. Y., and Jung, K. E. 2017. Development of Multiplex PCR for Simultaneous Detection of Citrus Viruses and the Incidence of Citrus Viral Diseases in Late-Maturity Citrus Trees in Jeju Island. Plant Pathol J 33:307-317.

Inouye, N., Maeda, T., and Mitsuhata, K. 1979. Citrus tatter leaf virus isolated from lily. Annuals of the Phytopathological Society of Japan 45:712-720.

Kehoe, M. A., Coutts, B. A., Buirchell, B. J., and Jones, R. A. 2014. Plant virology and next generation sequencing: experiences with a Potyvirus. PLOS ONE 9:e104580.

King, A. M. Q., Adams, M. J., Carstens, E. B., and Lefkowitz, E. J. 2011. Virus Taxonomy: Ninth Report of the International Committee on Taxonomy of Viruses. International Committee on Taxonomy of Viruses, Elsevier Academic Press.

Kralik, P., and Ricchi, M. 2017. A Basic Guide to Real Time PCR in Microbial Diagnostics: Definitions, Parameters, and Everything. Frontiers in Microbiology 8.

Kutyavin, I. V., Afonina, I. A., Mills, A., Gorn, V. V., Lukhtanov, E. A., Belousov, E. S., Singer, M. J., Walburger, D. K., Lokhov, S. G., Gall, A. A., Dempcy, R., Reed, M. W., Meyer, R. B., and Hedgpeth, J. 2000. 3'-minor groove binder-DNA probes increase sequence specificity at PCR extension temperatures. Nucleic acids research 28:655-661.

Leutenegger, C. M. 2001. The real-time TaqMan PCR and applications in veterinary medicine. Vet Sci Tomorrow 1:1-15.

Liu, K. H., Song, Z., Zhou, Y., Li, Z. A., and Zhou, C. Y. 2011. Detection of Citrus tatter leaf virus by Real-time RT-PCR. in: Proceedings of 18th Conference of International Organization of Citrus Virologists.

Magome, H., Yoshikawa, N., Takahashi, T., Ito, T., and Miyakawa, T. 1997. Molecular variability of the genomes of capilloviruses from apple, Japanese pear, European pear, and citrus trees. Phytopathology 87:389-396.

Mingxiao, M., Jinhua, L., Yingjin, S., Li, L., and Yongfei, L. 2013. TaqMan MGB probe fluorescence real-time quantitative PCR for rapid detection of Chinese Sacbrood virus. PLOS ONE 8:e52670-e52670.

Miyakawa, T. 1980. Occurrence and varietal distribution of tatter leaf-citrange stunt virus and its effects on Japanese citrus. in: Proceedings of 8th Conference of International Organization of Citrus Virologists.

Miyakawa, T., and Matsui, C. 1976. A Bud-Union Abnormality of Satusma Mandarin on *Poncirus Trifoliata* Rootstock in Japan. Pages 125-131 in: Proceedings of 7th Conference of International Organization of Citrus Virologists.

Miyakawa, T., and Tsuji, M. 1988. The association of tatterleaf virus with budunion crease of trees on trifoliate orange rootstock. Pages 360-364 in: Proceedings of 10th Conference of International Organization of Citrus Virologists.

Moreno, P., Ambrós, S., Albiach-Martí, M. R., Guerri, J., and Peña, L. 2008. Citrus tristeza virus: a pathogen that changed the course of the citrus industry. Mol Plant Pathol 9:251-268.

Moya, A., Holmes, E. C., and González-Candelas, F. 2004. The population genetics and evolutionary epidemiology of RNA viruses. Nature Reviews Microbiology 2:279-288.

Navarro, L. 1986. Citrus certification in Mediterranean countries1. EPPO Bulletin 16:227-238.

Nishio, T., Kawai, A., Kato, M., and Kobayashi, T. 1982. A sap-transmissible closterovirus in citrus imported from China and Formosa. Research Bulletin of the Plant Protection Service (Japan).

Ohira, K., Namba, S., Rozanov, M., Kusumi, T., and Tsuchizaki, T. 1995. Complete sequence of an infectious full-length cDNA clone of citrus tatter leaf capillovirus: comparative sequence analysis of capillovirus genomes. J Gen Virol 76 (Pt 9):2305-2309.

Olival, K. J., Hosseini, P. R., Zambrana-Torrelio, C., Ross, N., Bogich, T. L., and Daszak, P. 2017. Host and viral traits predict zoonotic spillover from mammals. Nature 546:646-650.

Osman, F., Dang, T., Bodaghi, S., and Vidalakis, G. 2017. One-step multiplex RT-qPCR detects three citrus viroids from different genera in a wide range of hosts. J Virol Methods 245:40-52.

Osman, F., Hodzic, E., Kwon, S. J., Wang, J., and Vidalakis, G. 2015. Development and validation of a multiplex reverse transcription quantitative PCR (RT-qPCR) assay for the rapid detection of *Citrus tristeza virus, Citrus psorosis virus, a*nd *Citrus leaf blotch virus*. J Virol Methods 220:64-75.

Parrish, C. R., Holmes, E. C., Morens, D. M., Park, E. C., Burke, D. S., Calisher, C. H., Laughlin, C. A., Saif, L. J., and Daszak, P. 2008. Cross-species virus transmission and the emergence of new epidemic diseases. Microbiol Mol Biol Rev 72:457-470.

Pfaffl, M. W. 2004. Quantification strategies in real-time PCR. Pages 89-113 in: A-Z of Quantitative PCR. International University Line (IUL), La Jolla, CA, USA.

Polek, M. 2000. Report to the Agricultural Commissioners of Fresno and Tulare Counties on the status of C*itrus tristeza virus* infestation in SE Fresno County. Central California Tristeza Agency, Tulare, CA.

Radford, A. D., Chapman, D., Dixon, L., Chantrey, J., Darby, A. C., and Hall, N. 2012. Application of next-generation sequencing technologies in virology. J Gen Virol 93:1853-1868.

Rasmussen, R. 2001. Quantification on the LightCycler. Pages 21-34 in: Rapid Cycle Real-Time PCR: Methods and Applications. S. Meuer, C. Wittwer and K.-I. Nakagawara, eds. Springer Berlin Heidelberg, Berlin, Heidelberg.

Roistacher, C. N. 1991. Graft-Transmissible Diseases of Citrus -Handbook for detection and diagnosis of graft-transmissible diseases of citrus. Food and Agriculture Organization of the United Nations, Rome.

Roose, M. L. 2014. Rootstocks. Pages 95-105 in: Citrus Production Manual. L. Ferguson and E. E. Grafton-Cardwell, eds., University of California Agricultural and Natural Resources (UC ANR) Publication 3539.

Roose, M. L., Gmitter, F. G., Lee, R. F., and Hummer, K. E. 2015. Conservation of citrus germplasm: an international survey 2015. Pages 33-38 International Society for Horticultural Science (ISHS), Leuven, Belgium.

Roussel, S., Kummert, J., Salmon, M., Dutrecq, O., and Jijakli, M. H. 2005. Development of RT-PCR assays using fluorogenic-3' minor groove binder DNA probes for detection of fruit tree viruses. EPPO Bulletin 35:105-108.

Roy, A., Fayad, A., Barthe, G., and Brlansky, R. H. 2005. A multiplex polymerase chain reaction method for reliable, sensitive and simultaneous detection of multiple viruses in citrus trees. J Virol Methods 129:47-55.

Smith, I. M., McNamara, D.G., Scott, P.R., and Harris, K. M. 1992. Quarantine pests for Europe : data sheets on quarantine pests for the European Union and for the European and Mediterranean Plant Protection Organization. 2nd ed. ed. CAB International in association with the European and Mediterranean Plant Protection Organization, Wallingford.

Song, Z., Li, Z. A., Liu, K. H., and Zhou, C. Y. 2015. Complete genome sequence analysis of two Citrus tatter leaf virus (CTLV) isolates from China. Journal of Integrative Agriculture 15:4.

Su, H. J., and Cheon, J. U. 1984. Occurrence and distribution of tatter leaf-citrange stunt complex a Taiwanese citrus. Pages 42-48 National Taiwan University, Bull. Phytopathol. Entomol.

Svec, D., Tichopad, A., Novosadova, V., Pfaffl, M. W., and Kubista, M. 2015. How good is a PCR efficiency estimate: Recommendations for precise and robust qPCR efficiency assessments. Biomol Detect Quantif 3:9-16.

Tamura, K., Stecher, G., Peterson, D., Filipski, A., and Kumar, S. 2013. MEGA6: Molecular Evolutionary Genetics Analysis version 6.0. Mol Biol Evol 30:2725-2729.

Tatineni, S., Afunian, M. R., Hilf, M. E., Gowda, S., Dawson, W. O., and Garnsey, S. M. 2009. Molecular characterization of Citrus tatter leaf virus historically associated with Meyer lemon trees: complete genome sequence and development of biologically active in vitro transcripts. Phytopathology 99:423-431.

Vidalakis, G., Gumpf, D. J., Polek, M., and Bash, J. A. 2014. The California Citrus Clonal Protection Program. Pages 117-130 in: Citrus Production Manual. L. Ferguson and E. E. Grafton-Cardwell, eds., University of California Agricultural and Natural Resources (UC ANR) Publication 3539.

Villamor, D. E. V., Ho, T., Al Rwahnih, M., Martin, R. R., and Tzanetakis, I. E. 2019. High Throughput Sequencing For Plant Virus Detection and Discovery. Phytopathology 109:716-725.

Wallace, J. M., and Drake, R. J. 1962. Tatter leaf, a previously undescribed virus effect on citrus. Plant Disease Reporter 46:211-212

Weber, P. H., and Bujarski, J. J. 2015. Multiple functions of capsid proteins in (+) stranded RNA viruses during plant–virus interactions. Virus Research 196:140-149.

Woolhouse, M. E., Haydon, D. T., and Antia, R. 2005. Emerging pathogens: the epidemiology and evolution of species jumps. Trends Ecol Evol 20:238-244.

Worobey, M., and Holmes, E. C. 1999. Evolutionary aspects of recombination in RNA viruses. Journal of General Virology 80:2535-2543.

Yokomi, R. K., Selvaraj, V., Maheshwari, Y., Saponari, M., Giampetruzzi, A., Chiumenti, M., and Hajeri, S. 2017. Identification and Characterization of Citrus tristeza virus Isolates Breaking Resistance in Trifoliate Orange in California. Phytopathology 107:901-908.

Yoshikawa, N., Sasaki, E., Kato, M., and Takahashi, T. 1992. The nucleotide sequence of apple stem grooving capillovirus genome. Virology 191:98-105.

Yoshikawa, N., Imaizumi, M., Takahashi, T., and Inouye, N. 1993. Striking similarities between the nucleotide sequence and genome organization of citrus tatter leaf and apple stem grooving capilloviruses. J Gen Virol 74:2743-2747.

Zhang, T. M., and Liang, X. Y. 1988. Occurrence and detection of citrus tatter leaf virus (CTLV) in Huangyan, Zhejiang Province, China. Plant Disease 72:543-545.

Isolate	GenBank Accession No.	Partial sequence of citrus tatter leaf virus
ASGV-P-209* (apple)	NC001749	G G T T T T C G A G G C A G G T T C G G A A A G T A A C C T G G A A C T G G A G G G T T A G G A G T C G T G T G A A A T T C C G C A A A C T T G G T C G C G G T C T T G C A G G T T G A C
CTLV-IPPN122	MH108986	. . . . G . . . . C . . . . T . . . .
CTLV-TL100	MH108975	. . . . G . . . . A . . . .
CTLV-TL101	MH108976	. . . . G . . . . A . . . . A . . . .
CTLV-TL102	MH108977	. . . . G . . . . A . . . .
CTLV-TL103	MH108978	. . . . G . . . . G . . . .
CTLV-TL104	MH108979	. . . . G . . . . G . A . . . .
CTLV-TL110	MH108980	. . . . G . . . . G . . . .
CTLV-TL111	MH108981	. . . . G . . . . G . . . .
CTLV-TL112	MH108982	. . . . G . . . . A . A . . . . G . . . .
CTLV-TL113	MH108983	. . . . G . . . . G . . . . T . . . . T . A . . . .
CTLV-TL114	MH108984	. . . . G . . . . . . G . T . . . . T . A . . . . T . . . . A . . . . .
CTLV-TL115	MH108985	. . . . G . . . . G . A . . . .
CTLV-MTH	KC588948	. . . . G . . . . C . . . . T . . . .
CTLV-XHC	KC588947	. . . . G . . . . . . G . T . . . . T . A . . . . T . . . .
CTLV-Pk	JX416228	. . . . G . . . . G . . . . T . . . . T . A . . . .
CTLV-Ponkan8	KY706358	. . . . G . . . . G . . . . T . . . . T . A . . . .
CTLV-ML	EU553489	. . . . G . . . . G . . . .
CTLV-Kumquat1	AY646511	. . . . G . . . . . . G . T . . . . T . A . . . . T . . . . A . . . . .
CTLV-LCd-NA-1	FJ355920	. . . . . . T . . . . G . . . . T . . . . T . A . . . .
CTLV-Shatang Orange	JQ765412	. . . . G . . . . . . G . T . . . . T . A . . . . T . . . .
CTLV-HJY	MH144341	. . . . G . . . . . . G . T . . . . T . A . . . . T . . . .
CTLV-ASGV-1-HJY	MH144342	. . . . . . T . . . . G . . . . G . T . Y . . . .
CTLV-ASGV-2-HJY	MH144343	. . . . G . . . . C . . . . A . . . . G . T . . . .
ASGV-Matsuco	LC084659	. . . . . . T . . . . G . . . . T . . . . T . A . . . .
ASGV-FKSS2	LC143387	. . . . G . . . .
ASGV-N297	LC184610	. . . . . . T . . . . . G . . . . G . . . .
ASGV-Kiyomi	LC184611	. . . . G . . . . G . A . . . .
ASGV-Nagami	LC184612	. . . . G . . . . . G . . . . T . . . . T . . . .
CTLV 6315 F1		C G A G G C A G G T T C G G A G A G T A
CTLV 6314 F2		G A G G C G G G T T C G G A G A G T A
CTLV 6314 F3		T G A G G C A G G T T C G G A G A G T A A
CTLV 6337 P FAM		T G G A A C T G G A G G G T T A G
CTLV R		G G T C G C G G T C T T G C A G G

Figure 1.1 Citrus tatter leaf virus detection assay targeting region. Multiple nucleotide sequences alignment of citrus tatter leaf virus and apple stem grooving virus isolated from citrus and citrus relatives host. Citrus tatter leaf virus detection assay targeting region is highlighted in dark grey and primers-probe set is also shown. Apple stem grooving virus isolate P-209 (NCBI GenBank Accession No. NC001749) is used here to represent the species.

Figure 1.2 Schematic representation of the genome organization of citrus tatter leaf virus isolate TL100 (NCBI GenBank Accession No. MH108975). Open box represents open reading frame 1 (ORF1) which encoded a 2,105 amino acid (aa) polypeptide, a putative polyprotein around 242-kDa containing methyltransferase-like, papain-like protease, helicase-like, RdRp-like domains, and a coat protein (CP). Open reading frame 1 also contains variable region I (VRI) and variable region II (VRII). Open box with backslashes represents open reading frame 2 (ORF2) which is nested in open reading frame 1 and encoded a 36-kDa protein which belongs to 30-kDa superfamily of cell-to-cell movement protein (MP). Solid lines represent the 5' and 3' untranslated regions (UTRs). Short line with end points represent the citrus tatter leaf virus RT-qPCR detection assay targeting region designed in this study.

35
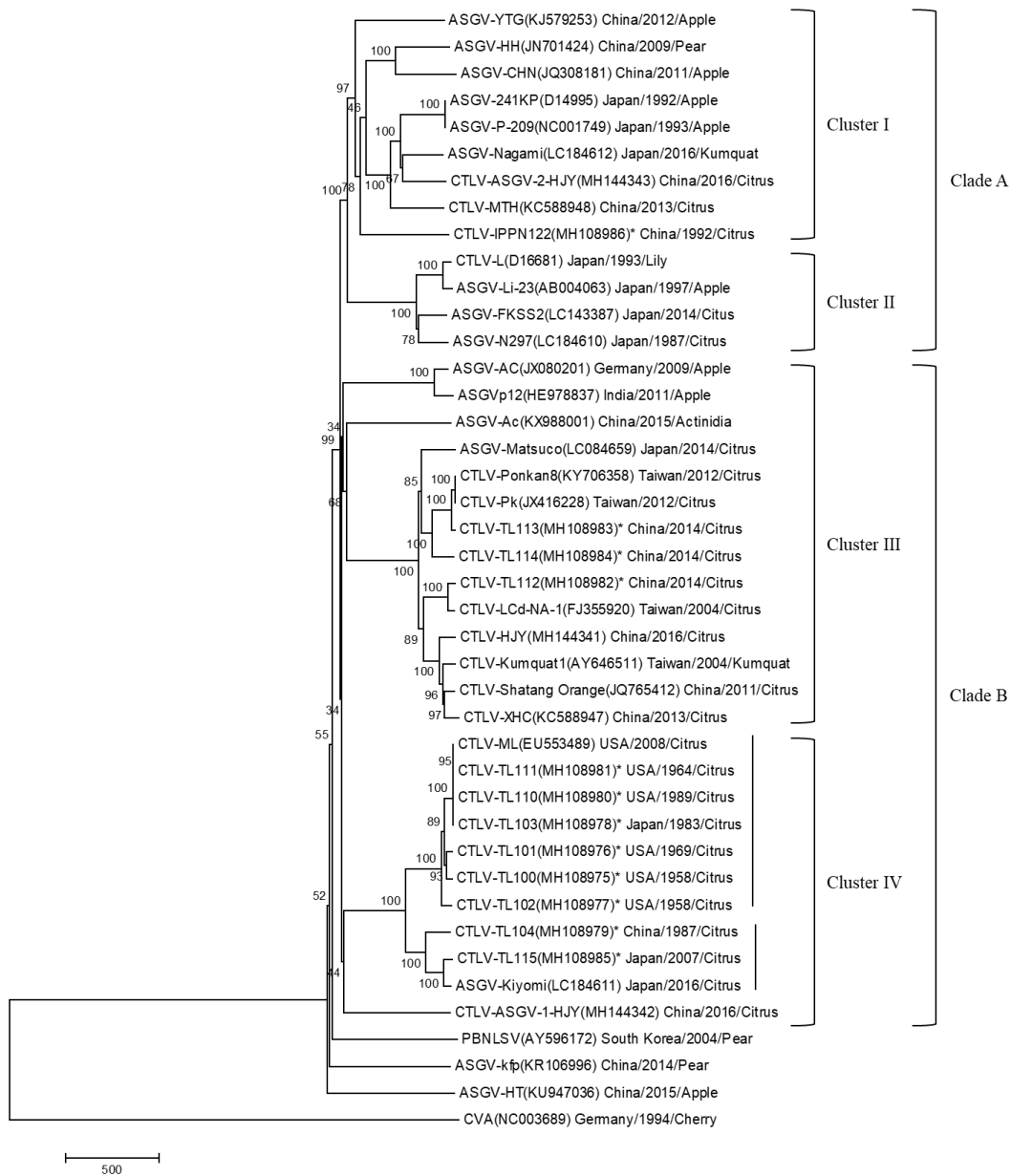
Figure 1.3 The unrooted phylogenetic tree based on full-length nucleotide sequences of citrus tatter leaf virus and apple stem grooving virus. Total 41 full-length virus genome sequences were used including 12 citrus tatter leaf virus isolates in this study, 12 of citrus tatter leaf virus, 16 isolates of apple stem grooving virus and one isolate of pear black necrotic leaf spot virus from NCBI GenBank database. Cherry virus A was used as an outgroup. The tree was constructed by MEGA 7.0.21 using neighbor-joining method with 1000 bootstrap replicates and bootstrap support is indicated at branch points. The scale bar shows the number of substitutions per base. (CTLV: citrus tatter leaf virus; ASGV: apple stem grooving virus; PBNLSV: pear black necrotic leaf spot virus; CVA: cherry virus A)
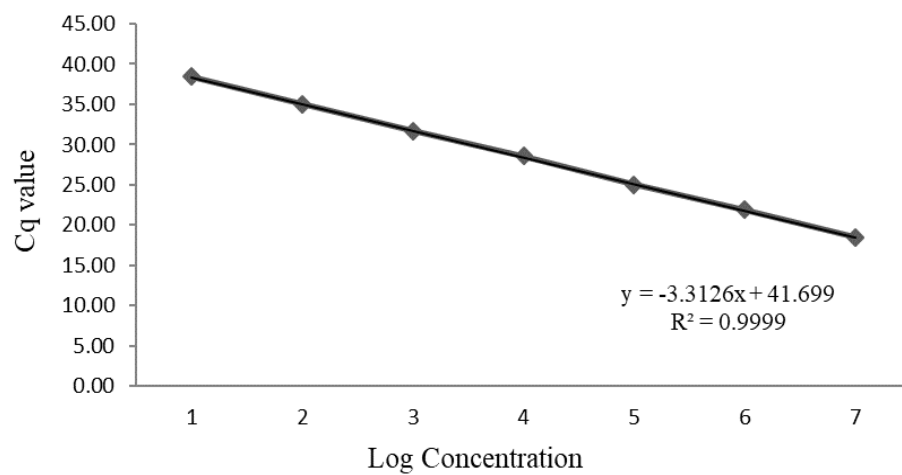
Figure 1.4 Standard curve analysis of RT-qPCR sensitivity. The X-axis displays the log concentration and the Y-axis represents the value of quantitative cycle (Cq).

Table 1.1 Isolates of citrus tatter leaf virus used in this study.

Sample	Citrus Host	Citrus Host Scientific Name	Geographic Origin	Isolation Year	Biological Indexing[1]	Genome Size (nt)	GenBank Accession No.
IPPN122	Sa Tou Satsuma	*C. unshiu* (Macf.) Marc.	China	1992	NA	6497	MH108986
TL100	Meyer Lemon	*C. limon* (L.) Burm.f. hyb.	TX, USA	1958	3	6495	MH108975
TL101	Meyer Lemon	*C. limon* (L.) Burm.f. hyb.	CA, USA	1969	3	6494	MH108976
TL102	Meyer Lemon	*C. limon* (L.) Burm.f. hyb.	CA, USA	1958	3	6495	MH108977
TL103	Hirado Buntan Pummelo	*C. grandis* (L.) Osb.	Japan	1983	NA	6495	MH108978
TL104	Kobeni Mikan Tangor	*C. reticulata* x *C. sinensis*	China	1987	NA	6495	MH108979
TL110	Little Sweetie Satsuma	*C. unshiu* (Macf.) Marc.	CA, USA	1989	NA	6495	MH108980
TL111	Meyer Lemon	*C. limon* (L.) Burm.f. hyb.	FL, USA	1964	NA	6495	MH108981
TL112	Citron	*C. medica* L.	China	2014	NA	6496	MH108982
TL113	Citron	*C. medica* L.	China	2014	NA	6496	MH108983
TL114	Citron	*C. medica* L.	China	2014	NA	6496	MH108984
TL115	Dekopan Tangor	*C. reticulata* x *C. sinensis*	Japan	2007	NA	6495	MH108985

[1.] The biological indexing was performed on *Citrus exclesa* and Rusk citrange. Symptom scores from 0 (no symptom) to 5 (severe symptoms).

Table 1.2 Oligonucleotide primers used in this study.

Primer Name	Primer Sequence 5'- 3'	Nucleotide Position[1]	Note
CTLV-Outer-1	CTGAGACCAATCACTCTATCTCTG	469-493	5' Outer CTLV gene specific primer, for CTLV isolates TL100, TL101, TL102, TL103, TL110, and TL111
CTLV-Outer-2	CTAAGACCAATCACTCTACTTCTA	469-493	5' Outer CTLV gene specific primer, for CTLV isolates TL115 and IPPN122
CTLV-Outer-3	CTAAGACCAATCACTCTATCTCTA	469-493	5' Outer CTLV gene specific primer, for CTLV isolates TL104
CTLV-Outer-4	CAAGCCAATCACTCTGTCTCTG	469-493	5' Outer CTLV gene specific primer, for CTLV isolates TL112, TL113, and TL114
CTLV-Inner-1	GGATGGGAATGTGACTTGAATC	222-244	5' Inner CTLV gene specific primer, for CTLV isolates IPPN122, TL100, TL101, TL102, TL103, TL110, and TL111
CTLV-Inner-2	GGATGGGAGTGTGACTTAAATC	222-244	5' Inner CTLV gene specific primer, for CTLV isolates TL104 and TL115
CTLV-Inner-3	GGATGAGAATGTGATTTAAATCCAATTGG	222-244	5' Inner CTLV gene specific primer, for CTLV isolates TL112, TL113, and TL114
CTLV-CP-Seq-5589-F	GRAAAGAGAGGRTTTAGGTCCCTCTCRGC	5589-5617	3' RACE CTLV gene specific primer

[1.] Nucleotide Position is based on reference genome of citrus tatter leaf virus isolate TL100 (NCBI GenBank Accession No. MH108975).

Abbreviation: CTLV: citrus tatter leaf virus.

Table 1.3 Full genome sequences of citrus tatter leaf virus isolates and capilloviruses used in phylogenetic and identity analysis.

Isolate	Host	Host Scientific Name	Geographic Origin	Isolation Year	GenBank Accession Number	GenBank Deposit Year	Cluster	Clade
AGSV-YTG	Apple	*Malus domestica*	China	2012	KJ579253	2014		
ASGV-HH	Pear	*Pyrus pyrifolia* cv. 'Huanghua'	China	2009	JN701424	2012		
ASGV-CHN	Apple	*Malus domestica*	China	2011	JQ308181	2013		
ASG-241KP	Apple	*Malus domestica*	Japan	1992	D14995	2008		
ASGV-P-209	Apple	*Malus domestica*	Japan	1993	NC001749	2018	I	
ASGV-Nagami	Kumquat	*Fortunella margarita* (Lour.)	Japan	2016	LC184612	2017		
CTLV-ASGV-2-HJY	Citrus- Huang Jin Mi You	*Citrus maxima* (Burm.) Merrill	China	2016	MH144343	2018		A
CTLV-MTH	Citrus- Ponkan Mandarin	*Citrus reticulata* Blanco	China	2013	KC588948	2013		
CTLV-IPPN122	Citrus- Sa Tou Satsuma	*Citrus unshiu* (Macf.) Marc.	China	1992	MH108986	2018		
CTLV-L	Lily	*Lilium longiflorum*	Japan	1993	D16681	2008		
ASGV-Li-23	Apple	*Malus domestica*	Japan	1997	AB004063	2000	II	
ASGV-FKSS2	Citrus	*Citrus junos* Sieb. ex Tanaka	Japan	2014	LC143387	2016		
ASGV-N297	Citrus- Satsuma	*Citrus unshiu* (Macf.) Marc.	Japan	1987	LC184610	2017		
ASGV-AC	Apple	*Malus domestica*	Germany	2009	JX080201	2012		
ASGVp12	Apple	*Malus domestica* cv. Red Chief	India	2011	HE978837	2015		
ASGV-Ac	Actinidia	*Actinidia* sp.	China	2015	KX988001	2017		
ASGV-Matsuco	Citrus	*Citrus tamurana*	Japan	2014	LC084659	2015		
CTLV-Ponkan8	Citrus- Ponkan Mandarin	*Citrus reticulata* Blanco	Taiwan	2012	KY706358	2018		
CTLV-Pk	Citrus- Ponkan Mandarin	*Citrus reticulata* Blanco	Taiwan	2012	JX416228	2012		
CTLV-TL113	Citrus- Citron	*Citrus medica* L.	China	2014	MH108983	2018	III	
CTLV-TL114	Citrus- Citron	*Citrus medica* L.	China	2014	MH108984	2018		
CTLV-TL112	Citrus- Citron	*Citrus medica* L.	China	2014	MH108982	2018		
CTLV-LCd-NA-1	Citrus- Sweet Orange	*Citrus sinensis* L. Osb.	Taiwan	2004	FJ355920	2008		
CTLV-HJY	Citrus- Huang Jin Mi You	*Citrus maxima* (Burm.) Merrill	China	2016	MH144341	2018		
CTLV-Kumquat1	Kumquat	*Fortunella margarita* (Lour.)	Taiwan	2004	AY646511	2004		
CTLV-Shatang Orange	Citrus- Shatang Mandarin	*Citrus reticulata* Blanco	China	2011	JQ765412	2012		B
CTLV-XHC	Citrus- Sweet Orange	*Citrus sinensis* L. Osb.	China	2013	KC588947	2013		
CTLV-ML	Citrus- Meyer Lemon	*Citrus limon* (L.) Burm.f. hyb.	FL, USA	2008	EU553489	2010		
CTLV-TL111	Citrus- Meyer Lemon	*Citrus limon* (L.) Burm.f. hyb.	FL, USA	1964	MH108981	2018		
CTLV-TL110	Citrus- Little Sweetie Satsuma	*Citrus unshiu* (Macf.) Marc.	CA, USA	1989	MH108980	2018		
CTLV-TL103	Citrus- Hirado Buntan	*Citrus maxima* (Burm.) Merrill	Japan	1983	MH108978	2018		
CTLV-TL101	Citrus- Meyer Lemon	*Citrus limon* (L.) Burm.f. hyb.	CA, USA	1969	MH108976	2018		
CTLV-TL100	Citrus- Meyer Lemon	*Citrus limon* (L.) Burm.f. hyb.	TX, USA	1958	MH108975	2018	IV	
CTLV-TL102	Citrus- Meyer Lemon	*Citrus limon* (L.) Burm.f. hyb.	CA, USA	1958	MH108977	2018		
CTLV-TL104	Citrus- Kobeni Mikan Tangor	*Citrus reticulata* x *Citrus sinensis*	China	1987	MH108979	2018		
CTLV-TL115	Citrus- Dekopon Tangor	*Citrus reticulata* x *Citrus sinensis*	Japan	2007	MH108985	2018		
ASGV-Kiyomi	Citrus	*Citrus unshiu x Citrus sinensis*	Japan	2016	LC184611	2017		
CTLV-ASGV-1-HJY	Citrus- Huang Jin Mi You	*Citrus maxima* (Burm.) Merrill	China	2016	MH144342	2018		
PBNLSV	Pear	*Pyrus pyrifolia*	South	2004	AY596172	2004		
ASGV-kfp	Pear	*Pyrus pyrifolia*	China	2014	KR106996	2015	Outgroup	
AGSV-HT	Apple	*Malus* spp. Crabapple	China	2015	KU947036	2017		
CVA	Cherry	*Prunus avium* L. cv. Sam	Germany	1994	NC003689	2018		

Abbreviations: CTLV: citrus tatter leaf virus; ASGV: apple stem grooving virus; PBNLSV: pear black necrotic leaf spot virus; CVA: cherry virus A.

Table 1.4 Oligonucleotide primers and probe of citrus tatter leaf virus detection assay designed in this study.

Primers/probes*	Sequence 5'- 3'	Nucleotide Position[1]	Amplicon size (bp)
CTLV 6315 F1	CGAGGCAGGTTCGGAGAGTA	6315-6334	
CTLV 6316 F2	GAGGCGGGTTCGGAGAGTA	6316-6334	
CTLV 6315 F3	TGAGGCAGGTTCGGAGAGTAA	6315-6335	82
CTLV R	CCTGCAAGACCGCGACC	6380-6396	
CTLV 6338 P FAM	TGGAACTGGAGGGTTAG	6338-6354	

[1.] Nucleotide position is based on reference genome of citrus tatter leaf virus isolate TL100 (NCBI GenBank Accession No. MH108975).

Abbreviations: CTLV: citrus tatter leaf virus; bp: base pairs.

*F: forward primer. R: reverse primer. P: qPCR probe.

Table 1.5 Full-length nucleotide sequence identities (%) of citrus tatter leaf virus isolates characterized in this study and capilloviruses from NCBI GenBank database.

Note: the data below form a lower-triangular pairwise-identity matrix. For each row, the listed values correspond, left to right, to the column isolates in the same order as the rows (AGSV-YTG, ASGV-HH, ASGV-CHN, ASG-241KP, ASGV-P-209, ASGV-Nagami, CTLV-ASGV-2-HJY, CTLV-MTH, CTLV-IPPN122, CTLV-L, ASGV-Li-23, ASGV-FKSS2, ASGV-N297, ASGV-AC, ASGVp12, ASGV-Ac, ASGV-Matsuco, CTLV-Ponkan8, CTLV-Pk, CTLV-TL113, CTLV-TL114, CTLV-TL112, CTLV-LCd-NA-1, CTLV-HJY, CTLV-Kumquat1, CTLV-Shatang Orange, CTLV-XHC, CTLV-ML, CTLV-TL111, CTLV-TL110, CTLV-TL103, CTLV-TL101, CTLV-TL100, CTLV-TL102, CTLV-TL104, CTLV-TL115, ASGV-Kiyomi, CTLV-ASGV-1-HJY, PBNLSV, ASGV-kfp, AGSV-HT).

Isolate	Clade	Cluster	Pairwise nucleotide identity (%) — values in column order
AGSV-YTG	A	I	
ASGV-HH	A	I	84.52
ASGV-CHN	A	I	83.23 90.54
ASG-241KP	A	I	86.78 87.12 86.34
ASGV-P-209	A	I	86.78 87.12 86.34 100.00
ASGV-Nagami	A	I	87.06 87.06 85.92 92.96 92.96
CTLV-ASGV-2-HJY	A	I	86.26 87.23 85.97 92.36 92.36 93.02
CTLV-MTH	A	I	86.63 86.49 85.78 91.07 91.07 91.42 90.84
CTLV-IPPN122	A	I	84.52 84.57 83.72 86.06 86.06 86.54 87.23 86.82
CTLV-L	A	II	83.04 84.09 83.12 82.98 82.98 82.95 83.11 83.45 83.48
ASGV-Li-23	A	II	82.78 84.08 83.03 82.97 82.97 83.17 83.27 83.41 83.41 98.47
ASGV-FKSS2	A	II	83.37 84.89 83.54 83.44 83.44 83.68 83.85 84.13 93.96 94.90 94.70
ASGV-N297	A	II	82.98 84.43 83.35 83.27 83.27 83.68 83.68 84.06 83.38 94.24 94.04 95.27
ASGV-AC	B	III	82.58 81.89 81.53 82.66 82.66 82.23 82.03 82.06 82.09 81.66 81.64 82.23 82.28
ASGVp12	B	III	82.12 81.16 80.90 81.76 81.76 81.42 80.99 81.49 81.42 80.84 80.87 81.47 81.42 97.31
ASGV-Ac	B	III	82.06 81.35 81.50 81.89 81.89 82.14 81.91 81.83 82.23 81.61 81.49 82.20 82.09 82.31 81.86
ASGV-Matsuco	B	III	82.54 81.66 81.44 81.81 81.81 82.25 81.55 82.57 81.14 81.37 81.37 81.78 81.72 81.71 81.55 82.23
CTLV-Ponkan8	B	III	82.43 81.97 81.60 81.72 81.72 82.23 81.66 82.13 81.11 81.58 81.57 81.74 81.61 81.86 81.61 82.20 95.13
CTLV-Pk	B	III	82.43 81.97 81.60 81.72 81.72 82.23 81.66 82.14 81.12 81.57 81.57 81.74 81.61 81.86 81.61 82.20 95.13 100.00
CTLV-TL113	B	III	82.35 82.01 81.60 81.64 81.64 82.15 81.66 82.08 81.18 81.49 81.46 81.75 81.54 81.98 81.73 82.26 95.05 99.43 99.43
CTLV-TL114	B	III	82.26 81.83 81.40 81.93 81.93 82.29 81.94 81.98 82.62 81.51 81.47 81.91 81.71 81.97 81.93 82.57 93.88 96.18 96.18 96.35
CTLV-TL112	B	III	82.30 81.71 81.60 82.07 82.07 82.60 81.94 82.37 81.58 81.60 81.61 81.95 81.78 82.29 81.92 82.49 93.51 93.27 93.27 93.75 92.67
CTLV-LCd-NA-1	B	III	82.14 81.46 81.41 81.66 81.66 82.32 81.58 82.01 81.26 81.28 81.29 81.66 81.43 82.11 81.72 82.43 94.24 93.95 93.93 94.47 93.42 98.73
CTLV-HJY	B	III	82.24 81.55 81.29 81.89 81.89 82.29 81.68 82.29 81.15 81.17 81.40 81.25 81.61 81.83 81.88 81.81 93.88 93.88 93.81 94.75 94.11 95.01
CTLV-Kumquat1	B	III	82.41 81.54 81.20 81.87 81.87 82.17 81.74 82.38 81.37 81.43 81.30 81.65 81.55 81.83 81.59 82.25 94.11 93.96 93.95 93.87 95.52 94.31 95.10 97.18
CTLV-Shatang Orange	B	III	82.27 81.66 81.35 81.69 81.69 82.31 81.52 82.34 81.45 81.18 81.18 81.43 81.41 81.85 81.59 82.34 94.45 94.10 94.11 94.10 95.18 94.53 95.35 97.53 97.96
CTLV-XHC	B	III	81.89 81.06 80.90 81.33 81.33 81.80 81.23 81.89 80.88 80.91 80.93 81.11 81.09 81.83 81.67 83.59 93.59 94.81 94.33 95.18 97.19 97.59 97.98
CTLV-ML	B	IV	81.95 81.12 81.52 81.64 81.64 82.27 81.33 82.09 82.18 81.38 81.27 81.66 81.61 81.77 81.42 81.50 81.86 81.84 81.84 81.98 81.93 82.04 81.90 81.98 81.86 81.72 81.43
CTLV-TL111	B	IV	81.95 81.12 81.52 81.64 81.64 82.27 81.33 82.09 82.18 81.38 81.27 81.66 81.61 81.77 81.42 81.50 81.86 81.84 81.84 81.98 81.93 82.04 81.90 81.98 81.86 81.72 81.43 100.00
CTLV-TL110	B	IV	81.95 81.12 81.52 81.64 81.64 82.27 81.33 82.09 82.18 81.38 81.27 81.66 81.61 81.77 81.42 81.50 81.86 81.84 81.84 81.98 81.93 82.04 81.90 81.98 81.86 81.72 81.43 100.00 100.00
CTLV-TL103	B	IV	82.00 81.15 81.50 81.66 81.66 82.23 81.35 82.10 82.20 81.40 81.29 81.67 81.63 81.78 81.44 81.52 81.87 81.86 81.86 82.00 81.95 82.06 81.92 82.00 81.87 81.73 81.44 99.95 99.95 99.95
CTLV-TL101	B	IV	81.99 81.29 81.47 81.61 81.61 82.18 81.30 82.10 82.18 81.25 81.16 81.61 81.53 81.95 81.58 81.39 81.81 81.87 81.87 82.01 82.02 82.04 81.92 81.86 81.89 81.64 81.36 98.70 98.70 98.70 98.66
CTLV-TL100	B	IV	82.04 81.29 81.53 81.84 81.84 82.32 81.47 82.17 82.10 81.30 81.23 81.77 81.81 81.95 81.55 81.55 81.86 81.93 81.93 82.07 82.03 82.12 81.98 81.97 81.89 81.69 81.41 98.52 98.52 98.52 98.47 98.98
CTLV-TL102	B	IV	82.23 81.35 81.64 81.95 81.95 82.40 81.67 82.18 82.40 81.49 81.40 81.93 81.83 81.92 82.04 82.01 82.30 81.87 81.98 82.00 81.73 81.43 97.99 97.99 97.99 98.01 98.56 98.33
CTLV-TL104	B	IV	81.73 81.47 81.83 81.80 81.80 82.46 81.92 82.46 82.03 81.37 81.29 82.14 81.90 82.06 81.58 81.97 81.78 82.03 82.03 82.10 82.40 82.00 81.81 81.86 81.95 81.70 81.47 92.51 92.51 92.51 92.56 92.87 92.60 92.54
CTLV-TL115	B	IV	81.50 81.15 81.27 81.87 81.87 82.18 81.61 82.35 81.81 81.49 81.29 82.03 81.73 81.93 81.47 81.67 81.95 82.01 82.01 82.06 82.44 82.00 81.75 82.00 82.10 81.89 81.66 92.02 92.02 92.02 92.04 92.30 92.20 92.05 95.73
ASGV-Kiyomi	B	IV	81.58 81.32 81.40 81.92 81.92 82.30 81.67 82.40 81.94 81.49 81.29 82.06 81.86 82.23 81.64 81.61 81.92 81.97 81.97 81.98 82.37 81.95 81.73 81.97 82.14 81.89 81.72 92.34 92.34 92.34 92.39 92.65 92.50 92.34 95.95 98.70
CTLV-ASGV-1-HJY	B	IV	82.60 81.86 81.50 82.49 82.49 82.54 82.34 82.32 82.35 82.00 81.92 82.29 82.37 82.68 81.78 82.12 80.77 80.94 80.94 80.92 81.31 81.46 80.88 81.03 80.88 80.91 80.74 81.78 81.78 81.78 81.80 81.82 81.87 82.03 82.81 82.49 82.57
PBNLSV		Outgroup	80.30 79.83 80.00 79.76 79.76 79.77 79.86 79.86 80.08 80.44 80.44 80.63 80.63 80.09 79.88 80.43 79.40 79.03 79.04 78.95 79.37 79.23 78.95 79.41 79.01 78.99 78.82 79.39 79.39 79.39 79.38 79.59 79.55 79.75 80.12 79.53 79.39 79.32
ASGV-kfp		Outgroup	79.98 79.65 79.50 79.64 79.64 80.13 79.92 79.98 79.76 79.58 79.52 79.93 80.01 80.06 79.22 79.41 80.26 80.12 80.10 80.01 80.27 80.06 80.12 79.92 80.15 80.10 80.01 79.90 79.52 79.52 79.56 79.59 79.52 79.48 79.72 79.70 79.61 80.27 79.19
AGSV-HT		Outgroup	80.87 79.34 78.90 79.09 79.09 79.41 79.09 79.65 79.29 78.94 78.82 79.23 78.97 79.23 79.19 79.20 79.12 79.64 79.29 79.23 79.23 79.26 79.31 78.97 79.67 79.67 79.67 79.69 79.68 79.79 79.79 79.81 79.44 79.47 79.41 78.78 78.43 79.21
CVA		Outgroup	26.57 26.69 26.20 26.89 26.89 26.70 26.30 26.61 26.33 25.73 25.86 25.91 25.76 26.16 25.88 26.15 25.98 26.41 26.41 26.43 26.15 26.33 26.10 25.95 26.12 26.04 25.91 26.82 26.82 26.82 26.82 26.82 26.75 26.98 26.80 26.60 26.58 26.67 26.31 25.99 26.24

Abbreviations: CTLV: citrus tatter leaf virus; ASGV: apple stem grooving virus; PBNLSV: pear black necrotic leaf spot virus; CVA: cherry virus A.

**Table 1.6** Variable sites (%) and nucleotide sequence identities (%) of citrus tatter leaf virus and apple stem grooving virus isolated from citrus and citrus relatives (n=28).

5'-Untranslated Region and Partial Polyprotein (1 - 5,640 nt)*			Coat Protein and 3'-Untranslated Region (5,641 - 6,495 nt)			Movement Protein (4,788 - 5,750 nt)		
Variable Sites (Variable/Total)	Minimum NSI[$]	NSI Mean ± SD	Variable Sites (Variable/Total)	Minimum NSI	NSI Mean ± SD	Variable Sites (Variable/Total)	Minimum NSI	NSI Mean ± SD
39.98 (2255/5640)	79.30	84.54 ± 6.66	23.63 (202/855)	89.60	92.78 ± 2.92	32.81 (316/963)	83.90	88.80 ± 4.77

Variable Region I (1,630 - 1,746 nt)			Variable Region II (4,783 - 5,640 nt)		
Variable Sites (Variable/Total)	Minimum NSI	NSI Mean ± SD	Variable Sites (Variable/Total)	Minimum NSI	NSI Mean ± SD
94.87 (111/117)	34.18	54.72 ± 21.80	35.08 (301/858)	82.05	87.87 ± 5.25

*Nucleotide position is based on reference genome of citrus tatter leaf virus isolate TL100 (NCBI GenBank Accession No. MH108975)

[$]NSI: Nucleotide Sequence Identity

Table 1.7 Variable sites (%) and nucleotide sequence identities (%) of the segmented coat protein and 3'-untranslated region of citrus tatter leaf and apple stem grooving virus isolated from citrus and citrus relatives (n= 28).

Position* (nt)	Variable Sites (Variable/Total)	Minimum NSI$	NSI Mean ± SD
5641 - 5840	22.50 (45/200)	86.00	94.36 ± 2.71
5841 - 6040	30.00 (60/200)	84.00	90.03 ± 4.76
6041 - 6240	25.50 (51/200)	87.00	91.98 ± 3.32
6241 - 6440	14.50 (29/200)	92.50	95.41 ± 1.99
6441 - 6495	30.91 (17/55)	78.18	90.49 ± 7.25

*Nucleotide position is based on reference genome of citrus tatter leaf virus isolate TL100 (NCBI GenBank Accession No. MH108975)

$NSI: Nucleotide Sequence Identity

Table 1.8 Comparison between RT-qPCR assays in detecting citrus tatter leaf virus inoculated and non-inoculated citrus plants (a) and their performance (b).

a.

Sample	Experiment	RNA Concentration (ng/µL)	260 / 280 Ratio	COX (n=4)	CTLV This study Lab A[1] (n=4)	CTLV This study Lab B[2] (n=2)	CTLV Liu et al. 2011 (n=4)	CTLV Cowell et al. 2017 (n=4)
CTLV Isolates (True Positive)								
IPPN122	TH2986-48	165.60	1.92	12.91 ± 0.04	22.16 ± 0.05	25.16 ± 0.03	27.82 ± 0.26	32.54 ± 0.37
TL100	1713-1	86.24	2.24	14.83 ± 0.13	24.20 ± 0.14	26.66 ± 0.58	27.11 ± 0.23	21.77 ± 0.28
	TL100A	94.88	2.07	15.05 ± 0.05	24.14 ± 0.06	24.92 ± 1.48	28.54 ± 0.20	22.07 ± 0.11
	TL100B	46.80	2.31	15.43 ± 0.06	22.55 ± 0.02	25.95 ± 1.35	26.49 ± 0.23	22.55 ± 0.04
TL101	1713-2	38.72	2.60	15.98 ± 0.04	20.80 ± 0.08	23.61 ± 2.39	25.24 ± 0.26	22.61 ± 0.05
	TL101A	115.04	2.09	14.76 ± 0.07	21.85 ± 0.10	24.09 ± 0.00	26.41 ± 0.22	21.98 ± 0.08
	TL101B	41.76	2.18	15.48 ± 0.26	21.62 ± 0.18	23.04 ± 1.21	25.89 ± 0.24	23.00 ± 0.15
	TL101-ND	130.32	2.06	14.63 ± 0.22	21.78 ± 0.13	21.27 ± 0.00	26.11 ± 0.14	20.75 ± 0.09
TL102	2-8-92	129.76	2.18	14.77 ± 0.20	22.66 ± 0.27	25.14 ± 0.21	27.26 ± 0.28	21.90 ± 0.04
TL103	3288-1	139.76	2.14	14.51 ± 0.10	24.71 ± 0.10	26.25 ± 0.23	28.54 ± 0.02	-
	3288-2	161.04	2.27	14.51 ± 0.39	22.40 ± 0.14	24.18 ± 0.26	26.20 ± 0.48	-
TL104	1855-12	73.44	2.24	15.80 ± 0.09	25.62 ± 0.11	22.92 ± 1.22	28.07 ± 0.20	-
	2881-1	104.72	2.05	15.19 ± 0.17	28.94 ± 0.21	26.44 ± 0.11	32.76 ± 0.40	-
	1855-13	148.40	2.15	14.25 ± 0.06	27.18 ± 0.09	24.64 ± 0.38	31.91 ± 0.28	-
TL110	3288-3	88.64	2.06	15.26 ± 0.12	22.90 ± 0.10	22.21 ± 0.06	31.01 ± 0.20	21.97 ± 0.05
	3288-4	120.64	2.11	14.81 ± 0.09	20.97 ± 0.06	23.47 ± 0.41	26.89 ± 0.10	20.35 ± 0.08
TL111	3288-6	189.60	2.03	14.01 ± 0.07	24.49 ± 0.08	28.22 ± 0.84	29.87 ± 0.34	21.09 ± 0.15
TL112	3291-9	140.08	2.15	14.64 ± 0.17	22.75 ± 0.10	24.53 ± 0.62	28.97 ± 0.21	22.66 ± 0.07
TL113	3291-10	119.12	2.24	14.75 ± 0.11	22.42 ± 0.06	23.72 ± 0.13	27.91 ± 0.16	26.34 ± 0.03
TL114	3291-11	197.28	2.11	13.88 ± 0.04	23.48 ± 0.09	24.54 ± 0.06	29.30 ± 0.17	24.31 ± 0.12
TL115	3170-1	221.20	2.09	13.68 ± 0.18	23.22 ± 0.10	26.12 ± 0.00	26.57 ± 0.13	-
	3170-2	176.00	2.22	14.06 ± 0.09	23.08 ± 0.06	27.17 ± 0.30	27.55 ± 0.09	-
CTLV-Non-inoculated (True Negative)								
Murcott Mandarin	1005674	44.24	2.12	16.41 ± 0.11	-	-	-	-
Fortune Mandarin	3014073	57.84	2.01	16.91 ± 0.10	-	-	-	-
Ponkan Mandarin	1005802	28.48	2.34	17.08 ± 0.11	-	-	-	-
Cleopatra Mandarin	1005683	40.56	2.12	17.89 ± 0.06	-	-	-	-
Parson Special Mandarin	3014062	35.44	2.00	16.52 ± 0.07	-	-	-	-
Tango Mandarin	1005668	39.76	2.00	15.71 ± 0.12	-	-	-	-
Primosole Mandarin	1005924	17.36	2.31	15.92 ± 0.04	-	-	-	-
Macetera Sweet Orange	3014130	52.88	1.99	15.65 ± 0.10	-	-	-	-
Pehrson #3 Valencia	1005873	40.48	2.07	15.33 ± 0.21	-	-	-	-
Pehrson #4 Valencia	3014051	44.96	2.10	15.98 ± 0.02	-	-	-	-
Rocky Hill Navel	1005796	47.92	2.07	16.26 ± 0.07	-	-	-	-
Rio Grande Navel	1005810	53.44	2.10	15.64 ± 0.10	-	-	-	-
Skaggs Bonanza Navel	1005797	49.92	2.02	16.19 ± 0.10	-	-	-	-
Autumn Gold Navel	1005884	58.96	2.21	15.91 ± 0.05	-	-	-	-
China S-9 Satsuma	1005895	61.68	2.02	15.61 ± 0.10	-	-	-	-
China S-18 Satsuma	3015105	29.92	2.38	17.05 ± 0.04	-	-	-	-
China S-1 Satsuma	3015102	39.52	2.01	16.61 ± 0.10	-	-	-	-
China S-17 Satsuma	3014074	12.48	3.18	15.96 ± 0.09	-	-	-	-
Minneola Tangelo	1005678	56.24	2.20	17.88 ± 0.04	-	-	-	-
Schaub Rough Lemon	1005710	22.32	2.23	17.06 ± 0.11	-	-	-	-
Marumi Kumquat	3014132	28.40	2.40	16.51 ± 0.17	-	-	-	-
Australian Finger Lime	1005608	53.28	2.32	17.05 ± 0.08	-	-	-	-
Eustis Limequat	1005814	28.40	2.38	16.49 ± 0.02	-	-	-	-
Valentine Pummelo	3014144	47.60	2.34	16.57 ± 0.09	-	-	-	-
X639	3014082	33.84	2.42	18.63 ± 0.09	-	-	-	-
RT-qPCR Controls								
Positive	H11 / UCD*	NT	NT	13.71 ± 0.08	17.96 ± 0.07	23.98 ± 0.37	24.38 ± 0.32	14.95 ± 0.19
No Template	H9	-	-	-	-	-	-	-
Negative	861-S-1	NT	NT	15.45 ± 0.15	-	-	-	-

Table 1.8 Comparison between RT-qPCR assays in detecting (a) citrus tatter leaf virus inoculated and non-inoculated citrus plants and (b) their performance (cont'd).

b.

	CTLV This study Lab A[1]	CTLV This study Lab B[2]	CTLV Liu *et al.* 2011	CTLV Cowell *et* *al.* 2017
RT-qPCR Performance				
Sn	1.00	1.00	1.00	0.68
Sp	1.00	1.00	1.00	1.00
LR+	UN	UN	UN	UN
LR-	0.00	0.00	0.00	0.32
J	1.00	1.00	1.00	0.68

Abbreviations: Cq: quantitative cycle; CTLV: citrus tatter leaf virus; COX: cytochrome oxidase gene of host plants used as positive internal control (Osman et al. 2015); NT: not tested; UN: undefined number (denominator equals 0).

[1] Lab A: Citrus Clonal Protection Program, University of California, Riverside, with ThermoFisher Scientific QuantStudio 12K Flex Real-Time PCR System.

[2] Lab B: Real-time PCR Research & Diagnostic Core Facility, University of California, Davis, with ThermoFisher 7900HT FAST Real-time PCR system.

* Different controls were used at Lab B.

Table 1.9 Citrus tatter leaf virus RT-qPCR assay validated for robustness.

Isolates	Experiment	CTLV RT-qPCR Cq Value				
		Optimum[1]	Annealing Temperature[2]		Pipetting Errors[2]	
		58 ℃ / 12 μL	-2 ℃	+2 ℃	-2 μL	+2 μL
IPPN122	TH2986-48	22.16 ± 0.05	29.59 ± 0.72	30.18 ± 0.38	30.41 ± 0.25	31.62 ± 2.04
TL100	TL100A	24.14 ± 0.06	23.62 ± 0.06	24.29 ± 0.38	24.57 ± 0.08	23.93 ± 0.35
TL101	TL101A	21.85 ± 0.10	21.14 ± 0.02	21.49 ± 0.09	21.45 ± 0.13	21.12 ± 0.27
TL103	3288-1	24.71 ± 0.10	25.82 ± 0.25	25.81 ± 0.07	26.32 ± 0.06	26.01 ± 0.09
TL112	3291-9	22.75 ± 0.10	23.44 ± 0.13	23.46 ± 0.02	23.82 ± 0.35	24.61 ± 2.18
TL113	3291-10	22.42 ± 0.06	22.28 ± 0.10	22.04 ± 0.11	22.29 ± 0.11	21.47 ± 0.15
TL115	3170-1	23.22 ± 0.10	24.66 ± 0.15	25.47 ± 0.25	25.19 ± 0.05	25.29 ± 0.10

Abbreviations: Cq: quantitative cycle; CTLV: citrus tatter leaf virus.

[1]Optimum setup was using the conditions validated and optimized in this study including volume, primer probe concentrations, annealing temperature, etc. And the reactions were run on ThermoFisher Scientific QuantStudio 12K Flex Real-Time PCR System.

[2]The RT-qPCR reactions were setup with same concentration of primers and probe and using Bio-Rad iTaq™ Universal Probes One-Step Kit per manufacturer's instruction. The reactions were run on Bio-Rad CFX-96 Real-Time PCR Detection System.

Table 1.10 Citrus tatter leaf virus RT-qPCR assay testing citrus tatter leaf virus-inoculated controls.

Sample	Origin	CTLV RT-qPCR Cq Value
FL202 PA A 7/27/10	FL, USA	16.62
FL202 Volk sub 1	FL, USA	23.09
CTLV #1, FL	FL, USA	23.32
CTLV #2, FL	FL, USA	24.50
CTLV #3, FL	FL, USA	23.33
CTLV #4, FL	FL, USA	24.94
CTLV #5, FL	FL, USA	32.82
CTLV #6, FL	FL, USA	21.28
Positive #1	South Korea	19.07
Positive #2	South Korea	32.04
Positive #3	South Korea	37.61
Positive #4	South Korea	25.11
H3	HI, USA	26.90
H29	HI, USA	26.28
Navel NSW Sample 1	Australia	20.98*
Navel NSW Sample 2	Australia	20.25*
Beltsville ARS	MD, USA	17.83*

Abbreviations: Cq: quantitative cycle; CTLV: citrus tatter leaf virus.

* RT-qPCR test was performed at Elizabeth Macarthur Agricultural Institute.

Table 1.11 Citrus tatter leaf virus RT-qPCR assay testing non-inoculated citrus controls.

Citrus Host	Source / Registration	RT-qPCR Cq Value	
		COX	CTLV
Mandarin (*C. reticulata* Blanco)			
Murcott Mandarin	1005674	16.49	-
Fortune Mandarin	3014073	17.21	-
Ponkan Mandarin	1005802	16.13	-
Cleopatra Mandarin	1005683	16.56	-
Parson Special Mandarin	3014062	16.24	-
Tango Mandarin	1005668	16.46	-
Primosole Mandarin	1005926	16.99	-
Imperial Mandarin	3014131	16.00	-
Hansen Mandarin	3014136	15.93	-
Encore Ls Mandarin	3003020	15.94	-
Sweet Orange (*C. sinensis* L. Osb.)			
Macetera Sweet Orange	3014130	16.11	-
Pehrson #3 Valencia	1005873	15.69	-
Pehrson #4 Valencia	3014051	16.58	-
Rocky Hill Navel	1005796	16.50	-
Gillette Navel	3014134	15.55	-
Rio Grande Navel	1005810	17.49	-
Cogan Navel	1005936	16.05	-
Ricalate Navel	3014068	16.93	-
Johnson Navel	3014096	16.47	-
Skaggs Bonanza Navel	1005797	16.93	-
Autumn Gold Navel	1005884	16.42	-
Robertson Navel	3014125	16.51	-
Ceridwen Navel	3014140	16.96	-
Satsuma (*C. unshiu* (Macf.) Marc.)			
China S-9 Satsuma	1005895	17.39	-
China S-18 Satsuma	3015105	16.11	-
China S-1 Satsuma	3015102	16.52	-
China S-17 Satsuma	3014074	15.85	-
China S-20 Satsuma	3014064	15.95	-
China 6-18 Satsuma	3014065	16.69	-
Tangelo (*C. reticulata* x *Citrus paradisi*)			
Minneola Tangelo	1005678	17.05	-

Abbreviations: Cq: quantitative cycle; CTLV: citrus tatter leaf virus; COX: cytochrome oxidase gene of host plants used as positive internal control (Osman et al. 2015).

Table 1.11 Citrus tatter leaf virus RT-qPCR assay testing non-inoculated citrus controls (cont'd).

Citrus Host	Source / Registration	COX	CTLV
Lemon (*C. limon* (L.) Burm.f.)			
Schaub Rough Lemon	1005710	16.95	-
Kumquat (*Fortunella* sp.)			
Centennial Variegated Kumquat	1005684	16.69	-
Nagami Kumquat	3014145	17.40	-
Marumi Kumquat	3014132	16.29	-
Clementine (*C. clementina* Hort. ex Tan.)			
Fina Sodea Clementine	3003054	16.43	-
Marisol Clementine	3014101	16.72	-
Lime (*C. aurantifolia* (Christm.) Swing.)			
Australian Finger Lime	1005608	16.95	-
Persian Lime	1005617	15.80	-
Limequat (*Fortunella* sp. x *C. aurantifolia*)			
Eustis Limequat	1005814	16.66	-
Pummelo (*C. grandis* (L.) Osb.)			
Valentine Pummelo	3014144	16.73	-
Citrange (*P. trifoliata* x *C. sinensis*)			
Furr C-57 Citrange	1005930	17.51	-
Citron (*C. medica* L.)			
'Etrog' Citron Arizona 861-S-1	1005966	14.02	-
Others			
X639	3014082	16.25	-

The RT-qPCR Cq Value columns (COX and CTLV) are grouped under the header "RT-qPCR Cq Value"; Source / Registration is a separate column.

Abbreviations: Cq: quantitative cycle; CTLV: citrus tatter leaf virus; COX: cytochrome oxidase gene of host plants used as positive internal control (Osman et al. 2015).

Table 1.12 Citrus tatter leaf virus RT-qPCR assay testing samples inoculated with non-targeted citrus pathogens.

Citrus Pathogen Isolate	Source / Registration number	RT-qPCR Cq Value		
		COX	CTLV	Target
Citrus tristeza virus (CTV)				
T514	T514-2	14.55	-	25.75
T538	3275-4	14.23	-	22.46
SY568	2761-114	13.87	-	20.30
Citrus psorosis virus (CPsV)				
P201	1766-5	14.56	-	26.52
P203	2-26-98	14.93	-	28.38
P218	3175-2	14.06	-	28.67
Citrus leaf blotch virus (CLBV)				
CLBV, Spain	3069-1	14.86	-	27.89
Citrus vein enation virus (CVEV)				
VE702	2923-2	14.46	-	(+)*
VE703	2923-3	14.33	-	(+)*
VE704	2923-4	14.42	-	(+)*
Citrus yellow vein virus (CYVV)				
YV3163-1	3163-1	14.54	-	21.28
YV3163-3	3163-3	15.09	-	20.72
YV920C	3163-20	14.66	-	21.94
Infectious variegation virus (IVV)				
IV400	IV400 3-26-03	13.82	-	13.63
IV401	IV401A 1993	14.62	-	28.41
Concave gum				
CG302	CG302 7-8-04	14.30	-	(+)**
CG308	2355-4	14.58	-	(+)**
CG309	CG309 11-14-96	13.86	-	(+)**

Abbreviations: Cq: quantitative cycle; CTLV: citrus tatter leaf virus; COX: cytochrome oxidase gene of host plants used as positive internal control (Osman et al. 2015).

*Citrus vein enation virus was tested by conventional RT-PCR

** Concave gum was tested by biological indexing

Table 1.12 Citrus tatter leaf virus RT-qPCR assay testing samples inoculated with non-targeted citrus pathogens (cont'd).

Citrus Pathogen Isolate	Source / Registration number	RT-qPCR Cq Value		
		COX	CTLV	Target
Citrus viroids				
Citrus exocortis viroid (CEVd)	2765-1	14.43	-	26.17
Citrus bent leaf viroid	2765-2	14.69	-	26.46
Citrus bent leaf viroid- LSS	3237-3	17.05	-	32.76
Hop stunt viroid, non-cachaxia	2765-4	14.92	-	21.62
Hop stunt viroid, cachaxia	2765-6	17.39	-	27.34
Citrus dwarfing viroid	2765-12	14.88	-	27.92
Citrus bark cracking viroid	3200-1	15.13	-	23.45
Citrus viroid V	3195-5	13.54	-	26.32
Candidatus Liberibacter				
asiaticus	HLB B	17.49	-	26.69
asiaticus	HLB G	16.78	-	29.55
Spiroplasma citri				
C189	C189 7-8-09	16.95	-	30.11
S616	S600 7-8-09	17.09	-	29.26

Abbreviations: Cq: quantitative cycle; CTLV: citrus tatter leaf virus; COX: cytochrome oxidase gene of host plants used as positive internal control (Osman et al. 2015).

Table 1.13 Nucleotide (below diagonal) and amino acid (above diagonal) sequence identities (%) of coat protein (CP).

Isolate	Genbank Accession No.	CTLV-IPPN122	CTLV-TL100	CTLV-TL101	CTLV-TL102	CTLV-TL103	CTLV-TL104	CTLV-TL110	CTLV-TL111	CTLV-TL112	CTLV-TL113	CTLV-TL114	CTLV-TL115	CTLV-MTH	CTLV-XHC	CTLV-Pk	CTLV-Ponkan8	CTLV-ML	CTLV-Kumquat1	CTLV-LCd-NA-1	CTLV-Shatang Orange	CTLV-HJY	CTLV-ASGV-1-HJY	CTLV-ASGV-2-HJY	CTLV-L	ASGV-Li-23	ASGV-P-209	ASGVp12	ASGV-AC	ASGV-HH	ASGV-241KP	ASGV-Matsuco	ASGV-FKSS2	ASGV-N297	ASGV-Kiyomi	ASGV-Nagami	ASGV-kfp	ASGV-Ac	ASGV-CHN	ASGV-YTG	ASGV-HT	PBNLSV
CTLV-IPPN122	MH108986		94.53	94.95	96.21	94.95	95.37	94.95	94.95	94.95	94.95	94.95	94.95	98.73	94.11	94.95	94.95	94.95	94.95	96.21	94.53	95.37	93.69	100.00	97.47	97.47	96.63	97.47	97.05	97.05	96.63	94.53	97.05	96.63	95.37	96.21	94.53	97.05	96.63	97.47	95.37	94.95
CTLV-TL100	MH108975	91.31		99.57	97.05	99.57	97.89	99.57	99.57	95.37	92.01	93.69	97.05	94.53	92.43	92.01	92.01	99.57	93.69	94.11	92.85	93.69	93.27	94.53	95.79	95.79	94.11	95.37	95.37	95.37	94.11	93.69	95.37	95.79	97.89	94.11	94.53	94.11	95.37	96.63	94.53	94.95
CTLV-TL101	MH108976	91.59	99.71		97.47	100.00	98.31	100.00	100.00	95.79	92.01	94.11	97.47	94.95	92.85	92.01	92.01	100.00	94.11	94.53	93.27	94.11	93.69	94.95	95.79	95.79	94.53	95.79	95.79	95.79	94.53	93.69	95.79	96.21	98.31	94.53	94.95	94.53	94.95	97.05	94.95	95.37
CTLV-TL102	MH108977	93.27	96.63	96.91		97.47	97.05	97.47	97.47	98.31	93.27	95.37	97.05	95.79	94.11	93.27	93.27	97.47	95.37	95.79	94.53	95.37	94.11	96.21	97.05	97.05	96.63	96.63	95.79	94.95	97.05	96.63	95.79	97.05	96.21	94.95	95.37	96.21	97.89	95.79	96.21	
CTLV-TL103	MH108978	91.59	99.15	99.43	96.35		98.31	100.00	100.00	95.79	92.01	94.11	97.47	94.95	92.85	92.01	92.01	100.00	94.11	94.53	93.27	94.11	93.69	94.95	95.79	95.79	95.79	94.53	93.69	95.79	96.21	98.31	94.53	94.95	94.53	94.95	97.05	94.95	95.37			
CTLV-TL104	MH108979	91.87	96.49	96.77	95.37	96.21		98.31	98.31	95.37	92.01	94.11	99.15	94.53	92.85	92.01	92.01	98.31	94.11	94.53	93.27	94.11	94.11	95.37	96.63	96.63	94.95	96.21	96.21	96.21	94.95	93.69	96.21	96.63	100.00	95.79	95.37	94.95	95.37	97.47	95.37	95.79
CTLV-TL110	MH108980	91.59	99.15	99.43	96.35	100.00	96.21		100.00	95.79	92.01	94.11	97.47	94.95	92.85	92.01	92.01	100.00	94.11	94.53	93.27	94.11	93.69	94.95	95.79	95.79	95.79	94.53	93.69	95.79	96.21	98.31	94.53	94.95	94.53	94.95	97.05	94.95	95.37			
CTLV-TL111	MH108981	91.59	99.15	99.43	96.35	100.00	96.21	100.00		95.79	92.01	94.11	97.47	94.95	92.85	92.01	92.01	100.00	94.11	94.53	93.27	94.11	93.69	94.95	95.79	95.79	95.79	94.53	93.69	95.79	96.21	98.31	94.53	94.95	94.53	94.95	97.05	94.95	95.37			
CTLV-TL112	MH108982	92.43	91.59	91.87	94.67	91.59	92.43	91.59	91.59		92.01	94.11	95.37	92.85	92.01	92.01	95.79	94.53	95.79	95.79	93.27	95.79	95.79	94.53	95.79	95.79	95.37	95.37	94.95	96.21	94.11	94.53										
CTLV-TL113	MH108983	90.19	90.05	90.33	90.75	90.05	90.33	90.05	90.05	90.19		95.37	91.59	94.95	94.11	100.00	100.00	92.01	95.37	95.79	94.95	95.79	91.59	94.95	94.53	94.53	93.69	94.11	94.53	94.11	93.69	95.79	94.53	93.69	92.01	93.69	92.01	92.85	93.27	94.53	93.27	92.01
CTLV-TL114	MH108984	90.47	90.75	91.03	91.31	90.75	91.17	90.75	90.75	90.89	96.63		93.69	94.95	97.47	95.37	95.37	94.11	100.00	98.73	98.31	99.57	92.85	94.95	96.21	96.21	94.95	95.37	95.79	95.79	94.95	94.53	95.79	96.21	94.11	96.63	94.11	94.95	95.37	94.11	94.53	94.11
CTLV-TL115	MH108985	92.01	96.07	96.35	94.95	96.07	97.89	96.07	96.07	92.57	89.91	90.75		94.11	92.43	91.59	91.59	97.47	93.69	94.53	92.85	93.69	93.27	94.95	96.21	96.21	94.95	95.79	95.79	95.79	94.53	93.27	95.79	95.79	99.15	95.37	94.95	94.53	94.95	97.05	94.95	95.37
CTLV-MTH	KC588512	97.89	91.45	91.73	92.99	91.73	91.73	91.73	91.73	92.71	90.33	91.17	91.59		94.11	94.95	94.95	94.95	94.95	95.79	94.53	95.37	92.43	98.73	97.05	97.05	96.21	96.21	96.63	96.63	96.21	94.53	96.63	96.21	94.53	95.37	94.11	96.21	95.37	97.05	94.11	94.53
CTLV-XHC	KC588947	89.77	90.05	90.33	90.33	90.05	90.47	90.05	90.05	89.91	95.65	89.91	95.65	98.17		90.47	94.11	94.11	92.85	97.47	97.05	97.05	97.89	95.93	95.93	96.63	96.63	95.65	94.25	89.63	89.77	89.77	89.91	90.75	89.91	89.49	90.05	90.33	89.91	90.61		
CTLV-Pk	JX416228	90.19	90.05	90.33	90.75	90.05	90.33	90.05	90.05	90.19	100.00	96.63	89.91	90.33	95.65		100.00	92.01	95.37	95.79	94.95	95.79	91.59	94.95	94.53	94.53	93.69	94.11	94.53	94.11	93.69	95.79	94.53	93.69	92.01	93.69	92.01	92.85	93.27	94.53	93.27	92.01
CTLV-Ponkan8	KY706358	90.19	90.05	90.33	90.75	90.05	90.33	90.05	90.05	90.19	96.63	90.33	95.65	100.00			92.01	95.79	94.95	95.79	91.59	94.95	94.53	94.53	93.69	94.11	94.53	94.11	93.69	95.79	94.53	93.69	92.01	93.69	92.01	92.85	93.27	94.53	93.27	92.01		
CTLV-ML	EU553489	91.59	99.15	99.43	96.35	100.00	96.21	100.00	100.00	91.59	90.05	90.75	96.07	91.73	90.05	90.05	90.05		94.11	94.53	93.27	94.11	93.69	94.95	95.79	95.79	94.53	95.79	95.79	95.79	94.53	93.69	95.79	96.21	98.31	94.53	94.95	94.95	94.95	97.05	94.95	95.37
CTLV-Kumquat1	AY646511	90.47	90.75	91.03	91.31	90.75	91.17	90.75	90.75	90.89	96.63	100.00	90.75	91.17	98.17	96.63	96.63	90.75		98.73	98.31	99.57	92.85	94.95	96.21	96.21	94.95	95.37	95.79	95.79	94.95	94.53	95.37	96.21	95.37	94.11	94.95	94.11	94.11	94.53	96.63	94.53	94.11
CTLV-LCd-NA-1	FJ355920	90.33	90.47	90.75	90.75	90.47	91.45	90.47	90.47	90.33	95.93	97.47	97.33	95.93	95.93	90.47	97.47		87.89	97.47	97.47	97.47	96.63	94.95	97.47	97.47	96.63	94.95	98.31	97.47	95.37	95.37	97.47	95.37	94.11							
CTLV-Shatang Orange	JQ765412	90.33	90.33	90.61	90.89	90.33	90.75	90.33	90.33	90.47	96.21	98.45	90.33	91.03	98.31	96.21	96.21	90.33	98.45	97.61		98.73	92.01	94.53	95.79	95.79	94.53	94.95	95.37	95.37	94.53	97.05	95.79	94.95	93.27	94.95	93.69	93.69	94.11	95.79	93.69	93.27
CTLV-HJY	MH144341	90.47	91.17	91.45	91.45	91.17	91.59	91.17	91.17	90.75	96.63	99.01	91.17	98.59	96.63	96.63	91.17	99.01	91.17	98.59	98.87		92.85	95.37	96.63	96.63	95.37	96.21	97.89	96.63	94.95	94.11	94.95	94.11	94.11	94.53	96.63	94.53	94.11			
CTLV-ASGV-1-HJY	MH144342	91.17	89.49	89.77	91.17	89.77	90.61	89.77	89.77	94.11	88.65	89.21	90.19	91.31	88.51	88.65	88.65	89.77	89.21	89.21	88.79	89.35		93.69	95.37	95.37	93.69	94.53	94.11	94.53	93.69	92.43	94.95	95.37	94.11	93.69	92.85	92.85	94.53	94.95	92.43	92.85
CTLV-ASGV-2-HJY	MH144343	98.17	90.75	91.03	92.71	91.03	91.45	91.03	91.03	91.59	89.49	89.49	90.19	91.59	90.91	89.49	89.49	89.49	91.03	90.19	90.05	90.05	90.19	90.33		97.47	97.47	96.63	97.47	97.05	97.05	96.63	94.53	97.05	96.63	95.37	96.21	94.53	97.05	96.63	97.47	95.37	94.95
CTLV-L	D16681	94.67	91.59	91.87	92.99	92.01	92.85	92.01	92.01	92.85	89.77	90.61	90.05	90.19	90.47	91.03	90.61	89.77	90.61	90.33	90.47	91.31	91.03	93.97		100.00	98.31	98.31	98.73	98.73	98.31	96.21	99.57	99.15	96.63	96.63	96.21	97.05	98.31	99.15	95.79	96.63
ASGV-Li-23	AB004063	94.39	91.87	92.15	93.27	92.29	93.13	92.29	92.29	92.85	89.77	90.61	93.13	94.25	89.91	89.77	89.77	92.29	89.91	90.33	90.47	91.31	91.31	93.97	99.71		98.31	98.31	98.73	98.73	98.31	96.21	99.57	99.15	96.63	96.63	96.21	97.05	98.31	99.15	95.79	96.63
ASGV-P-209	NC001749	92.29	90.05	90.33	92.15	90.33	90.33	90.33	90.33	92.29	89.49	90.19	89.49	89.35	89.49	89.49	90.19	89.49	89.21	89.35	89.49	90.19	92.15	92.43		97.47		97.47	97.89	97.47	97.47	96.63	94.95	98.31	97.47	95.37	95.37	94.53	96.21	97.89	98.73	95.79	95.79
ASGVp12	HE978837	92.29	91.03	91.03	92.29	90.61	91.03	90.61	90.61	91.31	89.35	89.49	91.03	91.59	89.07	89.35	89.35	90.61	89.49	89.77	89.63	89.91	88.93	92.01	92.71	92.71	90.33		99.57	97.89	97.47	95.37	97.89	97.47	96.21	96.21	95.37	96.63	98.31	98.31	95.79	95.79
ASGV-AC	KX988001	92.57	90.75	90.75	92.01	90.33	91.03	90.33	90.33	91.17	89.21	89.35	91.03	92.15	88.93	89.21	89.21	91.03	89.35	89.63	89.49	89.77	89.07	92.29	93.13	93.13	90.89	98.87		98.31	97.89	95.79	98.31	97.89	96.21	96.21	95.79	96.63	97.89	98.73	95.37	96.21
ASGV-HH	JN701424	92.15	91.03	91.31	92.43	90.89	91.73	90.89	90.89	91.59	90.05	90.47	91.31	92.15	88.79	90.05	90.05	90.05	90.47	90.47	91.03	91.73	93.55	91.87	91.59	92.43			98.31	97.89	96.21	96.21	95.79	96.63	97.05	98.73	95.37	96.21				
ASGV-241KP	D14995	92.29	90.05	90.33	92.15	90.33	90.33	90.33	90.33	92.29	89.35	89.49	91.87	88.79	89.35	89.35	90.33	89.49	89.21	89.35	89.49	90.19	92.15	92.15	92.43	100.00	90.33	90.89	91.87		94.95	98.31	97.47	94.95	95.37	94.53	96.21	96.63	97.47	94.53	94.95	
ASGV-Matsuco	LC084659	90.33	90.75	91.03	91.31	90.75	91.03	90.75	90.75	90.47	96.35	97.05	90.61	91.31	96.35	96.35	96.35	90.75	97.05	96.77	96.77	97.19	89.35	89.91	90.61	90.89	89.35	89.63	89.49	89.91	89.35		96.21	95.37	93.69	94.11	94.53	94.11	94.95	96.21	94.11	93.69
ASGV-FKSS2	LC143387	94.39	92.01	92.29	93.69	92.15	93.27	92.15	92.15	92.85	90.47	91.31	90.75	90.89	91.17	91.59	93.41	98.03	77.75	92.85	93.27	93.41	92.15	91.31	98.31		96.21	96.63	95.79	96.63	97.89	98.73	95.79	96.21								
ASGV-N297	LC184610	93.69	91.87	92.15	93.27	92.01	93.13	92.01	92.01	92.71	89.91	90.47	90.19	90.33	90.61	92.01	93.27	97.61	97.89	91.73	92.01	92.71	92.71	91.73	90.75	97.89		96.63	95.79	95.37	97.05	97.47	98.31	94.95	95.79							
ASGV-Kiyomi	LC184611	92.15	96.77	97.05	95.37	96.49	98.59	96.49	96.49	92.43	90.33	91.45	90.05	91.17	90.75	91.59	90.61	91.73	90.33	90.75	91.45	91.45	91.73	90.33	90.75		95.79	95.37	94.95	95.37	97.47	97.47	95.37	95.79								
ASGV-Nagami	LC184612	94.39	90.05	90.33	92.15	90.33	91.59	90.33	90.33	92.57	89.35	89.35	90.33	90.47	91.03	90.61	90.75	91.87	93.41	93.13	93.13	91.45	90.61	91.31	91.59	91.45	89.21	92.85	92.99	91.87		94.11	95.37	95.37	97.05	94.53	94.53					
ASGV-kfp	KR106996	91.31	90.75	91.03	90.89	91.17	91.17	91.17	91.17	90.61	88.65	89.77	91.87	91.45	89.49	88.65	88.65	91.17	89.77	89.77	90.05	90.19	89.49	90.19	91.17	91.45	90.05	89.49	90.05	90.33	90.05	89.91	91.45	91.03	91.73	91.31		94.95	94.53	97.05	94.53	97.05
ASGV-Ac	JX080201	92.57	90.89	91.17	92.15	91.03	91.87	91.03	91.03	91.03	89.91	90.75	92.85	90.33	90.33	90.75	91.45	91.03	90.75	90.33	93.41	90.33	92.01	92.15	91.73	90.33	93.83	93.41	91.87	91.87	92.01		95.79	97.05	94.95	94.95						
ASGV-CHN	JQ308181	91.87	90.75	90.75	91.59	90.61	90.89	90.61	90.61	91.03	89.91	90.05	90.47	91.45	89.77	89.91	89.91	90.61	92.99	92.99	91.87	91.17	91.45	95.79	91.87	89.91	92.85	92.15	90.89	91.45	89.77	91.45		97.47	94.95	94.95						
ASGV-YTG	KJ579253	93.13	92.01	92.29	93.69	91.87	92.85	91.87	91.87	93.55	91.03	91.31	92.43	93.97	90.33	91.03	91.03	91.87	91.31	91.73	91.73	91.59	92.99	93.69	92.85	92.99	93.27	96.07	92.85	91.45	93.83	93.13	92.57	92.99	91.31	92.71	94.95		96.63	97.47		
ASGV-HT	KU947036	92.99	91.59	91.59	92.57	91.17	92.43	91.17	91.17	91.45	90.05	91.31	91.73	93.13	90.61	90.05	90.05	91.17	91.31	91.03	91.17	91.45	90.05	92.85	92.99	92.99	90.19	92.43	92.71	91.45	90.19	91.45	92.71	92.15	91.87	92.15	91.87	90.75	93.27			94.11
PBNLSV	AY596172	91.87	90.61	90.89	92.15	90.75	92.15	90.75	90.75	91.45	89.07	89.63	91.31	91.59	88.93	89.07	89.07	90.75	89.63	89.63	89.49	89.77	89.63	91.59	94.11	94.11	90.19	90.61	91.17	91.87	90.19	89.63	94.67	93.97	91.73	90.75	92.71	92.57	91.03	93.13	91.17	

CTLV: citrus tatter leaf virus; ASGV: apple stem grooving virus; PBNLSV: pear black necrotic leaf spot virus.

Table 1.14 Nucleotide (below diagonal) and amino acid (above diagonal) sequence identities (%) of polyprotein (PP).

Isolate	Genbank Accession No.	CTLV-IPPN122	CTLV-TL100	CTLV-TL101	CTLV-TL102	CTLV-TL103	CTLV-TL104	CTLV-TL110	CTLV-TL111	CTLV-TL112	CTLV-TL113	CTLV-TL114	CTLV-TL115	CTLV-MTH	CTLV-XHC	CTLV-Pk	CTLV-Ponkan8	CTLV-ML	CTLV-Kumquat1	CTLV-LCd-NA-1	CTLV-Shatang Orange	CTLV-HJY	CTLV-ASGV-1-HJY	CTLV-ASGV-2-HJY	CTLV-L	ASGV-Li-23	ASGV-P-209	ASGVp12	ASGV-AC	ASGV-HH	ASGV-241KP	ASGV-Matsuco	ASGV-FKSS2	ASGV-N297	ASGV-Kiyomi	ASGV-Nagami	ASGV-kfp	ASGV-Ac	ASGV-CHN	ASGV-YTG	ASGV-HT	PBNLSV
CTLV-IPPN122	MH108986		86.24	86.34	86.29	86.13	86.83	86.13	86.13	86.02	86.13	86.34	86.18	89.40	84.95	86.08	86.08	86.13	85.81	85.97	85.65	85.76	86.88	90.73	86.08	85.76	89.66	82.55	85.59	87.68	89.66	85.81	87.52	87.04	86.24	89.77	83.46	86.67	86.88	87.09	84.47	84.20
CTLV-TL100	MH108975	80.62		99.25	98.92	98.66	94.27	98.66	98.66	87.04	86.34	86.40	93.73	86.24	85.81	86.40	86.40	98.66	86.45	86.99	86.24	86.61	87.20	86.18	85.49	85.27	86.40	83.62	86.40	86.40	86.40	86.72	86.61	86.93	94.00	86.99	84.00	86.13	85.43	85.86	83.88	84.36
CTLV-TL101	MH108976	80.71	98.89		99.25	98.98	94.43	98.98	98.98	86.88	86.34	86.50	93.79	86.13	85.70	86.40	86.40	98.98	86.50	86.83	86.24	86.45	87.20	86.13	85.38	85.11	86.18	83.57	86.24	86.34	86.18	86.61	86.40	86.77	94.16	86.93	83.95	86.02	85.38	85.70	83.88	84.20
CTLV-TL102	MH108977	80.67	98.60	98.85		98.55	94.21	98.55	98.55	86.56	85.97	86.34	93.68	85.86	85.49	86.02	86.02	98.55	86.40	86.50	86.08	86.34	87.20	86.25	85.33	85.06	86.13	83.46	86.13	86.29	86.13	86.29	86.34	86.50	93.95	86.88	83.79	85.86	85.33	85.70	83.72	84.15
CTLV-TL103	MH108978	80.67	98.41	98.62	98.26		94.27	100.00	100.00	86.72	86.24	86.29	93.73	85.97	85.65	86.29	86.29	100.00	86.34	86.67	86.18	86.40	86.77	86.08	85.38	85.01	86.24	83.41	86.08	86.02	86.24	86.67	86.34	86.56	94.11	87.09	83.68	85.92	85.06	85.49	83.77	84.04
CTLV-TL104	MH108979	80.38	92.02	92.32	92.09	91.97		94.27	94.27	86.18	86.24	86.24	97.05	86.61	85.27	86.29	86.29	94.27	86.13	86.13	85.92	86.24	87.68	86.67	85.22	84.74	86.61	83.57	86.24	86.08	86.61	86.29	86.83	86.72	97.37	87.36	84.16	86.13	86.18	85.81	83.99	84.10
CTLV-TL110	MH108980	80.67	98.41	98.62	98.26	100.00	91.97		100.00	86.72	86.24	86.29	93.73	85.97	85.65	86.29	86.29	100.00	86.34	86.67	86.18	86.40	86.77	86.08	85.38	85.01	86.24	83.41	86.08	86.02	86.24	86.67	86.34	86.56	94.11	87.09	83.68	85.92	85.06	85.49	83.77	84.04
CTLV-TL111	MH108981	80.67	98.41	98.62	98.26	100.00	91.97	100.00		86.72	86.24	86.29	93.73	85.97	85.65	86.29	86.29	100.00	86.34	86.67	86.18	86.40	86.77	86.08	85.38	85.01	86.24	83.41	86.08	86.02	86.24	86.67	86.34	86.56	94.11	87.09	83.68	85.92	85.06	85.49	83.77	84.04
CTLV-TL112	MH108982	79.69	80.65	80.56	80.44	80.56	80.29	80.56	80.56		95.93	95.44	86.13	86.18	95.61	95.77	95.77	86.72	96.14	99.94	96.57	96.46	85.65	86.13	85.22	84.85	86.93	84.64	87.36	85.65	86.93	96.09	86.02	85.92	86.18	87.15	83.73	86.29	84.79	86.18	84.26	84.42
CTLV-TL113	MH108983	79.55	80.76	80.69	80.62	80.65	80.69	80.65	80.65	94.09		96.84	86.13	86.50	94.59	99.83	99.83	86.24	95.02	95.87	95.34	95.23	85.86	86.29	86.13	85.06	86.83	84.75	87.31	86.08	86.83	96.52	86.40	86.34	85.86	86.93	84.38	85.92	85.54	86.29	84.10	84.36
CTLV-TL114	MH108984	79.90	80.65	80.65	80.54	80.54	80.96	80.54	80.54	92.80	96.25		86.40	86.77	96.25	96.68	96.68	86.29	97.43	95.39	97.00	96.41	86.34	86.45	85.70	85.22	87.41	84.97	87.47	85.81	87.41	95.28	86.45	86.50	86.13	87.20	84.27	86.34	85.17	86.29	83.72	84.95
CTLV-TL115	MH108985	80.13	91.59	91.70	91.55	91.39	95.37	91.39	91.39	80.29	80.71	81.08		86.67	85.76	86.18	86.18	93.73	86.45	86.08	86.29	86.56	87.47	86.08	85.43	84.79	86.56	83.78	86.29	86.02	86.56	86.50	86.61	86.50	98.87	87.31	84.32	85.43	86.02	85.49	83.77	84.10
CTLV-MTH	KC588948	85.01	80.65	80.58	80.44	80.53	80.88	80.53	80.53	80.58	80.54	81.06	80.79		85.76	86.56	86.56	85.97	86.13	86.13	86.24	86.50	86.77	92.29	86.72	86.29	83.68	83.19	86.02	88.54	93.68	86.50	88.22	88.11	86.50	94.11	84.11	86.72	88.75	87.63	83.94	83.88
CTLV-XHC	KC588947	79.24	80.44	79.99	79.99	80.06	79.99	80.06	80.06	94.84	93.20	94.27	80.28	80.31		94.53	85.65	87.21	95.55	97.75	97.26	85.49	86.40	84.27	86.83	84.85	86.40	94.80	85.33	85.43	85.49	86.08	83.30	85.38	83.88	85.43	82.76	84.31				
CTLV-Pk	JX416228	79.47	80.63	80.56	80.49	80.53	80.63	80.53	80.53	93.54	99.37	96.09	80.69	80.62	93.29		100.00	86.29	94.96	95.71	95.28	95.18	85.81	86.18	85.97	85.49	86.77	84.59	87.15	85.97	86.77	96.46	86.24	86.18	85.92	86.88	84.38	85.81	85.59	86.24	84.20	84.42
CTLV-Ponkan8	KY706358	79.47	80.63	80.56	80.49	80.53	80.63	80.53	80.53	93.54	99.37	96.09	80.69	80.62	93.29	100.00		86.29	94.96	95.71	95.28	95.18	85.81	86.18	85.97	85.49	86.77	84.59	87.15	85.97	86.77	96.46	86.24	86.18	85.92	86.88	84.38	85.81	85.59	86.24	84.20	84.42
CTLV-ML	EU553489	80.67	98.41	98.62	98.26	100.00	91.97	100.00	100.00	80.56	80.65	80.54	91.39	80.53	80.06	80.53	80.53		86.34	86.67	86.18	86.40	86.77	86.08	85.38	85.01	86.24	83.41	86.08	86.02	86.24	86.67	86.34	86.56	94.11	87.09	83.68	85.92	85.06	85.49	83.77	84.04
CTLV-Kumquat1	AY646511	79.74	80.53	80.51	80.53	80.49	80.47	80.49	80.49	94.71	93.41	94.84	80.72	80.81	97.50	93.50	93.50	80.49		96.09	98.28	97.37	85.54	85.81	85.59	85.22	86.99	84.54	87.15	85.43	86.99	94.91	86.24	86.02	86.18	86.56	83.73	86.13	84.58	86.02	83.29	84.52
CTLV-LCd-NA-1	FJ355920	79.62	80.65	80.56	80.44	80.56	80.26	80.56	80.56	99.85	94.16	92.80	80.29	80.44	94.84	93.54	93.54	80.56	96.09		96.52	96.41	85.59	86.05	85.57	84.79	86.88	96.03	85.97	85.86	86.13	87.59	85.86	86.24	84.74	86.13	84.04					
CTLV-Shatang Orange	JQ765412	79.81	80.29	80.24	80.26	80.33	80.19	80.33	80.33	94.98	93.70	94.68	80.47	80.74	97.93	93.71	93.71	80.33	97.91	94.98		98.01	85.54	85.54	85.43	85.01	86.93	84.54	86.99	85.49	86.93	95.55	86.02	85.92	86.02	86.67	83.68	86.34	84.63	85.92	83.40	84.58
CTLV-HJY	MH144341	79.67	80.53	80.40	80.47	80.54	80.28	80.54	80.54	94.45	93.30	94.11	80.51	80.67	96.98	93.39	93.39	80.54	96.93	94.48	97.32		85.70	85.86	85.33	84.95	87.15	84.59	87.04	85.49	87.15	95.50	86.18	86.02	86.29	86.88	84.27	86.56	84.90	85.81	83.77	84.79
CTLV-ASGV-1-HJY	MH144342	80.74	80.58	80.53	80.51	80.44	81.42	80.44	80.44	79.37	79.47	79.87	81.12	80.67	79.28	79.49	79.49	80.44	79.72	79.42	79.49		87.04	86.43	85.11	86.99	85.76	86.29	87.52	87.36	85.81	86.24	84.20	85.01								
CTLV-ASGV-2-HJY	MH144343	85.47	79.99	79.80	79.94	79.80	80.31	79.80	79.80	80.17	80.19	80.49	79.96	89.82	79.69	80.19	80.19	79.80	80.21	80.03	79.94	80.08	80.83		86.77	86.50	93.68	83.09	86.18	89.29	93.68	86.02	88.49	88.27	86.13	94.27	84.11	86.50	89.02	88.06	84.15	84.90
CTLV-L	D16681	81.56	79.65	79.58	79.63	79.69	79.49	79.69	79.69	79.69	79.96	79.90	79.65	81.56	79.30	80.04	80.04	79.69	79.76	79.65	79.53	79.46	80.35	81.26		97.80	87.25	82.66	85.43	88.06	87.25	85.27	95.07	94.75	85.38	86.72	82.92	84.79	87.15	85.38	83.56	82.76
ASGV-Li-23	AB004063	81.53	79.55	79.47	79.53	79.55	79.38	79.55	79.55	79.71	79.92	79.85	79.40	81.37	79.24	80.01	80.01	79.55	79.65	79.67	79.49	79.44	80.22	81.33	98.30		84.05	86.88	89.93	100.00	86.99	88.97	88.75	86.40	84.86	83.89	86.67	89.82	87.90	84.31	84.74	
ASGV-P-209	NC001749	84.92	80.49	80.22	80.31	80.22	80.33	80.22	80.22	80.33	80.17	80.54	80.46	90.75	79.92	80.26	80.26	80.22	80.47	80.22	80.24	80.46	81.08	92.27	81.37	81.31		84.05	86.88	89.93	100.00	86.99	88.97	88.75	86.40	84.86	83.89	86.67	89.82	87.90	84.31	84.74
ASGVp12	HE978837	79.56	80.05	80.08	79.85	79.96	80.01	79.96	79.96	80.30	80.30	80.56	79.90	79.71	80.08	80.15	80.15	79.96	80.15	80.22	80.12	80.19	80.44	79.13	78.81	78.86	80.12		95.06	83.52	84.05	84.75	83.41	83.89	83.73	83.41	83.62	81.91	83.09			
ASGV-AC	KX988001	80.28	80.54	80.54	80.38	80.38	80.56	80.38	80.38	80.69	80.54	80.56	80.44	80.28	80.44	80.40	80.40	80.38	80.40	80.40	80.65	80.37	80.29	81.44	80.24	79.71	79.69	81.13		97.08	86.34	86.88	87.25	86.08	86.77	86.50	86.24	84.70	86.18	85.65	86.56	85.01
ASGV-HH	JN701424	83.17	79.71	79.71	79.56	79.53	79.74	79.53	79.53	79.96	80.51	80.29	79.46	85.40	79.44	80.46	80.46	79.53	79.96	79.83	80.08	79.88	80.33	86.34	82.44	82.42	86.18	79.33	80.04		89.93	85.54	89.29	89.29	86.08	89.56	83.68	85.22	93.09	87.15	83.83	83.51
ASGV-241KP	D14995	84.92	80.49	80.22	80.31	80.22	80.33	80.22	80.22	80.33	80.17	80.54	80.46	90.75	79.92	80.26	80.26	80.22	80.47	80.22	80.24	80.46	81.08	92.27	81.37	81.31	100.00	80.12	81.13	86.18		86.99	88.97	88.75	86.40	84.86	83.89	86.67	89.82	87.90	84.31	84.74
ASGV-Matsuco	LC084659	79.46	80.44	80.38	80.29	80.44	80.24	80.44	80.44	93.77	94.75	93.36	80.51	80.97	93.68	94.84	94.84	80.44	93.62	93.77	94.02	93.66	79.19	79.99	79.69	79.65	80.35	80.03	80.17	80.10	80.35		85.86	86.13	86.24	86.83	84.16	85.86	84.90	86.08	83.83	84.36
ASGV-FKSS2	LC143387	82.17	80.12	79.94	80.06	79.97	80.31	79.97	79.97	80.06	80.13	80.26	80.21	82.40	79.46	80.12	80.12	79.97	79.94	79.99	79.74	79.65	80.62	82.19	94.36	94.18	81.87	79.51	80.31	83.35	81.87	80.04		96.14	86.67	88.27	83.57	85.92	88.27	86.72	84.10	83.67
ASGV-N297	LC184610	81.58	80.19	79.87	79.99	79.94	80.06	79.94	79.94	79.88	79.96	80.13	79.88	82.36	79.49	80.04	80.04	79.94	79.96	79.81	79.78	79.55	80.65	82.01	93.66	93.39	81.72	79.56	80.44	82.90	81.72	80.04	94.78		86.40	88.49	84.22	86.02	88.22	86.50	84.04	84.15
ASGV-Kiyomi	LC184611	80.24	91.86	92.04	91.86	91.73	95.52	91.73	91.73	80.28	80.58	80.92	98.64	80.85	80.28	80.60	80.60	91.73	80.69	80.24	80.44	80.44	81.17	80.03	79.65	79.40	80.51	80.06	80.74	79.60	80.51	80.47	80.24	79.99		87.15	84.00	85.38	85.97	85.54	83.45	83.94
ASGV-Nagami	LC184612	85.26	81.01	80.85	80.88	80.92	80.97	80.92	80.92	80.92	80.92	80.92	98.82	80.92	80.45	80.92	80.92	80.92	80.87	80.85	80.87	80.83	81.26	81.28	93.12	79.88	92.13	82.11	80.78	84.22	87.20	89.23	87.94	83.89	88.75		86.40	84.89	86.67	89.82	87.90	84.74
ASGV-kfp	KR106996	77.86	77.83	77.88	77.72	77.77	77.90	77.77	77.77	78.33	78.35	78.53	77.84	78.08	78.26	78.56	78.56	77.77	78.38	78.29	78.40	78.58	78.72	78.19	77.63	77.58	77.88	77.45	78.31	77.83	77.88	78.56	77.99	78.15	77.74	78.38		83.89	83.19	83.79	82.76	84.32
ASGV-Ac	JX080201	80.44	80.03	79.85	79.78	79.96	80.29	79.96	79.96	80.96	80.88	81.15	80.03	79.92	80.67	80.81	80.81	79.96	80.78	80.99	80.83	81.01	80.74	80.15	79.65	79.47	80.31	80.08	80.60	79.51	80.31	80.74	80.21	80.13	79.92	80.53	77.34		85.17	86.13	82.76	84.47
ASGV-CHN	JQ308181	82.31	80.10	80.03	80.12	80.10	80.38	80.10	80.10	79.94	80.10	79.88	80.13	80.10	79.70	80.10	80.10	80.10	80.10	79.85	79.83	79.69	79.97	85.09	81.47	81.37	85.36	79.13	79.80	89.70	85.36	79.90	81.94	81.81	79.92	86.04	78.38	85.81		83.56	83.19	
ASGV-YTG	KJ579253	83.01	80.49	80.44	80.46	80.40	79.92	80.40	80.40	80.42	80.79	80.71	79.76	85.42	80.31	80.88	80.88	80.40	80.88	80.42	80.71	80.60	81.01	85.08	81.22	80.92	85.65	80.24	80.76	82.60	85.65	80.94	81.54	81.19	79.81	86.08	78.10	80.22	81.35		84.52	85.01
ASGV-HT	KU947036	77.46	78.24	78.12	78.15	78.15	77.71	78.15	78.15	77.64	77.64	78.06	77.85	77.83	77.37	77.73	77.73	78.15	77.62	77.65	77.69	77.56	77.26	77.23	77.03	76.90	77.62	77.16	77.87	77.67	77.62	77.56	77.42	77.30	77.76	77.65	77.52	77.26	77.28	79.26		83.02
PBNLSV	AY596172	78.10	77.78	77.80	77.81	77.58	78.21	77.58	77.58	77.15	77.15	77.62	77.65	77.87	77.05	77.26	77.26	77.58	77.21	77.10	77.15	77.62	77.55	77.90	78.24	78.24	77.94	78.01	78.17	77.80	77.94	77.58	78.37	78.44	77.46	77.96	77.00	78.40	77.98	78.21	76.71	

CTLV: citrus tatter leaf virus; ASGV: apple stem grooving virus; PBNLSV: pear black necrotic leaf spot virus.

CHAPTER 2: Citrus vein enation virus Full Genome Characterization and Development of a Detection Assay

Abstract

Citrus vein enation virus (CVEV) belongs to the genus *Enamovirus* in the family of *Luteoviridae* and is a relatively newly characterized citrus virus. Several CVEV isolates had been sequenced from different geographic locations including Spain, China, Japan and Korea. However, very little is known about its genomic diversity and how such diversity among different isolates may influence virus detection assays by PCR. In this study, full-length genome sequences of 10 CVEV isolates from different citrus growing areas, United States of America (USA) and Australia, maintained for the past 50 years at the Citrus Clonal Protection Program (CCPP, University of California, Riverside), were characterized using next generation sequencing. High genomic identities were observed among isolates from different geographic locations. Phylogenetic analysis highlighted that isolates from Spain, Japan and Korea have close evolutionary relationship while isolates from USA and Australia were well supported in another clade. In addition, a China isolate was found to have its own niche during evolution. Furthermore, a reverse transcription quantitative polymerase chain reaction (RT-qPCR) assay was designed at the most conserved area by genome-wise analysis and developed through a systemic approach as presented in chapter 1 which benefit the high value germplasm and certification programs.

Introduction

Citrus vein enation disease was first reported by Wallace and Drake in California, USA (Wallace and Drake 1953). The symptoms were described as vein swelling and small papillae grew from veins in leaf underside of sour orange (*Citrus aurantium* L.), Mexican lime (*C. aurantifolia* (Christm.) Swing.) and other reactive species (Wallace and Drake 1953; Wallace and Drake 1959, 1961). And nearly all citrus species are susceptible to vein enation (Wallace and Drake 1959). It was also found that vein enation disease results in the formation of tumor-like woody galls on certain varieties of citrus including Rough lemon (*C. limon* (L.) Burm. f.) and sour lime (*C. aurantifolia* (Christm.) Swing.) (Fraser 1958; Wallace and Drake 1960, 1961). Both disease symptoms have been observed in many citrus growing areas including Australia, Brazil, China, Japan, India, Peru, Chile, South Africa, Egypt, Spain, Turkey and USA (Azeri and Heper 1972; Bazan de Segura and Ferrand 1969; Chen et al. 1992; Fraser 1958; Jacomino and Salibe 1993; Manjunath 1987; McClean 1954; Sheta et al. 2002; Tanaka and Yamada 1961; Vives et al. 2013; Wallace and Drake 1953). This disease was proved to be graft-transmissible and can be also transmitted by several aphid species including *Toxoptera citricida*, *Myzus persicae* and *Aphis gossypii* (Laird and Weathers 1961; Wallace and Drake 1959, 1960). Thus, the causal agent was assumed to be a new virus. And later, it showed that both vein enation and woody gall diseases were induced by same viral pathogen named as citrus vein enation virus (CVEV) (Wallace and Drake 1960, 1961) and it has been categorized as a quarantine pathogen within the European Union (Vives et al. 2013).

CVEV is a single-stranded RNA virus that belongs to genus *Enamovirus*, family *Luteoviridae* (Vives et al. 2013). Genome size of CVEV is 5,983 nucleotides (nt) and it has five open reading frames (ORFs) in its positive-sense strand along with untranslated regions (UTR) of 207 and 198 nt at the 5' and 3' termini, respectively. After the original virus description in 2013 by Vives et al., CVEV genome sequences have been reported by several research groups from China (Huang et al. 2015; Wu et al. 2019), Japan (Nakazono-Nagaoka et al. 2017) and Korea (Yang et al. 2019).

Bioindicators for indexing of CVEV such as Mexican lime and sour orange display symptoms of small papillae or projections in the leaf underside and the corresponding indentations on the upper leaf at scattered locations on the veins (Vives et al. 2013; Wallace and Drake 1960). However, the bioindicator indexing takes long time (2 to 6 months) and require well-defined greenhouse conditions and well-trained personnel to identify the symptoms (Roistacher 1991; Vives et al. 2013). Thus, biological indexing of this disease can be slow and expensive and cannot be used for a large number of samples (Vives et al. 2013). Enzyme-linked immunosorbent assay (ELISA), dot-blot hybridization and conventional RT-PCR tests have been developed for the detection of CVEV (Clark and da Graça 2000; Vives et al. 2013). However, these assays were developed based on limited genomic information which the first full-length sequence published by Vives et al. in 2013. Today, a total of 11 full-genome sequences are available in the GenBank (Nakazono-Nagaoka et al. 2017; Vives et al. 2013; Wu et al. 2019; Yang et al. 2019). Due to the limited number of CVEV full-genome sequences, very little is known about the genomic diversity and how such diversity may influence virus detection.

Next generation sequencing (NGS) technologies combined with bioinformatics have proven to be powerful tools for the assembly of full-genome viral sequences (Kehoe et al. 2014; Radford et al. 2012; Villamor et al. 2019). In addition, well-defined guidelines for the design and validation of qualitative real-time qPCR methods (Broeders et al. 2014; Bustin et al. 2009) in compilation with the approach developed in the previous chapter (chapter 1), a real-time RT-qPCR detection assay can be designed and validated efficiently for CVEV. Therefore, the purpose of this study is to characterize genomic and phylogenetic relationship of CVEV and further develop a robust and high-throughput CVEV RT-qPCR detection assay through the systematic analysis of newly generated full-length genome data from multiple virus isolates maintained for the past 50 years at the CCPP, UC Riverside. And the RT-qPCR assay can serve citrus germplasm and certification programs to distribute pathogen-tested propagative materials in a timely manner.

Materials and Methods

Virus isolates and RNA extraction for full-length genome sequencing.

Ten CVEV isolates from various citrus varieties introductions, originating from different citrus growing regions, were intercepted and maintained *in planta* under quarantine at the CCPP disease collection between 1973 and 2013 (Table 2.1). Sweet orange (*Citrus sinensis* (L.) Osbeck) seedlings were graft-inoculated with the different CVEV isolates and total RNA was extracted from phloem-rich bark tissues of the last

matured vegetative flush (i.e. one-year-old budwood) using TRIzol® reagent (Invitrogen, Carlsbad, California, USA) per manufacturer's instructions. The purity, integrity, and concentration of the RNA were tested using a NanoPhotometer™ (Implen, Germany) and Agilent 2100 Bioanalyzer (Agilent Technologies, Santa Clara, California, USA) per manufacturer's instructions.

NGS library preparation and bioinformatics.

CVEV RNA libraries were constructed using 4μg of total RNA with TruSeq Stranded mRNA Library Prep Kit (Illumina, San Diego, California, U.S.A.) per manufacturer's instructions. The RNA libraries were sequenced on an Illumina HiSeq 2500 instrument with high-output mode and single-end 50 or 100 base pairs (bp) at SeqMatic LLC (Fremont, California, USA). All sequencing data was generated by SeqMatic using an Illumina Genome Analyzer IIx and filtered through the default parameters of the Illumina QC pipeline and demultiplexed. The files were uploaded onto the VirFind bioinformatics server and mapped to the reference genome by Bowtie 2, followed by outputting mapped and unmapped contig sequences (Ho and Tzanetakis 2014). Unmapped sequences were *de novo* assembled by Trinity (Ho and Tzanetakis 2014). Assembled contigs were analyzed through BLASTn with an E-value cutoff of 10^{-2} against all virus sequences in GenBank and generated outputs of reads and report for virus sequences.

Rapid amplification of cDNA ends (RACEs) of genomic viral RNA.

The 5' and 3' end sequences were obtained via rapid amplification of cDNA ends (RACEs) and cloned for further sequencing at Molecular Cloning Laboratories (MCLAB, South San Francisco, California, USA). The contigs containing CTLV sequences from NGS along with RACE sequence data were then analyzed and assembled as consensus full-length genomes, using Vector NTI Advance™11 software (Thermo Fisher Scientific, Carlsbad, California, USA).

Phylogenetic and genomic identity analysis of full-length virus sequences.

Phylogenetic analysis was performed using the Molecular Evolutionary Genetics Analysis tool (MEGA v. 7.0.21) (Tamura et al. 2013). ClustalW was used to align the 10 newly generated CVEV full-length cDNA sequences along with 11 full genome sequences of CVEV and one pea enation mosaic virus 1 (PEMV-1, Enamovirus) available in the GenBank (Table 2.2). Phylogenetic topologies were reconstructed using three different methods: neighbor-joining, maximum likelihood and minimum evolution and tested with 1,000 bootstrap replicates. All phylogenetic methods gave similar results and the neighbor-joining tree was presented in this study. Nucleotide (nt) percentage differences were calculated for sequence identities of CVEV complete or specific areas of the genome using the pairwise sequence identity and similarity in a web-based analyzing program (http://imed.med.ucm.es/Tools/sias.html).

Citrus sample processing and RNA extraction for RT-qPCR detection of CVEV.

To account for the possible uneven distribution of the virus within a plant, budwood samples from four to six different branches around the tree canopy were randomly collected and combined into a single sample. Samples from the citrus trees' phloem-rich bark of matured budwood (approximately 12 to 18 months old) were collected and processed by freeze-drying and grinding as described by Osman et al. 2017. Total RNA was extracted from the ground sample using MagMAX™ Express-96 (Thermo Fisher Scientific, Carlsbad, California, USA) using a modified 5X MagMax™-96 Viral RNA Isolation Kit optimized for citrus tissues (Osman et al. 2017). Total RNA was eluted in 100 µl elution buffer and used as template for RT-qPCR.

RT-qPCR assay design and validation.

For the specific detection of the virus in citrus tissues an RT-qPCR assay was designed based on sequence conservation alignment of a total 21 full genome sequences of CVEV: 10 in house sequences generated in this study and 11 sequences from GenBank (Figure 2.1). Primers and probe were designed using the Primer Express™ software (Thermo Fisher Scientific, Carlsbad, California, USA) and following the guidelines for designing RT-qPCR assays a 60 °C optimum melting temperature for primers and a 10 °C increase for qPCR probes was used to prevent the formation of primer dimers (Table 2.3).

The fluorophore used for the CVEV probe was 6-carboxyfluorescein VIC and the 3'
quencher was Black Hole Quencher (BHQ). The homology of the primers and qPCR probe
was confirmed by a BLASTn search against the GenBank database.

The RT-qPCR reaction (12 µl total volume) was performed using the AgPath-ID^{TM}
One-Step RT-PCR Kit (Thermo Fisher Scientific, Carlsbad, California, USA) with 2.65
µL water, 6.25 µL 2X RT buffer, 0.6 µL primer probe mix (417 nM for primers and 83 nM
for probe as final concentrations), 0.5 µL 25X RT mix and 2 µL of RNA for each reaction.
The cycling conditions were 45 °C for 10 minutes, 95 °C for 10 minutes during the first
cycle, followed by 40 cycles of 95 °C for 15 seconds and 60 °C for 45 seconds. All samples
were analyzed using a Applied Biosystems™ 7900HT Fast Real-Time PCR System and
Applied Biosystems™ QuantStudio 12K Flex Real-Time PCR System (Thermo Fisher
Scientific, Carlsbad, California, USA). Fluorescent signals were collected during the
amplification cycle and the quantitative cycle (Cq) was calculated and exported with a
threshold of 0.2 and a baseline of 3 - 15 for the targets of interest. The Cq was calculated
by the qPCR machine using an algorithm with a set range of cycles at which the first
detectable significant increase in fluorescence occurs. Sample quality was assessed using
the COX qPCR assay where the internal control is the citrus cytochrome oxidase (COX)
gene (Osman et al. 2015).

RT-qPCR assay validation.

The newly designed CVEV RT-qPCR assay was validated using applicable parameters proposed in the "Guidelines for validation of qualitative real-time PCR methods" (Broeders et al. 2014) as well as the approach for the design and validation of molecular virus detection assays developed in the previous chapter (chapter 1). Applicability, practicability and transferability were evaluated by deploying the assay at two different laboratories, University of California (UC) Riverside- CCPP and UC Davis-Real-Time PCR Research & Diagnostic Core Facility. The robustness of the assay was evaluated with deviation in annealing temperatures (± 2 °C), reaction volumes (± 2 μL), and different qPCR instruments (CFX96 Real-Time PCR Detection System, Bio-Rad, Hercules, California, USA), and master mixes (iTaq™ Universal Probes One-Step Kit, Bio-Rad, Hercules, California, USA).

The specificity of the assay was evaluated both *in silico* and experimentally, using a variety of citrus samples with known CVEV infection status from different geographical origins and isolation times. All virus isolates exotic to California were received as nucleic acids under the auspices of the USDA APHIS-PPQ permits P526P-19-02049 and P526P-19-02050. Cross-reactivity was assessed using RNA of different non-inoculated citrus species and varieties and RNA from citrus inoculated with other non-targeted graft-transmissible pathogens of citrus.

The sensitivity (absolute limit of detection, LOD_6) and quantification of the amount of CVEV in samples was calculated by generating an absolute standard curve to determine

the starting number of copies. More specifically, amplicon of CVEV was obtained from the primer set (Table 2.3) and cloned into a plasmid (Eurofins MWG Operon, Huntsville, Alabama, USA). The extracted plasmid DNA was linearized using *Hind*III enzyme, to increase the efficiency of dilutions. Serial 10-fold dilution of plasmids carrying a known copy number of CVEV inserts were made to construct a DNA standard curve. The standard curves for CVEV were run in singleplex RT-qPCR setting utilizing 6-carboxyfluorescein VIC fluorophores. Reactions were performed in triplicate to establish the linear response between the Cq values and the log of known copy numbers. The copy numbers for each sample were calculated as previously described (Leutenegger 2001). The slope of the standard curve and the coefficient of determination (R^2) were calculated using linear regression (Rasmussen 2001). Amplification efficiency (E) was calculated with the formula $E = 10^{(-1/\text{slope})} - 1$ (Pfaffl 2004; Svec et al. 2015).

Based on the principal that a well performing diagnostic test correctly identifies the diseased individuals in a population, a series of statistical measurements, as reviewed by Bewick et al. (2004), were used to confirm the performance of the CVEV RT-qPCR detection assays. An assay is performing well when sensitivity (Sn) = true positives / (true positives + false negatives) and specificity (Sp) = true negatives / (true negatives + false positives) approach 100%. High positive likelihood ratio (LR^+) = sensitivity / (1-specificity) and low (close to zero) negative likelihood ratio (LR^-) = (1-sensitivity) / specificity also indicate a well performing diagnostic test. Finally, Youden's index (J) = sensitivity + specificity – 1, can attain the maximum value of 1, when the diagnostic test is

perfect and the minimum value of zero, when the test has no diagnostic value (Bewick et al. 2004).

Results

Full-length sequence of 10 CVEV isolates and genomic identity analysis.

Full-length viral genome sequences of 10 CVEV isolates were obtained by RNA-Seq and covered 51.8% to 96.0% of the viral genome. Primer walking sequencing and RACEs methods were used to identify the nucleotide gaps and obtain the genome sequences of CVEV. The full-length cDNA sequences were deposited in GenBank under the accession numbers MN187035 to MN187044 (Table 2.1). The genome size of 10 CVEV complete sequences identified in this study ranged from 5,982 to 5,983 nt with 5'-UTR range from 206 to 207 nt and 198 nt for 3'-UTR. The viral genome structure of CVEV is similar to other enamoviruses with five open reading frames (ORFs; Figure 2.2).

Among the 10 CVEV complete sequences in this study and 11 available from GenBank, the genomic identity analysis showed that CVEV full-length nucleotide sequences possessed 96.92 to 99.88% identities while two sequences of VE-1 were identical (NC_021564 and HF679486) (Table 2.2). In contrast, PEMV-1, another specie of genus *Enamovirus*, showed lower identities (52.50 to 52.85%) (Table 2.2) when compared to CVEV sequences.

The sequence of ORF0 (219 - 1,283 nt) overlaps with ORF1 and encodes a 39-kDa protein. The nucleotide and amino acid sequence analysis of ORF0 showed average of 99.03% and 98.91% in identities, respectively, among 21 isolates (Table 2.4 and 2.5). ORF1 (208 - 2,916 nt) potentially encodes a 100-kDa protein containing a conserved serine proteinase domain followed by the genome-linked viral protein (VPg). The degree of identity of ORF1 ranged from 96.82% to 99.92% for the nucleotide sequence with two identical isolates of VE-1 from Spain (Table 2.4 and 2.6). The amino acid identity showed average of 98.22% (Table 2.4 and 2.6). ORF2 (2,202 - 4,178 nt) was translated by a -1 ribosomal frameshift from ORF1 and encoded a 148-kDa fusion protein of 1,323 amino acids that contained helicase and polymerase (POL) domains. The degree of identity had an average of 98.19% for the nucleotide sequence and 97.87% for the amino acid sequence (Table 2.4 and 2.7). ORF3 (4,301 - 4,876 nt) encodes a 21-kDa protein as a putative CP which showed average of 99.17% and 99.80% in identity of nucleotide and amino acid sequences, respectively (Table 2.4 and 2.8). ORF3 also had the lowest variable site percentage in both nucleotide and amino acid sequences among the different CVEV ORFs (Table 2.4). ORF5 (4,877 - 5,785 nt) is expressed by readthrough the CP amber stop codon as a 55-kDa fusion protein. The nucleotide and amino acid comparison of ORF5 among CVEV isolates showed average of 98.14% and 98.40% in identity, respectively (Table 2.4 and 2.9).

Phylogenetic analysis of CVEV full-length sequences.

Using three different methods, phylogenetic trees were generated with the 10 full-length nucleotide sequences of CVEV isolates in this study and 11 CVEV isolates from NCBI GenBank. PEMV-1 from GenBank was used as outgroup. All three methods obtained similar topologies. The unrooted tree from the neighbor-joining analysis identified two distinct clades. One isolate from China, VE-SM, stood by itself as an outgroup (Figure 2.3). Ten isolates of CVEV clustered in clade A contained isolates from Japan (VE-STM-1, VE-STM-2, VE-IBK, VE-NGS, and VE-YM1), Korea (VE-JJ, VE-PTC, and VE-PCJ) and Spain (VE-1) (Figure 2.3). Clade B contained 10 isolates originating from Australia (VE709) and USA (VE701, VE702, VE703, VE704, VE705, VE706, VE707, VE708, and VE823) which were intercepted by the CCPP during variety introduction as well as regular field testing (Figure 2.3).

Genomic analysis for CVEV RT-qPCR assay design.

To identify conserved genomic regions for the design of a detection assay, the CVEV full genome was divided into three sections for further nucleotide sequence identity (NSI) analysis: (1) 5'-UTR ORF1 (1 - 2,201 nt), (2) ORF2 and non-coding region (2,202 - 4,300 nt), and (3) ORF3, ORF5 and 3'-UTR (4,301 - 5,983 nt) (Table 2.10). Sequence identity analysis showed that the ORF3, ORF5 and 3'-UTR (4,301 - 5,983 nt) region was the most conserved with average of identities at 98.56% and minimum of 97.14% (Table

2.10). This region also had the smallest standard deviation of identities (0.44%) and lowest rate for variable sites (8.02%) (Table 2.10). Therefore, ORF3, ORF5 and 3'-UTR (4,301 - 5,983 nt) region was selected as detection assay targeting area.

The highly conserved region, ORF3, ORF5 and 3'-UTR (4,301 - 5,983 nt), was further analyzed and revealed that nucleotides 4,301 to 4,530 nt had the highest identity (99.57 ± 0.55%) and the lowest rate for variable sites (3.48%) (Table 2.11). Therefore, the newly developed RT-qPCR detection primers and probe were designed to target this most conserved nucleotide region (Figure 2.1, Table 2.3).

CVEV RT-qPCR assay validation.

The applicability, practicability and transferability of this assay was validated by two independent laboratories with consistent reproducible results (Table 2.12). The assay was also proven to be robust since different annealing temperatures, reaction volumes, qPCR instruments, and master mixes had a minor effect at the Cq values and did not affect the classification of samples as positive or negative (Table 2.13). The specificity of the assay was determined *in silico* by analyzing the sequence of amplicons from different samples followed by a BLASTn search that recognized the amplicon sequences associated only with CVEV. Additionally, the specificity of the assay was evaluated qualitatively with the correct classification (false negative and positive rate 0%) of 144 known CVEV positive and negative samples (Table 2.12, 2.14, 2.15 and 2.16). More specifically, the

assay detected the virus in 34 known CVEV positive samples from various geographic locations (Table 2.12 and 2.14) and did not cross-react with 69 known CVEV negative samples of non-inoculated citrus varieties (Table 2.15) and a series of 41 non-targeted graft-transmissible citrus pathogens (Table 2.16).

When samples were tested with 10-fold serial dilutions and run in triplicate, the sensitivity of the CVEV RT-qPCR showed a linear dynamic range from 10^7 copies to < 10 copies per µl which indicates the detection assay reached the level of LOD_6 with R^2 equal to 0.9936 and 100.3% as its efficiency (Figure 2.4). The mean of viral load was 7.31 x 10^6 copies of CVEV per µl of infected sample extraction measured by the newly designed CVEV RT-qPCR assay. And the performance measurements (Sn, Sp, LR^+, LR^- and J) were all optimum.

Discussion

The most efficient citrus virus management practices are based on sensitive, reliable, and cost-effective detection assays for large-scale virus surveys in orchards, nurseries, and germplasm programs (Belasque Jr et al. 2010; Navarro 1986; Santos Filho et al. 2000; Von Broembsen and Lee 1988). This study presented the development of a RT-qPCR detection assay for CVEV by following the guidelines developed in chapter 1 of this dissertation using a systematic approach with advanced technology platforms for the characterization and analysis of genomic information and development and validation of

the diagnostic assay following the "Guidelines for validation of qualitative real-time PCR methods" (Broeders et al. 2014).

First, the sequence data obtained via NGS were *de novo* assembled onto 51.8% to 96.0% of the complete CVEV genome which demonstrated the strength of this technology to identification of a novel viral pathogen and characterize its genome sequence (Villamor et al. 2019). With RACE and primer walking sequencing data from each isolate, the full-length sequences were assembled in relatively short time compared to traditional sequencing methods. This allowed for a more comprehensive genome analysis, molecular and genetic characteristics of the CVEV not limited by the available sequences of a small number of virus isolates or parts of the virus genome.

Twenty-one CVEV full-length nucleotide sequences including 10 isolates from this study and 11 available in the GenBank database contributed molecular and genetic information to produce more complete phylogenetic tree as well as confirmed the previously reported size and structure of its viral genome (Chen et al. 1992; Nakazono-Nagaoka et al. 2017; Vives et al. 2013; Wu et al. 2019; Yang et al. 2019). The sequence analysis showed that full genome sequences of CVEV had high degree of identities among different isolates. When comparing among different genes of CVEV, the ORF3, a putative CP, had the most conserved nucleotide and amino acid sequences. The high degree of identities might be due to the functions of ORF3 as a CP in virus entry, disassembly, translation of viral RNAs, RNA replication, virus movement, transmission and symptom development which are critical in virus infection cycle (Weber and Bujarski 2015). CVEV

ORF2 contained helicase and polymerase domains had highest variable rate in amino acid sequence while ORF5 has highest variable rate in nucleotide sequence. These data assumed that both ORF2 and ORF5 might involve in host interaction and adaptation including pathogenicity and recruitment of host machinery for virus replication, translation, and symptom expression. ORF5 has been proven it involves in virus accumulation, systemic spread in hosts as well as transmission efficiency, specificity and virus persistence within the aphid vector (Vives et al. 2013).

The untranslated region (UTR) at the 5' end also showed high degree of variability which might be due to the virus-host interaction such as the infection process and adaptation its fitness to the host (Burrell et al. 2017; Vives et al. 2013). Opposite to 5'-UTR, 3'-UTR was more conserved among other non-coding regions assumed that it has important functions to the virus itself (Burrell et al. 2017).

Phylogenetic analysis of the full-length sequences showed a correlation between geographical locations. Two identical isolates from Spain were in clade A along with Japanese and Korean isolates which assumed to have same ancestor or origin. The distribution of CVEV in Japan and Korea might be due to the human impact or vector transmission between these two counties and were further introduced into Europe through human activities such as travel and trade. The clade B contained isolates from Australia, California and Louisiana which indicated that USA isolates might be originated from Australia during citrus variety introductions and then the vector distributes similar isolates among different states.

The VE-SM was isolated from a pummelo tree in China. This isolate stood by itself assuming VE-SM has its own niche in this geographic location during evolution, probably to adapt to the different citrus varieties, environment, weather, and/or vector species. However, only one isolate is not sufficient to generally characterize isolates from China as a whole. More sequence data are needed to conclude such significantly characteristics. The phylogenetic analysis also suggested that all CVEV isolates share a common ancestor which was divergent from PEMV-1.

Since the genetic variation within the targeted virus population can lead to false negative RT-qPCR results, for the design of the CVEV detection assay, the aim was to locate the most conserved region on the virus genome beyond the traditional approaches that focus on individual genes presumed conserved due to their function (Weber and Bujarski 2015). The newly developed detection assay was further validated according to the guidelines for validation of qualitative real-time PCR methods (Broeders et al. 2014; Kralik and Ricchi 2017). Through the development of a RT-qPCR assay for citrus tatter leaf virus as mentioned in chapter 1, the data showed that the most conserved region was not confined in a single gene, but it sometimes spanned across different regions. Through the genome-wise identity analysis, the CVEV RT-qPCR detection assay was designed and targeting at the most conserved region. In this case, the ORF3, a putative CP of CVEV, contained the targeting area. The conserved nature of the CVEV ORF3 could be a result of its functions in several stage of infection cycle including virion assembly (Weber and Bujarski 2015).

Compared to traditional published qPCR assays that were designed on limited or partial sequences of isolates, the assay in this study was developed using a high number of virus sequences and able to detect a diverse range of CVEV isolates from different geographic locations, citrus varieties, and isolation times. These results agree with Roussel et al. (Roussel et al. 2005) who reported that the RT-qPCR designed for prune dwarf virus (PDV) failed to detect many virus isolates because the assay was designed from very few published PDV sequences in the GenBank.

In addition, the sensitivity and specificity of this assay were improved by using MGB probes (Kutyavin et al. 2000; Mingxiao et al. 2013), designed from the multiple sequence alignment, that targeted the identified conserved genomic region among ORF3. Furthermore, measuring viral loads and performing reactions under variable conditions showed that the newly developed RT-qPCR is robust and can detect minimal quantities of the CVEV. The proposed CVEV RT-qPCR detection assay will be essential for high value citrus germplasm screening programs and citrus certification programs to ensure the availability of pathogen tested materials for propagation and variety introduction (Bostock et al. 2014; Navarro 1986; Vidalakis et al. 2014).

NGS technologies combined with bioinformatics analysis have proven again to be powerful tools in identifying and characterizing novel sequences of pathogens, in studying disease occurrence, genome variability, and phylogeny (Kehoe et al. 2014; Radford et al. 2012; Villamor et al. 2019). Using a systemic approach with the help of NGS technologies as well as the well-defined qPCR design, development and validation protocol (Broeders

et al. 2014; Bustin et al. 2009), the current qPCR assay can be regularly updated as more target pathogen genomes are sequenced, therefore, increasing the value of the assays in preventing virus outbreaks and managing virus spread and induced diseases.

References

Azeri, T., and Heper, E. 1972. Citrus vein-enation virus on Satsuma mandarins in the Aegean Coast of Turkey. Plant disease reporter 56:352-353.

Bazan de Segura, C., and Ferrand, A. 1969. Woody galls, its distribution and importance in new and old citrus plantings in Peru. Pages 1449-1451 in: 1st International Citrus Symposium.

Belasque Jr, J., Bassanezi, R. B., Yamamoto, P. T., Ayres, A. J., Tachibana, A., Violante, A. R., Tank Jr, A., Di Giorgi, F., Tersi, F. E. A., and Menezes, G. M. 2010. Lessons from huanglongbing management in São Paulo State, Brazil. Journal of Plant Pathology 92:285-302.

Bewick, V., Cheek, L., and Ball, J. 2004. Statistics review 13: receiver operating characteristic curves. Critical care (London, England) 8:508-512.

Bostock, R. M., Thomas, C., Hoenisch, R., Golino, D. A., and Vidalakis, G. 2014. Excluding Pests and Pathogens: Plant health: How diagnostic networks and interagency partnerships protect plant systems from pests and pathogens. California Agriculture 68:117-124.

Broeders, S., Huber, I., Grohmann, L., Berben, G., Taverniers, I., Mazzara, M., Roosens, N., and Morisset, D. 2014. Guidelines for validation of qualitative real-time PCR methods. Trends in Food Science & Technology 37:115-126.

Burrell, C. J., Howard, C. R., and Murphy, F. A. 2017. Chapter 4 - Virus Replication. Pages 39-55 in: Fenner and White's Medical Virology (Fifth Edition). C. J. Burrell, C. R. Howard and F. A. Murphy, eds. Academic Press, London.

Bustin, S. A., Benes, V., Garson, J. A., Hellemans, J., Huggett, J., Kubista, M., Mueller, R., Nolan, T., Pfaffl, M. W., and Shipley, G. L. 2009. The MIQE guidelines: minimum information for publication of quantitative real-time PCR experiments. Clinical chemistry 55:611-622.

Chen, G. Q., Yan, S. X., and Roistacher, C. N. 1992. First report of citrus vein enation disease in China. Plant Disease 76:1077.

Clark, C., and da Graça, J. 2000. Detection of citrus vein enation virus using cereal yellow dwarf virus ELISA kits. in: Proceedings of 14th Conference of International Organization of Citrus Virologists.

Fraser, L. R. 1958. Virus diseases of citrus in Australia. Pages 9-19 in: Proceedings of the Linnean Society of New South Wales.

Ho, T., and Tzanetakis, I. E. 2014. Development of a virus detection and discovery pipeline using next generation sequencing. Virology 471-473:54-60.

Huang, A.-j., Song, Z., Cao, M.-j., Chen, H.-m., Li, Z.-a., and Zhou, C.-y. 2015. The complete genome sequence of Citrus vein enation virus from China. Journal of Integrative Agriculture 14:598-601.

Jacomino, A. P., and Salibe, A. A. 1993. Occurrence of woody gall disease in citrus in siio paulo state, Brazil. in: Proceedings of 12th Conference of International Organization of Citrus Virologists.

Kehoe, M. A., Coutts, B. A., Buirchell, B. J., and Jones, R. A. 2014. Plant virology and next generation sequencing: experiences with a Potyvirus. PLOS ONE 9:e104580.

Kralik, P., and Ricchi, M. 2017. A Basic Guide to Real Time PCR in Microbial Diagnostics: Definitions, Parameters, and Everything. Frontiers in Microbiology 8.

Kutyavin, I. V., Afonina, I. A., Mills, A., Gorn, V. V., Lukhtanov, E. A., Belousov, E. S., Singer, M. J., Walburger, D. K., Lokhov, S. G., Gall, A. A., Dempcy, R., Reed, M. W., Meyer, R. B., and Hedgpeth, J. 2000. 3'-minor groove binder-DNA probes increase sequence specificity at PCR extension temperatures. Nucleic acids research 28:655-661.

Laird, E. F., and Weathers, L. G. 1961. Aphis gossypii, a vector of citrus vein-enation virus. Plant Diseases Reporter 45:877.

Leutenegger, C. M. 2001. The real-time TaqMan PCR and applications in veterinary medicine. Vet Sci Tomorrow 1:1-15.

Manjunath, K. L. 1987. Studies on vein enation virus disease of citrus in South India. Indian Journal of Plant Pathology 5:121-125.

McClean, A. P. D. 1954. Citrus vein-enation virus. South African Journal of Science 50:147.

Mingxiao, M., Jinhua, L., Yingjin, S., Li, L., and Yongfei, L. 2013. TaqMan MGB probe fluorescence real-time quantitative PCR for rapid detection of Chinese Sacbrood virus. PLOS ONE 8:e52670-e52670.

Nakazono-Nagaoka, E., Fujikawa, T., and Iwanami, T. 2017. Nucleotide sequences of Japanese isolates of citrus vein enation virus. Arch Virol 162:879-883.

Navarro, L. 1986. Citrus certification in Mediterranean countries1. EPPO Bulletin 16:227-238.

Osman, F., Dang, T., Bodaghi, S., and Vidalakis, G. 2017. One-step multiplex RT-qPCR detects three citrus viroids from different genera in a wide range of hosts. J Virol Methods 245:40-52.

Osman, F., Hodzic, E., Kwon, S. J., Wang, J., and Vidalakis, G. 2015. Development and validation of a multiplex reverse transcription quantitative PCR (RT-qPCR) assay for the rapid detection of Ci*trus tristeza virus, C*i*trus psorosis virus, a*nd Ci*trus leaf blotch virus*. J Virol Methods 220:64-75.

Pfaffl, M. W. 2004. Quantification strategies in real-time PCR. Pages 89-113 in: A-Z of Quantitative PCR. International University Line (IUL), La Jolla, CA, USA.

Radford, A. D., Chapman, D., Dixon, L., Chantrey, J., Darby, A. C., and Hall, N. 2012. Application of next-generation sequencing technologies in virology. J Gen Virol 93:1853-1868.

Rasmussen, R. 2001. Quantification on the LightCycler. Pages 21-34 in: Rapid Cycle Real-Time PCR: Methods and Applications. S. Meuer, C. Wittwer and K.-I. Nakagawara, eds. Springer Berlin Heidelberg, Berlin, Heidelberg.

Roistacher, C. N. 1991. Graft-Transmissible Diseases of Citrus -Handbook for detection and diagnosis of graft-transmissible diseases of citrus. Food and Agriculture Organization of the United Nations, Rome.

Roussel, S., Kummert, J., Salmon, M., Dutrecq, O., and Jijakli, M. H. 2005. Development of RT-PCR assays using fluorogenic-3' minor groove binder DNA probes for detection of fruit tree viruses. EPPO Bulletin 35:105-108.

Santos Filho, H. P., Passos, O. S., da Cunha Sobrinho, A. P., Barbosa, C. d. J., and Nickel, O. 2000. The citrus variety improvement program in northeastern Brazil after 15 Years. Pages 403-404 in: Proceedings of 14th Conference of International Organization of Citrus Virologists.

Sheta, E., Salem, E., Abou-Zeid, A., Osman, M., Shafik, M., El-Hawari, A., Safurim, J., D'Onghia, A., and Camacho, A. 2002. Development of a citrus certification program in Egypt. in: Proceedings of 15th Conference of International Organization of Citrus Virologists.

Svec, D., Tichopad, A., Novosadova, V., Pfaffl, M. W., and Kubista, M. 2015. How good is a PCR efficiency estimate: Recommendations for precise and robust qPCR efficiency assessments. Biomol Detect Quantif 3:9-16.

Tamura, K., Stecher, G., Peterson, D., Filipski, A., and Kumar, S. 2013. MEGA6: Molecular Evolutionary Genetics Analysis version 6.0. Mol Biol Evol 30:2725-2729.

Tanaka, S., and Yamada, S. 1961. Citrus virus diseases in Japan. in: Proceedings of 2nd Conference of International Organization of Citrus Virologists.

Vidalakis, G., Gumpf, D. J., Polek, M., and Bash, J. A. 2014. The California Citrus Clonal Protection Program. Pages 117-130 in: Citrus Production Manual. L. Ferguson and E. E. Grafton-Cardwell, eds., University of California Agricultural and Natural Resources (UC ANR) Publication 3539.

Villamor, D. E. V., Ho, T., Al Rwahnih, M., Martin, R. R., and Tzanetakis, I. E. 2019. High Throughput Sequencing For Plant Virus Detection and Discovery. Phytopathology 109:716-725.

Vives, M. C., Velázquez, K., Pina, J. A., Moreno, P., Guerri, J., and Navarro, L. 2013. Identification of a new enamovirus associated with citrus vein enation disease by deep sequencing of small RNAs. Phytopathology 103:1077-1086.

Von Broembsen, L., and Lee, A. T. C. 1988. South Africa's citrus improvement programme. Pages 407-416 in: Proceedings of 10th Conference of International Organization of Citrus Virologists.

Wallace, J. M., and Drake, R. J. 1953. A virus-induced vein enation in citrus. Citrus leaves 33:22-24.

Wallace, J. M., and Drake, R. J. 1959. Citrus vein enation. Pages 163-165 in: Citrus Virus Diseases. J. M. Wallace, ed. University of California Press, Berkeley and Los Angeles.

Wallace, J. M., and Drake, R. J. 1960. Woody galls on Citrus associated with vein enation virus infection. Plant Disease Reporter 44:580-584.

Wallace, J. M., and Drake, R. J. 1961. Induction of woody galls by wounding of citrus infected with vein-enation virus. Plant Disease Reporter 45:682-586.

Weber, P. H., and Bujarski, J. J. 2015. Multiple functions of capsid proteins in (+) stranded RNA viruses during plant–virus interactions. Virus Research 196:140-149.

Wu, J., Liu, Q., Qiu, Y., Zhang, S., Li, Z., Li, R., Zhou, C. Y., and Cao, M. 2019. First report of citrus vein enation virus from citrus cv. Huangguogan in Sichuan province, China. Plant Disease.

Yang, H.-J., Oh, J., Lee, H.-K., Lee, D.-S., Kim, S.-Y., Kim, M.-H., Park, C. Y., Kim, H., Yi, S.-I., Jeong, R.-D., Moon, J. S., and Lee, S.-H. 2019. First report of Citrus vein enation virus in Satsuma mandarin (*Citrus unshiu*) in Korea. Plant Disease.

Isolate	GenBank Accession No.	Partial Sequence of citrus vein enation virus
VE-1	NC_021564	T C G T C G G C G G C G T G C G G T T A A T A G A T C A A C C G G A G A G A T G C G T C C T T A C C A C T T G T A T G G G C T T A A A T G C A A C G A C A A G G G T T A T C T C A C T T T T G
VE701	MN187035	. . . .
VE702	MN187036	. . . .
VE703	MN187037	. . . . T . . . .
VE704	MN187038	. . . .
VE705	MN187039	. . . . A . . . . T . . . .
VE706	MN187040	. . . .
VE707	MN187041	. . . .
VE708	MN187042	. . . . T . . . .
VE709	MN187043	. . . . T . . . .
VE823	MN187044	. . . .
VE-STM-2	LC089854	. . . .
VE-STM-1	LC089853	. . . .
VE-IBK	LC089852	. . . . T . . . .
VE-NGS	LC089851	. . . .
VE-YM1	LC089850	. . . .
VE-1	HF679486	. . . .
VE-SM	KY303624	. . . .
VE-JJ	LC360112	. . . C . . . . C . . . .
CVEV F		C G G C G T G C G G T T A A T A G A T C A A
CVEV P		A G A G A T G C G T C C T T A C C
CVEV R		A A T G C A A C G A C A A G G G T T A T C T C

Figure 2.1 Multiple nucleotide sequences alignment of citrus vein enation virus. Citrus vein enation virus detection assay targeting region is highlighted in dark grey and primers-probe set is also shown. Citrus vein enation virus isolate VE-1 (NCBI GenBank Accession No. NC_021564) is used here to represent the species.
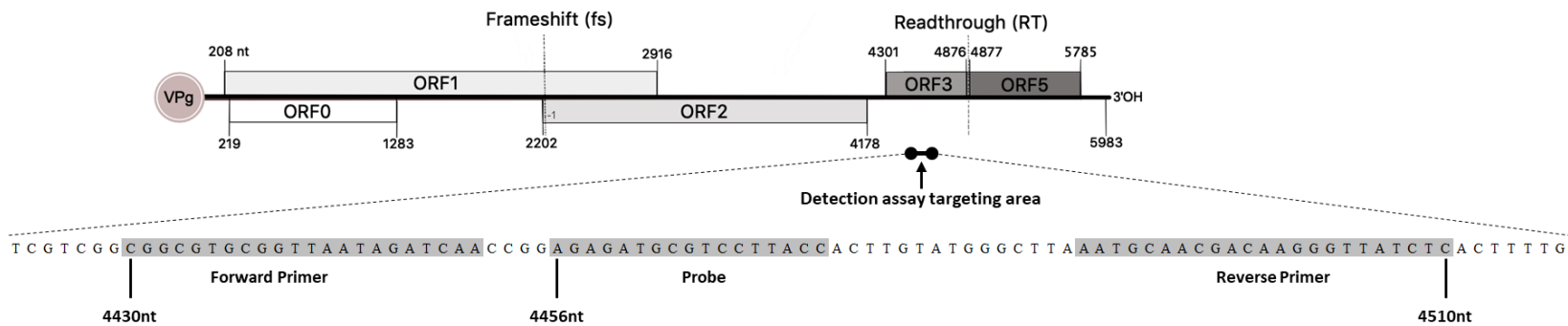
Figure 2.2 Schematic representation of the genome organization of citrus vein enation virus isolate VE701 (NCBI GenBank Accession No. MN187035). Open box represents open reading frames (ORFs). Solid lines alone represent untranslated regions (UTRs) at the termini and non-coding region within the genome. Short line with end points represent the citrus vein enation virus RT-qPCR detection assay targeting region designed in this study. Illustrations are not to scale.
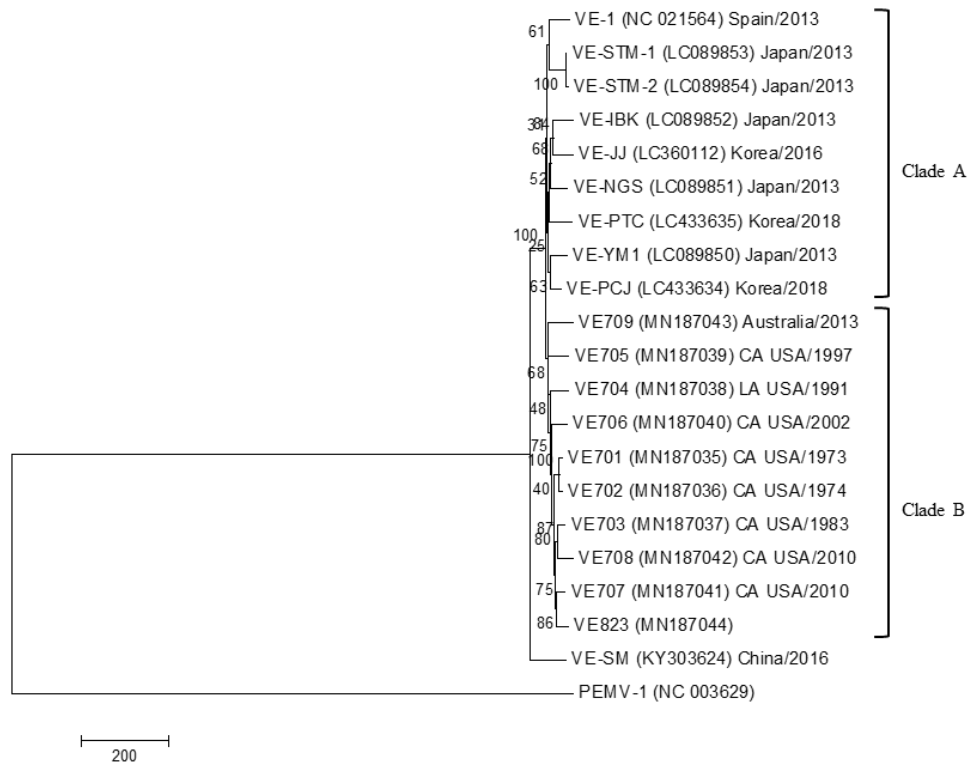
Figure 2.3 The unrooted phylogenetic tree based on full-length nucleotide sequences of 10 citrus vein enation virus isolates in this study and 11 isolates from NCBI GenBank database. Pea enation mosaic virus-1 was used as an outgroup. The tree was constructed by MEGA 7.0.21 using neighbor-joining method with 1000 bootstrap replicates and bootstrap support is indicated at branch points. The scale bar shows the number of substitutions per base. The identities were analyzed among isolates in the cluster. (VE: citrus vein enation virus; PEMV-1: pea enation mosaic virus 1)
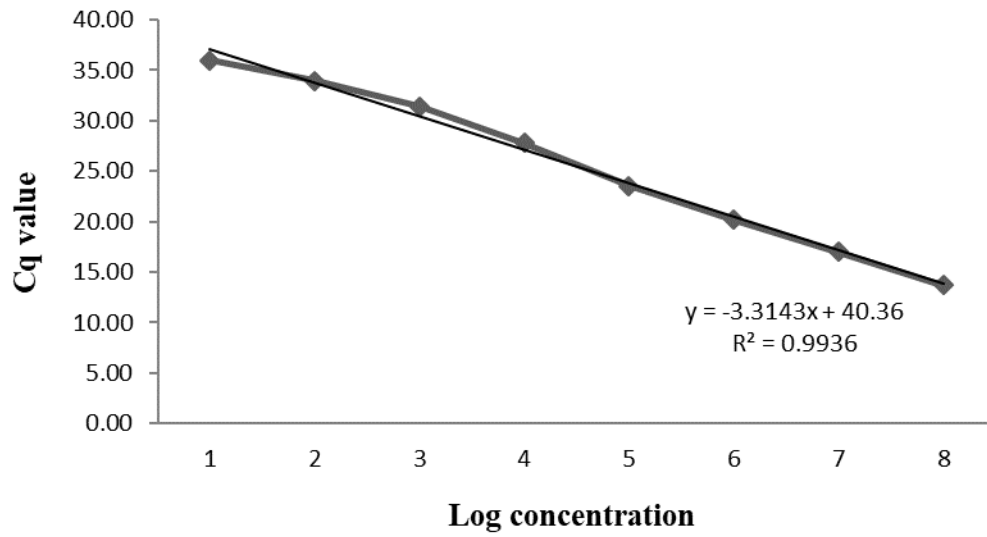
Figure 2.4 Standard curve analysis of RT-qPCR sensitivity. The X-axis displays the log copies/well and the Y-axis represents the value of quantitative cycle (Cq).

Table 2.1 Isolates of citrus vein enation virus used in this study.

Sample	Citrus Host	Citrus Host Scientific Name	Geographic Origin	Isolation Year	Biological Indexing[1]	Genome Size (nt)	GenBank Accession No.
VE701	Parent Navel Orange	*Citrus sinensis* L. Osb.	CA, USA	1973	2	5983	MN187035
VE702	Olinda Valencia Orange	*Citrus sinensis* L. Osb.	CA, USA	1974	3	5983	MN187036
VE703	Sweet Orange	*Citrus sinensis* L. Osb.	CA, USA	1983	3	5983	MN187037
VE704	Armstrong Satsuma	*Citrus unshiu* (Macf.) Marc.	LA, USA	1991	NA	5983	MN187038
VE705	Valencia Orange	*Citrus sinensis* L. Osb.	CA, USA	1997	4	5983	MN187039
VE706	Gillette Navel Orange	*Citrus sinensis* L. Osb.	CA, USA	2002	NA	5983	MN187040
VE707	Dweet Tangor	*Citrus reticulata* x *Citrus sinesis*	CA, USA	2010	3	5983	MN187041
VE708	Dweet Tangor	*Citrus reticulata* x *Citrus sinesis*	CA, USA	2010	3	5983	MN187042
VE709	Finger Lime	*Citrus australasica*	Australia	2013	NA	5983	MN187043
VE823	Citrus	NA	NA	1983	NA	5982	MN187044

[1] The biological indexing was performed on Mexican lime. Symptom scores from 0 (no symptom) to 5 (severe symptom).

Abbreviation: VE: citrus vein enation virus.

Table 2.2 Full-length nucleotide sequence identities (%) of citrus vein enation virus isolates characterized in this study and from NCBI GenBank database.

Isolate	Citrus Host	Host Scientific Name	Geographic Origin	Isolation Year	GenBank Accession Number	GenBank Deposit Year	Cluster	Clade	VE-1	VE-1	VE-STM-1	VE-STM-2	VE-IBK	VE-JJ	VE-NGS	VE-PTC	VE-YM1	VE-PCJ	VE709	VE705	VE704	VE706	VE701	VE702	VE703	VE708	VE707	VE823	VE-SM	PEMV-1
VE-1	Washington Navel Orange	*Citrus sinensis* (L.) Osb.	Spain	2013	NC_021564	2013	I	A																						
VE-1	Washington Navel Orange	*Citrus sinensis* (L.) Osb.	Spain	2013	HF679486	2014			100.00																					
VE-STM-1	Yuzu	*Citrus junos* Sieb. ex Tanaka	Japan	2013	LC089853	2017			98.59	98.59																				
VE-STM-2	Yuzu	*Citrus junos* Sieb. ex Tanaka	Japan	2013	LC089854	2017			98.54	98.54	99.88																			
VE-IBK	Yuzu	*Citrus junos* Sieb. ex Tanaka	Japan	2013	LC089852	2017			98.11	98.11	98.14	98.09																		
VE-JJ	Satsuma	*Citrus unshiu* (Macf.) Marc.	Korea	2016	LC360112	2017			98.02	98.02	98.22	98.21	98.47																	
VE-NGS	Yuzu	*Citrus junos* Sieb. ex Tanaka	Japan	2013	LC089851	2017			98.34	98.34	98.51	98.46	98.42	98.57																
VE-PTC	Trifoliate Orange	*Poncirus trifoliata*	Korea	2018	LC433635	2018			98.16	98.16	98.22	98.14	98.17	98.19	98.47															
VE-YM1	Yuzu	*Citrus junos* Sieb. ex Tanaka	Japan	2013	LC089850	2017			98.34	98.34	98.59	98.51	98.29	98.34	98.52	98.34														
VE-PCJ	Trifoliate Orange	*Poncirus trifoliata*	Korea	2018	LC433634	2018			98.61	98.61	98.87	98.79	98.62	98.61	98.79	98.61	98.96													
VE709	Finger Lime	*Citrus australasica*	Australia	2013	MN187043	2019	II		98.14	98.14	98.09	98.04	97.94	97.82	98.29	97.99	98.12	98.29												
VE705	Valencia Orange	*Citrus sinensis* L. Osb.	CA, USA	1997	MN187039	2019			98.29	98.29	98.19	98.14	98.04	98.02	98.22	98.12	98.57	98.42	98.21											
VE704	Armstrong Satsuma	*Citrus unshiu* (Macf.) Marc.	LA, USA	1991	MN187038	2019			98.39	98.39	98.29	98.27	98.04	98.04	98.26	98.07	98.22	98.42	98.19	98.36										
VE706	Gillette Navel Orange	*Citrus sinensis* L. Osb.	CA, USA	2002	MN187040	2019			98.32	98.32	98.31	98.26	98.11	98.14	98.44	98.17	98.36	98.51	98.37	98.52	98.74									
VE701	Parent Navel Orange	*Citrus sinensis* L. Osb.	CA, USA	1973	MN187035	2019			98.51	98.51	98.41	98.32	98.29	98.31	98.56	98.39	98.54	98.62	98.61	98.74	98.77	99.14								
VE702	Olinda Valencia Orange	*Citrus sinensis* L. Osb.	CA, USA	1974	MN187036	2019			98.57	98.57	98.44	98.36	98.31	98.26	98.56	98.34	98.57	98.66	98.54	98.76	98.79	98.99	99.74							
VE703	Sweet Orange	*Citrus sinensis* L. Osb.	CA, USA	1983	MN187037	2019			98.46	98.46	98.36	98.34	98.21	98.24	98.57	98.22	98.44	98.54	98.42	98.74	98.72	98.79	99.16	99.19						
VE708	Dweet Tangor	*Citrus reticulata* x *Citrus sinensis*	CA, USA	2010	MN187042	2019			98.17	98.17	98.07	98.02	97.87	97.92	98.24	97.94	98.16	98.29	98.14	98.41	98.51	98.56	98.94	99.03	99.16					
VE707	Dweet Tangor	*Citrus reticulata* x *Citrus sinensis*	CA, USA	2010	MN187041	2019			98.37	98.37	98.37	98.36	98.19	98.14	98.47	98.26	98.46	98.59	98.51	98.74	98.67	98.94	99.23	99.26	99.33	98.89				
VE823	Citrus	NA	NA	1983	MN187044	2019			98.24	98.24	98.19	98.14	98.04	98.04	98.32	98.09	98.19	98.37	98.42	98.62	98.52	98.79	99.14	99.14	99.09	98.69	99.24			
VE-SM	Pummelo	*Citrus grandis* (L.) Osb.	China	2016	KY303624	2017		B	97.20	97.20	97.25	97.17	96.92	96.94	97.12	97.22	97.24	97.37	96.99	97.12	97.10	97.17	97.42	97.35	97.22	96.94	97.15	97.15		
PEMV-1	Pea	Pisum sativum L. cv. 8221		1991	NC_003629	2002	Outgroup		52.69	52.69	52.64	52.64	52.83	52.69	52.61	52.50	52.75	52.85	52.55	52.73	52.69	52.82	52.83	52.76	52.62	52.66	52.68	52.68	52.80	

Abbreviations: VE: citrus vein enation virus; PEMV-1: pea enation mosaic virus-1.

Table 2.3 Oligonucleotide primers and probe of citrus vein enation virus detection assay designed in this study.

Primers and Probe	Sequence 5'- 3'	Nucleotide Position[1]	Amplicon size (bp)
CVEV F	CGGCGTGCGGTTAATAGATCAA	4430-4451	
CVEV R	GAGATAACCCTTGTCGTTGCATT	4488-4510	81
CVEV Probe VIC	AGAGATGCGTCCTTACC	4456-4472	

[1]Nucleotide Position is based on reference genome of citrus vein enation virus isolate VE701 (NCBI GenBank Accession No. MN187035).

Abbreviation: CVEV: citrus vein enation virus; F: forward primer; R: reverse primer.

Table 2.4 Variable sites (%) and sequence identities (%) of full genome, genes and untranslated regions of citrus vein enation virus isolates in this study and from NCBI GenBank database.

Region / Sequence	Full-length genome (1 - 5,983 nt)			5'-Untranslated Region (UTR) (1 - 207 nt)			3'-Untranslated Region (UTR) (5,786 - 5,983 nt)			Non-coding Region (4,179 - 4,300 nt)		
	Variable Sites (Variable/Total)	Minimum SI	SI[$] Mean ± SD	Variable Sites (Variable/Total)	Minimum SI	SI Mean ± SD	Variable Sites (Variable/Total)	Minimum SI	SI Mean ± SD	Variable Sites (Variable/Total)	Minimum SI	SI Mean ± SD
Nucleotide	8.76 (524/5983)	96.92	98.32 ± 0.51	17.87 (37/207)	90.73	95.49 ± 1.92	8.08 (16/198)	97.47	98.76 ± 0.57	9.84 (12/122)	94.26	97.76 ± 1.17

Gene / Sequence	Open Reading Frame 0 (ORF0) (219 - 1,283 nt)			Open Reading Frame1 (ORF1) (208 - 2,916 nt)			Open Reading Frame 2 (ORF2) (2,202 - 4,178 nt)		
	Variable Sites (Variable/Total)	Minimum SI	SI Mean ± SD	Variable Sites (Variable/Total)	Minimum SI	SI Mean ± SD	Variable Sites (Variable/Total)	Minimum SI	SI Mean ± SD
Nucleotide	5.82 (62/1065)	97.93	99.03 ± 0.42	8.56 (232/2709)	96.82	98.41 ± 0.56	9.36 (185/1977)	96.10	98.19 ± 0.67
Amino acid	7.04 (23/355)	97.74	98.91 ± 0.56	9.75 (88/903)	96.23	98.22 ± 0.68	11.23 (74/659)	95.90	97.87 ± 0.78

Gene / Sequence	Open Reading Frame 3 (ORF3) (4,301 - 4,876 nt)			Open Reading Frame5 (ORF5) (4,877 - 5,785 nt)		
	Variable Sites (Variable/Total)	Minimum SI	SI Mean ± SD	Variable Sites (Variable/Total)	Minimum SI	SI Mean ± SD
Nucleotide	4.69 (27/576)	98.43	99.17 ± 0.29	10.12 (92/909)	95.70	98.14 ± 0.71
Amino acid	2.08 (4/192)	98.43	99.80 ± 0.36	8.25 (25/303)	95.70	98.40 ± 0.86

Note: Nucleotide Position is based on reference genome of citrus vein enation virus isolate VE701 (NCBI GenBank Accession No. MN187035).

[$]SI: Sequence Identity.

Table 2.5 Nucleotide (below diagonal) and amino acid (above diagonal) sequence identities (%) of citrus vein enation virus open reading frame 0 (ORF0).

Isolate	GenBank Accesssion Number	VE-1	VE-1	VE-SM	VE-YM1	VE-NGS	VE-IBK	VE-STM-1	VE-STM-2	VE-JJ	VE-PTC	VE-PCJ	VE701	VE702	VE703	VE704	VE705	VE706	VE707	VE708	VE709	VE823
VE-1	NC_021564		100.00	98.30	99.43	99.71	98.87	99.43	99.43	98.30	98.87	99.15	99.71	100.00	99.43	99.15	99.15	98.87	99.43	99.43	98.30	99.43
VE-1	HF679486	100.00		98.30	99.43	99.71	98.87	99.43	99.43	98.30	98.87	99.15	99.71	100.00	99.43	99.15	99.15	98.87	99.43	99.43	98.30	99.43
VE-SM	KY303624	98.40	98.40		98.87	98.59	97.74	98.30	98.30	97.74	98.02	98.59	98.59	98.30	98.30	98.02	98.59	97.74	98.30	98.30	98.30	98.87
VE-YM1	LC089850	99.34	99.34	98.49		99.71	98.87	99.43	99.43	98.87	98.87	99.71	99.71	99.43	99.43	99.15	99.15	98.87	99.43	99.43	98.87	99.43
VE-NGS	LC089851	99.81	99.81	98.40	99.34		99.15	99.15	99.15	98.59	99.15	99.43	100.00	99.71	99.71	99.43	98.87	99.15	99.71	99.71	98.59	99.71
VE-IBK	LC089852	99.24	99.24	98.02	99.15	99.24		98.30	98.30	97.74	98.30	98.59	99.15	98.87	98.87	98.59	98.02	98.30	98.87	98.87	97.74	98.87
VE-STM-1	LC089853	99.62	99.62	98.59	99.53	99.43	99.06		100.00	98.30	98.30	99.15	99.15	99.43	98.87	98.59	99.15	98.30	98.87	98.87	98.30	98.87
VE-STM-2	LC089854	99.62	99.62	98.59	99.53	99.43	99.06	100.00		98.30	98.30	99.15	99.15	99.43	98.87	98.59	99.15	98.30	98.87	98.87	98.30	98.87
VE-JJ	LC360112	98.77	98.77	97.93	99.06	98.77	98.59	98.96	98.96		97.74	98.59	98.59	98.30	98.30	98.02	98.02	97.74	98.30	98.30	97.74	98.30
VE-PTC	LC433635	98.96	98.96	98.21	99.06	98.96	98.77	98.96	98.96	98.49		98.59	99.15	98.87	98.87	98.59	98.02	98.30	98.87	98.87	98.02	99.15
VE-PCJ	LC433634	99.06	99.06	98.40	99.53	99.06	98.87	99.24	99.24	98.77	98.77		99.43	99.15	99.15	99.43	98.87	98.59	99.15	99.15	98.59	99.15
VE701	MN187035	99.71	99.71	98.49	99.62	99.71	99.53	99.53	99.53	99.06	99.24	99.34		99.71	99.71	99.43	98.87	99.15	99.71	99.71	98.59	99.71
VE702	MN187036	99.71	99.71	98.30	99.62	99.53	99.34	99.53	99.53	98.87	99.06	99.15	99.81		99.43	99.15	99.15	98.87	99.43	99.43	98.30	99.43
VE703	MN187037	99.53	99.53	98.30	99.24	99.53	99.15	99.15	99.15	98.68	98.87	98.96	99.62	99.43		99.15	98.59	98.87	99.43	99.43	98.30	99.43
VE704	MN187038	99.15	99.15	98.12	99.24	99.15	98.96	98.96	98.96	98.68	98.68	98.96	99.43	99.43	99.24		98.30	99.15	99.15	99.71	98.02	99.15
VE705	MN187039	99.06	99.06	98.21	99.34	98.87	98.68	99.06	99.06	98.40	98.59	98.87	99.15	99.34	98.77	98.77		98.02	98.59	98.59	98.02	98.59
VE706	MN187040	99.24	99.24	98.02	99.34	99.24	99.06	99.06	99.06	98.59	98.77	99.06	99.53	99.34	99.15	99.15	98.87		99.43	99.43	97.74	98.87
VE707	MN187041	99.34	99.34	98.12	99.43	99.34	99.15	99.15	99.15	98.68	98.87	99.15	99.62	99.43	99.24	99.06	98.96	99.71		99.43	98.30	99.43
VE708	MN187042	99.15	99.15	98.12	99.06	99.15	98.77	98.77	98.77	98.30	98.68	98.77	99.24	99.06	99.43	99.06	98.59	99.15	99.06		98.30	99.43
VE709	MN187043	98.87	98.87	98.02	98.77	98.87	98.68	98.87	98.87	98.21	98.49	98.49	98.96	98.77	98.59	98.40	98.49	98.49	98.59	98.21		98.87
VE823	MN187044	99.24	99.24	98.21	99.15	99.24	99.06	99.06	99.06	98.59	99.06	99.06	99.53	99.34	99.15	98.96	98.87	99.24	99.34	98.77	98.87	

Abbreviation: VE: citrus vein enation virus.

Table 2.6 Nucleotide (below diagonal) and amino acid (above diagonal) sequence identities (%) of citrus vein enation virus open reading frame 1 (ORF1).

Isolate	GenBank Accesssion Number	VE-1	VE-1	VE-SM	VE-YM1	VE-NGS	VE-IBK	VE-STM-1	VE-STM-2	VE-JJ	VE-PTC	VE-PCJ	VE701	VE702	VE703	VE704	VE705	VE706	VE707	VE708	VE709	VE823
VE-1	NC_021564		100.00	97.56	98.56	98.78	98.22	99.00	99.00	98.00	98.00	98.78	99.11	99.00	98.89	98.67	98.56	98.67	98.67	98.33	97.67	98.22
VE-1	HF679486	100.00		97.56	98.56	98.78	98.22	99.00	99.00	98.00	98.00	98.78	99.11	99.00	98.89	98.67	98.56	98.67	98.67	98.33	97.67	98.22
VE-SM	KY303624	97.26	97.26		97.56	97.56	97.00	97.12	97.12	96.89	96.67	97.56	97.67	97.56	97.45	97.23	97.23	97.23	97.23	96.89	96.23	97.00
VE-YM1	LC089850	98.22	98.22	97.41		99.00	98.56	98.44	98.44	98.44	98.11	99.33	98.89	99.00	98.44	98.44	98.89	98.67	98.67	97.89	97.45	98.00
VE-NGS	LC089851	98.63	98.63	97.41	98.85		98.33	98.44	98.44	98.22	97.89	98.89	98.78	98.67	98.56	98.11	98.11	98.33	98.33	97.78	97.56	97.89
VE-IBK	LC089852	97.93	97.93	97.04	98.22	98.41		98.11	98.11	98.22	97.56	98.78	98.22	98.11	97.78	97.56	97.89	97.78	97.78	97.00	97.23	97.78
VE-STM-1	LC089853	98.63	98.63	97.37	98.70	98.74	98.11		100.00	97.89	97.67	98.78	98.56	98.44	98.11	98.11	98.00	98.11	98.11	97.34	97.34	97.67
VE-STM-2	LC089854	98.63	98.63	97.30	98.63	98.74	98.11	99.92		97.89	97.67	98.78	98.56	98.44	98.11	98.11	98.00	98.11	98.11	97.34	97.34	97.67
VE-JJ	LC360112	97.89	97.89	97.00	98.33	98.44	98.33	98.15	98.15		97.45	98.44	98.11	98.00	97.89	97.67	97.56	97.67	97.67	97.12	96.67	97.45
VE-PTC	LC433635	98.15	98.15	97.37	98.44	98.63	97.85	98.33	98.26	97.96		98.11	98.22	98.11	97.56	97.78	97.89	97.56	97.78	97.23	96.78	97.56
VE-PCJ	LC433634	98.59	98.59	97.60	99.04	99.07	98.37	98.92	98.85	98.56	98.67		99.00	98.89	98.56	98.33	98.67	98.78	98.78	98.00	97.78	98.11
VE701	MN187035	98.74	98.74	97.56	98.70	98.78	98.15	98.70	98.63	98.11	98.37	98.74		99.88	99.33	99.11	99.33	99.33	99.55	98.78	98.11	99.11
VE702	MN187036	98.74	98.74	97.48	98.70	98.70	98.08	98.70	98.63	98.04	98.30	98.67	99.92		99.22	99.22	99.44	99.22	99.44	98.67	98.00	99.00
VE703	MN187037	98.67	98.67	97.34	98.44	98.70	98.08	98.48	98.48	97.96	98.08	98.52	99.26	99.18		98.89	98.67	98.89	98.89	99.00	97.67	98.44
VE704	MN187038	98.56	98.56	97.12	98.33	98.44	97.78	98.41	98.41	97.78	98.04	98.41	99.04	99.04	99.04		98.67	98.67	98.67	98.11	97.45	98.22
VE705	MN187039	98.56	98.56	97.37	98.63	98.30	97.82	98.37	98.37	97.71	97.96	98.41	98.85	98.92	98.63	98.56		98.89	99.11	98.33	97.67	98.67
VE706	MN187040	98.56	98.56	97.30	98.52	98.67	97.89	98.59	98.59	97.93	98.11	98.63	99.37	99.29	99.07	99.00	98.67		99.33	98.33	97.67	98.67
VE707	MN187041	98.70	98.70	97.37	98.56	98.74	98.04	98.67	98.67	98.00	98.26	98.70	99.52	99.44	99.22	99.07	98.89	99.48		98.56	97.89	98.89
VE708	MN187042	98.52	98.52	97.19	98.30	98.48	97.78	98.26	98.26	97.74	98.00	98.37	99.11	99.04	99.48	98.89	98.56	99.00	99.15		96.89	97.89
VE709	MN187043	98.00	98.00	96.82	98.08	98.19	97.60	98.15	98.15	97.45	97.67	98.22	98.56	98.48	98.41	98.26	98.22	98.30	98.59	98.19		97.67
VE823	MN187044	98.63	98.63	97.30	98.26	98.52	97.96	98.44	98.44	97.93	98.15	98.56	99.22	99.15	99.00	98.85	98.67	99.18	99.33	98.85	98.44	

Abbreviation: VE: citrus vein enation virus.

Table 2.7 Nucleotide (below diagonal) and amino acid (above diagonal) sequence identities (%) of citrus vein enation virus open reading frame 2 (ORF2).

Isolate	GenBank Accesssion Number	VE-1	VE-1	VE-SM	VE-YM1	VE-NGS	VE-IBK	VE-STM-1	VE-STM-2	VE-JJ	VE-PTC	VE-PCJ	VE701	VE702	VE703	VE704	VE705	VE706	VE707	VE708	VE709	VE823
VE-1	NC_021564		100.00	96.96	97.57	97.42	97.42	97.26	97.42	97.57	97.57	97.87	98.63	98.63	98.78	97.72	98.78	97.87	98.48	98.63	97.72	98.33
VE-1	HF679486	100.00		96.96	97.57	97.42	97.42	97.26	97.42	97.57	97.57	97.87	98.63	98.63	98.78	97.72	98.78	97.87	98.48	98.63	97.72	98.33
VE-SM	KY303624	96.81	96.81		96.35	96.35	95.90	96.05	96.20	96.20	96.50	96.81	97.11	97.11	97.26	96.50	96.96	96.96	96.96	97.11	96.35	96.50
VE-YM1	LC089850	97.87	97.87	96.81		98.63	98.02	97.72	97.72	98.33	98.48	98.48	97.72	97.72	97.87	96.81	97.87	97.57	97.57	97.72	97.42	97.11
VE-NGS	LC089851	98.07	98.07	96.71	98.68		98.17	97.42	97.57	98.48	98.02	98.33	97.57	97.57	97.72	96.66	97.72	97.42	97.42	97.57	97.26	96.96
VE-IBK	LC089852	97.77	97.77	96.10	98.17	98.48		97.11	97.26	98.17	97.57	98.48	97.57	97.57	97.72	96.66	97.87	96.81	97.42	97.57	96.96	96.96
VE-STM-1	LC089853	98.07	98.07	96.66	97.97	98.38	97.87		99.84	97.42	97.11	97.87	97.72	97.72	97.87	97.11	97.57	97.87	97.87	97.87	97.11	97.42
VE-STM-2	LC089854	98.07	98.07	96.66	97.97	98.38	97.87	99.89		97.57	97.26	98.02	97.87	97.87	98.02	97.26	97.72	98.02	98.02	98.02	97.26	97.57
VE-JJ	LC360112	97.87	97.87	96.50	98.48	98.78	98.48	98.07	98.17		97.87	98.33	97.72	97.72	97.72	96.66	97.72	97.26	97.42	97.57	96.96	96.96
VE-PTC	LC433635	97.92	97.92	96.86	98.33	98.68	98.02	98.02	98.02	98.33		98.02	97.72	97.72	97.87	96.81	97.87	97.26	97.57	97.72	97.11	97.11
VE-PCJ	LC433634	98.28	98.28	96.86	98.68	98.98	98.88	98.48	98.48	98.78	98.63		98.02	98.02	98.17	97.11	98.33	97.57	97.87	98.02	97.72	97.42
VE701	MN187035	98.58	98.58	97.11	98.28	98.17	97.77	97.97	97.97	98.07	98.12	98.38		100.00	99.54	98.48	98.93	98.93	99.54	99.39	98.48	98.78
VE702	MN187036	98.58	98.58	97.11	98.28	98.17	97.77	97.97	97.97	98.07	98.12	98.38	100.00		99.54	98.48	98.93	98.93	99.54	99.39	98.48	98.78
VE703	MN187037	98.58	98.58	97.11	98.38	98.28	97.87	98.07	98.17	98.38	98.12	98.48	99.49	99.49		98.63	99.08	98.78	99.69	99.54	98.93	98.93
VE704	MN187038	98.17	98.17	96.76	97.67	97.77	97.36	97.82	97.92	97.77	97.72	97.97	98.68	98.68	98.78		98.02	98.33	98.63	98.63	97.57	98.17
VE705	MN187039	98.48	98.48	97.11	98.68	98.28	97.87	98.07	98.07	98.17	98.22	98.53	99.08	99.08	99.08	98.28		98.17	98.78	98.93	98.02	98.63
VE706	MN187040	98.02	98.02	96.96	97.92	97.92	97.42	98.07	98.07	97.72	97.72	98.12	98.83	98.83	98.73	98.58	98.43		98.78	98.78	98.02	98.33
VE707	MN187041	98.38	98.38	97.01	98.28	98.17	97.87	98.07	98.07	98.07	98.12	98.48	99.69	99.69	99.59	98.68	99.08	98.83		99.39	98.63	98.93
VE708	MN187042	98.38	98.38	96.81	98.07	97.97	97.57	97.77	97.77	97.97	97.92	98.17	99.49	99.49	99.39	98.38	98.88	98.43	99.39		98.48	98.93
VE709	MN187043	98.12	98.12	96.50	98.02	98.02	97.62	97.82	97.82	97.82	97.87	98.33	98.73	98.73	98.83	98.12	98.33	98.33	98.73	98.53		97.87
VE823	MN187044	98.22	98.22	96.76	98.02	97.92	97.62	97.92	97.92	97.82	97.87	98.12	99.34	99.34	99.24	98.43	98.93	98.48	99.44	99.14	98.38	

Abbreviation: VE: citrus vein enation virus.

Table 2.8 Nucleotide (below diagonal) and amino acid (above diagonal) sequence identities (%) of citrus vein enation virus open reading frame 3 (ORF3).

Isolate	GenBank Accesssion Number	VE-1	VE-1	VE-SM	VE-YM1	VE-NGS	VE-IBK	VE-STM-1	VE-STM-2	VE-JJ	VE-PTC	VE-PCJ	VE701	VE702	VE703	VE704	VE705	VE706	VE707	VE708	VE709	VE823
VE-1	NC_021564		100.00	99.47	100.00	100.00	99.47	100.00	100.00	98.95	100.00	100.00	100.00	100.00	100.00	100.00	100.00	100.00	100.00	100.00	100.00	100.00
VE-1	HF679486	100.00		99.47	100.00	100.00	99.47	100.00	100.00	98.95	100.00	100.00	100.00	100.00	100.00	100.00	100.00	100.00	100.00	100.00	100.00	100.00
VE-SM	KY303624	99.13	99.13		99.47	99.47	98.95	99.47	99.47	98.43	99.47	99.47	99.47	99.47	99.47	99.47	99.47	99.47	99.47	99.47	99.47	99.47
VE-YM1	LC089850	99.30	99.30	99.13		100.00	99.47	100.00	100.00	98.95	100.00	100.00	100.00	100.00	100.00	100.00	100.00	100.00	100.00	100.00	100.00	100.00
VE-NGS	LC089851	98.78	98.78	98.95	98.78		99.47	100.00	100.00	98.95	100.00	100.00	100.00	100.00	100.00	100.00	100.00	100.00	100.00	100.00	100.00	100.00
VE-IBK	LC089852	98.95	98.95	99.13	98.95	99.13		99.47	99.47	98.43	99.47	99.47	99.47	99.47	99.47	99.47	99.47	99.47	99.47	99.47	99.47	99.47
VE-STM-1	LC089853	99.30	99.30	99.47	99.47	99.13	99.30		100.00	98.95	100.00	100.00	100.00	100.00	100.00	100.00	100.00	100.00	100.00	100.00	100.00	100.00
VE-STM-2	LC089854	99.13	99.13	99.30	99.30	98.95	99.13	99.82		98.95	100.00	100.00	100.00	100.00	100.00	100.00	100.00	100.00	100.00	100.00	100.00	100.00
VE-JJ	LC360112	98.43	98.43	98.61	98.43	98.95	98.78	98.78	98.61		98.95	98.95	98.95	98.95	98.95	98.95	98.95	98.95	98.95	98.95	98.95	98.95
VE-PTC	LC433635	99.13	99.13	99.30	99.13	99.30	99.47	99.47	99.30	98.95		100.00	100.00	100.00	100.00	100.00	100.00	100.00	100.00	100.00	100.00	100.00
VE-PCJ	LC433634	99.13	99.13	99.30	99.13	99.30	99.47	99.47	99.30	98.95	99.65		100.00	100.00	100.00	100.00	100.00	100.00	100.00	100.00	100.00	100.00
VE701	MN187035	98.78	98.78	98.95	98.78	99.47	99.13	99.13	98.95	98.95	99.30	99.30		100.00	100.00	100.00	100.00	100.00	100.00	100.00	100.00	100.00
VE702	MN187036	98.78	98.78	98.95	98.78	99.47	99.13	99.13	98.95	98.95	99.30	99.30	100.00		100.00	100.00	100.00	100.00	100.00	100.00	100.00	100.00
VE703	MN187037	98.95	98.95	99.13	98.95	99.47	99.30	99.30	99.13	99.13	99.47	99.47	99.82	99.82		100.00	100.00	100.00	100.00	100.00	100.00	100.00
VE704	MN187038	98.95	98.95	99.13	98.95	99.13	99.30	99.30	99.13	98.78	99.47	99.47	99.13	99.13	99.30		100.00	100.00	100.00	100.00	100.00	100.00
VE705	MN187039	98.95	98.95	99.13	98.95	99.47	99.30	99.30	99.13	99.13	99.47	99.47	99.47	99.47	99.65	99.30		100.00	100.00	100.00	100.00	100.00
VE706	MN187040	99.13	99.13	98.95	98.78	99.30	99.13	99.13	98.95	98.95	99.30	99.30	99.30	99.30	99.47	99.47	99.47		100.00	100.00	100.00	100.00
VE707	MN187041	98.95	98.95	99.13	98.95	99.13	99.30	99.30	99.13	98.78	99.47	99.47	99.47	99.47	99.65	99.30	99.30	99.13		100.00	100.00	100.00
VE708	MN187042	98.78	98.78	98.95	98.78	99.30	99.13	99.13	98.95	98.95	99.30	99.30	99.65	99.65	99.82	99.13	99.47	99.30	99.47		100.00	100.00
VE709	MN187043	99.13	99.13	98.95	98.78	98.95	99.13	99.13	98.95	98.61	99.30	99.30	98.95	98.95	99.13	99.47	99.13	99.65	99.13	98.95		100.00
VE823	MN187044	98.61	98.61	98.78	98.61	99.30	98.95	98.95	98.78	98.78	99.13	99.13	99.82	99.82	99.65	99.30	99.30	99.47	99.30	99.47	99.13	

Abbreviation: VE: citrus vein enation virus.

Table 2.9 Nucleotide (below diagonal) and amino acid (above diagonal) sequence identities (%) of citrus vein enation virus open reading frame 5 (ORF5).

Isolate	GenBank Accesssion Number	VE-1	VE-1	VE-SM	VE-YM1	VE-NGS	VE-IBK	VE-STM-1	VE-STM-2	VE-JJ	VE-PTC	VE-PCJ	VE701	VE702	VE703	VE704	VE705	VE706	VE707	VE708	VE709	VE823
VE-1	NC_021564		100.00	95.70	99.00	98.34	99.00	99.00	99.00	98.01	98.34	98.67	97.02	98.01	98.01	97.68	98.01	97.68	98.01	98.01	98.34	98.01
VE-1	HF679486	100.00		95.70	99.00	98.34	99.00	99.00	99.00	98.01	98.34	98.67	97.02	98.01	98.01	97.68	98.01	97.68	98.01	98.01	98.34	98.01
VE-SM	KY303624	96.69	96.69		96.36	96.69	96.69	95.70	95.70	96.36	97.02	96.69	96.69	96.69	96.03	95.70	96.03	97.35	96.03	96.03	97.35	96.03
VE-YM1	LC089850	98.67	98.67	96.69		98.67	99.33	99.33	99.33	99.00	99.33	99.66	98.01	99.00	99.00	98.67	99.00	98.67	99.00	99.00	98.67	99.00
VE-NGS	LC089851	98.01	98.01	96.69	98.45		99.33	98.01	98.01	98.34	98.67	99.00	98.01	98.34	98.34	98.01	98.34	98.67	98.34	98.34	99.33	98.34
VE-IBK	LC089852	98.78	98.78	97.02	99.22	98.78		98.67	98.67	99.00	99.33	99.66	98.01	99.00	99.00	98.67	99.00	98.67	99.00	99.00	99.33	99.00
VE-STM-1	LC089853	98.67	98.67	96.69	98.67	98.23	98.56		100.00	98.34	98.67	99.00	97.35	98.34	98.34	98.01	98.34	98.01	98.34	98.34	98.01	98.34
VE-STM-2	LC089854	98.56	98.56	96.58	98.56	98.12	98.45	99.88		98.34	98.67	99.00	97.35	98.34	98.34	98.01	98.34	98.01	98.34	98.34	98.01	98.34
VE-JJ	LC360112	97.90	97.90	96.58	98.56	98.78	98.67	98.34	98.23		99.00	99.33	97.68	98.67	98.67	98.34	98.67	98.34	98.67	98.67	98.34	98.67
VE-PTC	LC433635	98.23	98.23	96.69	98.89	98.45	99.22	98.23	98.12	98.56		99.66	98.34	99.00	99.00	98.67	99.00	99.00	99.00	99.00	99.33	99.00
VE-PCJ	LC433634	98.67	98.67	96.91	99.33	98.67	99.44	98.67	98.56	98.78	99.11		98.34	99.33	99.33	99.00	99.33	99.00	99.33	99.33	99.00	99.33
VE701	MN187035	97.79	97.79	96.91	98.45	98.23	98.78	98.23	98.12	98.12	98.45	98.67		99.00	98.34	97.68	98.01	99.33	98.34	98.01	98.34	98.34
VE702	MN187036	98.23	98.23	97.13	98.89	98.45	99.22	98.67	98.56	98.56	98.89	99.11	99.55		99.33	98.67	99.00	99.00	99.33	99.00	98.34	99.33
VE703	MN187037	98.01	98.01	96.69	98.67	98.23	98.78	98.45	98.34	98.34	98.67	98.67	98.67	99.11		98.67	99.00	98.34	99.33	99.00	98.34	99.33
VE704	MN187038	98.34	98.34	96.47	98.67	98.01	98.78	98.34	98.23	98.12	98.45	98.89	98.23	98.67	98.23		99.00	98.01	98.67	98.67	98.01	98.67
VE705	MN187039	97.57	97.57	95.81	98.23	97.79	98.34	97.57	97.46	97.68	98.23	98.23	97.79	98.23	98.67	97.79		98.34	99.00	99.00	98.34	99.00
VE706	MN187040	97.90	97.90	96.80	98.56	98.34	98.89	97.90	97.79	98.34	98.78	98.78	99.00	98.78	98.34	98.12	98.12		98.34	98.34	99.00	98.34
VE707	MN187041	97.68	97.68	96.36	98.56	97.90	98.45	98.12	98.23	98.01	98.34	98.34	98.34	98.78	99.44	97.90	98.34	98.01		99.00	98.34	99.33
VE708	MN187042	97.02	97.02	95.70	97.46	97.24	97.57	97.46	97.35	97.35	97.46	97.68	97.46	97.90	97.46	97.57	96.91	97.13	97.13		98.34	99.00
VE709	MN187043	98.01	98.01	96.91	98.23	98.45	98.78	98.01	97.90	97.90	98.45	98.45	98.45	98.67	98.23	97.79	98.12	98.12	97.90	97.24		98.34
VE823	MN187044	97.68	97.68	96.80	98.34	97.90	98.45	98.12	98.01	98.01	98.34	98.34	98.56	99.00	99.44	97.90	98.56	98.01	99.11	97.35	98.12	

Abbreviation: VE: citrus vein enation virus.

Table 2.10 Variable sites (%) and nucleotide sequence identities (%) of genomic regions of citrus vein enation virus isolates in this study and from NCBI GenBank database.

Genomic Region Sample Size	5'-Untranslated Region and Open Reading Frame 1 (1 - 2,201 nt)			Open Reading Frame 2 and Non-Coding Region (2,202 - 4,300 nt)			Open Reading Frame 3, 5 and 3'-Untranslated Region (4,301 - 5,983 nt)		
	Variable Sites (Variable/Total)	Minimum NSI*	NSI Mean ± SD	Variable Sites (Variable/Total)	Minimum NSI*	NSI Mean ± SD	Variable Sites (Variable/Total)	Minimum NSI*	NSI Mean ± SD
n= 21	8.72 (192/2201)	96.72	98.29 ± 0.59	9.10 (191/2099)	96.26	98.24 ± 0.64	8.02 (135/1683)	97.14	98.56 ± 0.44

Note: Nucleotide Position is based on reference genome of citrus vein enation virus isolate VE701 (NCBI GenBank Accession No MN187035).

*NSI: Nucleotide Sequence Identity.

Table 2.11 Variable sites (%) and nucleotide sequence identities (%) of the segmented open reading frame 3, 5 and 3'-untranslated region of citrus vein enation virus isolates in this study and from NCBI GenBank database (n=21).

Position (nt)	Variable Sites (Variable/Total)	Minimum NSI*	NSI Mean ± SD
4,301 - 4,530	3.48 (8/230)	97.82	99.57 ± 0.55
4,531 - 4,760	6.09 (14/230)	97.39	98.73 ± 0.62
4,761 - 4,990	4.78 (11/230)	97.82	99.18 ± 0.56
4,991 - 5,220	10.87 (25/230)	96.52	98.21 ± 0.72
5,221 - 5,450	10.43 (24/230)	94.34	98.24 ± 1.12
5,451 - 5,680	10.00 (23/230)	93.47	97.95 ± 1.24
5,681 - 5,983	9.90 (30/303)	96.36	98.16 ± 0.78

Note: Nucleotide Position is based on reference genome of citrus vein enation virus isolate VE701 (NCBI GenBank Accession No. MN187035).

*NSI: Nucleotide Sequence Identity.

Table 2.12 Citrus vein enation virus RT-qPCR assay developed in this study in detecting citrus vein enation viruses inoculated citrus plants.

Sample	Experiment	RNA Concentration (ng/µl)	OD 260/280 Ratio	COX (n=1)	CVEV Lab A[1] (n=4)	CVEV Lab B[2] (n=2)
Citrus vein enation virus						
VE701	2923-1	79.84	1.87	15.76	31.60 ± 0.21	32.39 ± 0.57
	11-16-94	51.28	2.17	15.13	17.12 ± 0.19	21.74 ± 0.51
	2923-1-2	86.32	2.06	14.35	16.09 ± 0.10	19.07 ± 0.97
VE702	2923-2	53.68	2.40	17.16	15.02 ± 0.06	18.82 ± 0.57
	1-8-04	62.16	1.99	14.80	32.02 ± 0.23	36.00 ± 0.61
	10-2-01	90.16	2.03	14.28	16.20 ± 0.04	18.80 ± 0.22
VE703	2923-3	59.28	2.08	15.41	20.87 ± 0.16	23.28 ± 1.18
	3-17-98	99.84	1.95	14.27	15.74 ± 0.14	17.53 ± 0.16
VE704	2923-4	74.40	2.14	15.68	20.78 ± 0.51	20.67 ± 0.07
	3-3-94	92.88	1.99	14.16	17.36 ± 0.04	18.60 ± 0.01
	2761-22	100.00	1.92	14.17	15.05 ± 0.11	17.20 ± 0.07
	2761-23	89.76	2.10	14.30	15.65 ± 0.05	19.65 ± 0.54
	2761-24	64.56	2.18	14.77	16.18 ± 0.16	20.12 ± 0.58
VE705	2923-5	40.40	2.24	15.27	28.55 ± 0.04	27.05 ± 0.56
	10-30-98	96.80	2.09	14.33	17.98 ± 0.02	18.12 ± 1.65
	2761-109	96.08	2.05	14.32	29.15 ± 0.17	29.85 ± 0.22
	2761-110	75.76	2.01	14.62	26.68 ± 0.10	28.66 ± 0.26
	10-30-98-2	72.40	2.17	14.85	18.23 ± 0.19	22.12 ± 0.67
VE706	2833-1	82.56	2.19	15.78	24.14 ± 0.33	25.50 ± 0.71
	7-8-98	56.64	2.13	15.06	16.97 ± 0.06	20.55 ± 0.28
	2833-2	92.80	2.03	14.60	14.98 ± 0.06	17.95 ± 0.52
VE707	3184-5,6	63.68	1.98	15.62	19.53 ± 0.36	18.96 ± 0.20
VE708	3273-14	73.68	2.13	15.26	22.74 ± 0.36	22.85 ± 0.38
	3273-13	98.88	1.99	14.33	15.81 ± 0.09	17.14 ± 0.13
	3273-15	52.80	2.22	15.50	15.94 ± 0.16	19.08 ± 0.25
VE709	3273-16	84.32	2.11	17.59	25.92 ± 0.48	27.72 ± 0.01
	3354-5	79.04	2.10	14.75	16.53 ± 0.07	19.07 ± 0.04
	3354-6	75.92	2.08	14.71	15.21 ± 0.17	18.76 ± 0.42
	3273-18	79.76	2.21	14.53	16.84 ± 0.09	16.35 ± 2.09
VE823	2923-6	82.56	2.08	15.19	30.69 ± 0.38	30.72 ± 0.20
	10-1-98	86.32	1.94	14.45	15.01 ± 0.04	16.43 ± 0.80
RT-qPCR Controls						
Positive	H12 / UCD*	NT	NT	14.77	14.77 ± 0.12	23.42 ± 0.20
Negative	861-S-1 / UCD*	NT	NT	15.64	-	-
No Template	H9 / UCD*	-	-	-	-	-

Abbreviations: Cq: quantitative cycle; VE/CVEV: citrus vein enation virus; COX: cytochrome oxidase gene of host plants used as positive internal control (Osman et al. 2015); NT: not tested.

[1] Lab A: Citrus Clonal Protection Program, University of California, Riverside, with ThermoFisher Scientific QuantStudio 12K Flex Real-Time PCR System.

[2] Lab B: Real-time PCR Research & Diagnostic Core Facility, University of California, Davis, with ThermoFisher 7900HT FAST Real-time PCR system.

* Different controls were used at Lab B.

Table 2.13 Citrus vein enation virus RT-qPCR assay validated for robustness.

| Isolates | Experiment | Citrus vein enation virus RT-qPCR Cq Value | | | | |
| | | Optimum* | Annealing Temperature** | | Pipetting Errors** | |
		60 °C / 12 μL	-2 °C	+2 °C	-2 μL	+2 μL
VE701	2923-1	31.60 ± 0.21	29.98 ± 0.08	29.36 ± 0.25	29.20 ± 0.04	31.45 ± 0.12
VE703	2923-3	20.87 ± 0.16	20.49 ± 0.04	19.64 ± 0.02	19.62 ± 0.26	21.55 ± 0.22
VE704	2923-4	20.78 ± 0.51	19.72 ± 0.10	19.19 ± 0.06	18.73 ± 0.03	21.24 ± 0.09
VE705	2923-5	28.55 ± 0.04	26.39 ± 0.10	25.89 ± 0.20	25.38 ± 0.04	28.01 ± 0.12
VE706	2833-1	24.14 ± 0.33	23.32 ± 0.17	22.35 ± 0.06	22.37 ± 0.11	24.50 ± 0.13
VE707	3184-5,6	19.53 ± 0.36	17.85 ± 0.25	17.16 ± 0.12	17.00 ± 0.06	19.22 ± 0.11
VE708	3273-14	22.74 ± 0.36	22.26 ± 0.22	21.47 ± 0.10	21.44 ± 0.08	23.62 ± 0.12

* Optimum setup was using the conditions validated and optimized in this study including volume, primer probe concentrations, annealing temperature, etc. And the reactions were run on ThermoFisher Scientific QuantStudio 12K Flex Real-Time PCR System.

** The RT-qPCR reactions were setup with same concentration of primers and probe and using Bio-Rad iTaq™ Universal Probes One-Step Kit per manufacturer's instruction. The reactions were run on Bio-Rad CFX-96 Real-Time PCR Detection System.

Table 2.14 Citrus vein enation virus RT-qPCR assay testing citrus vein enation virus-inoculated controls.

Sample	Origin	CVEV RT-qPCR Cq Value
Navel NSW	Australia	31.85
Rough Lemon NSW	Australia	21.34
Lisbon Lemon NSW	Australia	14.09
South Africa RSA 1	South Africa	23.28
South Africa RSA 2	South Africa	21.73
Spain CEV 1	Spain	20.04
Spain CEV 2	Spain	28.70

* RT-qPCR test was performed at Elizabeth Macarthur Agricultural Institute.

Abbreviations: Cq: quantitative cycle; CVEV: citrus vein enation virus.

Table 2.15 Citrus vein enation virus RT-qPCR assay testing non-inoculated citrus controls.

Citrus Host	Source / Registration number	RT-qPCR Cq Value	
		COX	CVEV
Mandarin (*C. reticulata* Blanco)			
Murcott Mandarin	1005674	16.30	-
Fairchild LS Mandarin	3014099	16.06	-
Ponkan Mandarin	1005802	16.33	-
CPB 6B-1-12 Mandarin	3014123	15.47	-
Hasen Mandarin	3014136	16.73	-
Fortune Mandarin	3014073	16.11	-
Imperial Mandarin	3014131	16.20	-
Tango Mandarin	1005668	15.31	-
Hasen Mandarin	1005994	15.28	-
Cleopatra Mandarin	1005683	15.14	-
Encore LS Mandarin	3014071	15.86	-
Primosole Mandarin	1005924	15.98	-
Tango Mandarin	1005666	14.48	-
Parson Special Mandarin	3014062	15.25	-
Sweet Orange (*C. sinesis* L. Osb.)			
Rio Grande Navel	1005810	15.43	-
Macetera Sweet Orange	3014130	16.12	-
Skaggs Bonanza Navel	1005797	15.90	-
T.I. Sheldon Navel	1005940	16.57	-
Chislett Navel	3003023	17.22	-
Autumn Gold Navel	1005884	16.65	-
Rocky Hill Navel	1005796	15.93	-
Powell Navel	3014088	16.50	-
Pehrson#4 Valencia	3014051	15.48	-
Pehrson#3 Valencia	1005873	15.62	-
Ceridwen Navel	3014139	16.59	-
Dream Navel	1005867	16.68	-
Ceridwen Navel	3014140	15.89	-
Summer Gold Navel	3014116	16.23	-
Rio Grande Navel	3014138	17.90	-
Robertson Navel	1005688	17.98	-
Robertson Navel	3014125	15.95	-
Cluster Navel	1005855	15.69	-
Cogan Navel	3014086	16.34	-
Bahianinha Araras Navel	1005995	16.28	-
Palmer Navel	1005795	16.04	-
Rocky Hill Navel	3014124	14.97	-
Johnson Navel	3014096	15.92	-
Ricalate Navel	3014068	15.65	-
Robyn Navel	1005689	14.73	-

Abbreviations: Cq: quantitative cycle; CVEV: citrus vein enation virus; COX: cytochrome oxidase gene of host plants used as positive internal control (Osman et al. 2015).

Table 2.15 Citrus vein enation virus RT-qPCR assay testing non-inoculated citrus controls (cont'd).

Citrus Host	Source / Registration number	RT-qPCR Cq Value	
		COX	CVEV
Tangor (*C. reticulata* × *C. sinensis*)			
Iyo Mikan Tangor	1005799	16.50	-
Iyo Mikan Tangor	3014148	15.69	-
Satsuma (*C. unshiu* (Macf.) Marc.)			
China S-9 Satsuma	1005895	16.73	-
China S-18 Satsuma	3015105	16.50	-
China S-20 Satsuma	3014064	15.79	-
China S-1 Satsuma	3015102	16.33	-
China 6-15 Satsuma	3014076	15.76	-
Selma Satsuma	1005914	15.91	-
China S-17 Satsuma	3014074	16.31	-
China S-18 Satsuma	3015104	17.04	-
China 6-18 Satsuma	3014065	15.77	-
Miho Wase Satsuma	1005691	15.43	-
Lemon (*C. limon* (L.) Burm.f.)			
Interdonato Lemon	1005731	15.97	-
Interdonato Lemon	3014137	16.92	-
Schaub Rough Lemon	1005710	14.66	-
Milsweet Limetta	1005725	14.85	-
Kumquat (*Fortunella* sp.)			
Marumi Kumquat	3014132	15.75	-
Fukushu Kumquat	3003057	15.27	-
Sour Orage (*C. aurantium* L.)			
Smooth Flat Seville Sour Orange	3014147	15.56	-
Lime (*C. aurantifolia* (Christm.) Swing.)			
Australian Finger Lime	1005608	16.20	-
Australian Finger Lime	1005610	15.94	-
Clementine (*C. clementina* Hort. ex Tan.)			
Marisol Clementine	3014101	14.49	-
SRA 92 Clementine	1005735	16.29	-
Caffin Clementine	1005962	17.97	-
Pummelo (*C. grandis* (L.) Osb.)			
Valentine Pummelo	3014144	16.23	-
Valentine Pummelo	3014143	14.52	-
Tangelo (*C. reticulata* x *C. paradisi*)			
Minneola Tangelo	1005678	15.65	-
Limequat (*Fortunella* sp. x *C. aurantifolia*)			
Eustis Limequat	1005814	15.08	-
Others			
X639	3014082	15.51	-
Rubidoux Trifoliate	1005905	16.11	-

Abbreviations: Cq: quantitative cycle; CVEV: citrus vein enation virus; COX: cytochrome oxidase gene of host plants used as positive internal control (Osman et al. 2015).

Table 2.16 Citrus vein enation virus RT-qPCR assay testing samples inoculated with non-targeted citrus pathogens.

Citrus Pathogen Isolate	Source / Registration number	RT-qPCR Cq Value		
		COX	CVEV	Target
Citrus tristeza virus (CTV)				
SY558	2987-58	16.85	-	30.64
SY568	2761-114	16.22	-	25.00
T514	T514-2	16.24	-	35.48
T525	3347-63	16.25	-	30.86
T538	3275-4	16.31	-	24.12
Citrus psorosis virus (CPsV)				
P201	1766-5	16.46	-	29.20
P203	2-26-98	16.34	-	28.73
P205	3347-8	16.81	-	31.94
P215	3169-15	16.98	-	34.58
P218	3175-2	16.60	-	29.53
Citrus leaf blotch virus (CLBV)				
CLBV, Spain	3069-1	15.37	-	27.06
Mix viruses: CLBV & CTV	3300-7	15.41	-	24.75 / 22.35
Citrus tatter leaf virus (CTLV)				
IPPN122	TH2986-48	17.03	-	30.33
TL103	3288-1	15.49	-	25.40
TL112 3291-1	3291-1	16.12	-	25.45
TL112 3291-9	3291-9	16.30	-	23.92
TL113 3291-10	3291-10	16.79	-	22.71
TL114 3291-11	3291-11	16.37	-	24.60
TL114 3291-3	3291-3	15.51	-	23.58
TL115	3170-1	16.50	-	26.35

Abbreviations: Cq: quantitative cycle; CVEV: citrus vein enation virus; COX: cytochrome oxidase gene of host plants used as positive internal control (Osman et al. 2015).

Table 2.16 Citrus vein enation virus RT-qPCR assay testing samples inoculated with non-targeted citrus pathogens (cont'd).

Citrus Pathogen Isolate	Source / Registration number	RT-qPCR Cq Value		
		COX	CVEV	Target
Infectious variegation virus (IVV)				
IV402	2923-10	15.27	-	27.85
Concave gum				
CG302	CG302 7-8-04	17.03	-	(+)*
CG308	2355-4	17.20	-	(+)*
CG309	CG309 11-14-96	15.90	-	(+)*
Citrus viroids				
Citrus bent leaf viroid LSS	3237-3	17.05	-	32.76
Citrus bent leaf viroid	2765-2	16.17	-	28.18
Citrus bent leaf viroid	2597-2	16.58	-	30.24
Hop stunt viroid, non-cachaxia	2765-4	16.55	-	25.68
Hop stunt viroid, cachaxia	2765-6	17.39	-	27.34
Citrus dwarfing viroid	2765-11	17.57	-	36.45
Citrus dwarfing viroid LFS	2765-12	17.58	-	30.96
Citrus bark cracking viroid	3200-1	17.99	-	28.49
Citrus viroid V	3198-5	16.15	-	33.62
Citrus exocortis viroid (CEVd)	2765-1	17.25	-	30.02
Mix viroids: Citrus dwarfing viroid & Citrus bark cracking viroid	2765-14	16.79	-	33.76 / 28.45
Mix viroids	3207-8	16.39	-	30.15 / 25.30
Candidatus Liberibacter				
asiaticus	HLB Daisy	15.62	-	21.29
asiaticus	HLB Lemon	17.06	-	27.04
asiaticus	HLB Valencia	16.27	-	28.61
Spiroplasma citri				
C189	C189 7-8-09	14.94	-	26.76
S600	S600 7-8-09	16.05	-	32.88

Abbreviations: Cq: quantitative cycle; CVEV: citrus vein enation virus; COX: cytochrome oxidase gene of host plants used as positive internal control (Osman et al. 2015).

Note: mixed viroids were tested with two universal detection assays targeting at apscaviroids and non-apscaviroids of citrus, respectively.

* Concave gum was tested by biological indexing.

PART B- Identification and Characterization of Viral Suppressors of RNA Silencing Encoded by Citrus tatter leaf virus and Citrus vein enation virus

CHAPTER 3: Two Distinct Viral Suppressors of RNA Silencing Encoded by Citrus tatter leaf virus

Abstract

Upon entry into host cells, viral proteins manipulate specific physiological processes or signaling pathways to subvert host defenses. In this study, two viral proteins of citrus tatter leaf virus (CTLV) were identified and have function in the suppression of host antiviral RNA silencing. Both coat protein (CP) and movement protein (MP) suppressed RNA silencing in *GFP*-transgenic *Nicotiana benthamiana* 16c plants through *Agrobacterium* co-infiltration assay. MP acted as a local viral suppressor of RNA silencing (VSR) while the CP acted as a systemic VSR. When the potato virus X (PVX) infectious vector harbored either the CP or MP, they both promoted viral infection and symptoms development, likely through their RNA silencing suppression activities as a protein. The PVX deletion assay, revealed that the region associated with suppression function were located at amino acids (aa) 36 to 70 for CP and 112 to 143 for MP. When these aa regions were deleted, the VSR failed to promote PVX infection as well as silencing suppression in *Agrobacterium* co-infiltration assay in *GFP*-transgenic *N. benthamiana* 16c plants. The results of mass spectrometry-based immunoprecipitation proteomics showed that neither CTLV CP nor MP interact with cellular components directly involved in host antiviral RNA silencing pathways and they are probably using other indirect mechanisms. Based on the results of RNA immunoprecipitation and RNA-protein pull down assays, CTLV MP

interacts with double-stranded RNA (dsRNA) presumably through a protein complex or proteins contain RNA binding domains. By using this mechanism, MP prevents dsRNA cleavage and further leads to suppression of host antiviral RNA silencing. These findings confirmed that RNA silencing suppression as a CTLV strategy to cause disease and overcome host antiviral defense and are indicative of how CTLV can infect a wide range of hosts including a variety of woody and herbaceous plants.

Introduction

Citrus tatter leaf virus (CTLV, synonym: citrange stunt virus) was first discovered in Chico, California, United States, in 1962 (Garnsey 1970; Wallace and Drake 1962). It was found in latently infected Meyer lemon trees (*Citrus Limon* (L.) Burm. F. hyb.), a cultivar imported by F. Meyer from Beijing, China around 1908 (Garnsey 1970; Wallace and Drake 1962, 1963; Zhang and Liang 1988).

CTLV is an endemic virus particular to mainland China (Zhang and Liang 1988) and widespread in both Taiwan (Nishio et al. 1982; Su and Cheon 1984) and Japan (Miyakawa 1980; Miyakawa and Matsui 1976; Miyakawa and Tsuji 1988). It is also found in Australia (Broadbent et al. 1994; Fraser and Broadbent 1979), South Africa (da Graca 1977), and in USA, which has been reported in California (Wallace and Drake 1962), Florida (Garnsey 1964, 1970; Tatineni et al. 2009b), and Texas (da Graca and Sharia 1996; Herron and Skaria 2000).

Most citrus trees and varieties remain asymptomatic after CTLV infection (Garnsey 1964; Garnsey and Jones 1968; Roistacher 1991; Wallace and Drake 1963). However, seedlings of Mexican lime (*C. aurantifolia* (Christm.) Swing.) inoculated with Meyer lemon tissue displayed symptoms of deformed young leaves and blotching (Calavan et al. 1963; Garnsey 1964, 1974; Roistacher 1991; Wallace and Drake 1962, 1963). CTLV causes "tatterleaf" in *Citrus excelsa,* as well as stunted growth, deformed leaves, chlorotic spots, and mottling in citranges which are used as indicator plants (Garnsey 1964, 1974; Garnsey and Jones 1968; Wallace and Drake 1962, 1963).

CTLV can be mechanically transmitted to a wide range of herbaceous hosts. The virus can infect approximately 51 plant species within 15 families, including but not limited to *Apocynaceae, Aizoaceae, Amaranthaceae, Caryophyllaceae, Chenopodiaceae, Compositae, Convolvulaceae, Cucurbitaceae, Gramineae, Leguminosae, Liliaceae, Pedaliaceae, Rutaceae, Scrophulariaceae* and *Solanaceae* (Inouye et al. 1979; Semancik and Weathers 1965). CTLV causes necrotic local lesions and variable systemic necrosis in cowpeas (*Vigna unguiculata*) and beans (*Phaseolus vulgaris*) (Inouye et al. 1979; Semancik and Weathers 1965). Chlorotic local lesions and systemic chlorotic mottle are produced in *Chenopodium quinoa* (Inouye et al. 1979; Semancik and Weathers 1965).

CTLV causes various symptoms when infecting trees propagated on trifoliate (*Poncirus trifoliata* (L.) Raf.) and trifoliate hybrid (*P. trifoliata* x *C. sinensis*) rootstock. The symptoms include stunted growth, chlorotic, virus-pronounced bud-union crease, fluting of the rootstock, and decline of the canopy, which may shear off around the bud-

union at high winds (Calavan et al. 1963; Garnsey 1964; Garnsey and Jones 1968; Roistacher 1991). This virus is readily transmitted mechanically with no evidence of natural vectors (Calavan et al. 1963; Garnsey 1964, 1970; Wallace and Drake 1963).

CTLV was known as a citrus viral disease with limited economic importance. However, this changed when the citrus tristeza virus (CTV) epidemic required the use of the CTV-tolerant trifoliate and trifoliate hybrids rootstocks (Calavan et al. 1963; Garnsey 1964; Garnsey and Jones 1968; Moreno et al. 2008; Roose 2014; Roose et al. 2015; Tatineni et al. 2009b).

In the early 1900s, CTV was the most economically important and damaging virus to citrus trees (Moreno et al. 2008). The CTV epidemic destroyed almost 100 million trees on sour orange rootstock (*C. aurantium,* L.) worldwide (Moreno et al. 2008; Roistacher 1991). This led to the replacement of the horticulturally-desirable sour orange rootstock with the CTV-tolerant trifoliate and trifoliate hybrid, such as Carrizo and Troyer Citrange (*P. trifoliata* x *C. sinensis*) (Moreno et al. 2008; Roose 2014; Tatineni et al. 2009b). However, these CTV-tolerant rootstocks are susceptible to the bud union incompatibility associated with CTLV. Therefore, CTLV is posing a major economic threat to the multi-billion dollars citrus industry of USA (Calavan et al. 1963; Garnsey 1964; Garnsey and Jones 1968; Tatineni et al. 2009b).

CTLV belongs to the genus *Capillovirus* of the *Betaflexiviridare* family in *Tymovirales*. CTLV is a single-stranded, positive-sense RNA virus with a long, rod-shaped virion which is 600 to 650 nm long and 13 to 19 nm wide (Nishio 1989; Semancik and

Weathers 1965). The complete CTLV genome sequence of a Meyer lemon isolate was determined to be 6,495 nucleotides (nt). The genomic structure was similar to other capilloviruses with two overlapping open reading frames (ORFs) and a poly (A) tail at the 3' end (Ohira et al. 1994; Ohira et al. 1995; Yoshikawa et al. 1993). The ORF1 of CTLV encodes a putative 242-kDa polyprotein (Ohira et al. 1995; Tatineni et al. 2009a; Tatineni et al. 2009b). This polyprotein contains a replicase coding region which includes putative methyltransferase, papain-like protease, helicase, and RNA-dependent RNA polymerase domains plus a 27-kDa coat protein (CP) (Tatineni et al. 2009a; Tatineni et al. 2009b; Yoshikawa et al. 1993). ORF2 encodes a putative 36-kDa movement protein (MP) (Tatineni et al. 2009a; Tatineni et al. 2009b). In addition, there are two unique regions in ORF1, variable region I and II, with low sequence identities among different isolates (Liebenberg et al. 2012; Tatineni et al. 2009b). It has been suggesting that both variable region I and II might be critical for CTLV infection and pathogenicity (Tatineni et al. 2009b).

Plants have evolved and developed defenses designed to detect invading organisms and stop them before they are able to cause extensive damages (Ding 2010; Jones and Dangl 2006). In addition to physical barriers, plant cells have the ability to detect invading pathogens through pathogen-associated molecular patterns (PAMPs) and respond with inducible defenses including PAMP- triggered immunity (PTI) (Ding 2010; Jones and Dangl 2006; Weiberg et al. 2014). Moreover, effectors secreted by pathogens can also induce effector-triggered immunity (ETI) upon R protein recognition (Jones and Dangl 2006; Pumplin and Voinnet 2013; Zvereva and Pooggin 2012).

Increasing studies have shown the critical role of small RNAs associated with host RNA silencing and regulation of host defenses and responses against pathogens (Ding 2010; Díaz-Pendón and Ding 2008; Katiyar-Agarwal and Jin 2010; Padmanabhan et al. 2009; Ruiz-Ferrer and Voinnet 2009). Small RNAs are short, 20-30 nucleotides, noncoding RNA molecules present in most of eukaryotes (Weiberg et al. 2014). They target mRNA, guide silencing, and regulate gene expression transcriptionally and post-transcriptionally in a sequence-specific manner (Katiyar-Agarwal and Jin 2010; Weiberg et al. 2014). Plants contain two major groups of small RNAs namely small interfering RNAs (siRNAs) and microRNAs (miRNAs), distinguished by their biogenesis and structure of precursors. In general, double-stranded RNA (dsRNA) are processed to small RNAs, siRNAs and miRNAs, by a family of RNase III-like enzymes known as Dicer proteins (Csorba et al. 2015; Katiyar-Agarwal and Jin 2010; Weiberg et al. 2014). Perfectly base-paired long dsRNA is the precursor of siRNAs, whereas the miRNA is typically processed from an imperfectly base-paired stem-loop region known as primary miRNA (pri-miRNA) (Ding 2010; Katiyar-Agarwal and Jin 2010). siRNAs and miRNAs act in an RNA-induced silencing complex (RISC), of which Argonaute protein (AGO) is a core component and exhibits structural similarity to RNase H (Csorba et al. 2015; Ding 2010; Katiyar-Agarwal and Jin 2010; Weiberg et al. 2014). The RISC loaded with siRNA or miRNA recognizes the complementary messenger RNA (mRNA), activates AGO1, cleaves such mRNA transcript and leads to RNA silencing or interfering (RNAi) (Díaz-Pendón and Ding 2008; Katiyar-Agarwal and Jin 2010). Through RNAi, small RNAs regulate many biological processes in plants including abiotic stress responses, development, metabolism,

maintenance of genome integrity, and immunity against pathogens (Baulcombe 2004; Khraiwesh et al. 2012).

It has been found that viral infection in most eukaryotic hosts induces production of virus-derived small interfering RNAs (vsiRNAs), which share similar features to host endogenous small RNAs and mediate RNAi resulting in specific antiviral immunity (Csorba et al. 2015; Ding 2010; Díaz-Pendón and Ding 2008; Pumplin and Voinnet 2013). In plant cells, viral dsRNA formed during replication is recognized as a virus-associated molecular pattern (VAMP), a category of PAMP, is processed into primary vsiRNAs by Dicers (Incarbone and Dunoyer 2013; Pumplin and Voinnet 2013). Secondary vsiRNAs can be further produced by the amplification process. The vsiRNA-loaded AGOs can target viral genomes or transcripts and promote antiviral immunity through RNA silencing (Csorba et al. 2015; Ding 2010; Incarbone and Dunoyer 2013; Pumplin and Voinnet 2013). In addition, spread of the mobile silencing signals from cell-to-cell and long distance with or ahead of the virus can direct specific antiviral silencing, thereby inhibit systemic infection (Díaz-Pendón and Ding 2008; Incarbone and Dunoyer 2013).

An invariable principle of the never-ending molecular arms race between pathogens and hosts is the ability of pathogens to avoid, actively suppress, or even hijack host defense pathways. Upon viral infection, plants can process viral genomes into vsiRNAs and use them to guide antiviral silencing (Csorba et al. 2015; Ding 2010; Díaz-Pendón and Ding 2008; Pumplin and Voinnet 2013). Therefore, successful infection requires viral elements which attenuate or completely inhibit this host defense process.

Viruses encode proteins for their replication, encapsidation and movement within their hosts. Some of the proteins have multiple functions and play a role in interfering with host RNA silencing pathways. These proteins are known as viral suppressors of RNA silencing (VSRs) (Li and Ding 2006). VSRs are associated with virus pathogenicity and can directly or indirectly suppress host silencing pathways and ultimately lead to enhanced virus accumulation, intensified disease symptoms, and facilitation of cell-to-cell and long-distance movement (Incarbone and Dunoyer 2013). The VSR-mediated silencing suppression can be divided into three major categories: (1) inhibition of vsiRNAs generation, (2) binding to vsiRNAs and inhibition of the RISC loading and (3) inhibition of RISC components (Katiyar-Agarwal and Jin 2010). Cucumber mosaic virus 2b protein interacts physically with siRNA-loaded RISC and inhibits RNA silencing action (Goto et al. 2007; Katiyar-Agarwal and Jin 2010; Zhang et al. 2006). The 2b protein also inhibits the production of RNA-dependent RNA polymerases 1 (RDR1)-dependent vsiRNAs (Díaz-Pendón and Ding 2008). In potyviruses, the helper component-proteinase (HC-Pro) is a multifunctional protein involved in aphid transmission, genome amplification, polyprotein processing, long-distance movement, synergism, and silencing suppression (Anandalakshmi et al. 1998; Brigneti et al. 1998; Carrington et al. 1996; Kasschau and Carrington 1998). More specifically, HC-Pro acts as a VSR and plays a critical role in the suppression of miRNAs, *trans*-acting siRNAs (tasiRNAs), and virus-induced gene silencing (VIGS) pathways. Analysis of the HC-Pro mutants illustrated that proteolytic activity, genome replication, and long-distance movement were dependent on the VSR activity (Kasschau and Carrington 2001).

Given the fact that CTLV has a wide range of hosts across at least 15 different families including herbaceous and woody plants, it can be assumed that the virus uses its viral proteins successfully to suppress host antiviral immunity and replicate inside all the different plants. Therefore, the purpose of this study is to identify and characterize the VSRs of CTLV and further reveal their targets in host and their suppression mechanisms.

Materials and Methods

Virus isolate, cloning of viral genes, microbial strains and growth conditions.

CTLV isolate TL100 was characterized in chapter 1 and used in this study. Its viral genes of CP and MP were cloned and studied. TL100 was collected from Texas, USA in 1958 and has been maintained in a Meyer lemon tree at the greenhouse of Citrus Clonal Protection Program (CCPP), University of California, Riverside. Total RNA of TL100 was extracted from 100 mg of phloem-rich bark of the last matured vegetative flush using TRIzol™ (Invitrogen™, Carlsbad, California, USA), a standard protocol with phenol-chloroform extraction, followed by isopropanol precipitation, and re-suspended in 50 µl of nuclease-free water. The total RNA was reverse-transcribed to cDNA using SuperScript™ II Reverse Transcriptase (Invitrogen™, Carlsbad, California, USA) with Oligo(dT)$_{12-18}$ (Invitrogen™, Carlsbad, California, USA) primer. Gene specific primers were designed to target CP and MP of TL100 isolate (Table 3.1). The CP and MP were individually amplified with Platinum$^{®}$ *Pfx* DNA polymerase (Invitrogen™, Carlsbad, California, USA)

and then cloned into entry vector of Gateway® system by using pENTR™ directional TOPO® cloning kit (Invitrogen™, Carlsbad, California, USA). With Gateway® LR Clonase™ II Enzyme Mix (Invitrogen™, Carlsbad, California, USA), the *in vitro* recombination was catalyzed between entry vector pENTR™ and destination vector, pEarleyGate100 (pEG100; no protein tag sequence) (Earley et al. 2006) or modified pEG100 with FLAG protein tag sequence downstream of the coding region to generate a plant expression clone pEG1001. Bacterial strains and constructs used in this study are listed in Table 3.2. *Escherichia coli* strain Top10 (Invitrogen™, Carlsbad, California, USA) and NEB® 5-alpha (New England Biolabs®, Ipswich, Massachusetts, USA) were used for molecular cloning (Table 3.2). Plasmids were transformed into *Agrobacterium tumefaciens* strain GV3101 (Wroblewski et al. 2005) and used for transiently expression of proteins in plants (Table 3.2). Both *E. coli* and *A. tumefaciens* were grown in Luria-Bactani (LB) liquid medium and/or agar with appropriate antibiotics supplements at 37°C and 28°C, respectively (Table 3.2).

Plants and growth conditions.

N. benthamiana wild-type and the transgenic line 16c which constitutively expresses GFP protein (Ruiz et al. 1998) were grown and maintained in a temperature-controlled growth room (20 - 24°C) and light (16h light/8h dark). Plants about 4 to 6-week-old were used for the experiments.

***Agrobacterium*-mediated transient expression in *N. benthamiana* leaves.**

A. tumefaciens strain GV3101 (Wroblewski et al. 2005) carrying desired constructs were used for transient expression experiments in *N. benthamiana* plants. Bacterial cells were resuspended in an infiltration buffer [10 mM $MgCl_2$, 10 mM 2-(N-Morpholino) ethanesulfonic acid (MES), pH 5.6, and 150 µM acetosyringone] to a final OD_{600} of 0.8 to 1.0 and incubated for at least 3 hours at room temperature before infiltration (Renovell et al. 2012). Fully expanded leaves of *N. benthamiana* plants at the six-leaf stage (4 to 6-week-old) were infiltrated with a 3 ml syringe without a needle.

RNA silencing suppression co-infiltration assay by *Agrobacterium*-mediated transient expression in *N. benthamiana* 16c plants and GFP imaging.

In RNA silencing suppression co-infiltration assays, equal volumes of an *Agrobacterium* cell suspension carrying the *35S*::*GFP* gene and another construct harboring CTLV viral gene or control were mixed to a final solution with OD_{600} 0.8 to 1.0 of each construct before infiltration. *Agrobacterium* carrying an empty vector with no insertion was used as a negative control. Constructs expressing cucumber mosaic virus protein 2b (CMV 2b) and citrus leaf blotch virus movement protein (CLBV MP) which belongs to *Betaflexiviridae* like CTLV, under the *35S* promoter, were used as positive VSR controls (Lucy et al. 2000; Renovell et al. 2012). Fully expended leaves of *N.*

benthamiana 16c plants at the six-leaf stage (4 to 6-week-old) were infiltrated with 3 ml syringe without a needle. The signal of green fluorescence was visualized under a handheld long-wavelength UV lamp at 5 days post inoculation (dpi) for local tissue and 14 dpi for systemic tissue (Blak-Ray® Model B-100 AP, Ultraviolet Products, Upland, California, USA). Experiments were repeated at least three times.

RNA blotting of *GFP* mRNA and siRNA.

The abundance of *GFP* mRNA and siRNA were examined at 5 dpi after *Agrobacterium* co-infiltration for the silencing suppression assay in the infiltrated leaf areas by RNA blotting. Non-infiltrated systemic tissue located at the upper part of *N. benthamiana* was also examined for *GFP* mRNA abundance at 14 dpi. Total RNA of each sample was extracted using TRIzol™ (Invitrogen™, Carlsbad, California, USA) as described previously. RNA quality and concentration were measured in a NanoPhotometer™ (Implen, Germany) and equal amount of RNA was loaded for electrophoresis and RNA blotting.

The abundance of *GFP* mRNA and siRNA were determined using non-radiolabeled digoxigenin (DIG)-labeled RNA probe specifically and complementary to the *GFP* sequence. The probe was generated by *in vitro* transcription and DIG-RNA labeling (Roche Sigma-Aldrich, St. Louis, Missouri, USA) using linearized plasmid pGEMT-Easy-GFP-T7 (Table 3.2) which the *GFP* sequence was cloned into pGEM®-T Easy Vector

Systems (Promega, Madison, Wisconsin, USA) with T7 promoter located at the downstream site. The ribosomal RNA (rRNA) and nucleolar small RNA U6 gene of *N. benthamiana* were used as loading controls.

RNA blotting was conducted using DIG Northern Starter Kit (Roche Sigma-Aldrich, St. Louis, Missouri, USA). 1 µg of total RNA was denatured at 65°C for 10 minutes in loading buffer contained 50% formamide, chilled on ice for at least 1 minute, separated by electrophoresis in formamide-formaldehyde denaturing 2% agarose gels in 3-(N-Morpholino) propanesulfonic acid (MOPS) buffer (20 mM MOPS, 5 mM sodium acetate, and 2 mM ethylenediaminetetraacetic acid (EDTA)) and capillary-transferred onto positively charged nylon membranes (GE Healthcare Amersham Hybond-N+) overnight or at least 6 hours using 20X saline sodium citrate (SSC) buffer (3 M sodium chloride and 0.3 M sodium citrate, pH 7.0).

To analyze *GFP*-derived siRNAs, 10 µg of total RNA were mixed with loading buffer which contained 50% formamide, heated at 70°C for 10 minutes, and separated in a 15% polyacrylamide Tris-borate-EDTA(TBE)-urea gel in TBE buffer and transferred onto membranes as mentioned above.

Then, the membranes were UV cross-linked with 12,000 µJoules per cm^2 for 2 minutes. The ribosomal RNA of *N. benthamiana* was detected to confirm equal loading amount by staining with methylene blue after the UV cross-linking step. Both mRNA and siRNA membranes were hybridized with DIG-labeled RNA probes specific for the *GFP* sequence to detect *GFP* mRNA or siRNA. The DIG-labeled U6 DNA probe (Table 3.1)

was used as well to confirm same loading amount of siRNA. The membranes were washed and developed to detect the chemiluminescent signals with ChemiDoc™ Imaging Systems (Bio-Rad, Hercules, California, USA).

Relative gene expression of *GFP* by RT-qPCR.

Primers and probe for a *GFP* RT-qPCR assay were designed using the Primer Express™ software (Thermo Fisher Scientific, Carlsbad, California, USA) and following the guidelines for designing RT-qPCR assays a 60°C optimum melting temperature for primers and a 10°C increase for qPCR probes was used to prevent the formation of primer dimers. The fluorophore used for the *GFP* probe was 6-carboxyfluorescein FAM and the 3' quencher was nonfluorescent quencher (NFQ) (Table 3.1). The homology of the primers and qPCR probe was confirmed by BLASTn search against the GenBank database.

Total RNA of each sample was extracted by TRIzol™ (Invitrogen™, Carlsbad, California, USA) and treated with DNase I (New England Biolabs®, Ipswich, Massachusetts, USA) before loading into PCR reactions. The *GFP* RT-qPCR reaction (10 µl) was performed using the TaqMan® RNA-to-C_T 1-Step Kit (Applied Biosystems, Carlsbad, California, USA) with 2.8 µL water, 5.0 µL 2X TaqMan RT-PCR Mix, 0.6 µL of each primer (600 nM as final concentrations), 0.25 µL probe (250 nM as final concentrations), 0.25 µL 40X TaqMan RT Enzyme Mix and 0.5 µL of RNA (50 ng) for each reaction. The cycling conditions were 48°C for 15 minutes for the reverse

transcription step, 95°C for 10 minutes during the first cycle to inactivate the RT enzyme and activate the PCR polymerase, followed by 40 cycles of 95°C for 15 seconds and 60°C for 45 seconds. This assay was validated and analyzed using a QuantStudio™ 12K Flex Real-Time PCR System (Thermo Fisher Scientific, Carlsbad, California, USA). Fluorescent signals were collected during the amplification cycle and the number of cycles required for the fluorescent signal to cross the threshold (Ct) was calculated and exported.

An RT-qPCR assay of *N. benthamiana* housekeeping gene protein phosphatase 2A (*NbPP2A*) (Liu et al. 2012) was designed (Table 3.1) and used as a normalizer in the quantitative gene expression analysis. The PCR reaction setup for *NbPP2A* was similar to *GFP* assay except the final concentration of each primer was 900 nM.

The relative standard curves for both assays were conducted to analyze their dynamic range, precision and efficiency. The slope of the standard curve and the coefficient of determination (R^2) were calculated using linear regression (Rasmussen 2001). Amplification efficiency (E) was calculated with the formula $E = 10^{(-1/\text{slope})} - 1$ (Pfaffl 2001; Svec et al. 2015).

Relative expression levels (fold change) of the genes of interest were calculated using the Pfaffl method (Pfaffl 2001), with buffer-treated sample as the mock control (expression level of 1) and *NbPP2A* as the reference gene (endogenous control). Gene expression data for sample were the mean of three biological replicates; each biological replicate was the mean of three qPCR technical replicates.

The relative expression data was analyzed and calculated by Duncan's Multiple Range Test (MRT) with significance level α=0.05. Duncan proposed this test in 1955, and provides a series of shortest significant ranges in order to compare differences between means (Bewick et al. 2004; Duncan 1955; Tallarida and Murray 1987). Each pair of means was compared against a different critical value which depends on the ranks of these means in the ordered array (Bewick et al. 2004; Duncan 1955; Tallarida and Murray 1987).

Potato virus X (PVX) Assay.

PCR products of CTLV CP and MP were digested with *Asc*I and *Not*I restriction enzymes (New England Biolabs®, Ipswich, Massachusetts, USA) and ligated into the PVX infectious clone, pGR106 (Jones et al. 1999), which carries the full PVX genome (Table 3.1 and 3.2). Recombinant plasmids were transformed into *A. tumefaciens* strain GV3101 (pMP90::pSOUP) (Table 3.2), and the resulting strains were used to infiltrate six-leaf stage wild-type *N. benthamiana* plants. The frameshift mutations of CTLV CP and MP were also constructed with the same nucleotide sequence of the gene but a stop codon at the beginning of the reading frame.

Total RNA was extracted from samples collected at 21 dpi which were infiltrated with pGR106 (PVX), pGR106-CTLV-CP (PVX-CTLV-CP), and pGR106-CTLV-MP (PVX-CTLV-MP) by using TRIzol™ (Invitrogen™, Carlsbad, California, USA). Viral RNAs were detected by RNA blotting with DIG-labeled RNA probe which was

complementary to the PVX coat protein (CP) encoding gene by *in vitro* transcription and DIG-RNA labeling (Roche Sigma-Aldrich, St. Louis, Missouri, USA) using the linear plasmid, pGEMT-Easy-PVX-CP-T7, with T7 promoter located at the downstream site. Northern blotting setup and analysis were the same as mentioned above.

The relative expression level of each sample was quantified by the RT-qPCR designed for targeting PVX CP gene with housekeeping gene *NbPP2A* used as a normalizer. Primers and probe of PVX CP RT-qPCR assay was designed using the Primer Express™ software (Thermo Fisher Scientific, Carlsbad, California, USA) and following the guidelines for designing RT-qPCR assays a 60°C optimum melting temperature for primers and a 10°C increase for qPCR probes was used to prevent the formation of primer dimers. The fluorophore used for the PVX CP probe was 6-carboxyfluorescein FAM and the 3' quencher was nonfluorescent quencher (NFQ) (Table 3.1). The homology of the primers and qPCR probe was confirmed by a BLASTn search against the GenBank database. RT-qPCR setup, run, and analysis were the same as described previously with 600 nM as final concentration of each primer and 250 nM as final concentration of probe.

The relative standard curves for the PVX assay was conducted to analyze its dynamic range, precision and efficiency. The slope of the standard curve and the coefficient of determination (R^2) were calculated using linear regression (Rasmussen 2001). Amplification efficiency (E) was calculated with the formula $E = 10^{(-1/\text{slope})} - 1$ (Pfaffl 2001; Svec et al. 2015).

Relative expression levels (fold change) of the genes of interest were also calculated using the Pfaffl method (Pfaffl 2001), with PVX (pGR106 without insertion) sample as the control (expression level of 1) and *NbPP2A* as the reference gene (endogenous control). Gene expression data for the sample were the mean of three biological replicates; each biological replicate was the mean of three qPCR technical replicates. The relative expression data was analyzed and calculated by Duncan's Multiple Range Test (MRT) as mentioned above.

Serial deletion assay of CTLV CP and MP on PVX infectious vector pGR106.

Serial deletion clones were constructed using PVX infectious vector harboring CTLV CP (pGR106-CTLV-CP) and MP (pGR106-CTLV-MP) with Q5 Site-Directed Mutagenesis Kit (New England Biolabs®, Ipswich, Massachusetts, USA) per manufacturer's instructions. Primer sets for each deletion clone were designed by using NEBaseChanger® online tool on New England Biolabs® website (http://nebasechanger. neb.com/) with deletion ranging from 42 to 117 base pairs (14 to 39 amino acids) on each deletion clone (Table 3.1, 3.2 and Figure 3.1). The deletion constructs were transformed into *A. tumefaciens* strain GV3101 (pMP90::pSOUP) (Table 3.2), and the resulting strains were then used to infiltrate six-leaf stage wild-type *N. benthamiana* plants. Total RNA was extracted from samples collected at 21 dpi which were infected with pGR106, pGR106-CTLV-CP, pGR106-CTLV-MP, and their deletion clones. Viral RNAs were detected and

quantified by the PVX CP RT-qPCR with housekeeping gene *NbPP2A* used as normalizers in quantitative relative gene expression analysis as mentioned above.

Protein extraction and western blotting analysis.

Total protein was extracted from 500 mg of agroinfiltrated *N. benthamiana* leaves tissue using 1mL extraction buffer GTEN (10% [v/v] glycerol, 25 mM Tris-HCl pH 7.5, 1 mM EDTA, 150 mM NaCl) with supplements of 2% [w/v] polyvinylpolypyrrolidone (PVPP), 10 mM dithiothreitol (DTT), 0.1% Tween 20, and 1X protease inhibitor cocktail for plant cell (Sigma-Aldrich, St. Louis, Missouri, USA) before use (modified from Moffett et al. 2002). The samples were mixed with the buffer by vortexing and incubated on ice for 10 minutes. Subsequently, the samples were centrifuged twice at 4°C and 13,500 rpm for 10 minutes to remove plant debris. The supernatant was transferred into a new tube for further analysis and testing.

The presence of specific proteins was detected by western blotting. The sample lysates were run on Mini-PROTEAN® TGX Stain-Free™ Gels (Bio-Rad, Hercules, California, USA) with 2X Laemmli sample buffer (Bio-Rad, Hercules, California, USA) using Mini-PROTEAN® Tetra Vertical Electrophoresis Cell System (Bio-Rad, Hercules, California, USA). The proteins were subsequently transferred to PVDF membranes using a wet transfer method with Mini Trans-Blot® Cell System (Bio-Rad, Hercules, California, USA). Following protein transfer, the membranes were blocked with blocking buffer (5%

nonfat powdered milk buffered in 20 mM Tris-HCl, pH 7.5, 150 mM NaCl, and 0.1% Tween 20 (TBST)). The primary antibody, monoclonal ANTI-FLAG® M2 antibody produced in mouse (Sigma-Aldrich, St. Louis, Missouri, USA), was diluted in blocking buffer at optimized dilution ratio 1:2000 and incubated with the membranes at 4°C, overnight. Following incubation with the primary antibody, the membranes were washed three times for 10 minutes each with TBST. After washing, the secondary antibody, anti-mouse IgG HRP-linked antibody (Cell Signaling Technology, Danvers, Massachusetts, USA), was diluted in blocking buffer at optimized dilution ratio 1:5000 and incubated with the membrane for at least 1 hour at room temperature with agitation. The membranes were washed three times with TBST and developed using SuperSignal™ West Pico PLUS Chemiluminescent Substrate (Thermo Fisher Scientific, Carlsbad, California, USA). The blots were incubated for 5 minutes and exposed to ChemiDoc™ Imaging Systems (Bio-Rad, Hercules, California, USA) to acquire image.

Mass spectrometry-based immunoprecipitation (IP) proteomics.

To profile the interacting proteins, co-immunoprecipitation followed by mass spectrometry proteomics was used as a high-throughput methodology to analyze and characterize such interactions (ten Have et al. 2011; Turriziani et al. 2016). To start, the total protein was extracted with GTEN buffer as previously described from the *N. benthamiana* infiltrated leaves overexpressing CTLV CP or MP and incubated with the anti-Flag M2 affinity gel (Sigma-Aldrich, St. Louis, Missouri, USA) overnight at 4°C with

gentle agitation. The bead control was included and run in parallel. The unbound proteins were washed out with cold GTEN washing buffer (10% [v/v] glycerol, 25 mM Tris-HCl pH 7.5, 1 mM EDTA, 150 mM NaCl) for 5 times. Proteins bound with the anti-Flag affinity gel were eluted using elution buffer (0.1 M glycine-HCl, pH 3.5). The IP products were analyzed by western blotting and submitted to IIGB Proteomics Core at the University of California, Riverside for mass spectrometry analysis. Briefly, the submitted IP products were digested using trypsin protease at 37°C overnight and then analyzed by LC-MS/MS. Both Ultraperformance Liquid Chromatography coupled with Quadrupole Time of Flight Mass Spectrometry (UPLC/QTOF-MS) and the next generation LTQ-Orbitrap Fusion LC/MS (Thermo Fisher Scientific, Carlsbad, California, USA) were used in this study. Protein identities of top candidates were determined by using the Mascot search engine against the *N. benthamiana* proteomic database (Boyce Thompson Institute for Plant Research, http://bti.cornell.edu/nicotiana-benthamiana/). The whole set of mass spectrometry-based IP proteomic screening was repeated twice.

Sample preparation and RNA immunoprecipitation (RIP).

RIP is largely used method to identify the physical association between individual proteins and RNA molecules *in vivo* (Gagliardi and Matarazzo 2016; Ramanathan et al. 2019; Selth et al. 2011). The approach is based on the use of a specific antibody against the protein of interest to pull down the target-RNA complexes. Any RNA that is associated

with this protein complex will be isolated and can be further analyzed by polymerase chain reaction-based methods.

First, the leaf samples of *N. benthamiana* 16c plants were collected from the *Agrobacterium*-mediated transient expression assay after 2 days of co-infiltration with *Agrobacterium* strains carrying *35S::GFP* and individual viral gene constructs. The total protein of each sample was extracted from 200 mg plant tissue by using 1 ml phosphate buffered saline (PBS) with supplements of 0.05% Tween 20, 1 mM PMSF (Invitrogen™, Carlsbad, California, USA) and 1X protease inhibitor cocktail for plant cell (Sigma-Aldrich, St. Louis, Missouri, USA). The samples were incubated on ice for 30 minutes and mixed briefly by vortexing every 10 minutes. Then, the samples were centrifuged twice at 4°C, 13,500 rpm for 10 minutes to remove plant debris. The supernatant was transferred into a new tube.

RIP assay was conducted using Immunoprecipitation Kit Dynabeads® Protein A (Invitrogen™, Carlsbad, California, USA) per manufacturer's instruction. In brief, 3.5 µg anti-Flag M2 as ligand (Sigma-Aldrich, St. Louis, Missouri, USA) was added to 35 µl magnet Dynabeads® to establish the binding and form the beads-antibody complex in PBS buffer plus 0.05% Tween 20 (PBST) (Figure 3.2). The protein lysate was added to the beads-antibody complex and incubated at room temperature for 15 minutes. After incubation, the "beads-antibody-target protein interacting complex" was washed three times with PBST buffer. Subsequently, the target protein and its interacting nucleic acids were eluted and further treated with DNase I (New England Biolabs®, Ipswich,

Massachusetts, USA) to remove DNA. The RT-PCR analysis was carried out targeting the *GFP* gene using specific primers (Table 3.1) and QIAGEN OneStep RT-PCR kit in a 25 µl reaction (5 µl 5X RT-PCR Buffer, 1 µl 10 mM dNTP, 1.5 µl 10 µM forward/reverse primer, 1 µl QIAGEN OneStep RT-PCR Enzyme Mix, 1 µl of RNA, and 14 µl nuclease-free water) per manufacturer's instruction running with 57°C as annealing temperature 35 cycles and examined by 1.5% agarose gel electrophoresis.

RNA-protein pull-down assay.

The dsRNA of *GFP* was transcribed using MEGAscript® RNAi Kit (Invitrogen™, Carlsbad, California, USA) per manufacturer's instruction. Two separate clones were made to incorporate T7 promoter at upstream (5' end) as well as at downstream (3' end) of *GFP* sequence, respectively (Figure 3.3; Table 3.2). The plasmids were digested either with *Mlu*I or *Nco*I restriction enzyme (New England Biolabs®, Ipswich, Massachusetts, USA) to linearize the plasmid and served as templates for *in vitro* transcription. The reaction contained 5 µg of linear DNA template, 2 µl 10X T7 reaction buffer, 2 µl of each 75 mM ATP/CTP/GTP/UTP solution, 2 µl T7 enzyme mix, and adjusted with nuclease-free water to 20 µl. The reactions were incubated at 37°C for 4 hours. Subsequently, both *GFP* transcripts were mixed (1:1 ratio), heated at 75°C for 5 minutes and left the mixture on the bench to cool down to room temperature. This allowed sense and antisense *GFP* to anneal and form dsRNA. Small interfering RNA of *GFP* was prepared by digesting *GFP* dsRNA with *E. coli* RNase III (Applied Biosystem, Carlsbad, California, USA) and further purified

by running the reaction over an Amicon® Ultra-0.5 centrifuge filter unit (MilliporeSigma, Burlington, Massachusetts, USA) and collecting the flow-through containing the small RNA.

The dsRNA and small RNA of *GFP* were labeled with a single biotinylated nucleotide to the 3' terminus using Pierce™ RNA 3' End Desthiobiotinylation Kit (Thermo Fisher Scientific, Carlsbad, California, USA) by adding 3 µl 10X RNA ligase reaction buffer, 1 µl RNase inhibitor, 1 µl biotinylated cytidine bisphosphate, 2 µl T4 RNA ligase, 15 µl 30% PEG, 50 pmol RNA, and adjusted to 30 µl with nuclease-free water. The reactions were incubated at 16°C overnight and further purified by chloroform:isoamyl alcohol extraction and ethanol precipitation. Then, the labeled RNA was used in RNA-protein pull-down assay using Pierce™ Magnetic RNA-Protein Pull-Down Kit (Thermo Fisher Scientific, Carlsbad, California, USA) per manufacturer's instruction. The labeled RNA (50 pmol), either dsRNA or small RNA, was captured by streptavidin magnetic beads (50 µl). Then, the protein lysate (60 µl) extracted by GTEN buffer as mentioned above was added to the beads-RNA complex along with 10 µl 10X protein-RNA bunding buffer and 30 µl 50% glycerol. The reactions were incubated at 4°C for 60 minutes with agitation followed by the washing and the elution steps. The elute was examined by western blot analysis as described previously. The inputs of protein samples and RNA species were also examined by using western blot and polyacrylamide gel electrophoresis, respectively.

Results

CTLV CP and MP are viral suppressors of RNA silencing (VSRs) as identified by *Agrobacterium*-mediated transient expression in *N. benthamiana* 16c plants.

RNA silencing in plants is commonly induced and visualized using the *Agrobacterium* co-infiltration assay in *N. benthamiana* line 16c (Ruiz et al. 1998) with a stable integrated expressed *GFP* gene (endogenous) under the control of the cauliflower mosaic virus *35S* promoter. This assay provides a convenient system to screen and identify VSRs by co-infiltration with *Agrobacterium* containing a *GFP* expressing plasmid (exogenous) to induce *GFP* silencing and a test plasmid carrying CTLV VSR candidate to suppress such silencing. The siRNA-mediated RNA silencing is induced by endogenous and exogenous *GFP* genes expressing low, or no, green fluorescence in infiltrated areas at 5 to 7 dpi (Figure 3.4 a; no suppression / silenced). However, if the VSR candidate protein has the ability to suppress siRNA-mediated RNA silencing, such as CMV 2b, a strong green fluorescence is detected (Figure 3.4 a; suppression- local VSR). The *GFP* transgene silencing is typically observed in upper leaves and axillary shoots with little or no detectable GFP signal at 14 to 21 dpi (Figure 3.4 b; no suppression / silenced). However, if VSR inhibits systemic siRNA biogenesis or movement, it will also suppress systemic silencing of *GFP* (Figure 3.4 b; suppression- systemic VSR).

To identify the VSR of CTLV, both CP and MP were cloned individually under *35S* promoter in plant expression binary vectors. All the expression clones were agroinfiltrated and examined by western blotting to confirm the protein expression in *N.*

126

benthamiana (Figure 3.5 a). The expression vector without insertion was used as a negative empty vector control (Figure 3.5 a). CMV 2b and CLBV-MP, were used as VSR controls which suppressed both local and systemic RNA silencing (Figure 3.5 b and Table 3.3). When observed under UV light at 5 dpi, the CP of CTLV had no local silencing suppression ability since it produced similar patterns with the empty vector control in which a GFP fluorescence signal was not visualized locally (Figure 3.5 b and Table 3.3). On the other hand, the CTLV MP co-infiltration area had local suppression of RNA silencing at 5 dpi with 46% suppression rate which was similar to CLBV MP (41%) but less than CMV 2b (100%) (Figure 3.5 b and Table 3.3). Non-inoculated upper / systemic leaves were observed at 14 dpi. The showed that CTLV CP induced higher silencing suppression rate (44%) than CLBV MP (15%) but less in comparison to CMV 2b (100%) (Figure 3.5 b and Table 3.3). The CTLV MP did not display any suppression in non-inoculated systemic leaves (Figure 3.5 b and Table 3.3).

The abundance of *GFP* mRNA and *GFP* siRNA were examined by northern blot to confirm the suppression of RNA silencing. Northern blot hybridization was conducted using Digoxigenin (DIG) RNA labeling probes specifically for the positive strand of *GFP* RNA. In infiltrated leaf areas, the empty vector control and CTLV CP showed reduced *GFP* mRNA accumulation with increased abundance of *GFP* siRNA (Figure 3.5 c; local). However, leaves co-infiltrated with *GFP* expressing vector and CMV 2b, CLBV MP or CTLV MP strongly reduced the abundance of *GFP* siRNA, leading to increased accumulation of *GFP* transcripts (Figure 3.5 c; local).

Both empty vector and CTLV MP showed lower abundance of *GFP* transcripts in upper and non-inoculated tissue which small RNAs might act as signals that move systemically to induce small RNA-mediated gene silencing in newly emerging leaves (Figure 3.5 c; systemic). However, CMV 2b, CLBV MP and CTLV CP suppressed the systemic silencing of *GFP* with higher *GFP* mRNA accumulation (Figure 3.5 c; systemic). These results confirmed that CTLV has two VSRs. MP has suppression activity in local RNA silencing and CP has the ability to interfere with RNA silencing systemically.

In order to quantify the relative gene expression level of *GFP* in each sample, RT-qPCR assays for *GFP* and one endogenous gene control, *NbPP2A*, were designed and validated. The *GFP* RT-qPCR showed a linear dynamic range with R^2 equal to 0.9999 and 102.1% as its efficiency (Figure 3.6 a). The *NbPP2A* RT-qPCR also showed a linear dynamic range with R^2 equal to 0.9996 and 103.3% as its efficiency (Figure 3.6 b). Relative expression levels (fold change) of the *GFP* were calculated using the Pfaffl method (Pfaffl 2001) with mock as the control (expression level of 1) and *NbPP2A* as the endogenous gene control.

In local and infiltrated leaves, CMV 2b, CLBV MP and CTLV MP had significantly higher *GFP* expression than empty vector control (Figure 3.7 a; significance level α=0.05). In systemic and non-infiltrated leaves, CMV 2b, CLBV MP and CTLV CP had the *GFP* expression level significantly higher than empty vector control (Figure 3.7 b; significance level α=0.05). The results were consistent with the UV observation and RNA blot analysis and further confirmed that CTLV CP and MP are VSRs.

PVX infectious vector harboring CTLV CP or MP induced more severe symptoms and had higher viral RNA accumulation.

To test whether CTLV CP and MP are capable of suppressing siRNA-mediated host immunity, CP and MP were introduced individually into the PVX genome in an infectious clone, pGR106, and examined their effects on viral virulence. Unlike *N. benthamiana* plants infected with wild-type PVX (pGR106 without insertion), plants infected with PVX harboring either CTLV-CP (PVX-CTLV-CP) or MP (PVX-CTLV-MP) showed more severe mosaic and leaf deformation symptoms on newly emerged leaves along the apical shoots (Figure 3.8 a). Consistent with enhanced disease symptoms, northern blot analysis showed that viral RNAs accumulated to a much higher level in PVX-CTLV-CP infected tissues compared to wild-type PVX (Figure 3.8 b). PVX-CTLV-MP also enhanced disease symptoms and viral RNA accumulation (Figure 3.8 b), although to a lesser extent than PVX-CTLV-CP.

The relatively gene expression level of PVX viral RNAs in each sample were quantified by using RT-qPCR assays targeting PVX CP gene and *NbPP2A* as endogenous gene control. The PVX RT-qPCR assay validation showed a linear dynamic range with R^2 equal to 0.9998 and 100.1% as its efficiency (Figure 3.9). PVX-CTLV-CP and PVX-CTLV-MP infected tissues had nearly 25-fold and 10-fold more viral RNAs, respectively, than the wild-type PVX. Frameshifting mutation controls of CTLV CP and MP exhibited

mild or no mosaic symptoms and had similar virulence and fold change in comparison to wild-type PVX (Figure 3.10 a and b; significance level α=0.05).

PVX infectious vector harboring CTLV CP with deletion from 36 to 70 amino acids lost its function in promoting symptoms development and viral RNA accumulation.

To identify the regions of CTLV CP associated with host silencing suppression, clones with serial deletions were constructed in the PVX infectious vector and agroinfiltrated into wild type *N. benthamiana* (Figure 3.11 a). The newly emerged leaves along the apical shoots were observed at 21 dpi. Among PVX-CTLV-CP deletion clones, leaves infected with PVX-CTLV CP$^{\Delta 36-70}$ (D2) did not show mosaic symptoms and leaf deformation which were similar to the leaves infected with wild-type PVX (Figure 3.11 a). The symptom development of other deletion clones was similar to PVX-CTLV-CP (Figure 3.11 a). Quantitative analysis also showed that CTLV CP$^{\Delta 36-70}$ (D2) had the lowest PVX viral RNA accumulation (Figure 3.11 b; significance level α=0.05). Therefore, it can be assumed that the functional region associated with silencing suppression activity on CP is located within 36 and 70 amino acids.

PVX infectious vector harboring CTLV MP with deletion from 112 to 143 amino acids lost its function in promoting symptoms development and viral RNA accumulation.

To identify the regions of CTLV MP associated with host silencing suppression, clones with serial deletions were constructed in the PVX infectious vector and agroinfiltrated into wild type *N. benthamiana* (Figure 3.1 b). The newly emerged leaves along the apical shoots were observed at 21 dpi. Among PVX-CTLV-MP deletion clones, leaves infected with PVX-CTLV MP$^{\Delta112-143}$ (D4) did not show mosaic symptoms and leaf deformation were similar to the leaves infected with wild-type PVX (Figure 3.12 a). The symptom development of other deletion clones was similar to PVX-CTLV-MP (Figure 3.12 a). Quantitative analysis also showed that CTLV MP$^{\Delta112-143}$ (D4) had the lowest PVX viral RNA accumulation (Figure 3.12 b; significance level $\alpha=0.05$). Therefore, it can be assumed that the functional region associated with silencing suppression activity on MP is located within 112 and 143 amino acids.

CTLV CP$^{\Delta36-70}$ and MP$^{\Delta112-143}$ lost their activity in silencing suppression.

To confirm the associated functional regions identified in the CTLV CP and MP, an *Agrobacterium*-mediated transient expression assay in *N. benthamiana* 16c plants was used with co-infiltration of expressing vectors *GFP* and CP$^{\Delta36-70}$ (D2) or MP$^{\Delta112-143}$ (D4). The protein expression level of CP$^{\Delta36-70}$ and MP$^{\Delta112-143}$ were confirmed by western blot analysis (Figure 3.13 a). When observed at 5 dpi under UV light, the infiltrated area with MP of CTLV had mild-to-strong silencing suppression ability and a GFP signal was visualized. However, CTLV MP$^{\Delta112-143}$ lost its local silencing suppression activity and showed no or low GFP signal (Figure 3.13 b; local). The systemic leaves were observed at

14 dpi and CTLV CP$^{\Delta 36\text{-}70}$ also lost its systemic silencing suppression activity with no or low GFP signal (Figure 3.13 b; systemic). The suppression rate of both CTLV CP$^{\Delta 36\text{-}70}$ and MP$^{\Delta 112\text{-}143}$ was also decreased (Table 3.4). The results of the quantitative analysis were consistent with the UV light observations (Figure 3.13 b, c and d). The analysis of local infiltrated leaves confirmed that MP$^{\Delta 112\text{-}143}$ had lower *GFP* relative expression level than the wild-type MP and empty vector control (Figure 3.13 c; significance level α=0.05). The analysis of systemic leaves also confirmed that CP$^{\Delta 36\text{-}70}$ had lower *GFP* expression than the wild-type CP and empty vector control (Figure 3.13 d; significance level α=0.05). These results indicated that both CTLV CP$^{\Delta 36\text{-}70}$ and MP$^{\Delta 112\text{-}143}$ lost their suppression activity due to the deletion of their functional regions associated with host RNA silencing suppression.

Mass spectrometry-based immunoprecipitation proteomics showed that CTLV CP and MP did not directly interact with major host cellular proteins in RNA silencing pathway.

To reveal the identity of the CTLV CP and MP-associated proteins, products of immunoprecipitation were analyzed by mass spectrometry. The analysis of both CTLV CP and MP generated long lists of identified proteins. The exponentially modified protein abundance index (emPAI) was used to filter data based on the abundances of the proteins interacted with either CP or MP. The emPAI is quite useful for obtaining a broad overview of proteome profiles. With emPAI equal or greater than 1, total 100 protein hits were found

in CP-expressing sample but not in the control (Table 3.5). For MP, total 98 protein hits were found (Table 3.6). However, the major protein components in host RNA silencing pathway were not identified in either CTLV CP or MP expressing samples (Table 3.5 and 3.6). These results indicated that the CTLV CP and MP do not suppress host RNA silencing through direct interactions with the protein components of the pathway.

CTLV MP interacted with the dsRNA of GFP in RNA Immunoprecipitation (RIP) assay.

Other than targeting protein components, the VSRs can interact with dsRNA and/or siRNA species produced in the host RNA silencing pathway (Csorba et al. 2015; Incarbone and Dunoyer 2013; Mérai et al. 2006; Vargason et al. 2003). To investigate if CP and MP interact with dsRNA, an RNA immunoprecipitation (RIP) assay was conducted using *Agrobacterium* transient expression assay co-infiltrated with both VSR and *GFP* expressing vectors into *N. benthamiana* 16c plants where the host silencing was induced and the dsRNA of *GFP* was formed *in planta*. Turnip crinkle virus (TCV) P38 protein was used as a VSR control proven previously to interact with long dsRNAs to suppress host RNA silencing (Incarbone and Dunoyer 2013; Mérai et al. 2006). The dsRNAs of *GFP* were precipitated along with CTLV MP and TCV P38 (Figure 3.14). In addition, the deletion clone, MP$^{\Delta112-143}$, lost the binding ability to dsRNA (Figure 3.14). On the other hand, CTLV CP did not show any interaction with dsRNA (Figure 3.14).

CTLV CP and MP did not interact directly with dsRNA of *GFP* in an *in vitro* RNA-protein pull-down assay.

To further investigate if CTLV CP and MP interact with dsRNA, an RNA-protein pull-down assay was performed. In this assay, the *in vitro* transcribed and 3' end biotinylated dsRNA of *GFP* was used to pull down the interactive proteins that have ability to bind to dsRNA. Western blot analysis showed that the P38 of TCV was pulled down by the dsRNA of *GFP* (Figure 3.15 a). However, the CTLV CP and MP were not detected in the blot (Figure 3.15 a).

CTLV CP and MP had no direct interaction with siRNA of *GFP* in an *in vitro* RNA-protein pull-down assay.

To investigate if CTLV CP and MP interact with siRNA, an RNA-protein pull-down assay was performed. The siRNA of *GFP* were produced from *in vitro* transcribed dsRNA with subsequent RNase III digestion and 3' end biotinylation. Tomato bushy stunt virus (TBSV) P19 protein was used as a VSR control proven previously to interact with siRNA to suppress host RNA silencing (Incarbone and Dunoyer 2013; Vargason et al. 2003). TBSV P19 protein was pulled down and detected in western blot analysis, however, CTLV CP and MP did not show any direct interaction with siRNA (Figure 3.15 b).

Discussion

Viruses have been found to evolve and utilize silencing suppressors or VSRs to counteract the host antiviral defense mechanisms such as RNA silencing by inhibiting or blocking such mechanisms at different levels (Burgyán and Havelda 2011; Csorba et al. 2015; Ding 2010; Díaz-Pendón and Ding 2008; Incarbone and Dunoyer 2013; Pumplin and Voinnet 2013; Roth et al. 2004; Song et al. 2011; Wang et al. 2012; Wu et al. 2010). In this study, two VSRs of CTLV were identified exhibiting distinct features in silencing suppression.

Co-infiltration assays of *GFP*-transformed *N. benthamiana* 16c plants showed that CTLV MP was able to inhibit local RNA silencing and reduce siRNA accumulation. In addition, CTLV CP was shown to prevent *GFP* silencing in systemic tissues. However, these assays, along with observations under UV light and northern blot analysis, tend to be more qualitative rather than quantitative (Stephan et al. 2011). Therefore, *GFP* RT-qPCR as well as the RT-qPCR targeting the endogenous *NbPP2A* gene were designed and validated to access relative expression level of *GFP* in each sample. Our results showed that RT-qPCR allows an accurate assessment of *GFP* expression to be determined in plants when comparing to *GFP* mRNA detection via northern blots. This approach was also highly compatible with the widely used agroinfiltration assay.

The CTLV MP was confirmed as a local VSR which is similar to the CLBV MP (Renovell et al. 2012). Since both CTLV and CLBV belong to the *Betaflexiviridae* family, it is possible that viruses within this family use their MPs as universal local VSRs despite

135

their low sequence similarity. In addition, both CLBV MP and CTLV MP possess activities in silencing suppression which might benefit their evolutionary and adaptation to different hosts.

Previous studies showed that CLBV MP had activity only in suppression of local RNA silencing (Renovell et al. 2012). However, in this study, the systemic silencing suppression of CLBV-MP was demonstrated. The suppression rate was very low (15%; Table 3.3) and the relative expression levels were similar when compared to the CMV 2b (Figure 3.7 b).

CTLV MP also showed significantly higher *GFP* expression levels than the empty vector control in systemic tissues indicating that MP had some suppression activity toward systemic silencing. However, when compared to other systemic VSR controls such as CMV 2b and CLBV MP, the relative expression level of the CTLV MP was significantly lower with more than 50% difference (Figure 3.7 b). Previous studies have suggested that VSRs not only contribute to suppression of host gene silencing but also interfere with host microRNA (miRNA) pathway required for normal plant growth and development (Liu et al. 2017; Wang et al. 2012). VSRs can also cause developmental abnormalities in processes such as cell division, leaf deformation, and flower development by affecting the function of miRNA and the expression machinery in plant cells (Wang et al. 2012). Therefore, it is possible that the observed systemic suppression activity of CTLV MP may be due to the potential of the VSR in interfering with plant development, resistance

responses, host gene expression as well as disruption of miRNA function (Liu et al. 2017; Wang et al. 2012).

The CP of CTLV was proven to carry silencing suppression activity in systemic tissues but with low suppression rate. These results indicated that there might be other determinants affecting the silencing suppression efficiency and activity of CP. Besides working as VSRs, viral proteins also fulfill other functions during virus infection. For instance, the CP of RNA virus usually has multiple functions including but not limited to virus entry, disassembly, translation of viral RNAs, RNA replication, virus movement, transmission and symptom development (Weber and Bujarski 2015). Silencing functions could have become established in the cases where a balance between the positive effects on the virus life cycle and negative effects on the host was achieved (Csorba et al. 2015). Therefore, the trade-off among the different CP functions might have influenced the silencing suppression activity of CTLV CP.

The VSR activity of both CTLV CP and MP was also confirmed by agroinfiltration assays in wild-type *N. benthamiana* plants following expression with PVX infectious vector in a virus-induced gene silencing (VIGS) background (Galiakparov et al. 2003; Jones et al. 1999). In this experiment, CTLV CP and MP expressed from PVX infectious clone had dramatic effects on symptom development and viral RNA accumulation on *N. benthamiana*. Both proteins acted as pathogenicity determinants to promote PVX viral infection, likely through their RNA silencing suppression activities (Galiakparov et al. 2003; Qiao et al. 2013; Zhou et al. 2006). The frameshifting controls also proved that the

137

silencing suppression activity was determined by the proteins themselves instead of their mRNA sequences.

In conclusion, our experiments clearly demonstrated that both CTLV CP and MP suppress viral and transgene-induced RNA silencing and reduce or abolish the accumulation of silencing-associated siRNAs.

VSRs usually have functional domains that interact with host proteins or RNA targets leading to suppression of host RNA silencing (Kasschau et al. 1997; Qu and Morris 2005). Therefore, deletion or interruption of such functional regions should result to failure of VSRs to suppress host RNA silencing. Based on the data, the regions associated with silencing suppression are bearing within 36 to 70 amino acid of CP and 112 to 143 amino acid of MP. However, further experiments are needed to identify the specific domains, motifs or amino acid sites required for suppression.

VSRs interact with several host proteins associated with the antiviral RNA silencing pathway and inhibit the silencing through multiple mechanisms. VSRs have been found to target AGOs as well as Dicer proteins, Dicer-like (DCL) proteins, RNA-dependent RNA polymerases (RDRs), double-stranded RNA binding (DRB) proteins and co-factors of host (Burgyán and Havelda 2011; Csorba et al. 2015; Díaz-Pendón and Ding 2008; Incarbone and Dunoyer 2013; Pumplin and Voinnet 2013). According to mass-spectrometry proteomics analysis, CTLV MP, as a local VSR, did not directly interact with any protein components associated with host RNA silencing pathway and might target

other endogenous host regulators and factors to further modulate host antiviral defense indirectly (Csorba et al. 2015).

Several studies showed that VSRs suppress host gene silencing systemically by inhibiting or blocking the proteins involved in amplification of secondary vsiRNAs and the spread of vsiRNAs which move through plasmodesmata for cell-to-cell movement and further to the phloem and induce silencing in systemic tissues (Csorba et al. 2015; Díaz-Pendón and Ding 2008; Incarbone and Dunoyer 2013; Martín-Hernández and Baulcombe 2008; Qu et al. 2005; Schwach et al. 2005). However, based on the mass-spectrometry proteomics analysis, CTLV CP, a systemic VSR, did not show any direct interactions with host RDRs or cofactors. There is a possibility that CTLV CP interacts with other host regulators that contribute to inhibition of silencing signal amplification and its spread through an indirect mechanism.

Instead of targeting at proteins associated with the silencing pathway, some VSRs bind to RNA components such as long dsRNA or siRNA to suppress the antiviral defense (Burgyán and Havelda 2011; Csorba et al. 2015; Díaz-Pendón and Ding 2008; Incarbone and Dunoyer 2013; Pumplin and Voinnet 2013). The RIP results showed that CTLV MP was able to bind to dsRNA contributing to the silencing suppression probably by preventing dsRNA to be processed by the Dicer proteins. However, we could not rule out the possibility that CTLV MP can also interact with single-stranded RNA of *GFP* in this RIP setup. Therefore, the interaction between MP and dsRNA was further examined by RNA-protein pull-down assay using *in vitro* transcribed dsRNA and MP-overexpressed

protein lysate. The interaction between dsRNA and CTLV MP was not found indicating that MP might either bind to dsRNA indirectly with the help of a protein or protein complex contains RNA binding domains or utilize other indirect mechanisms to suppress host RNA silencing.

CTLV CP, as a systemic VSR, did not show any direct interaction with siRNAs which can move systemically (Martín-Hernández and Baulcombe 2008; Qu et al. 2005; Schwach et al. 2005). This assumed that CTLV CP uses indirect strategies to suppress systemic gene silencing.

Both CTLV CP and MP are weak VSRs, similar to CLBV MP, when compared to CMV 2b (Renovell et al. 2012). A virus carrying weak VSRs tends to co-exist with hosts rather than accumulate high virus titer and cause severe damage or death to the plants (Renovell et al. 2012). This is more beneficial to the co-evolution between CTLV and its hosts in the pathogenicity point of view. These two VSRs could be the key factors responsible for the evolution and pathogenicity of the CTLV which only causes mild symptoms or remains symptomless on most its wide range of hosts.

Actually, the potential of CTLV causing serious problems to citrus production is a man-made situation in which a CTLV-infected scion is grafted on a trifoliate or trifoliate hybrid rootstock leading to budunion incompatibility, canopy decline and tree death (Calavan et al. 1963; Garnsey 1964; Garnsey and Jones 1968; Roistacher 1991). The virus could not encounter the situation of scion grafted on rootstock under its natural evolutionary process. Therefore, the balance or non-pathogenic existence of the virus in its

host was disrupted due to this man-made host environment. This is not the first case in citrus pathology that such situation occurred. The most catastrophic virus epidemic in citrus occurred in a similar man-made scion-rootstock environment. Citrus tristeza virus (CTV) is causing stem pitting disease in some sensitive citrus hosts. Stem pitting reduces fruit yield but in general is not lethal (Moreno et al. 2008; Roistacher 1991). However, when CTV encountered man-made environment of sweet orange scion grafted on sour orange rootstock, the quick decline disease emerged (Moreno et al. 2008) and killed over 100 million trees worldwide. It appears that CTLV has the same potential since the fourth element of the plant disease tetrahedron- humans- have created an artificial host environment that CTLV had not have enough time to adapt and evolve in co-existence and balance with trifoliate and trifoliate hybrids since they have been largely used since 1950s (Moreno et al. 2008).

References

Anandalakshmi, R., Pruss, G. J., Ge, X., Marathe, R., Mallory, A. C., Smith, T. H., and Vance, V. B. 1998. A viral suppressor of gene silencing in plants. Proceedings of the National Academy of Sciences of the United States of America 95:13079-13084.

Baulcombe, D. 2004. RNA silencing in plants. Nature 431:356-363.

Bewick, V., Cheek, L., and Ball, J. 2004. Statistics review 9: one-way analysis of variance. Critical care (London, England) 8:130-136.

Brigneti, G., Voinnet, O., Li, W. X., Ji, L. H., Ding, S. W., and Baulcombe, D. C. 1998. Viral pathogenicity determinants are suppressors of transgene silencing in Nicotiana benthamiana. EMBO J 17:6739-6746.

Broadbent, P., Dephoff, C. M., and Gilkeson, C. 1994. Detection of citrus tatter leaf virus in Australia. Australasian Plant Pathology 23:20-24.

Burgyán, J., and Havelda, Z. 2011. Viral suppressors of RNA silencing. Trends in Plant Science 16:265-272.

Calavan, E. C., Christiansen, D. W., and Roistacher, C. N. 1963. Symptoms associated with tatter-leaf virus infection of Troyer citrange rootstocks. Plant Disease Reporter 47:971-975.

Carrington, J. C., Kasschau, K. D., Mahajan, S. K., and Schaad, M. C. 1996. Cell-to-Cell and Long-Distance Transport of Viruses in Plants. Plant Cell 8:1669-1681.

Csorba, T., Kontra, L., and Burgyan, J. 2015. viral silencing suppressors: Tools forged to fine-tune host-pathogen coexistence. Virology 479-480:85-103.

da Graca, J. V. 1977. Citrus tatter leaf virus in South African Meyer lemon. Citrus and sub-tropical fruit journal 529.

da Graca, J. V., and Sharia, M. 1996. Citrus Tatter Leaf Virus in the Rio Grande Valley of South Texas. Pages 198-200 in: Proceedings of 13th Conference of International Organization of Citrus Virologists.

Ding, S. W. 2010. RNA-based antiviral immunity. Nat Rev Immunol 10:632-644.

Duncan, D. B. 1955. Multiple Range and Multiple F Tests. Biometrics 11:1-42.

Díaz-Pendón, J. A., and Ding, S. W. 2008. Direct and indirect roles of viral suppressors of RNA silencing in pathogenesis. Annu Rev Phytopathol 46:303-326.

Earley, K. W., Haag, J. R., Pontes, O., Opper, K., Juehne, T., Song, K., and Pikaard, C. S. 2006. Gateway-compatible vectors for plant functional genomics and proteomics. Plant J 45:616-629.

Fraser, L. R., and Broadbent, P. 1979. Virus and related diseases of citrus in New South Wales. Dept. of Agriculture New South Wales.

Gagliardi, M., and Matarazzo, M. R. 2016. RIP: RNA Immunoprecipitation. Pages 73-86 in: Polycomb Group Proteins: Methods and Protocols. C. Lanzuolo and B. Bodega, eds. Springer New York, New York, NY.

Galiakparov, N., Tanne, E., Mawassi, M., Gafny, R., and Sela, I. 2003. ORF 5 of grapevine virus A encodes a nucleic acid-binding protein and affects pathogenesis. Virus Genes 27:257-262.

Garnsey, S. M. 1964. Detection of tatter leaf virus of citrus in Florida. Florida State Horticultural Society 77:106-109.

Garnsey, S. M. 1970. Viruses in Florida's Meyer lemon trees and their effects on other citrus. Florida State Horticultural Society 83:66-71.

Garnsey, S. M. 1974. Mechanical transmission of a virus that produces tatter leaf symptoms in *Citrus excela*. Pages 137-140 in: Proceedings of 6th Conference of International Organization of Citrus Virologists.

Garnsey, S. M., and Jones, J. W. 1968. Relationship of symptoms to the presence of tatter-leaf virus in several citrus hosts. Pages 206-212 in: Proceedings of 4th Conference of International Organization of Citrus Virologists.

Goto, K., Kobori, T., Kosaka, Y., Natsuaki, T., and Masuta, C. 2007. Characterization of silencing suppressor 2b of cucumber mosaic virus based on examination of its small RNA-binding abilities. Plant Cell Physiol 48:1050-1060.

Herron, C. M., and Skaria, M. 2000. Further Studies on Citrus Tatter Leaf Virus in Texas. Pages 185-194 in: Proceedings of 14th Conference of International Organization of Citrus Virologists.

Incarbone, M., and Dunoyer, P. 2013. RNA silencing and its suppression: novel insights from in planta analyses. Trends Plant Sci 18:382-392.

Inouye, N., Maeda, T., and Mitsuhata, K. 1979. Citrus tatter leaf virus isolated from lily. Annuals of the Phytopathological Society of Japan 45:712-720.

Jones, J. D., and Dangl, J. L. 2006. The plant immune system. Nature 444:323-329.

Jones, L., Hamilton, A. J., Voinnet, O., Thomas, C. L., Maule, A. J., and Baulcombe, D. C. 1999. RNA–DNA Interactions and DNA Methylation in Post-Transcriptional Gene Silencing. The Plant Cell 11:2291.

Kasschau, K. D., Cronin, S., and Carrington, J. C. 1997. Genome Amplification and Long-Distance Movement Functions Associated with the Central Domain of Tobacco Etch Potyvirus Helper Component–Proteinase. Virology 228:251-262.

Kasschau, K. D., and Carrington, J. C. 1998. A counterdefensive strategy of plant viruses: suppression of posttranscriptional gene silencing. Cell 95:461-470.

Kasschau, K. D., and Carrington, J. C. 2001. Long-distance movement and replication maintenance functions correlate with silencing suppression activity of potyviral HC-Pro. Virology 285:71-81.

Katiyar-Agarwal, S., and Jin, H. 2010. Role of small RNAs in host-microbe interactions. Annu Rev Phytopathol 48:225-246.

Khraiwesh, B., Zhu, J.-K., and Zhu, J. 2012. Role of miRNAs and siRNAs in biotic and abiotic stress responses of plants. Biochimica et Biophysica Acta (BBA) - Gene Regulatory Mechanisms 1819:137-148.

Li, F., and Ding, S.-W. 2006. Virus Counterdefense: Diverse Strategies for Evading the RNA-Silencing Immunity. Annual Review of Microbiology 60:503-531.

Liebenberg, A., Moury, B., Sabath, N., Hell, R., Kappis, A., Jarausch, W., and Wetzel, T. 2012. Molecular evolution of the genomic RNA of Apple stem grooving capillovirus. J Mol Evol 75:92-101.

Liu, D., Shi, L., Han, C., Yu, J., Li, D., and Zhang, Y. 2012. Validation of Reference Genes for Gene Expression Studies in Virus-Infected Nicotiana benthamiana Using Quantitative Real-Time PCR. PLOS ONE 7:e46451.

Liu, S.-R., Zhou, J.-J., Hu, C.-G., Wei, C.-L., and Zhang, J.-Z. 2017. MicroRNA-Mediated Gene Silencing in Plant Defense and Viral Counter-Defense. Frontiers in Microbiology 8

Lucy, A. P., Guo, H. S., Li, W. X., and Ding, S. W. 2000. Suppression of post-transcriptional gene silencing by a plant viral protein localized in the nucleus. The EMBO journal 19:1672-1680.

Martín-Hernández, A. M., and Baulcombe, D. C. 2008. Tobacco rattle virus 16-kilodalton protein encodes a suppressor of RNA silencing that allows transient viral entry in meristems. J Virol 82:4064-4071.

Miyakawa, T. 1980. Occurrence and varietal distribution of tatter leaf-citrange stunt virus and its effects on Japanese citrus. in: Proceedings of 8th Conference of International Organization of Citrus Virologists.

Miyakawa, T., and Matsui, C. 1976. A Bud-Union Abnormality of Satusma Mandarin on *Poncirus Trifoliata* Rootstock in Japan. Pages 125-131 in: Proceedings of 7th Conference of International Organization of Citrus Virologists.

Miyakawa, T., and Tsuji, M. 1988. The association of tatterleaf virus with budunion crease of trees on trifoliate orange rootstock. Pages 360-364 in: Proceedings of 10th Conference of International Organization of Citrus Virologists.

Moffett, P., Farnham, G., Peart, J., and Baulcombe, D. C. 2002. Interaction between domains of a plant NBS-LRR protein in disease resistance-related cell death. The EMBO journal 21:4511-4519.

Moreno, P., Ambrós, S., Albiach-Martí, M. R., Guerri, J., and Peña, L. 2008. Citrus tristeza virus: a pathogen that changed the course of the citrus industry. Mol Plant Pathol 9:251-268.

Mérai, Z., Kerényi, Z., Kertész, S., Magna, M., Lakatos, L., and Silhavy, D. 2006. Double-Stranded RNA Binding May Be a General Plant RNA Viral Strategy To Suppress RNA Silencing. Journal of Virology 80:5747.

Nishio, T., Kawai, A., Kato, M., and Kobayashi, T. 1982. A sap-transmissible closterovirus in citrus imported from China and Formosa. Research Bulletin of the Plant Protection Service (Japan).

Nishio, T. K., A.; Takahashi, T.; Namba, S.; Yamashita, S. 1989. Purification and properties of citrus tatter leaf virus. Annals of the Phytopathological Society of Japan 55:254-258.

Ohira, K., Namba, S., Rozanov, M., Kusumi, T., and Tsuchizaki, T. 1995. Complete sequence of an infectious full-length cDNA clone of citrus tatter leaf capillovirus: comparative sequence analysis of capillovirus genomes. J Gen Virol 76 (Pt 9):2305-2309.

Ohira, K., Ito, T., Kawai, A., Namba, S., Kusumi, T., and Tsuchizaki, T. 1994. Nucleotide sequence of the 3'-terminal region of citrus tatter leaf virus RNA. Virus Genes 8:169-172.

Padmanabhan, C., Zhang, X., and Jin, H. 2009. Host small RNAs are big contributors to plant innate immunity. Curr Opin Plant Biol 12:465-472.

Pfaffl, M. W. 2001. A new mathematical model for relative quantification in real-time RT-PCR. Nucleic acids research 29:e45-e45.

Pumplin, N., and Voinnet, O. 2013. RNA silencing suppression by plant pathogens: defence, counter-defence and counter-counter-defence. Nat Rev Microbiol 11:745-760.

Qiao, Y., Liu, L., Xiong, Q., Flores, C., Wong, J., Shi, J., Wang, X., Liu, X., Xiang, Q., Jiang, S., Zhang, F., Wang, Y., Judelson, H. S., Chen, X., and Ma, W. 2013. Oomycete pathogens encode RNA silencing suppressors. Nat Genet 45:330-333.

Qu, F., and Morris, T. J. 2005. Suppressors of RNA silencing encoded by plant viruses and their role in viral infections. FEBS Letters 579:5958-5964

Qu, F., Ye, X., Hou, G., Sato, S., Clemente, T. E., and Morris, T. J. 2005. RDR6 has a broad-spectrum but temperature-dependent antiviral defense role in Nicotiana benthamiana. J Virol 79:15209-15217.

Ramanathan, M., Porter, D. F., and Khavari, P. A. 2019. Methods to study RNA–protein interactions. Nature Methods 16:225-234.

Rasmussen, R. 2001. Quantification on the LightCycler. Pages 21-34 in: Rapid Cycle Real-Time PCR: Methods and Applications. S. Meuer, C. Wittwer and K.-I. Nakagawara, eds. Springer Berlin Heidelberg, Berlin, Heidelberg.

Renovell, Á., Vives, M. C., Ruiz-Ruiz, S., Navarro, L., Moreno, P., and Guerri, J. 2012. The Citrus leaf blotch virus movement protein acts as silencing suppressor. Virus Genes 44:131-140.

Roistacher, C. N. 1991. Graft-Transmissible Diseases of Citrus -Handbook for detection and diagnosis of graft-transmissible diseases of citrus. Food and Agriculture Organization of the United Nations, Rome.

Roose, M. L. 2014. Rootstocks. Pages 95-105 in: Citrus Production Manual. L. Ferguson and E. E. Grafton-Cardwell, eds., University of California Agricultural and Natural Resources (UC ANR) Publication 3539.

Roose, M. L., Gmitter, F. G., Lee, R. F., and Hummer, K. E. 2015. Conservation of citrus germplasm: an international survey. Pages 33-38 International Society for Horticultural Science (ISHS), Leuven, Belgium.

Roth, B. M., Pruss, G. J., and Vance, V. B. 2004. Plant viral suppressors of RNA silencing. Virus Res 102:97-108.

Ruiz-Ferrer, V., and Voinnet, O. 2009. Roles of plant small RNAs in biotic stress responses. Annu Rev Plant Biol 60:485-510.

Ruiz, M. T., Voinnet, O., and Baulcombe, D. C. 1998. Initiation and maintenance of virus-induced gene silencing. The Plant cell 10:937-946.

Schwach, F., Vaistij, F. E., Jones, L., and Baulcombe, D. C. 2005. An RNA-dependent RNA polymerase prevents meristem invasion by potato virus X and is required for the activity but not the production of a systemic silencing signal. Plant Physiol 138:1842-1852.

Selth, L. A., Close, P., and Svejstrup, J. Q. 2011. Studying RNA–Protein Interactions In Vivo By RNA Immunoprecipitation. Pages 253-264 in: Epigenetics Protocols. T. O. Tollefsbol, ed. Humana Press, Totowa, NJ.

Semancik, J. S., and Weathers, L. G. 1965. Partial purification of a mechanically transmissible virus associate with tatter leaf of citrus. Phytopathology 55:1354-1358.

Song, L., Gao, S., Jiang, W., Chen, S., Liu, Y., Zhou, L., and Huang, W. 2011. Silencing suppressors: viral weapons for countering host cell defenses. Protein Cell 2:273-281.

Spreen, T. H. 2010. The World Citrus Industry. Soil, Plant Growth and Crop Production.

Stephan, D., Slabber, C., George, G., Ninov, V., Francis, K. P., and Burger, J. T. 2011. Visualization of plant viral suppressor silencing activity in intact leaf lamina by quantitative fluorescent imaging. Plant Methods 7:25.

Su, H. J., and Cheon, J. U. 1984. Occurrence and distribution of tatter leaf-citrange stunt complex a Taiwanese citrus. Pages 42-48 National Taiwan University, Bull. Phytopathol. Entomol.

Svec, D., Tichopad, A., Novosadova, V., Pfaffl, M. W., and Kubista, M. 2015. How good is a PCR efficiency estimate: Recommendations for precise and robust qPCR efficiency assessments. Biomol Detect Quantif 3:9-16.

Tallarida, R. J., and Murray, R. B. 1987. Duncan Multiple Range Test. Pages 125-127 in: Manual of Pharmacologic Calculations: With Computer Programs. R. J. Tallarida and R. B. Murray, eds. Springer New York, New York, NY.

Tatineni, S., Afunian, M. R., Gowda, S., Hilf, M. E., Bar-Joseph, M., and Dawson, W. O. 2009a. Characterization of the 5'- and 3'-terminal subgenomic RNAs produced by a capillovirus: Evidence for a CP subgenomic RNA. Virology 385:521-528.

Tatineni, S., Afunian, M. R., Hilf, M. E., Gowda, S., Dawson, W. O., and Garnsey, S. M. 2009b. Molecular characterization of Citrus tatter leaf virus historically associated with Meyer lemon trees: complete genome sequence and development of biologically active in vitro transcripts. Phytopathology 99:423-431.

ten Have, S., Boulon, S., Ahmad, Y., and Lamond, A. I. 2011. Mass spectrometry-based immuno-precipitation proteomics – The user's guide. PROTEOMICS 11:1153-1159.

Turriziani, B., von Kriegsheim, A., and Pennington, S. R. 2016. Protein-Protein Interaction Detection Via Mass Spectrometry-Based Proteomics. Pages 383-396 in: Modern Proteomics – Sample Preparation, Analysis and Practical Applications. H. Mirzaei and M. Carrasco, eds. Springer International Publishing, Cham.

USDA-NASS. 2018. Agricultural Statistics 2018. United States Department of Agriculture- National Agricultural Statistics Service.

Vargason, J. M., Szittya, G., Burgyán, J., and Hall, T. M. T. 2003. Size Selective Recognition of siRNA by an RNA Silencing Suppressor. Cell 115:799-811.

Wallace, J. M., and Drake, R. J. 1962. Tatter leaf, a previously undescribed virus effect on citrus. Plant Disease Reporter 46:211-212

Wallace, J. M., and Drake, R. J. 1963. New information on symptom effects and host range of citrus tatter leaf virus. Plant Disease Reporter 47:352-353.

Wang, M. B., Masuta, C., Smith, N. A., and Shimura, H. 2012. RNA silencing and plant viral diseases. Mol Plant Microbe Interact 25:1275-1285.

Weber, P. H., and Bujarski, J. J. 2015. Multiple functions of capsid proteins in (+) stranded RNA viruses during plant–virus interactions. Virus Research 196:140-149.

Weiberg, A., Wang, M., Bellinger, M., and Jin, H. 2014. Small RNAs: a new paradigm in plant-microbe interactions. Annu Rev Phytopathol 52:495-516.

Wroblewski, T., Tomczak, A., and Michelmore, R. 2005. Optimization of Agrobacterium-mediated transient assays of gene expression in lettuce, tomato and Arabidopsis. Plant Biotechnology Journal 3:259-273.

Wu, Q., Wang, X., and Ding, S. W. 2010. Viral suppressors of RNA-based viral immunity: host targets. Cell Host Microbe 8:12-15.

Yoshikawa, N., Imaizumi, M., Takahashi, T., and Inouye, N. 1993. Striking similarities between the nucleotide sequence and genome organization of citrus tatter leaf and apple stem grooving capilloviruses. J Gen Virol 74:2743-2747.

Zhang, T. M., and Liang, X. Y. 1988. Occurrence and detection of citrus tatter leaf virus (CTLV) in Huangyan, Zhejiang Province, China. 72:543-545.

Zhang, X., Yuan, Y. R., Pei, Y., Lin, S. S., Tuschl, T., Patel, D. J., and Chua, N. H. 2006. Cucumber mosaic virus-encoded 2b suppressor inhibits Arabidopsis Argonaute1 cleavage activity to counter plant defense. Genes Dev 20:3255-3268.

Zhou, Z. S. h., Dell'Orco, M., Saldarelli, P., Turturo, C., Minafra, A., and Martelli, G. P. 2006. Identification of an RNA-silencing suppressor in the genome of Grapevine virus A. J Gen Virol 87:2387-2395.

Zvereva, A. S., and Pooggin, M. M. 2012. Silencing and innate immunity in plant defense against viral and non-viral pathogens. Viruses 4:2578-2597.
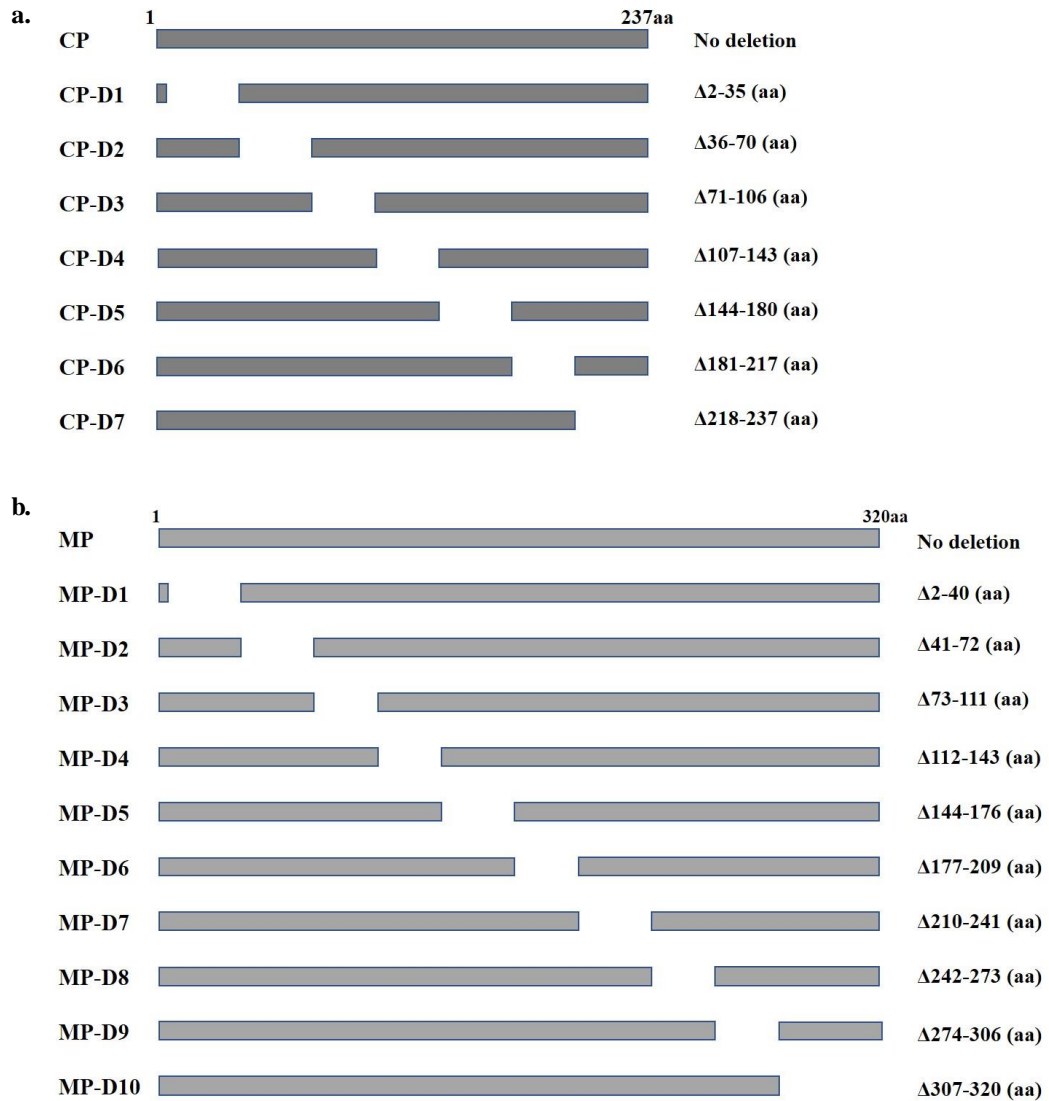
Figure 3.1 Serial deletion assay of coat protein and movement protein encoded by citrus tatter leaf virus to identify functional regions of suppression activity in viral suppressors of RNA silencing. Illustrations are not to scale. (a) coat protein serial deletions and (b) movement protein serial deletions. (CP: coat protein; MP: movement protein)
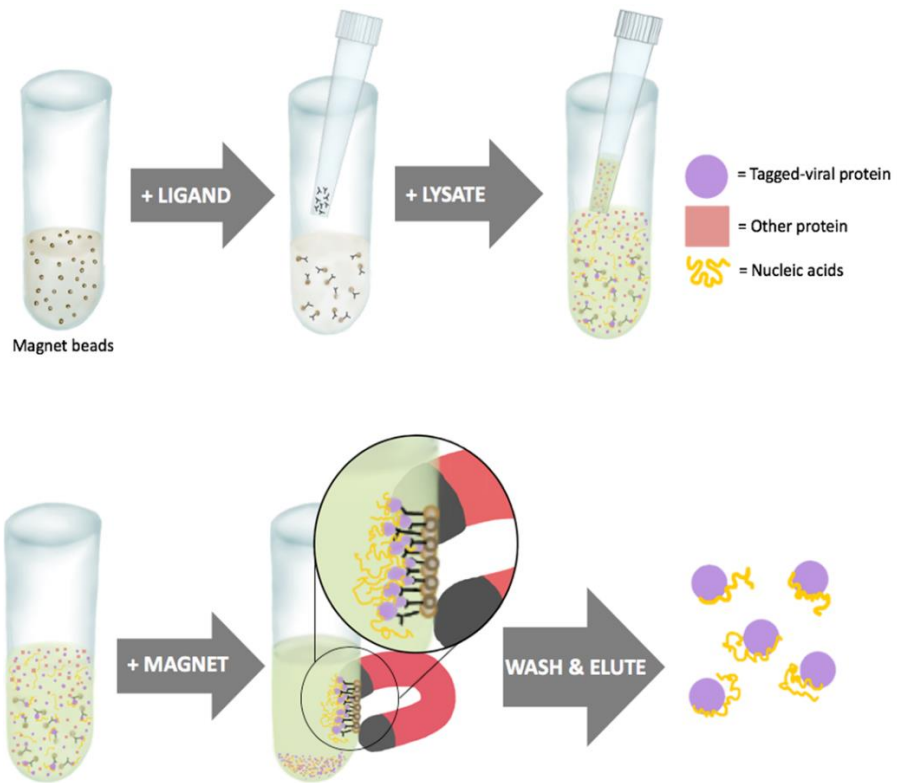
Figure 3.2 General procedure of RNA immunoprecipitation (RIP) assay used in this study to identify interactions between RNA and viral suppressor of RNA silencing (VSR). Illustrations are not to scale.
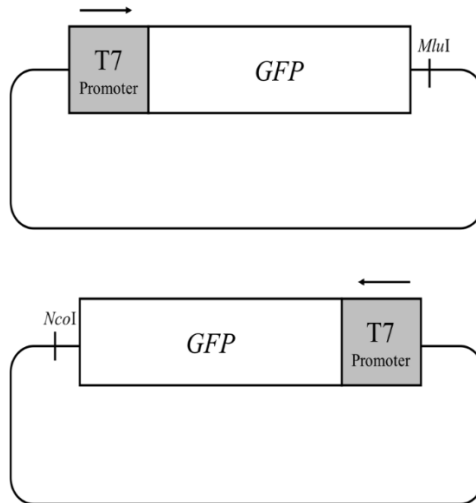
Figure 3.3 *GFP* constructs with T7 promoters either at the upstream or downstream of the gene, respectively, for *in vitro* transcription and to synthesize double-stranded RNA (dsRNA) for RNA-protein pull down assay. Illustrations are not to scale.
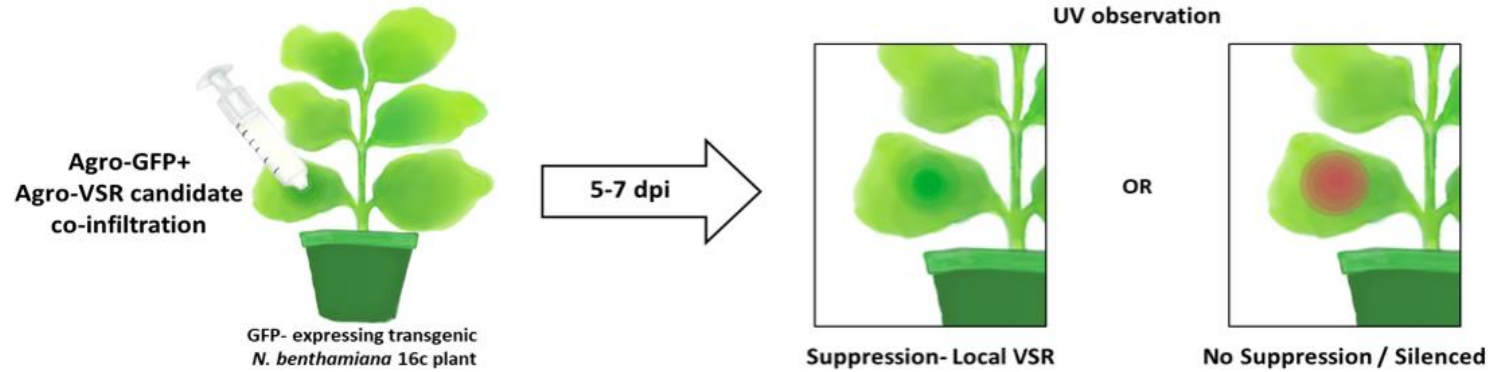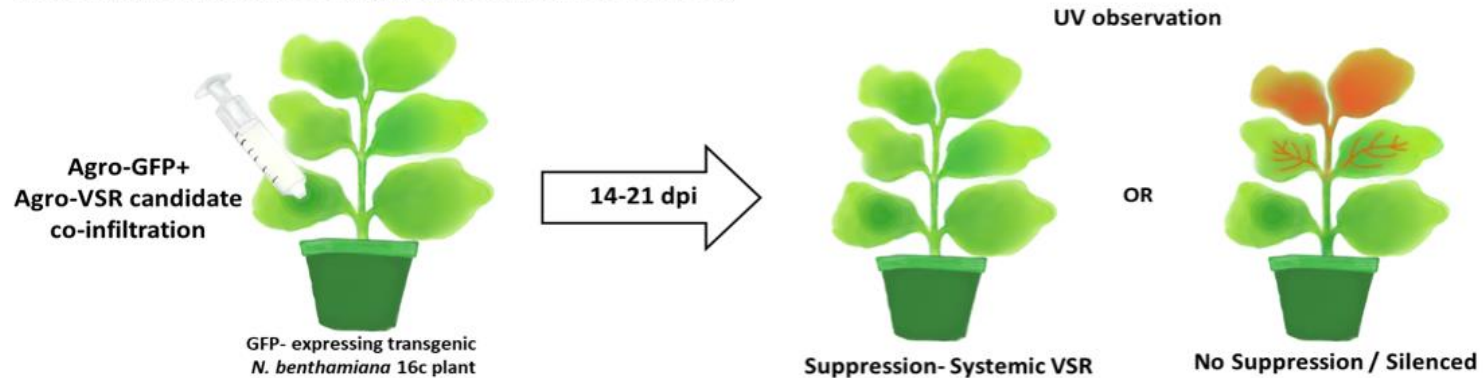
Figure 3.4 RNA silencing suppression co-infiltration assay by *Agrobacterium*-mediated transient expression in *Nicotiana benthamiana* 16c plants and GFP imaging with UV observation. Transient expression assay for (a) local RNA silencing and (b) systemic RNA silencing.
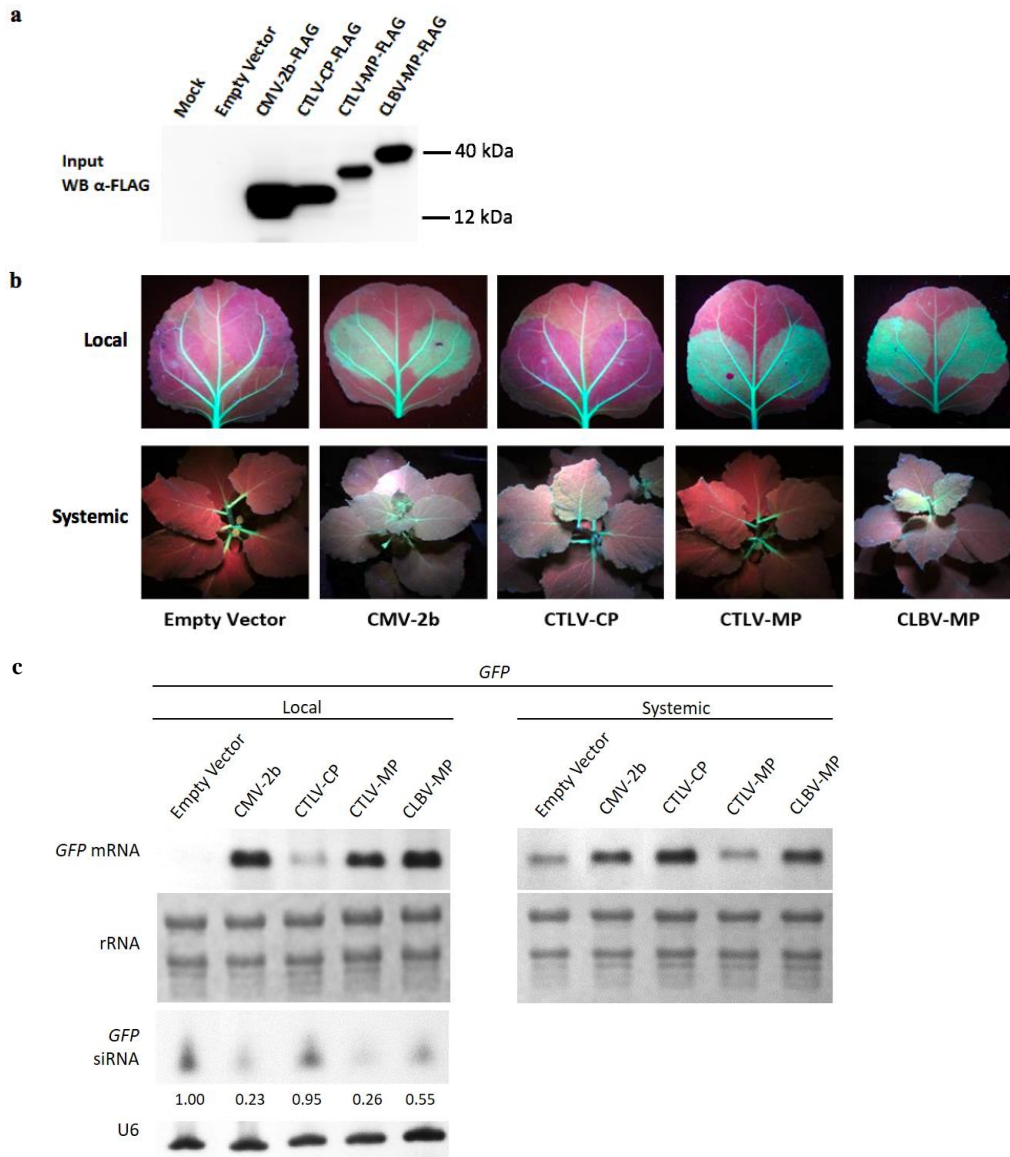
Figure 3.5 RNA silencing suppression co-infiltration assay of citrus tatter leaf virus coat protein and movement protein. Empty vector was used as negative control and cucumber mosaic virus 2b and citrus leaf blotch virus movement protein were used as controls of viral suppressor of RNA silencing. (a) Western blot analysis to confirm protein expression. (b) Local (upper row) and systemic (lower row) silencing suppression observed under UV light at 5 and 14 dpi, respectively. (c) Northern blot analysis for testing *GFP* mRNA level. siRNA of *GFP* was also examined for local infiltrated tissue. Number represents the intensity of signal compared to empty vector. Ribosomal RNA and U6 were used as loading control. (WB: western blot; CMV-2b: cucumber mosaic virus 2b; CTLV: citrus tatter leaf virus; CLBV: citrus leaf blotch virus; CP: coat protein; MP: movement protein; rRNA: ribosomal RNA)

153
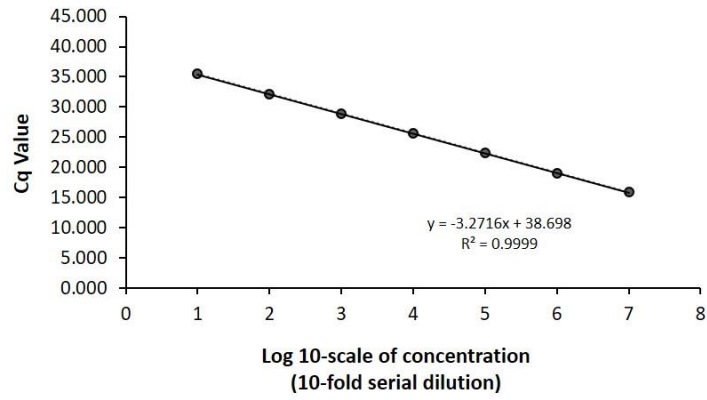
a *GFP* RT-qPCR
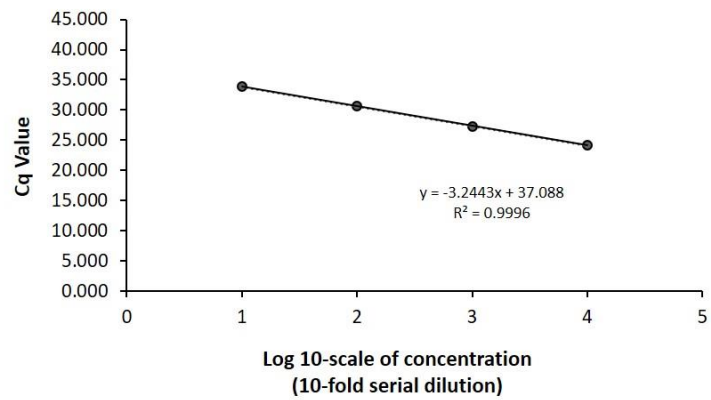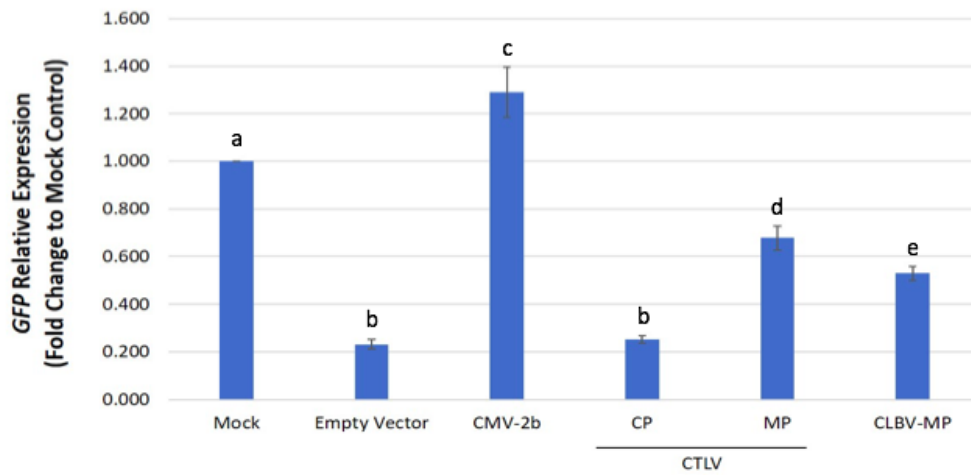

b *NbPP2A* RT-qPCR (reference control)

Figure 3.6 Standard curve analysis to validate RT-qPCR assays. The X-axis displays the log concentration and the Y-axis represents the value of quantitative cycle (Cq). (a) *GFP* RT-qPCR assay. (b) *NbPP2A* RT-qPCR assay.
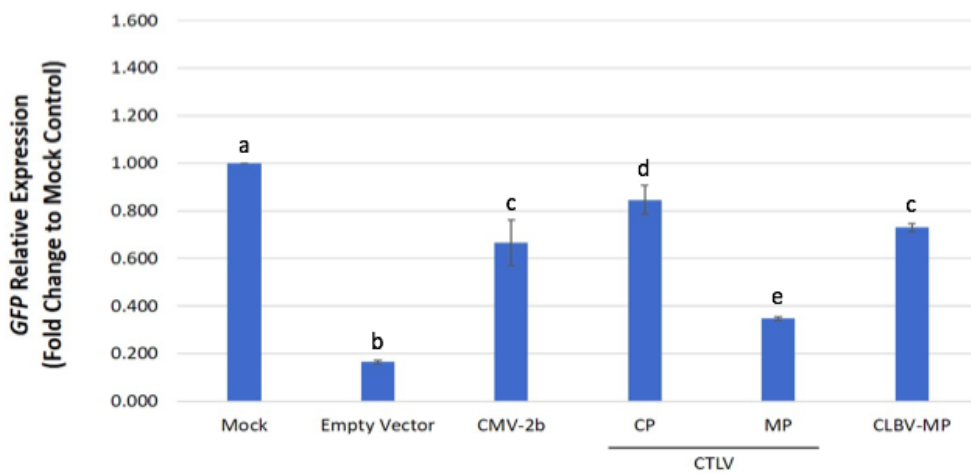
a. Local

b. Systemic

Figure 3.7 Relative expression analysis of *GFP* mRNA for silencing suppression co-infiltration assay with (a) local and infiltrated leaf tissue collected at 5 dpi and (b) systemic tissue collected at 14 dpi. (Significance level α=0.05) (CMV-2b: cucumber mosaic virus; CTLV: citrus tatter leaf virus; CLBV: citrus leaf blotch virus; CP: coat protein; MP: movement protein)
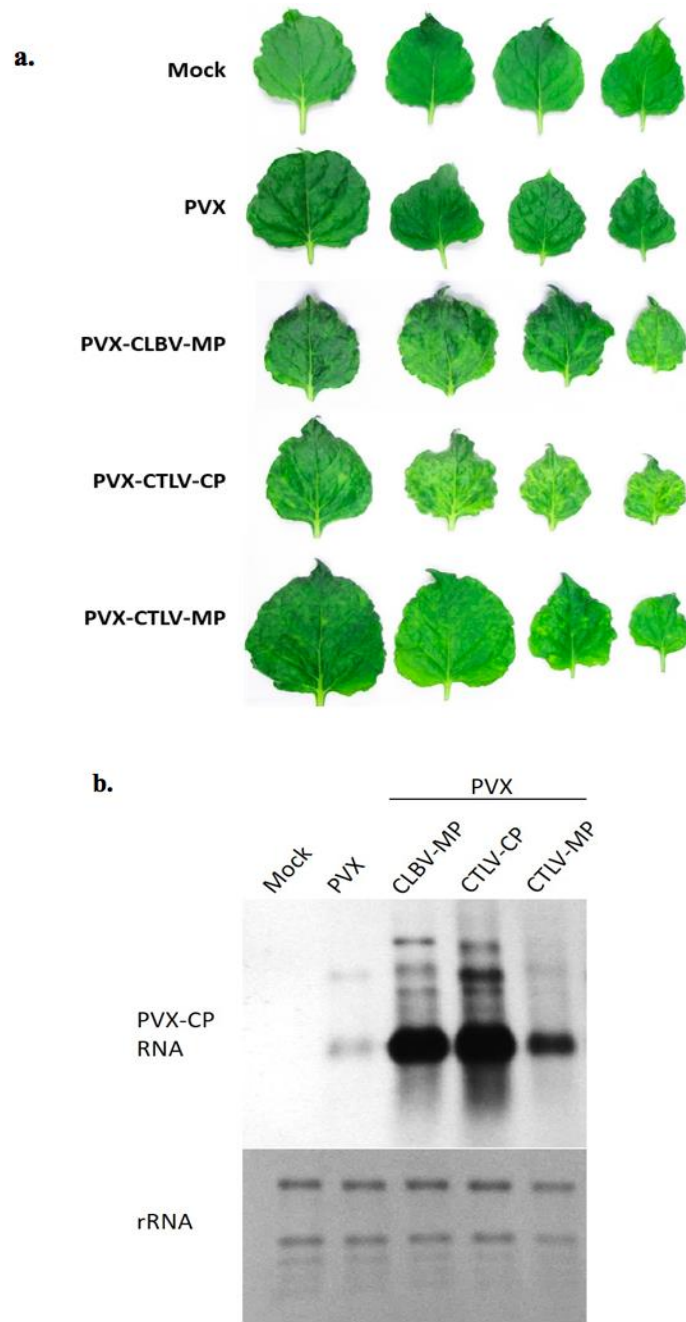
Figure 3.8 Potato virus X assay to test coat protein and movement protein encoded by citrus tatter leaf virus on the suppression of siRNA-mediated host immunity in *N benthamiana* plants. (a) Leaf symptoms. (b) Northern blot analysis with DIG-labeled PVX coat protein probe to detect viral accumulation. Ribosomal RNA was stained and visualized as loading control. (PVX: potato virus x; CLBV: citrus leaf blotch virus; CTLV: citrus tatter leaf virus; CP: coat protein; MP: movement protein)
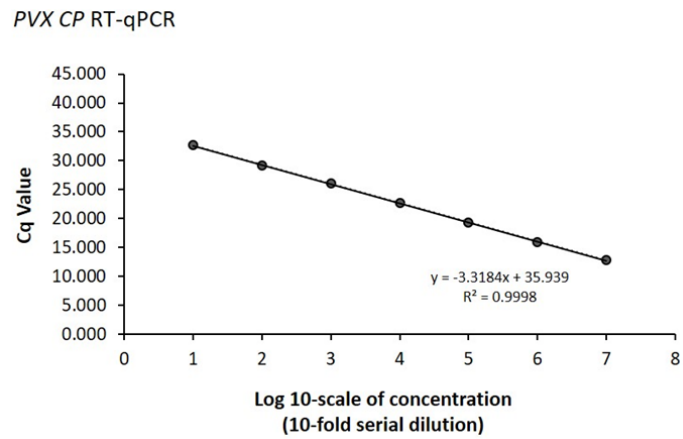
PVX CP RT-qPCR

y = -3.3184x + 35.939
R² = 0.9998

Figure 3.9 Standard curve analysis to validate RT-qPCR assay which targets coat protein (CP) of potato virus X (PVX). The X-axis displays the log concentration and the Y-axis represents the value of quantitative cycle (Cq).
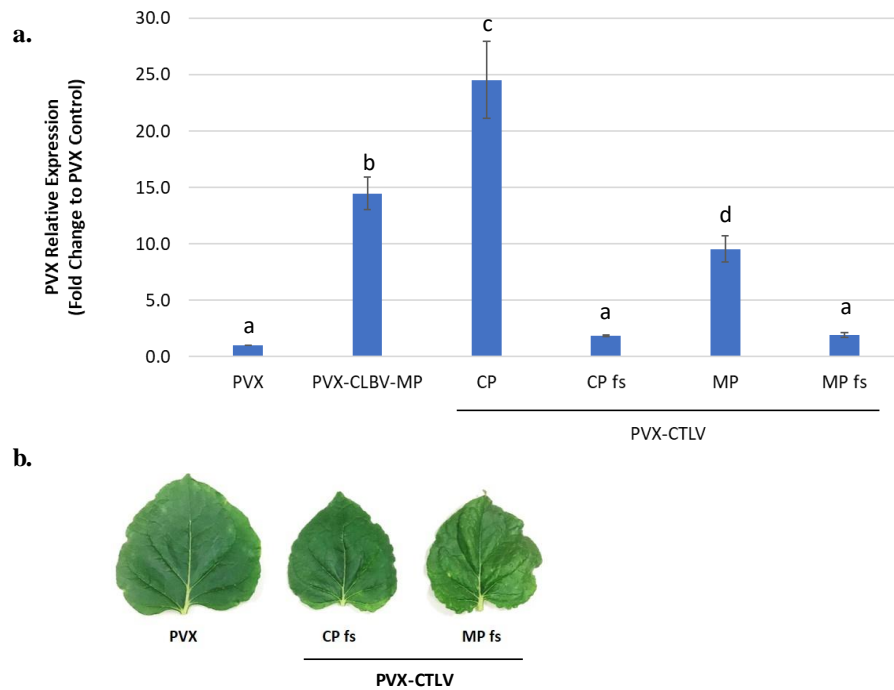
Figure 3.10 Potato virus X assay to test citrus tatter leaf virus coat protein, movement protein, and their frameshifting mutations on the suppression of siRNA-mediated host immunity in *N benthamiana* plants. (a) Relative expression level by PVX CP RT-qPCR (Significance level α=0.05). (b) Leaf symptoms of frameshifting mutations of citrus tatter leaf virus coat protein and movement protein. (PVX: potato virus x; CLBV: citrus leaf blotch virus; CTLV: citrus tatter leaf virus; CP: coat protein; MP: movement protein; fs: frameshifting mutation)
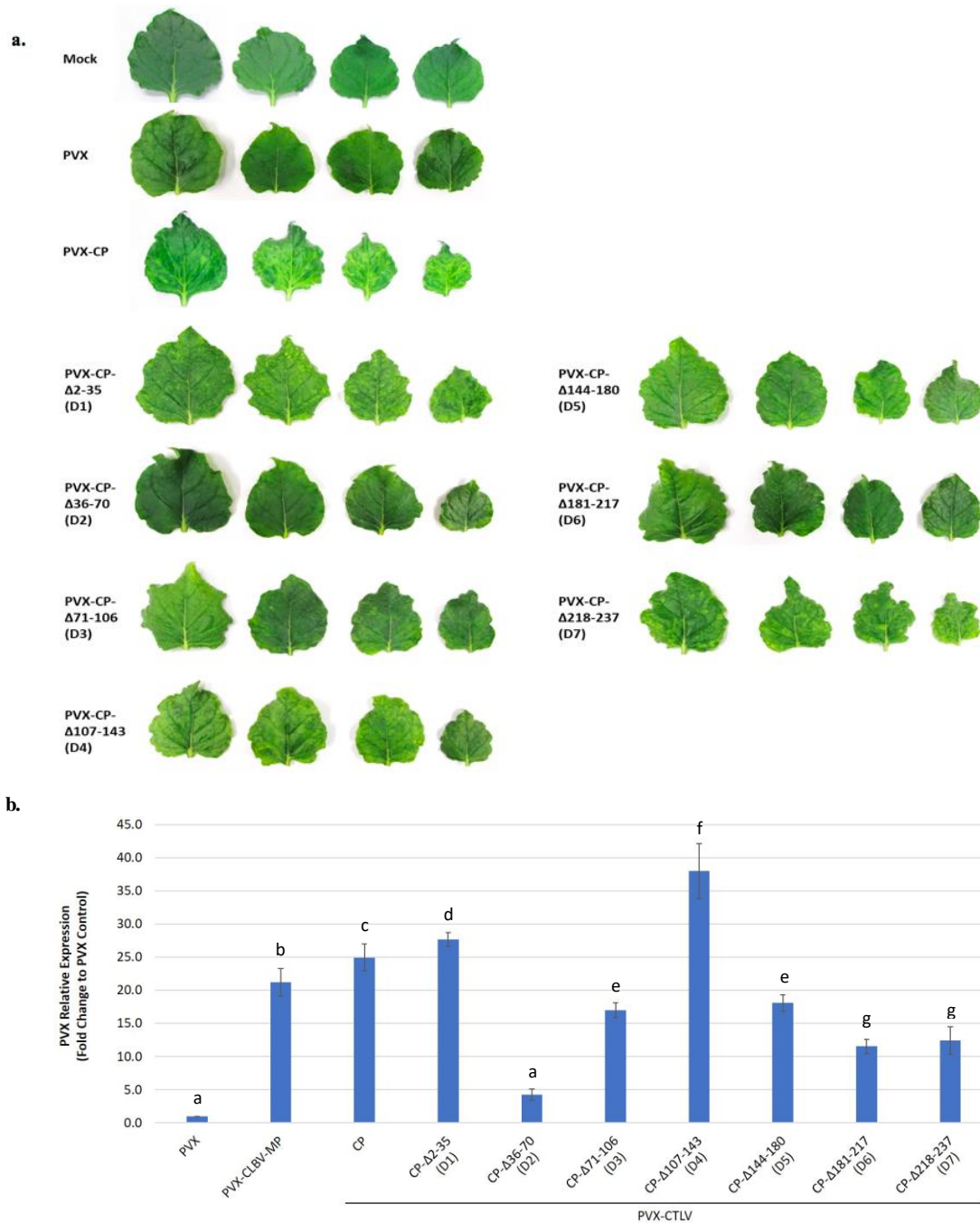
Figure 3.11 Citrus tatter leaf virus coat protein deletion assay by using potato virus X to test on the suppression of siRNA-mediated host immunity in *N benthamiana* plants. (a) Leaf symptoms of citrus tatter leaf virus coat protein and its deletions. (b) Relative expression level of citrus tatter leaf virus coat protein and its deletions by PVX CP RT-qPCR (Significance level α=0.05). (PVX: potato virus x; CLBV: citrus leaf blotch virus; CTLV: citrus tatter leaf virus; CP: coat protein; MP: movement protein)
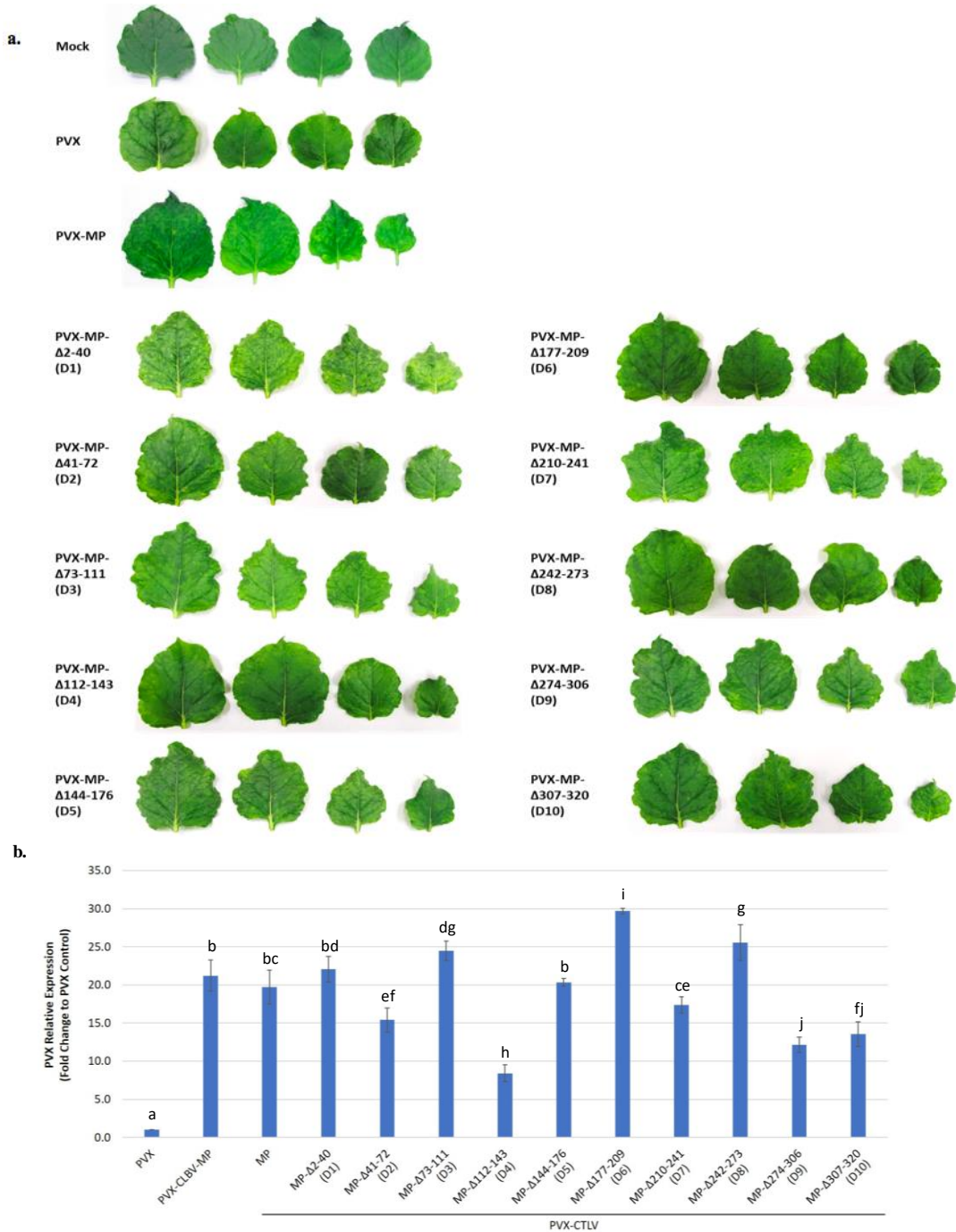
Figure 3.12 Citrus tatter leaf virus movement protein deletion assay by using potato virus X to test on the suppression of siRNA-mediated host immunity in *N benthamiana* plants. (a) Leaf symptoms of citrus tatter leaf virus movement protein and its deletions. (b) Relative expression level of citrus tatter leaf virus movement protein and its deletions by PVX CP RT-qPCR (Significance level α=0.05). (PVX: potato virus x; CLBV: citrus leaf blotch virus; CTLV: citrus tatter leaf virus; MP: movement protein)
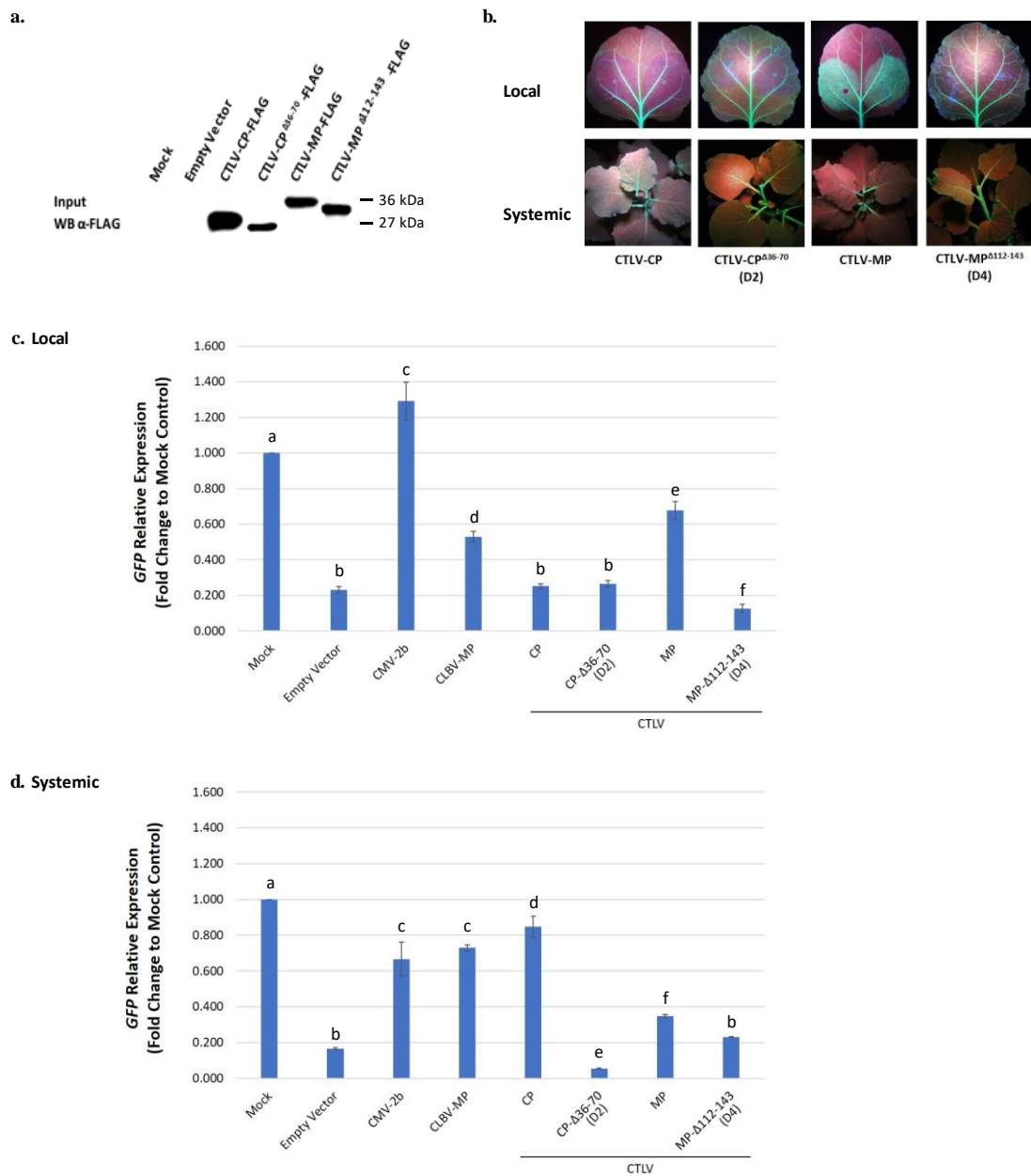
Figure 3.13 RNA silencing suppression co-infiltration assay of citrus tatter leaf virus coat protein, movement protein and their deletions. (a) Western blot analysis to confirm protein expression. (b) Local (upper row) and systemic (lower row) silencing suppression observed under UV light at 5 and 14 dpi, respectively. Relative expression level analysis for *GFP* mRNA level in both (c) local tissue and (d) systemic tissues by *GFP* RT-qPCR (Significance level α=0.05). (WB: western blot; CMV-2b: cucumber mosaic virus 2b; CLBV: citrus leaf blotch virus; CTLV: citrus tatter leaf virus; CP: coat protein; MP: movement protein)
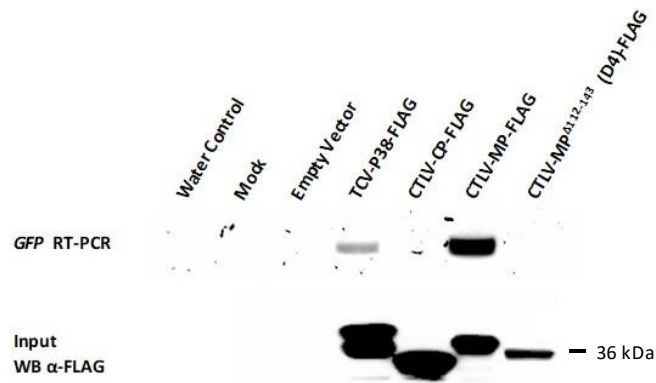
Figure 3.14 RNA immunoprecipitation (RIP) of citrus tatter leaf virus coat protein, movement protein and its deletion. The agarose gel electrophoresis of *GFP* RT-PCR products is shown in the upper part of the figure. The input of the protein was examined by western blot analysis and is shown in the lower panel. (TCV: turnip crinkle virus; CTLV: citrus tatter leaf virus; CP: coat protein; MP: movement protein; WB: western blot)
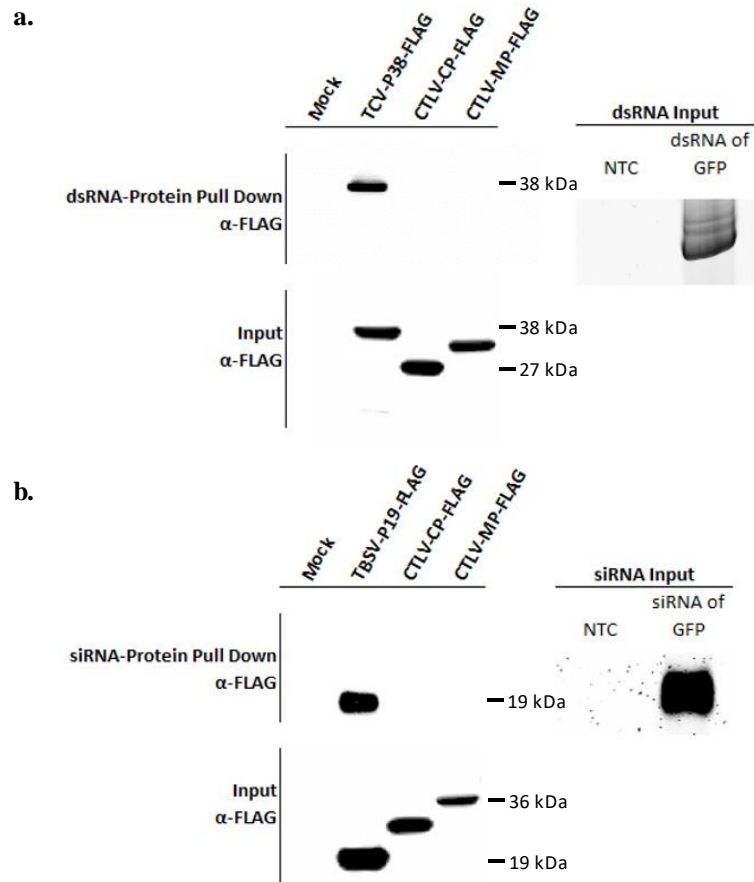
Figure 3.15 Western blot analysis of RNA-protein pull-down assay to examine citrus tatter leaf virus coat protein and movement protein RNA binding capability with (a) double-stranded RNA (dsRNA) of *GFP* and (b) small interfering RNA (siRNA). Inputs of dsRNA and siRNA were examined by polyacrylamide gel electrophoresis. (TCV: turnip crinkle virus; CTLV: citrus tatter leaf virus; TBSV: tomato bushy stunt virus; CP: coat protein; MP: movement protein)

Table 3.1 List of primers and probes used in this study.

No.	Name	Primer Sequence	Purpose of use
Cloning			
1	VSR_CP-F1	CACCGAATTCATGAGTTTGGAAGACGT	Viral gene cloning- pEarleyGate vectors
2	VSR_CP-R1	GCATGCACCCTCCAGTTCCA	Viral gene cloning- pEarleyGate vectors
3	VSR_MP-F1	CACCGAATTCATGGCNATCGTCAAYGTCAACCA	Viral gene cloning- pEarleyGate vectors
4	VSR_MP-R1	GCATGCGGGGGAGGAACCGTCA	Viral gene cloning- pEarleyGate vectors
5	VSR_CP-R2	GCATGCTCA ACCCTCCAGTTCCA	Viral gene cloning- pEarleyGate vectors
6	VSR_MP-R2	GCATGCTCAGGGGGAGGAACCGTCA	Viral gene cloning- pEarleyGate vectors
7	VSR_CLBV-MP-F	CACCATGGCATCCCTGATCAATGTAAG	Viral gene cloning- pEarleyGate vectors
8	VSR_CLBV-MP-R1	CTTGGTCCCAGTGTCACTGGC	Viral gene cloning- pEarleyGate vectors
9	VSR_CLBV-MP-R2	TCACTTGGTCCCAGTGTCACTGG	Viral gene cloning- pEarleyGate vectors
10	VSR_CMV-2b-F	CACCATGGAATTGAACGHRGGYG	Viral gene cloning- pEarleyGate vectors
11	VSR_CMV-2b-R1	RAAMGCACCTTCCGCCCA	Viral gene cloning- pEarleyGate vectors
12	VSR_CMV-2b-R2	TCARAAMGCACCTTCCGCCC	Viral gene cloning- pEarleyGate vectors
13	VSR_GFP-F	CACCATGAGTAAAGGAGAAGAACTTTTCACTGGA	Gene cloning- pEarleyGate vectors
14	VSR_GFP-R1	TTTGTATAGTTCATCCATGCCATGTGTAATCCCA	Gene cloning- pEarleyGate vectors
15	VSR_GFP-R2	TTATTTGTATAGTTCATCCATGCCATGTGTAATCCCA	Gene cloning- pEarleyGate vectors
16	pGR106-CTLV-CP-F	GGCGCGCCATGAGTTTGGAAGACGTG	Viral gene cloning- pGR106 vector
17	pGR106-CTLV-CP-R	GCGGCCGCTCAACCCTCCAGTT	Viral gene cloning- pGR106 vector
18	pGR106-CTLV-MP-F	GGCGCGCCATGGCAATCGTCA	Viral gene cloning- pGR106 vector
19	pGR106-CTLV-MP-R	GCGGCCGCTCAGGGGGAGGAAC	Viral gene cloning- pGR106 vector
20	pGR106-CLBV-MP-F	GGCGCGCCATGGCATCCCTG	Viral gene cloning- pGR106 vector
21	pGR106-CLBV-MP-R	GCGGCCGCTCACTTGGTCCCAG	Viral gene cloning- pGR106 vector
22	pGR106-CTLV-CP fs-F	CCAGAATTGACTTGTCAAATATAG	CTLV-CP frameshifting clone- pGR106 vector
23	pGR106-CTLV-CP fs-R	CCAAATTTTAGTTTTTTCACC	CTLV-CP frameshifting clone- pGR106 vector
24	pGR106-CTLV-MP fs-F1	ACTGTTGTTATTTTGGACTTAG	CTLV-MP frameshifting clone- pGR106 vector
25	pGR106-CTLV-MP fs-R1	GGACTCAAACTTGAACAAATAC	CTLV-MP frameshifting clone- pGR106 vector
26	pGR106-CTLV-MP fs-F2	AACGGTTCCTCCCCCTGAG	CTLV-MP frameshifting clone- pGR106 vector
27	pGR106-CTLV-MP fs-R2	CAGAATTTCCTTTCCCGGGTC	CTLV-MP frameshifting clone- pGR106 vector
28	pGR106-CTLV-CP-D1-F	CCTGAAGGGTTCAAGGAAGG	CTLV-CP deletion clone- pGR106 vector
29	pGR106-CTLV-CP-D1-R	CATGGCGCGCCAATCGAT	CTLV-CP deletion clone- pGR106 vector
30	pGR106-CTLV-CP-D2-F	TCATCTGATAAGACCCAGTTTC	CTLV-CP deletion clone- pGR106 vector
31	pGR106-CTLV-CP-D2-R	GGGAGGAACCGTCAGAAT	CTLV-CP deletion clone- pGR106 vector
32	pGR106-CTLV-CP-D3-F	AGGGAAGGGACGTCTGGT	CTLV-CP deletion clone- pGR106 vector
33	pGR106-CTLV-CP-D3-R	CCCAAAAACAGCTATATTTCCAAATAAATATTTAC	CTLV-CP deletion clone- pGR106 vector
34	pGR106-CTLV-CP-D4-F	TGTACGTTCAGAAAGCTTTG	CTLV-CP deletion clone- pGR106 vector
35	pGR106-CTLV-CP-D4-R	GGTCTTCTTTTGCTCTTC	CTLV-CP deletion clone- pGR106 vector
36	pGR106-CTLV-CP-D5-F	TTCGAAAAGAGCCCTTGG	CTLV-CP deletion clone- pGR106 vector
37	pGR106-CTLV-CP-D5-R	TTCGTTCAAAGAATTTTGCTTAG	CTLV-CP deletion clone- pGR106 vector
38	pGR106-CTLV-CP-D6-F	ACTGAAGGACAAAAGGGG	CTLV-CP deletion clone- pGR106 vector
39	pGR106-CTLV-CP-D6-R	AGCTTTGGGCCATTTCTT	CTLV-CP deletion clone- pGR106 vector
40	pGR106-CTLV-CP-D7-F	TGAGCATGCAAGGGTGGG	CTLV-CP deletion clone- pGR106 vector
41	pGR106-CTLV-CP-D7-R	ACGAAAAAGCCTCTTTGTCATTCTATC	CTLV-CP deletion clone- pGR106 vector
42	pGR106-CTLV-MP-D1-F	AACTGCATCAAAAGGTTTGAATCAAACG	CTLV-MP deletion clone- pGR106 vector
43	pGR106-CTLV-MP-D1-R	CATGGCGCGCCAATCGAT	CTLV-MP deletion clone- pGR106 vector
44	pGR106-CTLV-MP-D2-F	ATTGACTCCATTAGGAAAAAG	CTLV-MP deletion clone- pGR106 vector
45	pGR106-CTLV-MP-D2-R	GAGCACATCTGGCTTAAAAAAG	CTLV-MP deletion clone- pGR106 vector
46	pGR106-CTLV-MP-D3-F	TATGACGGAGCTTGCCTG	CTLV-MP deletion clone- pGR106 vector
47	pGR106-CTLV-MP-D3-R	TTCAGTGTCATCAAGGAGTTTG	CTLV-MP deletion clone- pGR106 vector
48	pGR106-CTLV-MP-D4-F	CACTGTCTTTCCACAACTG	CTLV-MP deletion clone- pGR106 vector
49	pGR106-CTLV-MP-D4-R	CACGATAACTCTCCCCTC	CTLV-MP deletion clone- pGR106 vector
50	pGR106-CTLV-MP-D5-F	CTTGATATTGGGGTTGCTTAC	CTLV-MP deletion clone- pGR106 vector
51	pGR106-CTLV-MP-D5-R	TTCAGGTCTAAGTCCAAAATAAC	CTLV-MP deletion clone- pGR106 vector
52	pGR106-CTLV-MP-D6-F	GAAGCACTCAAATTCAATG	CTLV-MP deletion clone- pGR106 vector
53	pGR106-CTLV-MP-D6-R	AGCAAACAGTTCTGTGTC	CTLV-MP deletion clone- pGR106 vector
54	pGR106-CTLV-MP-D7-F	AAAAGACTATTTAGGGGTGAC	CTLV-MP deletion clone- pGR106 vector
55	pGR106-CTLV-MP-D7-R	ACAACCGCTGATAGCTTG	CTLV-MP deletion clone- pGR106 vector
56	pGR106-CTLV-MP-D8-F	TCCCTCTCAGCAAGAATTG	CTLV-MP deletion clone- pGR106 vector
57	pGR106-CTLV-MP-D8-R	TTCAATGTGCACATTTGG	CTLV-MP deletion clone- pGR106 vector
58	pGR106-CTLV-MP-D9-F	CCATATAGACCCGGGAAAG	CTLV-MP deletion clone- pGR106 vector

Table 3.1 List of primers and probes used in this study (cont'd).

No.	Name	Primer Sequence	Purpose of use
Cloning			
59	pGR106-CTLV-MP-D9-R	CCTAAATCCTCTCTTTTCCTG	CTLV-MP deletion clone- pGR106 vector
60	pGR106-CTLV-MP-D10-F	TGAGCATGCAAGGGTGGG	CTLV-MP deletion clone- pGR106 vector
61	pGR106-CTLV-MP-D10-R	GTCTTCCACAGATATACTCCTACC	CTLV-MP deletion clone- pGR106 vector
62	VSR_TCV-P38-F	CACCATGGAAAATGATCCTAGAGTCCGGAAGTTC	Viral gene cloning- pEarleyGate vectors
63	VSR_TCV-P38-R	AATTCTGAGTGCTTGCCATTTACCCTTTGGC	Viral gene cloning- pEarleyGate vectors
64	VSR_TBSV-P19-F	CACCATGGAACGAGCTATACAAGGAAACGAC	Viral gene cloning- pEarleyGate vectors
65	VSR_TBSV-P19-R	CTCGCTTTCTTTTTCGAAGGTCTCAGTACCTTC	Viral gene cloning- pEarleyGate vectors
66	GFP-F-full gene	AAGGATCCATGGTAGATCTGACTAGTAAAGGAGAAG	Cloning GFP gene for northern blot probe production
67	GFP-R-full gene	ATCTCGAGTCACACGTGGTGGTGGTGGTGGT	Cloning GFP gene for northern blot probe production
68	PVX-CP full-F	ATGTCAGCACCAGCTAGCACAACACAGC	Cloning PVX CP gene for northern blot probe production
69	PVX-CP full-R	ATGGTGGTGGTAGAGTGACAACAGCCTCAG	Cloning PVX CP gene for northern blot probe production
DIG-Labeled DNA Probe			
70	U6 Probe	AGGGGCCATGCTAATCTTCTC /Dig_N/	Small RNA loading control DIG-labeled probe
RT-qPCR / RT-PCR Assays			
71	GFP-F	ACGGCATCAAAGCCAACTTC	GFP RT-qPCR
72	GFP-R	GCACGCCGCCGTCTT	GFP RT-qPCR
73	GFP Probe	/FAM/ CCCGCCACAACAT /NFQ/	GFP RT-qPCR, TaqMan™ MGB probe, Applied Biosystems™
74	PVX CP F	GGCCAGGGCACAATCCA	PVX RT-qPCR assay
75	PVX CP R	GACCTCGAGTGACAGCTGCAT	PVX RT-qPCR assay
76	PVX CP Probe	/FAM/ CGACTTTGCCAGCCTA /NFQ/	PVX RT-qPCR assay, TaqMan™ MGB probe, Applied Biosystems™
77	NbPP2A F	CCACTCGGTGGTGGAGAAA	NbPP2A RT-qPCR assay
78	NbPP2A R	CATCAGGGTCTTCAGCTAGCTCTA	NbPP2A RT-qPCR assay
79	NbPP2A Probe	CCATTCGCCCTAGTTT	NbPP2A RT-qPCR assay, TaqMan™ MGB probe, Applied Biosystems™
80	mgfp5 FWD	GGCCAACACTTGTCACTACT	GFP RT-PCR primer for RIP assay
81	mgfp5 REV	GGTCTTGAAGTTGGCTTTGATG	GFP RT-PCR primer for RIP assay

Table 3.2 List of plasmids, constructs, and bacterial strains used in this study.

Plasmids or Strains	Description	Source / Reference
Plasmids		
pEarleyGate100	pEG100; a Gateway binary vector with cauliflower mosaic virus *35S* promoter, Kan^R	Earley et al.
pEarleyGate100::*GFP*	pEG100 carrying *GFP* , Kan^R	This study
pEarleyGate100::*CMV2b*	pEG100 carrying *CMV2b* , Kan^R	This study
pEarleyGate100::*CLBV-MP*	pEG100 carrying *CLBV-MP* , Kan^R	This study
pEarleyGate100::*CTLV-CP*	pEG100 carrying *CTLV-CP* , Kan^R	This study
pEarleyGate100::*CTLV-MP*	pEG100 carrying *CTLV-MP* , Kan^R	This study
pEarleyGate1001	pEG1001; modified from pEG100 by adding *Flag* at the downstream of cloning site, Kan^R	This study
pEarleyGate1001::*GFP*	pEG1001 carrying *GFP* tagged with *Flag* at C-terminal, Kan^R	This study
pEarleyGate1001::*CMV2b*	pEG1001 carrying *CMV2b* tagged with *Flag* at C-terminal, Kan^R	This study
pEarleyGate1001::*CLBV-MP*	pEG1001 carrying *CLBV-MP* tagged with *Flag* at C-terminal, Kan^R	This study
pEarleyGate1001::*CTLV-CP*	pEG1001 carrying *CTLV-CP* tagged with *Flag* at C-terminal, Kan^R	This study
pEarleyGate1001::*CTLV-MP*	pEG1001 carrying *CTLV-MP* tagged with *Flag* at C-terminal, Kan^R	This study
pGR106	A binary and infectious vector carrying the Potato virus X genome, Kan^R	Jones et al.
pGR106::*CLBV-MP*	pGR106 carrying *CLBV-MP* , Kan^R	This study
pGR106::*CTLV-CP*	pGR106 carrying *CTLV-CP* , Kan^R	This study
pGR106::*CTLV-MP*	pGR106 carrying *CTLV-MP* , Kan^R	This study
pGR106::*CTLV-CP* -frameshift	pGR106 carrying *CTLV-CP* with framshifting, Kan^R	This study
pGR106::*CTLV-MP* -frameshift	pGR106 carrying *CTLV-MP* with framshifting, Kan^R	This study
pGR106::*CTLV-CP-D1*	pGR106 carrying *CTLV-CP* with deletion from 2 to 35 amino acid, Kan^R	This study
pGR106::*CTLV-CP-D2*	pGR106 carrying *CTLV-CP* with deletion from 36 to 70 amino acid, Kan^R	This study
pGR106::*CTLV-CP-D3*	pGR106 carrying *CTLV-CP* with deletion from 71 to 106 amino acid, Kan^R	This study
pGR106::*CTLV-CP-D4*	pGR106 carrying *CTLV-CP* with deletion from 107 to 143 amino acid, Kan^R	This study
pGR106::*CTLV-CP-D5*	pGR106 carrying *CTLV-CP* with deletion from 144 to 180 amino acid, Kan^R	This study
pGR106::*CTLV-CP-D6*	pGR106 carrying *CTLV-CP* with deletion from 181 to 217 amino acid, Kan^R	This study
pGR106::*CTLV-CP-D7*	pGR106 carrying *CTLV-CP* with deletion from 218 to 237 amino acid, Kan^R	This study

Abbreviations: ^{R}: Resistance Gene; Kan: kanamycin; Amp: ampicillin; Gen: gentamycin; Tet: tetracycline.

Table 3.2 List of plasmids, constructs, and bacterial strains used in this study (cont'd).

Plasmids or Strains	Description	Source / Reference
Plasmids		
pGR106::*CTLV-MP* -D1	pGR106 carrying *CTLV-MP* with deletion from 2 to 40 amino acid, Kan^R	This study
pGR106::*CTLV-MP* -D2	pGR106 carrying *CTLV-MP* with deletion from 41 to 72 amino acid, Kan^R	This study
pGR106::*CTLV-MP* -D3	pGR106 carrying *CTLV-MP* with deletion from 73 to 111 amino acid, Kan^R	This study
pGR106::*CTLV-MP* -D4	pGR106 carrying *CTLV-MP* with deletion from 112 to 143 amino acid, Kan^R	This study
pGR106::*CTLV-MP* -D5	pGR106 carrying *CTLV-MP* with deletion from 144 to 176 amino acid, Kan^R	This study
pGR106::*CTLV-MP* -D6	pGR106 carrying *CTLV-MP* with deletion from 177 to 209 amino acid, Kan^R	This study
pGR106::*CTLV-MP* -D7	pGR106 carrying *CTLV-MP* with deletion from 210 to 241 amino acid, Kan^R	This study
pGR106::*CTLV-MP* -D8	pGR106 carrying *CTLV-MP* with deletion from 242 to 273 amino acid, Kan^R	This study
pGR106::*CTLV-MP* -D9	pGR106 carrying *CTLV-MP* with deletion from 274 to 306 amino acid, Kan^R	This study
pGR106::*CTLV-MP* -D10	pGR106 carrying *CTLV-MP* with deletion from 307 to 320 amino acid, Kan^R	This study
pEarleyGate1001::*TCV-P38*	pEG1001 carrying *TCV-P38* tagged with *Flag* at C-terminal, Kan^R	This study
pEarleyGate1001::*TBSV-P19*	pEG1001 carrying *TBSV-P19* tagged with *Flag* at C-terminal, Kan^R	This study
pGEMT-Easy::*T7-GFP*	pGEM®-T Easy carrying *GFP*, upstream with T7 promoter, Amp^R	This study
pGEMT-Easy::*GFP-T7*	pGEM®-T Easy carrying *GFP*, downstream with T7 promoter, Amp^R	This study
pGEMT-Easy::*PVX-CP-T7*	pGEM®-T Easy carrying *PVX-CP*, downstream with T7 promoter, Amp^R	This study
Bacterial Strains		
Escherichia coli NEB® 5-alpha	*fhuA2 Δ(argF-lacZ)U169 phoA glnV44 Φ80Δ (lacZ)M15 gyrA96 recA1 relA1 endA1 thi-1 hsdR17*	New England Biolabs
Escherichia coli TOP10	F- *mcrA* Δ(*mrr-hsdRMS-mcrBC*) φ80*lacZ* ΔM15 *Δlac* X74 *rec* A1 *ara* D139 Δ(*araleu*)7697 *gal* U *gal* K *rps* L (Str^R) *end* A1 *nup* G	Thermal Fisher Scientific
Agrobacterium tumefaciens GV3101 (pMP90)	Rif^R, Gen^R	Wroblewski et al.
Agrobacterium tumefaciens GV3101 (pMP90::pSOUP)	Rif^R, Gen^R, Tet^R	This study

Abbreviations: ^{R}: Resistance Gene; Kan: kanamycin; Amp: ampicillin; Gen: gentamycin; Tet: tetracycline.

Table 3.3 Silencing suppression rate of co-infiltration assay of citrus tater leaf virus coat protein and movement protein.

Constructs	No. of Plants Infiltrated	No. of Plants Silencing Suppressed	
		Locally	Systemically
pEG100-GFP + pEG100	40	0 **(0%)**	0 **(0%)**
pEG100-GFP + pEG100-CMV-2b	40	40 **(100%)**	40 **(100%)**
pEG100-GFP + pEG100-CTLV-CP	39	0 **(0%)**	17 **(44%)**
pEG100-GFP + pEG100-CTLV-MP	39	18 **(46%)**	0 **(0%)**
pEG100-GFP + pEG100-CLBV-MP	39	16 **(41%)**	6 **(15%)**

Abbreviations: CMV-2b: cucumber mosaic virus 2b; CTLV: citrus tatter leaf virus; CLBV: citrus leaf blotch virus; CP: coat protein; MP: movement protein

Table 3.4 Silencing suppression rate of co-infiltration assay of citrus tatter leaf virus partial deletion of coat protein and movement protein.

Constructs	No. of Plants Infiltrated	No. of Plants Silencing Suppressed	
		Locally	Systemically
pEG100-GFP + pEG100-CTLV-CP	39	0 **(0%)**	17 **(44%)**
pEG100-GFP + pEG100-CTLV-CP$^{\Delta 36-70}$ (D2)	12	0 **(0%)**	2 **(17%)**
pEG100-GFP + pEG100-CTLV-MP	39	18 **(46%)**	0 **(0%)**
pEG100-GFP + pEG100-CTLV-MP$^{\Delta 122-143}$ (D4)	12	2 **(17%)**	0 **(0%)**

Abbreviations: CTLV: citrus tatter leaf virus; CP: coat protein; MP: movement protein

Table 3.5 List of potential citrus tatter leaf virus coat protein (CP)-associated proteins identified by UPLC/Q-TOF-MS in *N. benthamiana*.

N. benthamiana Accession No.	Best Match in *Arabidopsis thaliana*	Protein Name / Description	No. of Observed Peptides	emPAI	Mascot Score	Sequence Coverage
NbS00035989g0001.1	AT5G11580.1	Regulator of chromosome condensation (RCC1) family protein	21	26.12	777.08	37.80
NbS00027424g0009.1	AT1G09620.1	ATP binding/leucine-tRNA ligases/aminoacyl-tRNA ligase	48	11.83	1105.95	51.46
NbS00000088g0002.1	AT4G30010.1	ATP-dependent RNA helicase	2	9.00	23.15	20.93
NbS00019288g0006.1	AT5G23860.2	beta-tubulin	7	7.58	416.60	30.00
NbS00030810g0011.1	AT2G43160.1	ENTH/VHS family protein	17	7.11	454.54	26.11
NbS00003947g0013.1	AT5G64460.8	Phosphoglycerate mutase family protein	7	6.74	36.46	66.91
NbS00031412g0004.1	AT3G12110.1	Actin-11, ACT11	12	6.11	520.46	39.43
NbS00006458g0003.1	AT4G14960.2	alpha-tubulin isoform, TUA6	14	5.72	575.98	38.80
NbS00000030g0010.1	AT2G43160.4	ENTH/VHS family protein	17	5.66	437.14	20.02
NbS00044990g0002.1	AT2G39730.1	Rubisco activase, RCA	18	5.58	505.23	50.56
NbS00016397g0010.1	AT4G33090.1	Puromycin-sensitive aminopeptidase	31	5.56	485.22	45.77
NbS00046182g0007.1	AT5G59370.2	Actin 4	10	4.75	464.42	40.05
NbS00003962g0006.1	AT2G37370.1	Centrosomal protein of 135 kDa-like protein	13	4.62	164.01	52.91
NbS00027242g0004.1	AT5G59613.2	ATP synthase	2	4.62	13.32	31.34
NbS00003508g0016.1	AT3G13330.1	Proteasome activating protein 200	50	4.01	1034.15	37.56
NbS00019252g0009.1	AT3G20320.1	Trigalactosyldiacylglycerol2	6	3.92	50.49	28.72
NbS00002899g0003.1	AT1G04430.2	S-adenosyl-L-methionine-dependent methyltransferases superfamily protein	23	3.81	274.80	41.42
NbS00022532g0009.1	AT3G20320.1	Trigalactosyldiacylglycerol2	13	3.77	358.42	38.92
NbS00004706g0011.1	AT3G18480.1	CCAAT-displacement protein alternatively spliced product	22	3.73	179.03	38.15
NbS00054890g0003.1	AT4G00430.1	Plasma membrane intrinsic protein 1	9	3.64	54.18	41.81
NbS00003552g0008.1	AT3G18480.1	CCAAT-displacement protein alternatively spliced product	32	3.53	344.14	38.61
NbS00008003g0012.1	AT3G18480.1	CCAAT-displacement protein alternatively spliced product	32	3.53	322.91	43.87
NbS00057125g0003.1	AT1G04430.2	S-adenosyl-L-methionine-dependent methyltransferases superfamily protein	22	3.49	274.34	37.50
NbS00030134g0011.1	AT5G09880.1	Splicing factor, CC1-like	13	3.42	165.19	27.15
NbS00016385g0017.1	AT3G18480.1	CCAAT-displacement protein alternatively spliced product	30	3.24	254.68	41.60
NbS00006841g0003.1	AT4G00430.1	Plasma membrane intrinsic protein 1	9	3.22	56.87	41.81
NbS00003479g0020.1	AT5G54160.1	O-methyltransferase 1	8	3.22	96.88	30.58
NbS00045109g0006.1	AT5G54160.1	O-methyltransferase 1	7	3.06	100.14	30.58
NbS00003172g0001.1	AT3G23820.1	UDP-D-glucuronate 4-epimerase 6	13	3.05	145.85	37.11
NbS00043286g0001.1	AT1G65980.1	Thioredoxin-dependent peroxidase 1	2	2.98	27.69	16.67
NbS00021129g0002.1	AT4G30010.1	ATP-dependent RNA helicase	1	2.98	11.97	18.60
NbS00004413g0003.1	AT3G66654.2	Cyclophilin-like peptidyl-prolyl cis-trans isomerase family protein	8	2.88	143.93	30.27
NbS00056344g0007.1	AT1G78300.1	General regulatory factor 2	10	2.83	149.61	42.35
NbS00038051g0004.1	AT4G14960.2	Tubulin/FtsZ family protein	10	2.81	431.67	27.79

Table 3.5 List of potential citrus tatter leaf virus coat protein (CP)-associated proteins identified by UPLC/Q-TOF-MS in *N. benthamiana* (cont'd).

N. benthamiana Accession No.	Best Match in *Arabidopsis thaliana*	Protein Name / Description	No. of Observed Peptides	emPAI	Mascot Score	Sequence Coverage
NbS00046497g0001.1	AT5G64460.5	Phosphoglycerate mutase family protein	3	2.73	33.86	34.75
NbS00003962g0002.1	AT5G13560.1	Structural maintenance of chromosomes protein	5	2.59	79.66	31.80
NbS00017951g0015.1	AT1G19360.1	Nucleotide-diphospho-sugar transferase family protein	12	2.59	119.18	35.29
NbS00032256g0001.1	AT5G09880.1	Splicing factor, CC1-like	11	2.54	136.63	20.44
NbS00010545g0005.1	AT2G21620.1	Adenine nucleotide alpha hydrolases-like superfamily protein	4	2.46	32.14	29.94
NbS00017354g0008.1	AT1G04080.1	Tetratricopeptide repeat (TPR)-like superfamily protein	17	2.37	133.73	31.78
NbS00001653g0010.1	AT1G04080.1	Tetratricopeptide repeat (TPR)-like superfamily protein	16	2.35	164.81	29.50
NbS00010323g0009.1	AT3G23820.1	UDP-D-glucuronate 4-epimerase 6	11	2.30	102.74	41.28
NbS00034559g0014.1	ATCC 51363	GroES-like zinc-binding alcohol dehydrogenase family protein	4	2.16	32.05	22.93
NbS00044621g0001.1	AT2G21130.1	Peptidyl-prolyl cis-trans isomerase	5	2.16	69.68	29.07
NbS00052811g0006.1	AT1G04430.2	S-adenosyl-L-methionine-dependent methyltransferases superfamily protein	19	2.08	189.63	34.15
NbS00035212g0002.1	AT1G07890.6	Ascorbate peroxidase 1	8	2.03	85.46	39.66
NbS00002358g0009.1	AT1G07890.8	Ascorbate peroxidase 1	7	2.02	92.34	39.41
NbS00010073g0014.1	AT3G66654.2	Cyclophilin-like peptidyl-prolyl cis-trans isomerase family protein	8	1.99	140.31	26.42
NbS00041476g0008.1	AT1G18270.1	Ketose-bisphosphate aldolase class-II family protein	39	1.98	261.89	32.73
NbS00029456g0006.1	AT2G37170.1	Plasma membrane intrinsic protein 2	5	1.96	50.81	30.77
NbS00027349g0023.1	AT1G19360.1	Nucleotide-diphospho-sugar transferase family protein	10	1.91	120.49	29.02
NbS00012616g0008.1	AT2G22360.1	DNAJ heat shock family protein	6	1.89	59.42	46.63
NbC25340200g0001.1	AT3G48870.2	Clp ATPase	4	1.89	34.67	34.90
NbS00037522g0005.1	AT2G47680.1	Zinc finger (CCCH type) helicase family protein	22	1.89	187.03	28.26
NbS00055578g0001.1	AT3G49430.3	SER/ARG-rich protein 34	8	1.87	77.59	24.58
NbS00012784g0015.1	AT4G35090.1	Catalase 2	10	1.87	166.11	31.12
NbS00033243g0006.1	AT1G04430.2	S-adenosyl-L-methionine-dependent methyltransferases superfamily protein	17	1.85	192.63	32.15
NbS00020265g0006.1	AT5G13450.1	delta subunit of Mt ATP synthase	6	1.82	44.58	29.68
NbS00028134g0008.1	AT1G66070.2	Translation initiation factor eIF3 subunit	6	1.78	49.44	28.13
NbS00010354g0016.1	AT1G72660.3	P-loop containing nucleoside triphosphate hydrolases superfamily protein	8	1.72	63.40	30.09
NbS00055279g0004.1	AT1G52510.1	alpha/beta-Hydrolases superfamily protein	5	1.72	72.04	16.40
NbS00000471g0009.1	AT2G05100.1	Photosystem II light harvesting complex gene	4	1.68	52.85	18.94
NbS00014997g0006.1	AT5G13450.1	delta subunit of Mt ATP synthase	5	1.58	34.72	25.13
NbS00006116g0019.1	AT4G35090.1	Catalase 2	11	1.57	165.13	30.66
NbS00016897g0015.1	AT5G13500.3	Hyp O-arabinosyltransferase-like protein	7	1.57	55.56	27.98
NbS00009747g0010.1	AT5G55660.1	DEK domain-containing chromatin associated protein	14	1.56	147.72	23.55
NbS00015969g0002.1	AT1G09640.1	Translation elongation factor EF1B	10	1.51	129.67	26.02
NbS00013098g0009.1	AT3G07950.1	Rhomboid protein-related	4	1.51	14.48	43.09

Table 3.5 List of potential citrus tatter leaf virus coat protein (CP)-associated proteins identified by UPLC/Q-TOF-MS in *N. benthamiana* (cont'd).

N. benthamiana Accession No.	Best Match in *Arabidopsis thaliana*	Protein Name / Description	No. of Observed Peptides	emPAI	Mascot Score	Sequence Coverage
NbS00038547g0010.1	AT4G35785.1	RNA-binding (RRM/RBD/RNP motifs) family protein	5	1.51	56.22	26.64
NbS00038860g0017.1	AT1G02840.3	RNA-binding (RRM/RBD/RNP motifs) family protein	7	1.51	60.07	26.04
NbS00008464g0006.1	AT5G12110.1	Glutathione S-transferase, C-terminal-like;Translation elongation factor EF1B/ribosomal protein S6	5	1.42	20.85	25.66
NbS00050861g0003.1	AT1G45170.1	Outer envelope pore 24B-like protein	3	1.42	10.46	18.09
NbS00008999g0021.1	AT3G13772.1	Transmembrane nine 7	10	1.41	80.12	17.37
NbS00000252g0005.1	AT3G23600.1	alpha/beta-Hydrolases superfamily protein	4	1.37	27.48	26.36
NbS00032836g0007.1	AT1G02840.3	RNA-binding (RRM/RBD/RNP motifs) family protein	7	1.35	66.44	27.30
NbS00001183g0003.1	AT4G12910.1	Serine carboxypeptidase-like 20	8	1.35	57.07	18.16
NbS00021840g0003.1	AT3G05530.1	Regulatory particle triple-A ATPase 5A	10	1.33	97.66	25.77
NbS00007401g0003.1	AT5G13500.3	Hyp O-arabinosyltransferase-like protein	6	1.31	49.60	24.93
NbS00005601g0008.1	AT3G13772.1	Transmembrane nine 7	11	1.29	92.65	21.12
NbS00025239g0009.1	AT4G35100.2	Plasma membrane intrinsic protein 3	4	1.28	39.88	35.79
NbS00007385g0004.1	AT1G30230.1	Glutathione S-transferase	4	1.28	35.60	22.03
NbS00020461g0001.1	AT3G53520.1	UDP-glucuronic acid decarboxylase 1	9	1.28	76.15	26.67
NbS00043955g0003.1	AT1G30230.2	Glutathione S-transferase	5	1.25	41.24	21.59
NbS00037510g0012.1	AT2G01970.1	Endomembrane protein 70 protein family	10	1.25	135.01	17.37
NbS00019252g0008.1	AT3G20320.1	Trigalactosyldiacylglycerol2	6	1.24	231.24	27.15
NbS00056569g0004.1	AT3G25140.1	Nucleotide-diphospho-sugar transferases superfamily protein	12	1.23	112.27	22.61
NbS00008151g0013.1	AT1G77490.1	Thylakoidal ascorbate peroxidase	9	1.21	46.52	25.06
NbS00009733g0021.1	AT1G80480.1	Plastid transcriptionally active 17	8	1.21	93.65	18.48
NbS00005540g0006.1	AT2G01970.1	Endomembrane protein 70 protein family	11	1.20	98.27	15.80
NbS00023196g0008.1	AT5G41210.1	Glutathione S-transferase THETA 1	3	1.15	13.64	25.81
NbS00003754g0001.1	AT5G41685.1	Mitochondrial outer membrane translocase complex	1	1.15	8.10	20.78
NbS00060849g0001.1	AT5G19350.2	RNA-binding (RRM/RBD/RNP motifs) family protein	3	1.15	51.30	29.89
NbS00029324g0007.1	AT3G13570.1	SC35-like splicing factor 30A	5	1.15	55.25	21.01
NbS00019983g0006.1	AT5G46290.1	3-ketoacyl-acyl carrier protein synthase	3	1.15	46.02	22.06
NbS00028669g0013.1	AT4G35785.1	RNA-binding (RRM/RBD/RNP motifs) family protein	4	1.15	48.05	20.64
NbS00024706g0002.1	AT5G50920.1	CLPC homologue 1	20	1.13	179.05	30.40
NbS00034319g0004.1	AT5G65730.1	Xyloglucan endotransglucosylase/hydrolase 6	4	1.08	116.49	18.75
NbS00025171g0003.1	AT5G08680.1	ATP synthase alpha/beta family protein	3	1.05	40.87	18.55
NbS00003600g0001.1	AT1G44910.2	Pre-mRNA-processing protein 40A	10	1.02	109.06	13.72
NbS00039057g0010.1	AT1G11860.3	Glycine cleavage T-protein family	9	1.00	82.19	28.08

Table 3.6 List of potential citrus tatter leaf virus movement protein (MP)-associated proteins identified by UPLC/Q-TOF-MS in *N. benthamiana*.

N. benthamiana Accession No.	Best Match in *Arabidopsis thaliana*	Protein Name / Description	No. of Observed Peptides	emPAI	Mascot Score	Sequence Coverage
NbS00035989g0001.1	AT5G11580.1	Regulator of chromosome condensation (RCC1) family protein	21	26.12	777.08	37.80
NbS00056603g0002.1	AT1G75780.1	Tubulin beta-1 chain, TUB1	12	17.33	588.10	39.67
NbS00027424g0009.1	AT1G09620.1	ATP binding; leucine-tRNA ligases; aminoacyl-tRNA ligases; nucleotide binding	48	11.83	1105.95	51.46
NbS00030497g0004.1	AT5G23860.2	Tubulin beta 8, TUB8	8	10.66	428.48	27.81
NbS00000088g0002.1	AT4G30010.1	ATP-dependent RNA helicase	2	9.00	23.15	20.93
NbS00030810g0011.1	AT2G43160.1	ENTH/VHS family protein	17	7.11	454.54	26.11
NbS00003947g0013.1	AT5G64460.8	Phosphoglycerate mutase family protein	7	6.74	36.46	66.91
NbS00008911g0002.1	AT1G42970.1	Glyceraldehyde-3-phosphate dehydrogenase B subunit	19	5.66	639.11	46.28
NbS00000030g0010.1	AT2G43160.4	ENTH/VHS family protein	17	5.66	437.14	20.02
NbS00016397g0010.1	AT4G33090.1	Aminopeptidase M1	31	5.56	485.22	45.77
NbS00045823g0014.1	AT2G28900.1	Outer plastid envelope protein 16-1	4	4.62	27.36	47.77
NbS00003962g0006.1	AT5G13560.1	Structural maintenance of chromosomes protein	13	4.62	164.01	52.91
NbS00003508g0016.1	AT3G13330.1	Proteasome activating protein 200	50	4.01	1034.15	37.56
NbS00019252g0009.1	AT3G20320.1	Trigalactosyldiacylglycerol2	6	3.92	50.49	28.72
NbS00002899g0003.1	AT1G04430.2	S-adenosyl-L-methionine-dependent methyltransferases superfamily protein	23	3.81	274.80	41.42
NbS00022532g0009.1	AT3G20320.1	Trigalactosyldiacylglycerol2	13	3.77	358.42	38.92
NbS00004706g0011.1	AT3G18480.1	CCAAT-displacement protein alternatively spliced product	22	3.73	179.03	38.15
NbS00054890g0003.1	AT4G00430.1	Plasma membrane intrinsic protein 1	9	3.64	54.18	41.81
NbS00003552g0008.1	AT3G18480.1	CCAAT-displacement protein alternatively spliced product	32	3.53	344.14	38.61
NbS00008003g0012.1	AT3G18480.1	CCAAT-displacement protein alternatively spliced product	32	3.53	322.91	43.87
NbS00057125g0003.1	AT1G04430.2	S-adenosyl-L-methionine-dependent methyltransferases superfamily protein	22	3.49	274.34	37.50
NbS00030134g0011.1	AT5G09880.1	Splicing factor, CC1-like	13	3.42	165.19	27.15
NbS00016385g0017.1	AT3G18480.1	CCAAT-displacement protein alternatively spliced product	30	3.24	254.68	41.60
NbS00006841g0003.1	AT4G00430.1	Plasma membrane intrinsic protein 1	9	3.22	56.87	41.81
NbS00016445g0012.1	AT5G09810.1	Actin 7	8	3.22	317.00	35.16
NbS00003479g0020.1	AT5G54160.1	O-methyltransferase 1	8	3.22	96.88	30.58
NbS00045109g0006.1	AT5G54160.1	O-methyltransferase 1	7	3.06	100.14	30.58
NbS00003172g0001.1	AT3G23820.1	UDP-D-glucuronate 4-epimerase 6	13	3.05	145.85	37.11
NbS00021129g0002.1	AT4G30010.1	ATP-dependent RNA helicase	1	2.98	11.97	18.60
NbS00043286g0001.1	AT1G65980.1	Thioredoxin-dependent peroxidase 1	2	2.98	27.69	16.67
NbS00044851g0011.1	AT3G13920.1	Eukaryotic translation initiation factor 4A1	12	2.98	206.26	35.84
NbS00004413g0003.1	AT3G66654.2	Cyclophilin-like peptidyl-prolyl cis-trans isomerase family protein	8	2.88	143.93	30.27
NbS00056344g0007.1	AT1G78300.1	General regulatory factor 2	10	2.83	149.61	42.35
NbS00038051g0004.1	AT4G14960.2	Tubulin/FtsZ family protein	10	2.81	431.67	27.79

Table 3.6 List of potential citrus tatter leaf virus movement protein (MP)-associated proteins identified by UPLC/Q-TOF-MS in *N. benthamiana* (cont'd).

N. benthamiana Accession No.	Best Match in *Arabidopsis thaliana*	Protein Name / Description	No. of Observed Peptides	emPAI	Mascot Score	Sequence Coverage
NbS00021088g0005.1	AT5G48300.1	ADP glucose pyrophosphorylase 1	19	2.70	348.82	48.27
NbS00024386g0011.1	AT3G05560.3	Ribosomal L22e protein family	4	2.59	37.33	35.43
NbS00003962g0002.1	AT2G37370.1	Centrosomal protein of 135 kDa-like protein	5	2.59	79.66	31.80
NbS00017951g0015.1	AT1G19360.1	Nucleotide-diphospho-sugar transferase family protein	12	2.59	119.18	35.29
NbS00032256g0001.1	AT5G09880.1	Splicing factor, CC1-like	11	2.54	136.63	20.44
NbS00017354g0008.1	AT1G04080.1	Tetratricopeptide repeat (TPR)-like superfamily protein	17	2.37	133.73	31.78
NbS00001653g0010.1	AT1G04080.1	Tetratricopeptide repeat (TPR)-like superfamily protein	16	2.35	164.81	29.50
NbS00010323g0009.1	AT3G23820.1	UDP-D-glucuronate 4-epimerase 6	11	2.30	102.74	41.28
NbS00024811g0011.1	AT3G22890.1	ATP sulfurylase 1	11	2.16	112.83	28.79
NbS00034559g0014.1	AT5G63620.1	GroES-like zinc-binding alcohol dehydrogenase family protein	4	2.16	32.05	22.93
NbS00044621g0001.1	AT2G21130.1	Cyclophilin-like peptidyl-prolyl cis-trans isomerase family protein	5	2.16	69.68	29.07
NbS00052811g0006.1	AT1G04430.2	S-adenosyl-L-methionine-dependent methyltransferases superfamily protein	19	2.08	189.63	34.15
NbS00002358g0009.1	AT1G07890.8	Ascorbate peroxidase 1	7	2.02	92.34	39.41
NbS00010073g0014.1	AT3G66654.2	Cyclophilin-like peptidyl-prolyl cis-trans isomerase family protein	8	1.99	140.31	26.42
NbS00041476g0008.1	AT1G18270.1	Ketose-bisphosphate aldolase class-II family protein	39	1.98	261.89	32.73
NbS00029456g0006.1	AT2G37170.1	Plasma membrane intrinsic protein 2	5	1.96	50.81	30.77
NbS00027349g0023.1	AT1G19360.1	Nucleotide-diphospho-sugar transferase family protein	10	1.91	120.49	29.02
NbC25340200g0001.1	AT3G48870.2	Clp ATPase	4	1.89	34.67	34.90
NbS00037522g0005.1	AT2G47680.1	Zinc finger (CCCH type) helicase family protein	22	1.89	187.03	28.26
NbS00055578g0001.1	AT3G49430.3	SER/ARG-rich protein 34A	8	1.87	77.59	24.58
NbS00012784g0015.1	AT4G35090.1	Catalase 2	10	1.87	166.11	31.12
NbS00033243g0006.1	AT1G04430.2	S-adenosyl-L-methionine-dependent methyltransferases superfamily protein	17	1.85	192.63	32.15
NbS00020265g0006.1	AT5G13450.1	delta subunit of Mt ATP synthase	6	1.82	44.58	29.68
NbS00028134g0008.1	AT1G66070.2	Translation initiation factor eIF3 subunit	6	1.78	49.44	28.13
NbS00010354g0016.1	AT1G72660.3	P-loop containing nucleoside triphosphate hydrolases superfamily protein	8	1.72	63.40	30.09
NbS00055279g0004.1	AT1G52510.1	alpha/beta-Hydrolases superfamily protein	5	1.72	72.04	16.40
NbS00020631g0001.1	AT4G35100.2	Plasma membrane intrinsic protein 3	4	1.68	34.95	34.19
NbS00000471g0009.1	AT2G05100.1	Photosystem II light harvesting complex gene 2.1	4	1.68	52.85	18.94
NbS00022787g0008.1	AT5G06290.1	2-cysteine peroxiredoxin B	6	1.64	79.70	22.96
NbS00014997g0006.1	AT5G13450.1	delta subunit of Mt ATP synthase	5	1.58	34.72	25.13
NbS00006116g0019.1	AT4G35090.1	Catalase 2	11	1.57	165.13	30.66
NbS00016897g0015.1	AT5G13500.3	Hyp O-arabinosyltransferase-like protein	7	1.57	55.56	27.98
NbS00009747g0010.1	AT5G55660.1	DEK domain-containing chromatin associated protein	14	1.56	147.72	23.55
NbS00020892g0003.1	AT3G05560.3	Ribosomal L22e protein family	4	1.51	59.40	28.13

Table 3.6 List of potential citrus tatter leaf virus movement protein (MP)-associated proteins identified by UPLC/Q-TOF-MS in *N. benthamiana* (cont'd).

N. benthamiana Accession No.	Best Match in *Arabidopsis thaliana*	Protein Name / Description	No. of Observed Peptides	emPAI	Mascot Score	Sequence Coverage
NbS00015969g0002.1	AT1G09640.1	Translation elongation factor EF1B, gamma chain	10	1.51	129.67	26.02
NbS00013098g0009.1	AT3G07950.1	Rhomboid protein-related	4	1.51	14.48	43.09
NbS00038547g0010.1	AT4G35785.1	RNA-binding (RRM/RBD/RNP motifs) family protein	5	1.51	56.22	26.64
NbS00038860g0017.1	AT1G02840.3	RNA-binding (RRM/RBD/RNP motifs) family protein	7	1.51	60.07	26.04
NbS00005651g0008.1	AT1G09640.1	Translation elongation factor EF1B, gamma chain	10	1.45	127.40	26.81
NbS00008464g0006.1	AT5G12110.1	Glutathione S-transferase, C-terminal-like;Translation elongation factor EF1B/ribosomal protein S6	5	1.42	20.85	25.66
NbS00050861g0003.1	AT1G45170.1	Outer envelope pore 24B-like protein	3	1.42	10.46	18.09
NbS00000252g0005.1	AT3G23600.1	alpha/beta-Hydrolases superfamily protein	4	1.37	27.48	26.36
NbS00032836g0007.1	AT1G02840.3	RNA-binding (RRM/RBD/RNP motifs) family protein	7	1.35	66.44	27.30
NbS00001183g0003.1	AT4G12910.1	Serine carboxypeptidase-like 20	8	1.35	57.07	18.16
NbS00007401g0003.1	AT5G13500.3	Hyp O-arabinosyltransferase-like protein	6	1.31	49.60	24.93
NbS00005601g0008.1	AT3G13772.1	Transmembrane nine 7	11	1.29	92.65	21.12
NbS00025239g0009.1	AT4G35100.2	Plasma membrane intrinsic protein 3	4	1.28	39.88	35.79
NbS00007385g0004.1	AT1G30230.1	Glutathione S-transferase, C-terminal-like;Translation elongation factor EF1B/ribosomal protein S6	4	1.28	35.60	22.03
NbS00020461g0001.1	AT3G53520.1	UDP-glucuronic acid decarboxylase 1	9	1.28	76.15	26.67
NbS00037510g0012.1	AT2G01970.1	Endomembrane protein 70 protein family	10	1.25	135.01	17.37
NbS00043955g0003.1	AT1G30230.2	Glutathione S-transferase, C-terminal-like;Translation elongation factor EF1B/ribosomal protein S6	5	1.25	41.24	21.59
NbS00019252g0008.1	AT3G20320.1	Trigalactosyldiacylglycerol2	6	1.24	231.24	27.15
NbS00056569g0004.1	AT3G25140.1	Nucleotide-diphospho-sugar transferases superfamily protein	12	1.23	112.27	22.61
NbS00008151g0013.1	AT1G77490.1	Thylakoidal ascorbate peroxidase	9	1.21	46.52	25.06
NbS00005540g0006.1	AT2G01970.1	Endomembrane protein 70 protein family	11	1.20	98.27	15.80
NbS00003754g0001.1	AT5G41685.1	Mitochondrial outer membrane translocase complex	1	1.15	8.10	20.78
NbS00060849g0001.1	AT5G19350.2	RNA-binding (RRM/RBD/RNP motifs) family protein	3	1.15	51.30	29.89
NbS00029324g0007.1	AT3G13570.1	SC35-like splicing factor 30A	5	1.15	55.25	21.01
NbS00028669g0013.1	AT4G35785.1	RNA-binding (RRM/RBD/RNP motifs) family protein	4	1.15	48.05	20.64
NbS00024706g0002.1	AT5G50920.1	CLPC homologue 1	20	1.13	179.05	30.40
NbS00034319g0004.1	AT5G65730.1	Xyloglucan endotransglucosylase/hydrolase 6	4	1.08	116.49	18.75
NbS00017563g0004.1	AT1G78630.1	Ribosomal protein L13 family protein	3	1.05	48.52	17.99
NbS00060621g0001.1	AT3G48730.1	Glutamate-1-semialdehyde 2,1-aminomutase 2	8	1.04	105.85	29.08
NbS00003600g0001.1	AT1G44910.2	Pre-mRNA-processing protein 40A	10	1.02	109.06	13.72

CHAPTER 4: Two Distinct Viral Suppressors of RNA Silencing Encoded by Citrus vein enation virus

Abstract

Viral proteins have been known to have multiple functions in virus-host interactions. The P0 and open reading frame 3 (ORF3), a putative coat protein, encoded by citrus vein enation virus (CVEV) were identified as viral suppressors of RNA silencing (VSR) using *Agrobacterium*-mediated RNA silencing suppression co-infiltration assay on *GFP*-transgenic *Nicotiana benthamiana* 16c plants. CVEV uses P0 as a local and systemic VSR while the ORF3 as a systemic VSR. When the potato virus X (PVX) infectious vector harboring either CVEV P0 or ORF3 was inoculated on *N. benthamiana*, both constructs promoted viral infection and symptom development, likely through their RNA silencing suppression activities. Mass spectrometry-based immunoprecipitation (IP) proteomics identified CVEV P0, which possessed an F-box motif, interacting with the S-phase kinase-associated protein 1 (SKP1) and cullin 1 (CUL1) to form a multi-protein SCF E3 ubiquitin ligase complex. Co-immunoprecipitation (co-IP) confirmed the interaction between P0 and AtSKP1. Both co-IP and pull-down assays also confirmed the direct interaction between P0 and AGO1, one of the main components in the plant host RNA silencing pathway. The targeted degradation of AGO1 by P0 was found insensitive to the proteasome inhibitor MG132 but sensitive to host autophagic degradation pathway which was previously characterized in other P0s of viruses in *Luteoviridae* family. CVEV ORF3 did not interact

with any protein targets directly related to host silencing pathway and did not bind to any RNA species indicating that ORF3 uses indirect mechanisms to suppress RNA silencing. A robust hypersensitive response-like cell death triggered by P0 in *N. benthamiana* was also observed probably through gene-for-gene interaction.

Introduction

Citrus vein enation disease was first reported by Wallace and Drake in 1953 (Wallace and Drake 1953). The symptoms were described as vein swelling and small papillae-like growth from veins underside of the leaves at scattered locations over the surface and the upper side with corresponding indentations (Wallace and Drake 1953; Wallace and Drake 1959). Nearly all citrus and citrus relative species and varieties are susceptible to its infection (Wallace and Drake 1953; Wallace and Drake 1959). Fraser reported that the vein enation virus is widespread in the citrus of New South Wales, Australia (Fraser 1958). Furthermore, the symptom of woody gall was also observed on rough lemon rootstock at the same production area (Fraser 1958, 1960). The woody gall symptom can also be found on the trunk and branches of Mexican and Rangpur (*Citrus limonia* Osb.) limes, and Volkamer lemon (*C. volkameriana* Tan.). Woody gall was assumed to be caused by a viroid, but later on, it was shown that both vein enation and woody gall diseases were induced by same viral pathogen which was named as citrus vein enation virus (CVEV) (Wallace and Drake 1960, 1961). Both symptoms have been observed in many citrus growing areas including USA, China, Japan, Chile, Brazil, Egypt,

Turkey, South Africa, Australia, Peru, Spain and India (Azeri and Heper 1972; Bazan de Segura and Ferrand ; Chen et al. 1992; Fraser 1958; Jacomino and Salibe 1993; Manjunath 1987; McClean 1954; Sheta et al. 2002; Tanaka and Yamada 1961; Vives et al. 2013; Wallace and Drake 1953).

Vein enation disease was proved to be graft-transmissible and vectored by *Toxoptera citricida* (Kirk.) (McClean 1954) as well as green peach aphids (*Myzus persicae* (Sulz.)) (Wallace and Drake 1959) in a persistent transmission mode. Later, it was also proved that CVEV can be transmitted by *T. aurantii* (Boyer de Fonscolombe) and *Aphis gossypii* (Laird and Weathers 1961; Vives et al. 2013). The causal of agent was finally sequenced and characterized by Vives in 2013 as a new virus that belongs to *Enamovirus* genus of the *Luteoviridae* family (Vives et al. 2013).

CVEV has limited economic impact on citrus industry. It preliminarily effects on inducing seedling yellows in nursery production and woody gall formation on rough lemon rootstocks. Control of vein enation is based on inoculum exclusion and prevention of outbreaks preliminarily with the use of budwood produced in germplasm and budwood certification programs (Bostock et al. 2014; Navarro 1986; Vidalakis et al. 2014).

CVEV is a relatively newly characterized citrus virus. Several genome sequences of CVEV were reported from Spain, Japan, China, Korea as well as 10 sequences characterized in chapter 2 from Australia, California, and Louisiana, USA (Huang et al. 2015; Nakazono-Nagaoka et al. 2017; Vives et al. 2013; Yang et al. 2019). CVEV is a single-stranded, positive sense RNA virus (Vives et al. 2013). It has isometric virus-like

particles of approximately 28 nm in diameter when observed under electron microscope (Da Graça and Maharaj 1991; Maharaj and Da Graca 1988). The genome size of CVEV is 5,983 nucleotides (nt) and has five open reading frames (ORFs) (Vives et al. 2013).

As described in chapter 3, plants evolve different layers of defense systems against viral infection including physical barriers, basal defense, resistant gene responses and antiviral RNA silencing (Ding 2010; Jones and Dangl 2006). To counteract these defenses, viruses use viral proteins to suppress host RNA silencing pathways (Csorba et al. 2015; Ding 2010; Díaz-Pendón and Ding 2008; Pumplin and Voinnet 2013). These proteins are known as viral suppressors of RNA silencing (VSRs) and play critical roles in virus pathogenicity via direct or indirect suppression of host RNA silencing that ultimately leads to enhanced virus accumulation, intensified disease symptoms, and facilitation of cell-to-cell and long-distance movement (Incarbone and Dunoyer 2013).

The CVEV ORF3 which encodes a 21 kDa putative coat protein (CP) has been reported previously as a viral suppressor of RNA silencing (VSR) (Song et al. 2018). Other than ORF3, the proteins products of ORF0 and ORF5 also have potential to be VSRs. In the family of *Luteoviridae*, P0s encoded by ORF0s of several poleroviruses and enamoviruses were identified as strong VSRs despite their low nucleotide sequence identities (Almasi et al. 2015; Baumberger et al. 2007; Bortolamiol et al. 2007; Csorba et al. 2010; Derrien et al. 2012; Fusaro et al. 2012; Mangwende et al. 2009; Pazhouhandeh et al. 2006; Vives et al. 2013; Wang et al. 2015). Meanwhile, ORF 5 is expressed by readthrough of the ORF3 amber stop codon and encodes a 55 kDa CP-readthrough domain

(RTD) fusion protein (Stevens et al. 2005) and it is required for efficient aphid transmission in poleroviruses (Brault et al. 1995; Stevens et al. 2005). ORF5 is also known to have important roles in transmission efficiency, specificity, virus persistence within the aphid vector and involve in symptom expression, virus accumulation, and likely in systemic spread (Brault et al. 2003; Brault et al. 1995; Bruyère et al. 1997; Stevens et al. 2005; Ziegler-Graff 1996).

The purpose of this study is to identify and characterize the VSRs of CVEV using the model plant, *N. benthamiana,* and reveal CVEV VSRs' targets and mechanisms against host antiviral immunity. It is critical to understand more of CVEV and its pathogenicity along with their plant host interactions which will contribute to the development of disease management programs and breeding of CVEV tolerant or resistant citrus.

Materials and Methods

Virus isolate, cloning of viral genes, microbial strains, and growth conditions.

CVEV isolate VE701 characterized in chapter 2 was used in this study. The individual viral genes of ORF0, ORF3 and ORF5 were cloned and analyzed. VE701 was collected from California, USA in 1973 and has been maintained in a sweet orange tree at the greenhouse of Citrus Clonal Protection Program (CCPP), University of California, Riverside. Total RNA of VE701 was extracted from 100 mg of phloem-rich bark of the last matured vegetative flush using TRIzol™ (Invitrogen™, Carlsbad, California, USA), a

standard protocol with phenol-chloroform extraction, followed by isopropanol precipitation, and re-suspension in 50 µl of nuclease-free water. The total RNA was reverse-transcribed to cDNA using SuperScript™ II Reverse Transcriptase (Invitrogen™, Carlsbad, California, USA) with Oligo(dT)$_{12-18}$ (Invitrogen™, Carlsbad, California, USA) primer. Gene specific primers were designed to target ORF0, ORF3 and ORF5 of VE701 isolate (Table 4.1). The ORF0, ORF3 and ORF5 were individually amplified with Platinum® *Pfx* DNA polymerase (Invitrogen™, Carlsbad, California, USA) and then cloned into the entry vector of Gateway® system using the pENTR™ directional TOPO® cloning kit (Invitrogen™, Carlsbad, California, USA). With Gateway® LR Clonase™ II Enzyme Mix (Invitrogen™, Carlsbad, California, USA), the *in vitro* recombination was catalyzed between entry vector pENTR™ and destination vectors, pEarleyGate100 (pEG100; no protein tag sequence) (Earley et al. 2006), pEarleyGate203 (pEG203) with c-Myc coding region at N-terminal (Earley et al. 2006), or modified pEG100 with FLAG coding region at C-terminal (pEG1001) to generate a plant expression clone. Bacterial strains and constructs used in this study are listed in Table 4.2. *Escherichia coli* strains Top10 (Invitrogen™, Carlsbad, California, USA) and NEB® 5-alpha (New England Biolabs®, Ipswich, Massachusetts, USA) were used for molecular cloning (Table 4.2). Plasmids were transformed into *Agrobacterium tumefaciens* strain GV3101 (Wroblewski et al. 2005) and used for transiently expressing proteins in plants (Table 4.2). Both *E. coli* and *A. tumefaciens* were grown in Luria-Bactani (LB) liquid medium and/or agar with appropriate antibiotics supplements at 37°C and 28°C, respectively (Table 4.2).

Plants and growth conditions.

N. benthamiana wild-type and the transgenic line 16c which constitutively expresses GFP protein (Ruiz et al. 1988) were grown from seed and maintained in a temperature-controlled growth room (20 - 24°C) and light (16h light/8h dark). Plants about 4 to 6-week-old were used for the experiments.

Agrobacterium-**mediated transient expression in** *N. benthamiana* **leaves.**

A. tumefaciens strain GV3101 (Wroblewski et al. 2005) carrying the desired constructs were used for transient expression experiments in *N. benthamiana* plants. Bacterial cells were resuspended in an infiltration buffer [10 mM $MgCl_2$, 10 mM 2-(N-Morpholino) ethanesulfonic acid (MES), pH 5.6, and 150 µM acetosyringone] to a final OD_{600} of 0.8 to 1.0 and incubated for at least 3 hours at room temperature before infiltration (Renovell et al. 2012). Fully expanded leaves of *N. benthamiana* plants at the six-leaf stage (4 to 6-week-old) were infiltrated with a 3 ml syringe without a needle. Experiments were repeated at least three times.

RNA silencing suppression co-infiltration assay by *Agrobacterium*-**mediated transient expression in** *N. benthamiana* **16c plants and GFP imaging.**

In the RNA silencing suppression co-infiltration assays, equal volumes of an *Agrobacterium* cell suspension carrying the *35S*::*GFP* gene and another construct harboring CVEV viral gene or control were mixed to a final OD_{600} 0.8 to 1.0 for each construct before infiltration. *Agrobacterium* carrying an empty vector with no insertion was used as a negative control. Constructs expressing the cucumber mosaic virus protein 2b (CMV 2b) and citrus leaf blotch virus movement protein (CLBV MP) under the *35S* promoter were used as positive VSR controls (Lucy et al. 2000; Renovell et al. 2012). Fully expended leaves of *N. benthamiana* 16c plants at the six-leaf stage (4 to 6-week-old) were infiltrated with a 3 ml syringe without a needle. The signal of green fluorescence was visualized under a handheld long-wavelength UV lamp at 5 days post infiltration (dpi) for local tissue and 14 dpi for systemic tissue (Blak-Ray® Model B-100 AP, Ultraviolet Products, Upland, California, USA).

Relative gene expression of *GFP* by RT-qPCR.

Relative gene expression was analyzed using *GFP* RT-qPCR assay along with an RT-qPCR assay of *N. benthamiana* housekeeping gene protein phosphatase 2A (*NbPP2A*) as normalizers in the quantitative gene expression analysis. Both assays were designed and validated in chapter 3 (Table 3.1, 4.1 and Figure 3.6).

Total RNA of each sample was extracted by TRIzol™ (Invitrogen™, Carlsbad, California, USA) as mentioned above and treated with DNase I (New England Biolabs®,

Ipswich, Massachusetts, USA) before loading into PCR reactions. The *GFP* RT-qPCR reaction (10 µl) was performed using the TaqMan® RNA-to-C_T 1-Step Kit (Applied Biosystems, Carlsbad, California, USA) with 2.8 µL water, 5.0 µL 2X TaqMan RT-PCR Mix, 0.6 µL of each primer (600 nM as final concentrations), 0.25 µL probe (250 nM as final concentrations), 0.25 µL 40X TaqMan RT Enzyme Mix and 0.5 µL of RNA (50 ng) for each reaction. The cycling conditions were 48°C for 15 minutes for the reverse transcription step, 95°C for 10 minutes during the first cycle to inactivate the RT enzyme and activate the PCR polymerase, followed by 40 cycles of 95°C for 15 seconds and 60°C for 45 seconds. This assay was validated and analyzed using a QuantStudio™ 12K Flex Real-Time PCR System (Thermo Fisher Scientific, Carlsbad, California, USA). Fluorescent signals were collected during the amplification cycle and the number of cycles required for the fluorescent signal to cross the threshold (Ct) was calculated and exported. The RT-qPCR reaction setup for *NbPP2A* was similar to *GFP* assay except the final concentration of each primer was 900 nM.

Relative expression levels (fold change) of the genes of interest were calculated using the Pfaffl method (Pfaffl 2001), with a buffer-treated sample as the mock control (expression level of 1) and *NbPP2A* as the reference gene (endogenous control). Gene expression data for each sample were the mean of three biological replicates and each biological replicate was the mean of three qPCR technical replicates.

The relative expression data was analyzed and calculated by Duncan's Multiple Range Test (MRT) with significance level α=0.05. Duncan proposed this test in 1955 and

provides a series of shortest significant ranges in order to compare differences between means (Bewick et al. 2004; Duncan 1955; Tallarida and Murray 1987). Each pair of means was compared against a different critical value which depends on the ranks of these means in an ordered array (Bewick et al. 2004; Duncan 1955; Tallarida and Murray 1987).

RNA blotting of *GFP* siRNA.

The abundance of *GFP* small interference RNA (siRNA) of the local infiltrated leaves were examined at 5 dpi by RNA blotting. Total RNA of each sample was extracted using TRIzol™ (Invitrogen™, Carlsbad, California, USA) as described previously. RNA quality and concentration were measured in a NanoPhotometer™ (Implen, Germany) and equal amount of RNA was loaded for electrophoresis and RNA blotting. The abundance of *GFP* siRNA as determined using a non-radiolabeled digoxigenin (DIG)-labeled RNA probe specific and complementary to the *GFP* sequence which was generated by *in vitro* transcription and DIG-RNA labeling (Roche Sigma-Aldrich, St. Louis, Missouri, USA) using the linearized plasmid, pGEMT-Easy-GFP-T7 (Table 4.2), with *GFP* sequence cloned into pGEM®-T Easy Vector Systems (Promega, Madison, Wisconsin, USA) and T7 promoter located at the downstream site.

To analyze *GFP*-derived siRNAs, 10 µg of total RNA were mixed with loading buffer containing 50% formamide, heated at 70°C for 10 minutes, and separated in a 15% polyacrylamide Tris-borate-EDTA(TBE)-urea gel in TBE buffer and capillary-transferred

onto positively charged nylon membranes (GE Healthcare Amersham Hybond-N+) overnight or for at least 6 hours using 20X saline sodium citrate (SSC) buffer (3 M sodium chloride and 0.3 M sodium citrate, pH 7.0). Subsequently, the membranes were UV cross-linked with 12,000 µJoules per cm^2 for 2 minutes. The siRNA membranes were hybridized with DIG-labeled RNA probes specific to the *GFP* sequence to detect *GFP*-derived siRNA. The nucleolar small RNA U6 gene of *N. benthamiana* was used as a loading control (Table 4.1) to confirm same loading amount of siRNA. The membranes were washed and developed to detect the chemiluminescent signals with ChemiDoc^{TM} Imaging Systems (Bio-Rad, Hercules, California, USA).

Potato virus X (PVX) Assay.

PCR products of CVEV P0 and ORF3, identified as potential VSRs, were digested with *Asc*I and *Not*I restriction enzymes (New England Biolabs®, Ipswich, Massachusetts, USA) and ligated into the PVX infectious clone, pGR106 (Jones et al. 1999), which carries the full PVX genome (Table 4.1 and 4.2). Recombinant plasmids were transformed into the *A. tumefaciens* strain GV3101 (pMP90::pSOUP) (Table 4.2), and the resulting strains were then used to infiltrate six-leaf stage wild-type *N. benthamiana* plants. The frameshift mutations of CVEV P0 and ORF3 were also constructed which carried the same nucleotide sequence but with a stop codon at the beginning of the reading frame (Table 4.1 and 4.2).

Viral RNAs were detected and quantified by the RT-qPCR designed for targeting the PVX coat protein (CP) gene with the housekeeping gene *NbPP2A* used as a normalizer in quantitative gene expression analysis. Total RNA was extracted from samples collected at 21 dpi which were infiltrated with pGR106 (PVX), pGR106-CVEV-P0 (PVX-CVEV-P0), and pGR106-CVEV-ORF3 (PVX-CVEV-ORF3) by using TRIzol™ (Invitrogen™, Carlsbad, California, USA™).

Primers and probe of PVX CP RT-qPCR assay was designed and validated in chapter 3 (Table 3.1, 4.1 and Figure 3.9). Total RNA of each sample was treated with DNase I (New England Biolabs®, Ipswich, Massachusetts, USA) before loading into PCR reactions. The PVX CP RT-qPCR reaction (10 µl) was performed using the TaqMan® RNA-to-C_T 1-Step Kit (Applied Biosystems, Carlsbad, California, USA) with 2.8 µL water, 5.0 µL 2X TaqMan RT-PCR Mix, 0.6 µL of each primer (600 nM as final concentrations), 0.25 µL probe (250 nM as final concentrations), 0.25 µL 40X TaqMan RT Enzyme Mix and 0.5 µL of RNA (50 ng) for each reaction. The cycling conditions were 48°C for 15 minutes for the reverse transcription step, 95°C for 10 minutes during the first cycle to inactivate the RT enzyme and activate the PCR polymerase, followed by 40 cycles of 95°C for 15 seconds and 60°C for 45 seconds. This assay was validated and analyzed using a QuantStudio™ 12K Flex Real-Time PCR System (Thermo Fisher Scientific, Carlsbad, California, USA). Fluorescent signals were collected during the amplification cycle and the number of cycles required for the fluorescent signal to cross the threshold (Ct) was calculated and exported. The RT-qPCR reaction setup for *NbPP2A* was similar except the final concentration of each primer was 900 nM.

Relative expression levels (fold change) of the genes of interest were calculated using the Pfaffl method (Pfaffl 2001), with the pGR106 (PVX)-infiltrated sample as the control (expression level of 1) and *NbPP2A* as the reference gene (endogenous control). Gene expression data for each sample were the mean of three biological replicates and each biological replicate was the mean of three qPCR technical replicates. The relative expression data was analyzed and calculated by Duncan's Multiple Range Test (MRT) as mentioned above.

Serial deletion assay of CVEV P0 and ORF3 using RNA silencing suppression co-infiltration assay by *Agrobacterium*-mediated transient expression in *N. benthamiana* 16c plants.

Serial deletion clones were constructed using plant expressing vectors, pEG100 and pEG1001, harboring CVEV P0 and ORF3 with Q5 Site-Directed Mutagenesis Kit (New England Biolabs®, Ipswich, Massachusetts, USA) per manufacturer's instructions. Primer sets for each deletion clone were designed using NEBaseChanger® online tool on the New England Biolabs® (Ipswich, Massachusetts, USA) website (http://nebasechanger.neb. com/) with deletion ranging from 66 to 144 base pairs (22 to 48 amino acids) on each deletion clone (Table 4.1, 4.2; Figure 4.1). The deletion constructs were transformed into *A. tumefaciens* strain GV3101 (Table 4.2), and the resulting strains were then used to co-infiltrate six-leaf stage *N. benthamiana* 16c plants along with *GFP*-expressing construct. Total RNA was extracted at 5 dpi for local tissues and 14 dpi for systemic tissues from

plants infiltrated with empty vector, CVEV P0, CVEV ORF3 and their deletion clones. The RNA of *GFP* was detected and quantified by the *GFP* RT-qPCR with housekeeping gene *NbPP2A* used as a normalizer in quantitative relative gene expression analysis as described above.

Triple site mutation of P0 on F-box motif.

Through analysis of the amino acid sequence, a putative F-box motif was found in P0 of CVEV located at 52 to 67 amino acids. Based on this information, the deletion mutation $P0^{\Delta36-83}$ (D2) was used as F-box knockdown mutant. In addition, the $P0^{L52A,P53A,L56A}$ with mutations on the conserve amino acid sites of the F-box motif was also constructed by using plant expressing vectors, pEG100 and pEG1001, harboring CVEV P0 with Q5 Site-Directed Mutagenesis Kit (New England Biolabs®, Ipswich, Massachusetts, USA) per manufacturer's instructions. Primer sets for each deletion clone were designed using NEBaseChanger® online tool on the New England Biolabs® (Ipswich, Massachusetts, USA) website (http://nebasechanger.neb.com/) with mutations at amino acid sequence at 52, 53 and 56 sites (Table 4.1 and 4.2). The mutation constructs were transformed into *A. tumefaciens* strain GV3101 and the resulting strains were then used to co-infiltrate six-leaf stage *N. benthamiana* 16c plants along with *GFP*-expressing vector. Total RNA was extracted at 5 dpi for local tissues and 14 dpi for systemic tissues from plants infiltrated with empty vector, CVEV P0, and $P0^{L52A,P53A,L56A}$. The RNA of *GFP* was

detected and quantified by the *GFP* RT-qPCR with housekeeping gene *NbPP2A* used as a normalizer in quantitative relative gene expression analysis as described above.

Protein extraction and western blot analysis.

Total protein was extracted from 500 mg of agroinfiltrated *N. benthamiana* leaves tissue using 1mL extraction buffer GTEN (10% [v/v] glycerol, 25 mM Tris-HCl pH 7.5, 1 mM EDTA, 150 mM NaCl) with supplements of 2% [w/v] polyvinylpolypyrrolidone (PVPP), 10 mM dithiothreitol (DTT), 0.1% Tween 20, and 1X protease inhibitor cocktail for plant cell (Sigma-Aldrich, St. Louis, Missouri, USA-Aldrich) before use (modified from Moffett et al. 2002). The samples were mixed with buffer by vortexing and incubated on ice for 10 minutes. The samples were centrifuged twice at 4°C and 13,500 rpm for 10 minutes to remove plant debris. The supernatant was transferred to a new tube for further analysis and testing.

The presence of specific proteins was detected by western blot hybridization. The sample lysates were run on Mini-PROTEAN® TGX Stain-Free™ Gels (Bio-Rad, Hercules, California, USA) with 2X Laemmli sample buffer (Bio-Rad, Hercules, California, USA) using Mini-PROTEAN® Tetra Vertical Electrophoresis Cell System (Bio-Rad, Hercules, California, USA). The proteins were subsequently transferred to PVDF membranes using a wet transfer method with Mini Trans-Blot® Cell System (Bio-Rad, Hercules, California, USA). Following protein transfer, the membranes were blocked with blocking buffer (5%

nonfat powdered milk buffered in 20 mM Tris-HCl, pH 7.5, 150 mM NaCl, and 0.1% Tween 20 (TBST)). The primary antibodies were diluted in blocking buffer at optimized dilution ratio and incubated with the membranes at 4°C, overnight. The antibody information of this study can be found in Table 4.3. Following incubation with the primary antibody, the membranes were washed three times for 10 minutes each with TBST. After washing, the secondary antibody was diluted in blocking buffer at optimized dilution ratio and incubated with the membrane for at least 1 hour at room temperature with agitation (Table 4.3). The membranes were washed three times with TBST and developed using SuperSignal™ West Pico PLUS Chemiluminescent Substrate (Thermo Fisher Scientific, Carlsbad, California, USA). The blots were incubated for 5 minutes and exposed to ChemiDoc™ Imaging Systems (Bio-Rad, Hercules, California, USA) to acquire images.

Mass spectrometry-based immunoprecipitation (IP) proteomics.

To characterize the protein targets of a VSR, high-throughput methodologies to analyze protein-protein interactions were used. Mass spectrometry-based immunoprecipitation proteomics is a powerful tool to study protein-protein interactions, protein complexes characteristics and their response to regulatory mechanisms (ten Have et al. 2011). Co-immunoprecipitation of expressed proteins and their complexes followed by proteomic analysis allows for the discovery of specific protein interactions (Turriziani et al. 2016). To start, the total protein was extracted by GTEN buffer as previously described from the *N. benthamiana* infiltrated leaves overexpressing CVEV P0 or ORF3

and incubated with the anti-Flag M2 affinity gel (Sigma-Aldrich, St. Louis, Missouri, USA) overnight at 4°C with gentle agitation. The bead control was included and run in parallel. The unbound proteins were washed out with cold GTEN washing buffer (10% [v/v] glycerol, 25 mM Tris-HCl pH 7.5, 1 mM EDTA, 150 mM NaCl) for 5 times. Proteins bound with the anti-Flag affinity gel were eluted using elution buffer (0.1 M glycine-HCl, pH 3.5). The IP products were analyzed by western blotting and submitted to IIGB Proteomics Core at University of California, Riverside for mass spectrometry analysis. Briefly, the submitted IP products were digested using trypsin protease at 37°C overnight and then analyzed by LC-MS/MS. Both Ultraperformance Liquid Chromatography coupled with Quadrupole Time of Flight Mass Spectrometry (UPLC/QTOF-MS) and the next generation LTQ-Orbitrap Fusion LC/MS (Thermo Fisher Scientific, Carlsbad, California, USA) were used in this study. Protein identities of top candidates were determined by using the Mascot search engine against the *N. benthamiana* proteomic database (Boyce Thompson Institute for Plant Research, http://bti.cornell.edu/nicotiana-benthamiana/). The whole set of mass spectrometry-based IP proteomic screening was repeated twice.

Co-immunoprecipitation (co-IP).

Co-IP constructs were made using pENTR vectors, followed by pEG1001 as a destination vector with FLAG coding region at C-terminus for CVEV P0 or its mutations. pEG203 was used as a destination vector with c-Myc coding region at the N-terminus for

AtSKP1. Agrobacteria harboring the bait and prey constructs were mixed to a final OD_{600} 0.8 each and co-infiltrated into *N. benthamiana* leaves. Total protein of each sample was extracted by GTEN buffer, as previously described, and incubated with the anti-Flag M2 affinity gel (Sigma-Aldrich, St. Louis, Missouri, USA-Aldrich) for 4 hours to overnight at 4°C with gentle agitation. The unbound proteins were washed out with cold GTEN washing buffer (10% [v/v] glycerol, 25 mM Tris-HCl pH 7.5, 1 mM EDTA, 150 mM NaCl) for 3 to 5 times. Proteins bound with the anti-Flag affinity gel were eluted using 2X Laemmli sample buffer (Bio-Rad, Hercules, California, USA) and boiled for 5 minutes. The presence of specific proteins in the immunocomplex was detected by western blotting as described previously.

Protein degradation inhibition assay.

Agrobacterium harboring pEG1001 P0 or P0 with deletion at OD_{600} 0.8 were infiltrated into *N. benthamiana* leaves. The inoculated areas were infiltrated again 24 hours before sample collection either with 50 µM MG132 (Sigma-Aldrich, St. Louis, Missouri, USA-Aldrich) or 20 µM E-64d (Sigma-Aldrich, St. Louis, Missouri, USA-Aldrich) in 10 mM $MgCl_2$ buffer and buffer-treated sample as control. Total protein of each sample was extracted by GTEN buffer and analyzed by western blotting as previously described.

Pull-down assay.

The MagneGST™ Pull-Down System (Promega, Madison, Wisconsin, USA) was used to detect protein interactions between glutathione-S-transferase (GST)-fused P0 or P0 with deletion expressed in *E. coli* (strain B21(DE3)pLysS) and AGO1 as prey proteins expressed *in vitro* in the TNT® T7 Quick Coupled Transcription/Translation System (Promega, Madison, Wisconsin, USA). The pull-down experiment was conducted based on the technical manual of MagneGST™ Pull-Down System (Promega, Madison, Wisconsin, USA). The protocol was divided into three phases. First, the prey protein, AGO1, was expressed in the TNT® T7 Quick Coupled System. Second, GST-P0 or P0 with deletion as bait protein presented in crude *E. coli* lysate was immobilized on the MagneGST™ beads. Then, the prey protein, AGO1, was mixed with MagneGST™ beads carrying the bait protein, GST-P0 or P0 with deletion, and captured through bait-prey interaction. Nonspecifically bound proteins were washed away, and the prey and bait proteins were eluted from the resin with 1X sodium dodecyl sulfate (SDS) loading buffer (50 mM Tris-HCl, pH 6.8, 2% SDS, 0.1% bromophenol blue, 10% glycerol and 10 mM dithiothreitol). Prey proteins were analyzed by western blot as previously described.

Sample preparation and RNA immunoprecipitation (RIP).

RIP is a largely used method to study the physical association between individual proteins and RNA molecules *in vivo* (Gagliardi and Matarazzo 2016; Ramanathan et al.

2019; Selth et al. 2011). The approach is based on the use of a specific antibody against the protein of interest to pull down the target-RNA complexes. Any RNA that is associated with this protein complex will be isolated and can be further analyzed by polymerase chain reaction-based methods.

The leaf samples of *N. benthamiana* 16c plants were collected from *Agrobacterium*-mediated transient expression assay after 2 dpi of co-infiltration with *Agrobacterium* strains carrying *35S::GFP* and individual viral gene constructs. The total protein of each sample was extracted from 200 mg plant tissue using 1 ml phosphate buffered saline (PBS) with supplements of 0.05% Tween 20, 1 mM PMSF (Invitrogen™, Carlsbad, California, USA™) and 1X protease inhibitor cocktail for plant cell (Sigma-Aldrich, St. Louis, Missouri, USA-Aldrich). The samples were incubated on ice for 30 minutes and mixed briefly by vortexing every 10 minutes. Subsequently, the samples were centrifuged twice at 4°C and 13,500 rpm for 10 minutes to remove plant debris and the supernatant was transferred into a new tube.

The RIP assay was conducted using the Immunoprecipitation Kit Dynabeads® Protein A (Invitrogen™, Carlsbad, California, USA™) per manufacturer's instruction. In brief, as described in chapter 3, 3.5 µg anti-Flag M2 as the ligand (Sigma-Aldrich, St. Louis, Missouri, USA-Aldrich) was added to 35 µl Dynabeads® to establish the binding and form the beads-antibody complex in PBS buffer plus 0.05% Tween 20 (PBST) (Figure 3.2). The protein lysate was added to the beads-antibody complex and incubated at room temperature for 15 minutes. After incubation, the "beads-antibody-target protein

interacting complex" was washed three times with PBST buffer, the target protein and its interacting nucleic acids were eluted and further treated with DNase I (New England Biolabs®, Ipswich, Massachusetts, USA) to remove DNA. The RT-PCR analysis was carried out targeting the *GFP* gene using specific primers (Table 4.1). The reaction was performed with QIAGEN OneStep RT-PCR kit in a 25 µl reaction (5 µl 5X RT-PCR Buffer, 1 µl 10mM dNTP, 1.5 µl 10 µM forward/reverse primer, 1 µl QIAGEN OneStep RT-PCR Enzyme Mix, 1 µl of RNA, and 14 µl nuclease-free water) with annealing temperature 57°C, 35 cycles. Amplicons were examined by 1.5% agarose gel electrophoresis.

RNA-protein pull-down assay.

The dsRNA of *GFP* as transcribed using MEGAscript® RNAi Kit (Invitrogen™, Carlsbad, California, USA) per manufacturer's instruction. Two separate clones were made to incorporate a T7 promoter upstream (5'-end) or downstream (3'-end) of the *GFP* sequence as described in chapter 3 (Figure 3.3; Table 3.2 and 4.2). The plasmids were digested either with *Mlu*I or *Nco*I restriction enzyme (New England Biolabs®, Ipswich, Massachusetts, USA) to linearize the plasmid and served as template in the *in vitro* transcription reaction which contained 5 µg of linear DNA template, 2 µl 10X T7 reaction buffer, 2 µl of each 75 mM ATP/CTP/GTP/UTP solution, 2 µl T7 enzyme mix, and adjusted with nuclease-free water to 20 µl. The reactions were incubated at 37°C for 4 hours. Subsequently, both *GFP* transcripts were mixed (1:1 ratio) and heated at 75°C for 5

minutes. The mixtures were left on the bench to cool down to room temperature. This allowed sense and antisense *GFP* to anneal together and form dsRNA. Small RNA of *GFP* was prepared by digesting *GFP* dsRNA with *E. coli* RNase III (Applied Biosystem, Carlsbad, California, USA) and further purified by running the reaction over an Amicon® Ultra-0.5 centrifuge filter unit (MilliporeSigma, Burlington, Massachusetts, USA) and collecting the flow-through that contained the small RNAs. The dsRNA and small RNA of *GFP* were labeled with a single biotinylated nucleotide at the 3' terminus using Pierce™ RNA 3' End Desthiobiotinylation Kit (Thermo Fisher Scientific, Carlsbad, California, USA) by adding 3 µl 10X RNA ligase reaction buffer, 1 µl RNase inhibitor, 1 µl biotinylated cytidine bisphosphate, 2 µl T4 RNA ligase, 15 µl 30% PEG, 50 pmol RNA, and adjusted to 30 µl with nuclease-free water. The reactions were incubated at 16°C overnight and further purified by chloroform:isoamyl alcohol extraction and ethanol precipitation. The labeled RNA was used in RNA-protein pull-down assay using Pierce™ Magnetic RNA-Protein Pull-Down Kit (Thermo Fisher Scientific, Carlsbad, California, USA) per manufacturer's instruction. The labeled RNA (50 pmol), either dsRNA or small RNA, was captured by streptavidin magnetic beads (50 µl). The total protein lysate (60 µl) extracted by GTEN buffer as described above was added to the beads-RNA complex along with 10 µl 10X protein-RNA bunding buffer and 30 µl 50% glycerol. The reactions were incubated at 4°C for 60 minutes with agitation, followed by washing and elution steps. The elute was examined by western blot analysis as described above. The inputs of protein samples and RNA species were also examined using western blot and polyacrylamide gel electrophoresis, respectively.

Results

CVEV P0 and ORF3 are viral suppressors of RNA silencing (VSRs) identified using *Agrobacterium*-mediated transient expression in *N. benthamiana* 16c plants.

As mentioned in chapter 3, RNA silencing in plants is commonly induced and visualized using the *Agrobacterium* co-infiltration assay in *N. benthamiana* line 16c (Ruiz et al. 1998) with a stable integrated expressed *GFP* gene (endogenous) under the control of the cauliflower mosaic virus *35S* promoter. This assay provides a convenient system to screen and identify VSRs by co-infiltration with *Agrobacterium* containing a *GFP* expressing plasmid (exogenous), in order to induce *GFP* silencing, and a test plasmid carrying CVEV VSR candidate to suppress such silencing. The siRNA-mediated RNA silencing is induced by endogenous and exogenous *GFP* genes expressing low, or no, green fluorescence in infiltrated areas at 5 to 7 dpi (Figure 3.4 a; no suppression / silenced). However, if the VSR candidate protein has the ability to suppress siRNA-mediated RNA silencing, such as CMV 2b, a strong green fluorescence is detected (Figure 3.4 a; suppression- local VSR). The *GFP* transgene silencing is typically observed in upper leaves and axillary shoots with little or no detectable GFP signal at 14 to 21 dpi (Figure 3.4 b; no suppression / silenced). However, if VSR inhibits systemic siRNA biogenesis or movement, it will also suppress systemic silencing of *GFP* (Figure 3.4 b; suppression-systemic VSR).

To identify the VSR(s) of CVEV, the P0, ORF3 and ORF5 were individually cloned under *35S* promoter in plant expression binary vectors. The resulting constructs were agroinfiltrated and examined by western blotting to confirm the protein expression in *N. benthamiana* (Figure 4.2 a). The expression vector without insertion was used as a negative empty vector control (Figure 4.2 b). CMV 2b and CLBV MP were used as VSR controls. These VSRs suppressed both local and systemic RNA silencing (Figure 4.2 b, Table 4.4).

When observed under UV light at 5 dpi, the ORF3 and ORF5 of CVEV had no local silencing suppression activity since they produced similar GFP patterns with the empty vector control in which the fluorescence signal was not visualized locally (Figure 4.2 b, Table 4.4). On the other hand, the CVEV P0 co-infiltration area had local suppression of RNA silencing at 5 dpi with 96% suppression rate (Figure 4.2 b, Table 4.4) which was similar to CMV 2b (100%) and higher than CLBV MP (41%). Non-inoculated upper / systemic leaves were observed at 14 dpi and showed that CVEV P0 induced silencing suppression at high rate (96%) (Figure 4.2 b, Table 4.4). CVEV ORF3 had activity in systemic silencing suppression with 33% suppression rate, higher than CLBV MP (15%). The CVEV ORF5 did not display any suppression in upper / systemic leaves (Figure 4.2 b, Table 4.4).

In infiltrated leaf areas, the CVEV ORF3 and ORF5 showed increasing abundance of *GFP* siRNA and similar relative expression of *GFP* when compared to the empty vector control indicating that CVEV ORF3 and ORF5 do not have local silencing suppression activity (Figure 4.2 c and 4.3 a). CMV 2b, CLBV MP and CVEV P0 strongly reduced the

abundance of *GFP* siRNA, leading to significantly higher relative expression of *GFP* in agreement with the results of the UV co-infiltration experiments (Figure 4.2 c and 4.3 a; significance level α=0.05).

CVEV P0 and ORF3 suppressed the systemic silencing of *GFP* with significantly higher *GFP* relative expression level when compared to the empty vector control (Figure 4.3 b; significance level α=0.05). More specifically, P0 had 1.5-fold more *GFP* expression than both VSR controls (Figure 4.3 b; significance level α=0.05) while ORF3 displayed significant higher fold change than VSR controls but lower than P0 (Figure 4.3 b; significance level α=0.05). CVEV ORF5 displayed similar relative expression level to the empty vector (Figure 4.3 b; significance level α=0.05).

PVX infectious vector harboring CVEV P0 or ORF3 induced more severe symptoms and had higher viral RNA accumulation.

To test whether CVEV P0 and ORF3 are capable of suppressing siRNA-mediated host immunity, P0 and ORF3 were introduced individually into the PVX genome and examined their effects on viral virulence. Unlike *N. benthamiana* plants infected with PVX, the plants infected with PVX carrying CVEV P0 (PVX-CVEV-P0) and CVEV ORF3 (PVX-CVEV-ORF3) showed severe mosaic and leaf deformation symptoms on newly emerged leaves along the apical shoots (Figure 4.4 a). Consistent with enhanced disease symptoms, relative expression level analysis showed that viral RNAs accumulated to a

much higher level in PVX-CVEV-P0 and PVX-CVEV-ORF3 infected tissues compared to the wild-type PVX (Figure 4.4 b; significance level α=0.05). The frameshifting mutation controls of CVEV P0 and ORF3 exhibited similar virulence and fold change in virus accumulation to the wild-type PVX (Figure 4.4 b and c; significance level α=0.05). These frameshifting mutation controls had mild or no mosaic symptoms and did not promote PVX infection (Figure 4.4 b and c).

Plant protein expressing vector harboring CVEV P0 with deletion from 36 to 83 amino acids as well as 176 to 245 amino acids lost its function in silencing suppression.

To identify the regions of CVEV P0 associated with silencing suppression, clones with serial deletions of CVEV P0 in pEG1001 and pEG100 vectors were constructed and tested using *Agrobacterium*-mediated transient expression assay in *N. benthamiana* 16c plants co-infiltrated with GFP-expressing vector (Figure 4.1a). The protein expression level of each deletion clone was examined at 2 dpi by western blot hybridization to confirm the stability of proteins with deletions (Figure 4.5 a). The agroinfiltrated leaves were observed at 5 dpi under UV light (Figure 4.5 b). Among the P0 deletion clones, leaves infiltrated with $P0^{\Delta 36-83}$ (D2), $P0^{\Delta 176-210}$ (D6), and $P0^{\Delta 211-245}$ (D7) did not show local silencing suppression with no or low GFP signal (Figure 4.5 b). Quantitative analysis also displayed that $P0^{\Delta 36-83}$ (D2), $P0^{\Delta 176-210}$ (D6), and $P0^{\Delta 211-245}$ (D7) had low relative *GFP* expression level similar to the empty vector control (Figure 4.5 c; significance level α=0.05). These data indicated that the regions associated with silencing suppression

activity on P0 is locate within 36 to 83 and 176 to 245 amino acids. The systemic leaves were observed at 14 dpi under UV light (Figure 4.5 d). And none of the P0 with deletions lost their activity in systemic silencing suppression (Figure 4.5 d). The results of quantitative analysis were consistent with the UV light observation without any significant reduction of the expression level in any of the P0 deletions when compared to empty vector control (Figure 4.5 e; significance level α=0.05).

CVEV P0 contains an F-box motif which plays a critical role in local silencing suppression.

The protein expression of $P0^{L52A,P53A,L56A}$ (triple sites mutation) and $P0^{\Delta 36-83}$ (D2; F-box knockdown mutation) was confirmed with western blot analysis (Figure 4.6 a). When observed under UV light, both $P0^{\Delta 36-83}$ (D2) and $P0^{L52A,P53A,L56A}$ lost their silencing suppression function in the local infiltrated area but not in the systemic tissues (Figure 4.6 b). The relative expression analysis also showed that the *GFP* mRNA level of both $P0^{L52A,P53A,L56A}$ and $P0^{\Delta 36-83}$ (D2) infiltrated leaves were significantly decreased when compared to wild-type P0 (Figure 4.6 c; significance level α=0.05). However, in the systemic tissue, the *GFP* expression level of both $P0^{L52A,P53A,L56A}$ and $P0^{\Delta 36-83}$ (D2) was slightly lower than P0 but significantly higher than the empty vector (Figure 4.6 d; significance level α=0.05).

Plant protein expressing vector harboring CVEV ORF3 with deletion from 68 to 100 amino acids lost its function in silencing suppression.

To identify the region of CVEV ORF3 associated with silencing suppression, the clones with serial deletion of CVEV ORF3 on pEG1001 and pEG100 vectors were constructed and tested using *Agrobacterium*-mediated transient expression assay in *N. benthamiana* 16c plants co-infiltrated with GFP-expressing vector (Figure 4.1 b). The protein expression level of each deletion clones was examined at 2 dpi by western blot to confirm the stability of the proteins with deletions. (Figure 4.7 a). The newly emerged leaves along the apical shoots was observed at 14 dpi under UV light (Figure 4.7 b). Among deletion clones, leaves infected with ORF3$^{\Delta 68\text{-}100}$ (D3) did not show systemic silencing suppression with no or low GFP signal (Figure 4.7 b). Quantitative analysis also indicated that ORF3$^{\Delta 68\text{-}100}$ (D3) had significantly lower relative *GFP* expression level similar to the empty vector control (Figure 4.7 c; significance level $\alpha=0.05$). These results indicated that the region associated with silencing suppression activity on ORF3 should be located within 68 to 100 amino acids.

Mass spectrometry-based immunoprecipitation proteomics showed that CVEV P0 directly interacted with major host cellular proteins in the RNA silencing pathway.

To reveal the identity of the CVEV P0-associated proteins, products from immunoprecipitation were analyzed by mass spectrometry. The LC-MS/MS analysis of

CVEV P0 generated a long list of identified proteins with the help of the database searching. In this study, the exponentially modified protein abundance index (emPAI) was used to filter data, based on the abundances of the proteins interacted with P0. The emPAI was quite useful for obtaining a broad overview of proteome profiles. With emPAI equal or greater than 1, total 50 protein hits were found in the P0-expressing sample but not in the control (Table 4.5). Among them, S phase kinase-associated protein 1 (SKP1), and cullin1 (CUL1) were identified in multiple hits (Table 4.5).

Mass spectrometry-based immunoprecipitation proteomics showed that CVEV ORF3 did not directly interact with major host cellular proteins in the RNA silencing pathway.

To reveal the identity of the CVEV ORF3-associated proteins, products from immunoprecipitation were analyzed by mass spectrometry as mentioned above. With emPAI equal or greater than 1, total 58 protein hits were found in the ORF3-expressing sample but not in the control (Table 4.6). However, no major protein components in host RNA silencing pathway were identified in the ORF3-expressing sample (Table 4.6).

CVEV P0 interacted with SKP1 through F-box motif.

To confirm the interaction between P0 and SKP1, the pEG1001 harboring AtSKP1 was *Agrobacterium* co-infiltrated with P0 into *N. benthamiana*. At 2 dpi, leaf samples were

collected and extracted followed by co-immunoprecipitation (co-IP). Through western blot analysis, the interaction between P0 and AtSKP1 was confirmed (Figure 4.8). The P0$^{\Delta 36-83}$ (D2), an F-box knockdown mutant, lost the interaction with AtSKP1 (Figure 4.8). However, the triple site mutation on the F-box motif of P0 (P0^{L52A,P53A,L56A}) did not lost the interaction with AtSKP1 (Figure 4.8).

F-box motif and region within 176 to 245 amino acids of CVEV P0 involved in AGO1 degradation.

To identify if the AGO1 was degraded through either proteasomal or autophagic degradation, a inhibition assay was conducted. When expressed P0 in *N. benthamiana*, the protein level of AGO1 was barely detectable by western blot analysis even when samples were treated with proteasome inhibitor 50μM MG132 (Figure 4.9 a). However, when the samples were treated with autophagy inhibitor 20μM E-64d, the AGO1 protein expression level was rescued (Figure 4.9 a). In addition, P0$^{\Delta 36-83}$ (D2), P0$^{\Delta 176-210}$ (D6), and P0$^{\Delta 211-245}$ (D7) did not affect the expression level of AGO1 with different treatments (Figure 4.9 a). These results indicated that 36 - 83 and 176 - 245 aa of P0 contain critical regions and involve in guiding and leading AGO1 to its autophagic degradation.

CVEV P0 directly interacts with AGO1.

To reveal the protein regions of P0 interacting with AGO1, co-IP was conducted. The result showed that P0 interacts with AGO1. However, the interaction was lost when P0 carried the deletion between 211 to 245 aa, P0$^{\Delta 211\text{-}245}$ (D7) (Figure 4.9 b). In addition, the pull-down assay further confirmed the direct interaction between P0 and AGO1 (Figure 4.9 c). P0$^{\Delta 211\text{-}245}$ (D7) also lost its interaction with AGO1 which is consistent with the co-IP results (Figure 4.9 c). In the pull-down assay, P0$^{\Delta 176\text{-}210}$ (D6) only had slight interaction with AGO1 (Figure 4.9 c).

CVEV P0 interacts with dsRNA-*GFP* in RNA immunoprecipitation (RIP) but not in RNA-protein pull down assay.

Other than targeting the protein components, the VSRs can also interact with the dsRNA and/or siRNA species produced in the host RNA silencing pathway. To identify if P0 and ORF3 interact with dsRNA, the RNA immunoprecipitation (RIP) assay was conducted using *Agrobacterium* transient expression assay co-infiltrated with VSR and GFP-expressing vectors into *N. benthamiana* 16c plants, where host silencing was induced and dsRNA of *GFP* was formed *in planta*. Turnip crinkle virus (TCV) P38 protein was used as a VSR control which has been proven to interact with long dsRNA to suppress host RNA silencing (Incarbone and Dunoyer 2013; Mérai et al. 2006). Through RIP assay, the dsRNA of *GFP* were precipitated along with TCV P38 which has the ability to bind to

dsRNA (Figure 4.10). None of the P0 or ORF3 showed any interaction with dsRNA (Figure 4.10).

To further confirm if CVEV P0 and ORF3 interact with dsRNA, the RNA-protein pull-down assay was performed. In such assay, the *in vitro* transcribed and 3'-end biotinylated dsRNA of *GFP* was used to pull down proteins that have the ability to bind to dsRNA. From the western blot analysis, P38 protein of TCV was pulled down by the dsRNA of *GFP* (Figure 4.11 a). However, P0 and ORF3 were not detected in the blot.

Both CVEV P0 and ORF3 had no interaction with siRNA in RNA-protein pull down assay.

To further investigate if CVEV P0 and ORF3 interact with siRNA, the RNA-protein pull-down assay was also used. The siRNA of *GFP* were produced from *in vitro* transcribed dsRNA with RNase III digestion and 3'-end biotinylation. Tomato bushy stunt virus (TBSV) P19 protein was used as a VSR control which has been proven to interact with siRNA to suppress host RNA silencing (Incarbone and Dunoyer 2013; Vargason et al. 2003). Through such assay, TBSV P19 protein was pulled down and detected in western blot analysis. However, CVEV P0 and ORF3 did not show any interaction with siRNA (Figure 4.11 b).

CVEV P0 triggered hypersensitive response (HR)-like cell death.

During the agrobacterium infiltration assays, robust (HR)-like cell death was found at the infiltrated area of CVEV P0 at 1 to 2 dpi which might be triggered by gene-for-gene interaction in *N. benthamiana* (Figure 4.12). Further experiments are needed to identify the R protein of the host which recognized P0 and triggered this ETI response.

Discussion

To counteract the host antiviral RNA silencing mechanism, many plant and animal viruses have evolved silencing suppressors or VSRs to inhibit and block such mechanism at different levels (Burgyán and Havelda 2011; Csorba et al. 2015; Ding 2010; Díaz-Pendón and Ding 2008; Incarbone and Dunoyer 2013; Pumplin and Voinnet 2013; Roth et al. 2004; Song et al. 2011; Wang et al. 2012; Wu et al. 2010). In this study, two VSRs of CVEV, P0 and ORF3, were identified exhibiting distinct features in silencing suppression.

Co-infiltration assays of *GFP*-transformed *N. benthamiana* 16c plants along with qualitative and quantitative analysis showed that CVEV P0 has suppression activity in local RNA silencing and reduces siRNA accumulation. Both P0 and ORF3 have the ability to suppress RNA silencing systemically probably by blocking the associated amplification mechanism or the mobile small RNA silencing signals which move and spread systemically through cell-to-cell and vascular system mediating gene silencing in newly

emerging leaves (Csorba et al. 2015; Díaz-Pendón and Ding 2008; Incarbone and Dunoyer 2013; Wu et al. 2010).

CVEV ORF3 displayed only 33% suppression rate which indicated that there might be other determinants affecting its silencing suppression efficiency and activity. Besides working as VSRs, viral proteins also fulfill other functions during the infection. For instance, CPs of RNA viruses usually have multiple functions including but not limited to virus entry, disassembly, translation of viral RNAs, RNA replication, virus movement, transmission and symptom development (Weber and Bujarski 2015). Silencing functions could have become established in the cases when the balance between the positive effects on the viral life cycle and negative effects on host were beneficial to the virus itself (Csorba et al. 2015). Therefore, the trade-off between different protein functions might influence the silencing suppression activity of CVEV ORF3.

The suppressor activity of both CVEV P0 and ORF3 was further confirmed by agroinfiltration assays in wild-type *N. benthamiana* plants following expression from PVX infectious vector in a virus-induced gene silencing (VIGS) background (Galiakparov et al. 2003; Jones et al. 1999). In this experiment, CVEV P0 and ORF3 expressed from PVX infectious clone had dramatic effects on facilitating symptom development and viral RNA accumulation on *N. benthamiana* which both acted as pathogenicity determinants to promote viral infection, likely through their RNA silencing suppression activities (Galiakparov et al. 2003; Qiao et al. 2013; Zhou et al. 2006). The frameshifting controls

also showed that silencing suppression effects of both P0 and ORF3 were determined by the proteins themselves instead of their mRNA sequences.

Taken together, our results indicated that both CVEV P0 and ORF3 are VSRs which suppress viral and transgene-induced RNA silencing and reduce or abolish the accumulation of silencing-associated siRNAs.

The regions of CVEV P0 and ORF3 associated with host silencing suppression were identified through *Agrobacterium* co-infiltration assay on 16c *N. benthamiana*. VSRs usually have functional domains interacting with host proteins or RNA targets that lead to suppression of host RNA silencing. The deletion or interruption of such functional regions should fail to suppress host RNA silencing. Based on our results, CVEV P0$^{\Delta 36-83}$ (D2), P0$^{\Delta 176-210}$ (D6), and P0$^{\Delta 211-245}$ (D7) lost their local suppression activities due to deletion of regions associated with host RNA silencing suppression. However, the systemic suppression associated region of CVEV P0 was not found in the serial deletion assay assuming that the mechanism is much more complex. For ORF3, the region associated with silencing suppression was located within 68 to 100 amino acids and their deletion failed to suppress host systemic RNA silencing. Further studies are required to identify the specific domains, motifs or amino acid sites required for P0 and ORF3 systemic silencing suppression.

Viruses of both genera of *Polerovirus* and *Enamovirus* in *Luteoviridae* family have been found to use P0 as a VSR to suppress host antiviral silencing (Baumberger et al. 2007; Bortolamiol et al. 2007; Csorba et al. 2010; Derrien et al. 2012; Fusaro et al. 2012;

Mangwende et al. 2009; Pazhouhandeh et al. 2006). These P0s contain F-box motifs and interact with host proteins, SKP1 and CUL1, to form an SCF complex which is a multi-protein E3 ubiquitin ligase complex (Baumberger et al. 2007; Bortolamiol et al. 2007; Csorba et al. 2015; Csorba et al. 2010; Derrien et al. 2012; Fusaro et al. 2012; Pazhouhandeh et al. 2006). The amino acid (aa) sequence analysis found that CVEV P0 also has such motif and three aa sites are conserved, as other P0s, and located at 52, 53 and 56 aa. The triple site mutation of these three amino acids on CVEV P0 was unable to suppress host local RNA silencing, indicating that the F-box motif has an important role in local silencing suppression.

CVEV P0 also showed its interaction with host SKP and CUL proteins through F-box motif. These results indicated that CVEV P0 as well as other P0s could mimic the host mechanism to form SCF complex, a E3 ubiquitin ligase, and further catalyze the ubiquitination of host protein targets associated with antiviral RNA silencing pathway (Baumberger et al. 2007; Bortolamiol et al. 2007; Csorba et al. 2015; Csorba et al. 2010; Derrien et al. 2012; Fusaro et al. 2012; Pazhouhandeh et al. 2006). Through co-IP, the interactions between CVEV P0 and AtSKP1 were further confirmed and the deletion of the F-box motif proved that two proteins interact within this region. However, the CVEV P0 triple site mutation on F-box conserved amino acids did not affect the interaction with AtSKP1. Therefore, we assumed that there are more amino acids sites involved in this interaction.

Several studies have proved that P0s target at AGO1 as well as other AGO proteins (AGO 2, 4-6, 9) and guide them for autophagic degradation before holo-RISC assembly to suppress host RNA silencing (Baumberger et al. 2007; Bortolamiol et al. 2007; Csorba et al. 2015; Csorba et al. 2010; Derrien et al. 2012; Fusaro et al. 2012; Pazhouhandeh et al. 2006). According to the results of co-IP and pull-down assays, AGO1 directly interacted with CVEV P0 (Pazhouhandeh et al. 2006) through the functional region within 211 and 245 aa and guided AGO1 to its degradation and the region within 176 and 210 aa also has a role in assisting such degradation. The proteasome inhibitor did not affect the degradation of AGO1 by CVEV P0 which is consistent with previous studies (Baumberger et al. 2007; Derrien et al. 2012). However, when the autophagy inhibitor was applied, the AGO1 degradation was suppressed. This result indicated that CVEV P0 promotes the degradation of AGO1 through the host autophagy pathway as mentioned in previous studies (Derrien et al. 2012). It has been proposed that P0s inhibit RISC assembly by hijacking a normal host physiological process to promote selective autophagy of unloaded AGO1 before RISC assembly (Derrien et al. 2012). More studies are required to confirm the role of CVEV P0 and other P0s in autophagy pathway to see whether it acts as an cargo receptor or as an autophagic adapter which trafficking AGO1 to a cargo receptor for degradation (Leary et al. 2017). And despite the lack of any sequence similarity, the P0s of poleroviruses and enamoviruses in the family of *Luteoviridae* have a conserved mode of action upon the RNA silencing machinery which also supported their evolutionary scenario (Fusaro et al. 2012).

Systemic VSRs suppress host gene silencing by blocking the amplification and spread of silencing signals which could travel through plasmodesmata for cell-to-cell

movement and further to the vascular system and induce silencing in systemic tissue (Csorba et al. 2015; Díaz-Pendón and Ding 2008; Incarbone and Dunoyer 2013). However, we demonstrated that through mass spectrometry-based immunoprecipitation proteomics, CVEV ORF3 did not have any direct interaction with host RDRs or the cofactors which contribute to amplification of RNA silencing and spread of systemic signals by synthesis of vsiRNAs (Csorba et al. 2015; Díaz-Pendón and Ding 2008; Martín-Hernández and Baulcombe 2008; Qu et al. 2005; Schwach et al. 2005). These results indicated that ORF3 does not suppress host RNA silencing through direct interaction with protein components in the host RNA silencing pathway (Csorba et al. 2015). Moreover, RNA immunoprecipitation (RIP) and RNA-protein pull down assays showed that CVEV ORF3 was unable to bind RNA species directly. Therefore, there is a possibility that ORF3 utilizes indirect strategies such as interaction with other host regulators that contribute to inhibition of silencing signal amplification and spread or interaction with RNA species through a protein or protein complex containing RNA binding domains.

Recent studies showed that strong suppressors activity would allow high accumulation of virus in cells likely causing severe damages to infected plants and may also induce dramatic resistance responses (Renovell et al. 2012). In CVEV, both P0 and ORF3 are VSRs, thus could be the critical factors responsible for viral invasion, pathogenicity, and symptom development in its hosts. To counteract such viral proteins, plants have evolved a large group of host R proteins with nucleotide-binding and leucine-rich repeat (NB-LRR) domains to recognize the activity of viral proteins, including VSRs, to induce ETI accompanied by HR (Wang et al. 2015). Several P0s of poleroviruses have

been found to elicit HR in *N. glutinosa* which recognized by an R protein (Wang et al. 2015). An HR-like cell death reaction was also observed on the CVEV P0 infiltrated area on *N. benthamiana* in this study. Further investigation is needed to identify the R protein corresponding to CVEV P0 and prove the gene-for-gene interactions.

VSRs are usually out-selected during evolution (Csorba et al. 2015). A recent study found that several isolates of siratro latent polerovirus (SLPV) isolated from the same region in Australia, all lacked the start codon AUG in the ORF0, and some isolates even contained point mutations and deletions in this region, thus inhibiting translation of ORF0 (Filardo and Sharman 2019). Lack of a functional ORF0 might have affected the viral pathogenicity, suppression of antiviral immunity and the host range of the virus (Filardo and Sharman 2019). On the other hand, mutations on the ORF0 may give the ability to the virus to avoid R protein recognition and escape host immunity. Viral P0s of enamoviruses and poleroviruses are an excellent example of the endless arm race between host and pathogen in finding an evolutionary balance benefit both organizations.

References

Almasi, R., Miller, W. A., and Ziegler-Graff, V. 2015. Mild and severe cereal yellow dwarf viruses differ in silencing suppressor efficiency of the P0 protein. Virus Res 208:199-206.

Azeri, T., and Heper, E. 1972. Citrus vein-enation virus on Satsuma mandarins in the Aegean Coast of Turkey. Plant disease reporter 56:352-353.

Baumberger, N., Tsai, C. H., Lie, M., Havecker, E., and Baulcombe, D. C. 2007. The Polerovirus silencing suppressor P0 targets ARGONAUTE proteins for degradation. Curr Biol 17:1609-1614.

Bazan de Segura, C., and Ferrand, A. Woody galls, its distribution and importance in new and old citrus plantings in Peru. Pages 1449-1451.

Bewick, V., Cheek, L., and Ball, J. 2004. Statistics review 9: one-way analysis of variance. Critical care (London, England) 8:130-136.

Bortolamiol, D., Pazhouhandeh, M., Marrocco, K., Genschik, P., and Ziegler-Graff, V. 2007. The Polerovirus F box protein P0 targets ARGONAUTE1 to suppress RNA silencing. Curr Biol 17:1615-1621.

Bostock, R. M., Thomas, C., Hoenisch, R., Golino, D. A., and Vidalakis, G. 2014. Excluding Pests and Pathogens: Plant health: How diagnostic networks and interagency partnerships protect plant systems from pests and pathogens. California Agriculture 68:117-124.

Brault, V., Bergdoll, M., Mutterer, J., Prasad, V., Pfeffer, S., Erdinger, M., Richards, K. E., and Ziegler-Graff, V. 2003. Effects of Point Mutations in the Major Capsid Protein of Beet Western Yellows Virus on Capsid Formation, Virus Accumulation, and Aphid Transmission. Journal of Virology 77:3247.

Brault, V., van den Heuvel, J. F., Verbeek, M., Ziegler-Graff, V., Reutenauer, A., Herrbach, E., Garaud, J. C., Guilley, H., Richards, K., and Jonard, G. 1995. Aphid transmission of beet western yellows luteovirus requires the minor capsid read-through protein P74. The EMBO Journal 14:650-659.

Bruyère, A., Brault, V., Ziegler-Graff, V., Simonis, M. T., Van den Heuvel, J. F. J. M., Richards, K., Guilley, H., Jonard, G., and Herrbach, E. 1997. Effects of Mutations in the Beet Western Yellows Virus Readthrough Protein on Its Expression and Packaging and on Virus Accumulation, Symptoms, and Aphid Transmission. Virology 230:323-334.

Burgyán, J., and Havelda, Z. 2011. Viral suppressors of RNA silencing. Trends in Plant Science 16:265-272.

Chen, G. Q., Yan, S. X., and Roistacher, C. N. 1992. First report of citrus vein enation disease in China. Plant Disease 76:1077.

Csorba, T., Kontra, L., and Burgyan, J. 2015. viral silencing suppressors: Tools forged to fine-tune host-pathogen coexistence. Virology 479-480:85-103.

Csorba, T., Lozsa, R., Hutvagner, G., and Burgyan, J. 2010. Polerovirus protein P0 prevents the assembly of small RNA-containing RISC complexes and leads to degradation of ARGONAUTE1. Plant J 62:463-472.

Da Graça, J. V., and Maharaj, S. B. 1991. Citrus vein enation virus, a probable luteovirus. in: Proceedings of 11th Conference of International Organization of Citrus Virologists.

Derrien, B., Baumberger, N., Schepetilnikov, M., Viotti, C., De Cillia, J., Ziegler-Graff, V., Isono, E., Schumacher, K., and Genschik, P. 2012. Degradation of the antiviral component ARGONAUTE1 by the autophagy pathway. Proc Natl Acad Sci U S A 109:15942-15946.

Ding, S. W. 2010. RNA-based antiviral immunity. Nat Rev Immunol 10:632-644.

Duncan, D. B. 1955. Multiple Range and Multiple F Tests. Biometrics 11:1-42.

Díaz-Pendón, J. A., and Ding, S. W. 2008. Direct and indirect roles of viral suppressors of RNA silencing in pathogenesis. Annu Rev Phytopathol 46:303-326.

Earley, K. W., Haag, J. R., Pontes, O., Opper, K., Juehne, T., Song, K., and Pikaard, C. S. 2006. Gateway-compatible vectors for plant functional genomics and proteomics. Plant J 45:616-629.

Fraser, L. R. 1958. Virus diseases of citrus in Australia. Pages 9-19 in: Proceedings of the Linnean Society of New South Wales.

Fraser, L. R. 1960. Woody gall, a suspected virus disease of Rough Lemon and other Citrus varieties. in: Proceedings of the Linnean Society of New South Wales.

Fusaro, A. F., Correa, R. L., Nakasugi, K., Jackson, C., Kawchuk, L., Vaslin, M. F., and Waterhouse, P. M. 2012. The Enamovirus P0 protein is a silencing suppressor which inhibits local and systemic RNA silencing through AGO1 degradation. Virology 426:178-187.

Gagliardi, M., and Matarazzo, M. R. 2016. RIP: RNA Immunoprecipitation. Pages 73-86 in: Polycomb Group Proteins: Methods and Protocols. C. Lanzuolo and B. Bodega, eds. Springer New York, New York, NY.

Galiakparov, N., Tanne, E., Mawassi, M., Gafny, R., and Sela, I. 2003. ORF 5 of grapevine virus A encodes a nucleic acid-binding protein and affects pathogenesis. Virus Genes 27:257-262.

Huang, A.-j., Song, Z., Cao, M.-j., Chen, H.-m., Li, Z.-a., and Zhou, C.-y. 2015. The complete genome sequence of Citrus vein enation virus from China. Journal of Integrative Agriculture 14:598-601.

Incarbone, M., and Dunoyer, P. 2013. RNA silencing and its suppression: novel insights from in planta analyses. Trends Plant Sci 18:382-392.

Jacomino, A. P., and Salibe, A. A. 1993. Occurrence of woody gall disease in citrus in siio paulo state, Brazil. in: Proceedings of 12th Conference of International Organization of Citrus Virologists.

Jones, J. D., and Dangl, J. L. 2006. The plant immune system. Nature 444:323-329.

Jones, L., Hamilton, A. J., Voinnet, O., Thomas, C. L., Maule, A. J., and Baulcombe, D. C. 1999. RNA–DNA Interactions and DNA Methylation in Post-Transcriptional Gene Silencing. The Plant Cell 11:2291.

Koonin, E. V., Dolja, V. V., and Morris, T. J. 1993. Evolution and Taxonomy of Positive-Strand RNA Viruses: Implications of Comparative Analysis of Amino Acid Sequences. Critical Reviews in Biochemistry and Molecular Biology 28:375-430.

Laird, E. F., and Weathers, L. G. 1961. Aphis gossypii, a vector of citrus vein-enation virus. Plant Diseases Reporter 45:877.

Leary, A. Y., Sanguankiattichai, N., Duggan, C., Tumtas, Y., Pandey, P., Segretin, M. E., Salguero Linares, J., Savage, Z. D., Yow, R. J., and Bozkurt, T. O. 2017. Modulation of plant autophagy during pathogen attack. Journal of Experimental Botany 69:1325-1333

Lecker, S. H., Goldberg, A. L., and Mitch, W. E. 2006. Protein Degradation by the Ubiquitin–Proteasome Pathway in Normal and Disease States. Journal of the American Society of Nephrology 17:1807.

Lucy, A. P., Guo, H. S., Li, W. X., and Ding, S. W. 2000. Suppression of post-transcriptional gene silencing by a plant viral protein localized in the nucleus. The EMBO journal 19:1672-1680.

Maharaj, S. B., and Da Graca, J. V. 1988. Observation of isometric virus-like particles associated with citrus vein nation-infected citrus and the viruliferous aphid vector Toxoptera citricidus. Phytophylactica 20:357-360.

Mangwende, T., Wang, M. L., Borth, W., Hu, J., Moore, P. H., Mirkov, T. E., and Albert, H. H. 2009. The P0 gene of Sugarcane yellow leaf virus encodes an RNA silencing suppressor with unique activities. Virology 384:38-50.

Manjunath, K. L. 1987. Studies on vein enation virus disease of citrus in South India. Indian Journal of Plant Pathology 5:121-125.

Martín-Hernández, A. M., and Baulcombe, D. C. 2008. Tobacco rattle virus 16-kilodalton protein encodes a suppressor of RNA silencing that allows transient viral entry in meristems. J Virol 82:4064-4071.

McClean, A. P. D. 1954. Citrus vein-enation virus. South African Journal of Science 50:147.

Moffett, P., Farnham, G., Peart, J., and Baulcombe, D. C. 2002. Interaction between domains of a plant NBS-LRR protein in disease resistance-related cell death. The EMBO journal 21:4511-4519.

Mérai, Z., Kerényi, Z., Kertész, S., Magna, M., Lakatos, L., and Silhavy, D. 2006. Double-Stranded RNA Binding May Be a General Plant RNA Viral Strategy To Suppress RNA Silencing. Journal of Virology 80:5747.

Nakazono-Nagaoka, E., Fujikawa, T., and Iwanami, T. 2017. Nucleotide sequences of Japanese isolates of citrus vein enation virus. Arch Virol 162:879-883.

Navarro, L. 1986. Citrus certification in Mediterranean countries1. EPPO Bulletin 16:227-238.

Pazhouhandeh, M., Dieterle, M., Marrocco, K., Lechner, E., Berry, B., Brault, V., Hemmer, O., Kretsch, T., Richards, K. E., Genschik, P., and Ziegler-Graff, V. 2006. F-box-like domain in the polerovirus protein P0 is required for silencing suppressor function. Proc Natl Acad Sci U S A 103:1994-1999.

Pfaffl, M. W. 2001. A new mathematical model for relative quantification in real-time RT-PCR. Nucleic acids research 29:e45-e45.

Pumplin, N., and Voinnet, O. 2013. RNA silencing suppression by plant pathogens: defence, counter-defence and counter-counter-defence. Nat Rev Microbiol 11:745-760.

Qiao, Y., Liu, L., Xiong, Q., Flores, C., Wong, J., Shi, J., Wang, X., Liu, X., Xiang, Q., Jiang, S., Zhang, F., Wang, Y., Judelson, H. S., Chen, X., and Ma, W. 2013. Oomycete pathogens encode RNA silencing suppressors. Nat Genet 45:330-333.

Qu, F., Ye, X., Hou, G., Sato, S., Clemente, T. E., and Morris, T. J. 2005. RDR6 has a broad-spectrum but temperature-dependent antiviral defense role in Nicotiana benthamiana. J Virol 79:15209-15217.

Ramanathan, M., Porter, D. F., and Khavari, P. A. 2019. Methods to study RNA–protein interactions. Nature Methods 16:225-234.

Renovell, Á., Vives, M. C., Ruiz-Ruiz, S., Navarro, L., Moreno, P., and Guerri, J. 2012. The Citrus leaf blotch virus movement protein acts as silencing suppressor. Virus Genes 44:131-140.

Roth, B. M., Pruss, G. J., and Vance, V. B. 2004. Plant viral suppressors of RNA silencing. Virus Res 102:97-108.

Ruiz, M. T., Voinnet, O., and Baulcombe, D. C. 1998. Initiation and maintenance of virus-induced gene silencing. The Plant cell 10:937-946.

Schmitz, J., Stussi-Garaud, C., Tacke, E., Prüfer, D., Rohde, W., and Rohfritsch, O. 1997. In SituLocalization of the Putative Movement Protein (pr17) from Potato Leafroll Luteovirus (PLRV) in Infected and Transgenic Potato Plants. Virology 235:311-322.

Schwach, F., Vaistij, F. E., Jones, L., and Baulcombe, D. C. 2005. An RNA-dependent RNA polymerase prevents meristem invasion by potato virus X and is required for the activity but not the production of a systemic silencing signal. Plant Physiol 138:1842-1852.

Selth, L. A., Close, P., and Svejstrup, J. Q. 2011. Studying RNA–Protein Interactions In Vivo By RNA Immunoprecipitation. Pages 253-264 in: Epigenetics Protocols. T. O. Tollefsbol, ed. Humana Press, Totowa, NJ.

Sheta, E., Salem, E., Abou-Zeid, A., Osman, M., Shafik, M., El-Hawari, A., Safurim, J., D'Onghia, A., and Camacho, A. 2002. Development of a citrus certification

program in Egypt. in: Proceedings of 15th Conference of International Organization of Citrus Virologists.

Silva, J. M. F., Al Rwahnih, M., Blawid, R., Nagata, T., and Fajardo, T. V. M. 2017. Discovery and molecular characterization of a novel enamovirus, Grapevine enamovirus-1. Virus Genes 53:667-671.

Song, L., Gao, S., Jiang, W., Chen, S., Liu, Y., Zhou, L., and Huang, W. 2011. Silencing suppressors: viral weapons for countering host cell defenses. Protein Cell 2:273-281.

Song, Z., Wang, Y., Cui, T., Bin, Y., Yan, J., and Zhou, C. 2018. Identification of an RNA silencing suppressor encoded by citrus vein enation virus. Journal of Plant Pathology

Stevens, M., Freeman, B., Liu, H. Y., Herrbach, E., and Lemaire, O. 2005. Beet poleroviruses: close friends or distant relatives? Molecular Plant Pathology 6:1-9.

Tallarida, R. J., and Murray, R. B. 1987. Duncan Multiple Range Test. Pages 125-127 in: Manual of Pharmacologic Calculations: With Computer Programs. R. J. Tallarida and R. B. Murray, eds. Springer New York, New York, NY.

Tanaka, S., and Yamada, S. 1961. Citrus virus diseases in Japan. in: Proceedings of 2nd Conference of International Organization of Citrus Virologists.

ten Have, S., Boulon, S., Ahmad, Y., and Lamond, A. I. 2011. Mass spectrometry-based immuno-precipitation proteomics – The user's guide. PROTEOMICS 11:1153-1159.

Turriziani, B., von Kriegsheim, A., and Pennington, S. R. 2016. Protein-Protein Interaction Detection Via Mass Spectrometry-Based Proteomics. Pages 383-396 in: Modern Proteomics – Sample Preparation, Analysis and Practical Applications. H. Mirzaei and M. Carrasco, eds. Springer International Publishing, Cham.

Vargason, J. M., Szittya, G., Burgyán, J., and Hall, T. M. T. 2003. Size Selective Recognition of siRNA by an RNA Silencing Suppressor. Cell 115:799-811.

Vidalakis, G., Gumpf, D. J., Polek, M., and Bash, J. A. 2014. The California Citrus Clonal Protection Program. Pages 117-130 in: Citrus Production Manual. L. Ferguson and E. E. Grafton-Cardwell, eds., University of California Agricultural and Natural Resources (UC ANR) Publication 3539.

Vives, M. C., Velázquez, K., Pina, J. A., Moreno, P., Guerri, J., and Navarro, L. 2013. Identification of a new enamovirus associated with citrus vein enation disease by deep sequencing of small RNAs. Phytopathology 103:1077-1086.

Wallace, J. M., and Drake, R. J. 1953. A virus-induced vein enation in citrus. Citrus leaves 33:22-24.

Wallace, J. M., and Drake, R. J. 1959. Citrus vein enation. Pages 163-165 in: Citrus Virus Diseases. J. M. Wallace, ed. University of California Press, Berkeley and Los Angeles.

Wallace, J. M., and Drake, R. J. 1960. Woody galls on Citrus associated with vein enation virus infection. Plant Disease Reporter 44:580-584.

Wallace, J. M., and Drake, R. J. 1961. Induction of woody galls by wounding of citrus infected with vein-enation virus. Plant Disease Reporter 45:682-586.

Wang, K. D., Empleo, R., Nguyen, T. T., Moffett, P., and Sacco, M. A. 2015. Elicitation of hypersensitive responses in Nicotiana glutinosa by the suppressor of RNA silencing protein P0 from poleroviruses. Mol Plant Pathol 16:435-448.

Wang, M. B., Masuta, C., Smith, N. A., and Shimura, H. 2012. RNA silencing and plant viral diseases. Mol Plant Microbe Interact 25:1275-1285.

Weber, P. H., and Bujarski, J. J. 2015. Multiple functions of capsid proteins in (+) stranded RNA viruses during plant–virus interactions. Virus Research 196:140-149.

Wroblewski, T., Tomczak, A., and Michelmore, R. 2005. Optimization of Agrobacterium-mediated transient assays of gene expression in lettuce, tomato and Arabidopsis. Plant Biotechnology Journal 3:259-273.

Wu, Q., Wang, X., and Ding, S. W. 2010. Viral suppressors of RNA-based viral immunity: host targets. Cell Host Microbe 8:12-15.

Yang, H.-J., Oh, J., Lee, H.-K., Lee, D.-S., Kim, S.-Y., Kim, M.-H., Park, C. Y., Kim, H., Yi, S.-I., Jeong, R.-D., Moon, J. S., and Lee, S.-H. 2019. First report of Citrus vein enation virus in Satsuma mandarin (*Citrus unshiu*) in Korea. Plant Disease.

Zhou, Z. S. h., Dell'Orco, M., Saldarelli, P., Turturo, C., Minafra, A., and Martelli, G. P. 2006. Identification of an RNA-silencing suppressor in the genome of Grapevine virus A. J Gen Virol 87:2387-2395.

Ziegler-Graff, V. 1996. The coat protein of beet western yellows luteovirus is essential for systemic infection but the viral gene products P29 and P19 are dispensable for systemic infection and aphid transmission. Molecular plant-microbe interactions 9:501-510
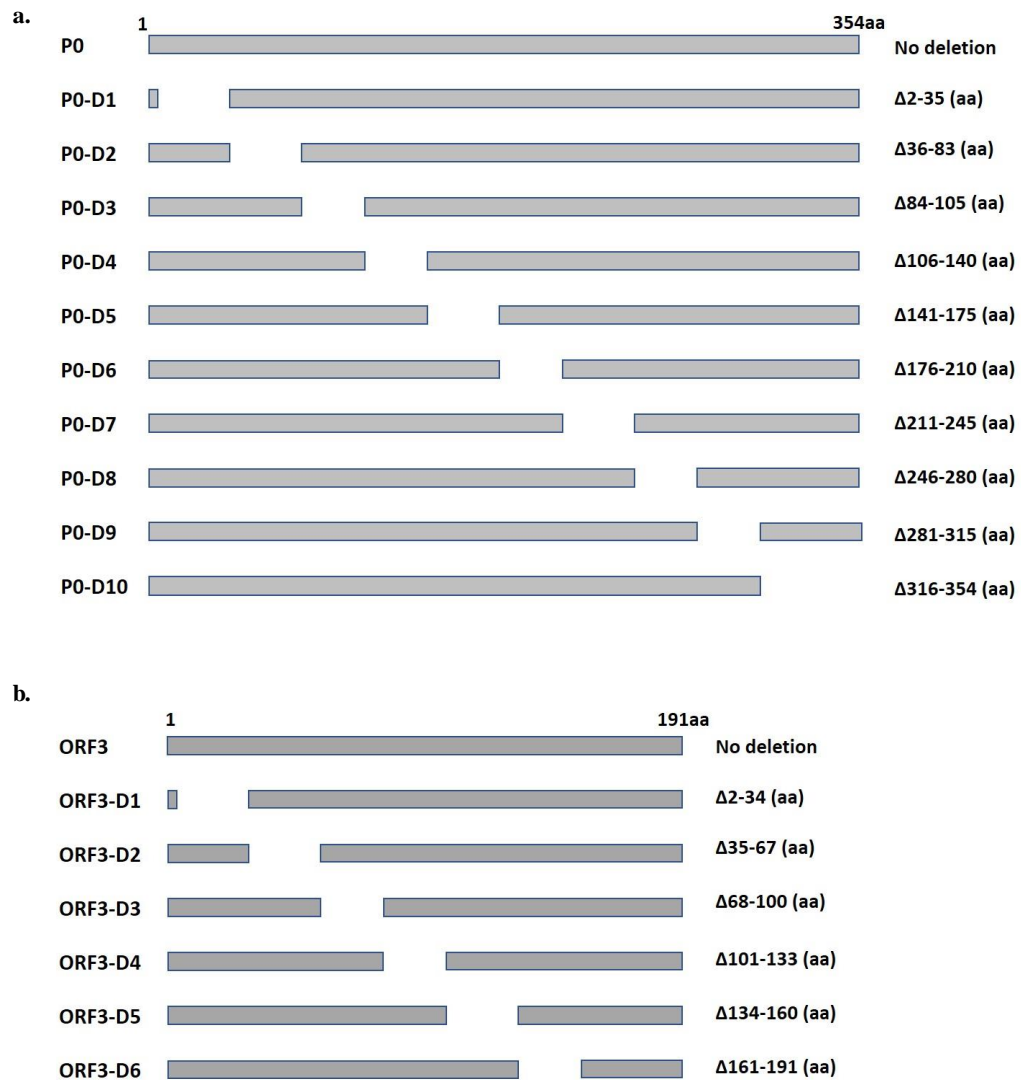
Figure 4.1 Serial deletion assay of P0 and open reading frame 3 (ORF3) encoded by citrus vein enation virus to identify functional regions of suppression activity in viral suppressors of RNA silencing (VSR). Illustrations are not to scale. (a) P0 serial deletions and (b) ORF3 serial deletions.
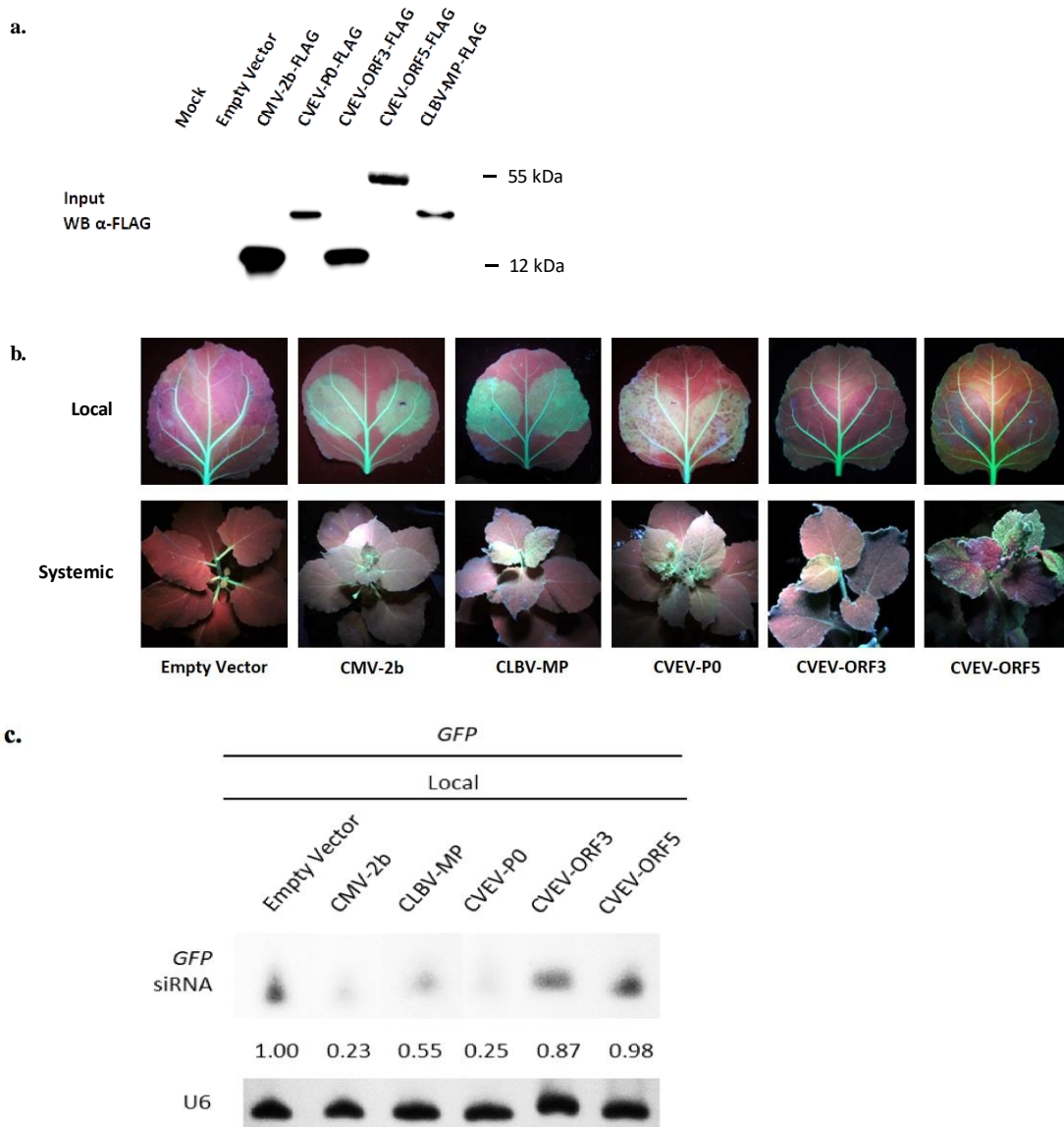
Figure 4.2 RNA silencing suppression co-infiltration assay of citrus vein enation virus P0, open reading frame 3 and 5. Empty vector was used as negative control and cucumber mosaic virus 2b and citrus leaf blotch virus movement protein were used as controls of viral suppressor of RNA silencing. (a) Western blot analysis to confirm protein expression. (b) Local (upper row) and systemic (lower row) silencing suppression observed under UV light at 5 and 14 dpi, respectively. (c) Northern blot analysis for testing *GFP* siRNA examined for local infiltrated tissue. Number represents the intensity of signal compared to empty vector. U6 were used as loading control. (CMV-2b: cucumber mosaic virus 2b; CLBV-MP: citrus leaf blotch virus movement protein; CVEV: citrus vein enation virus; ORF3: open reading frame 3; ORF5: open reading frame 5; WB: western blot)
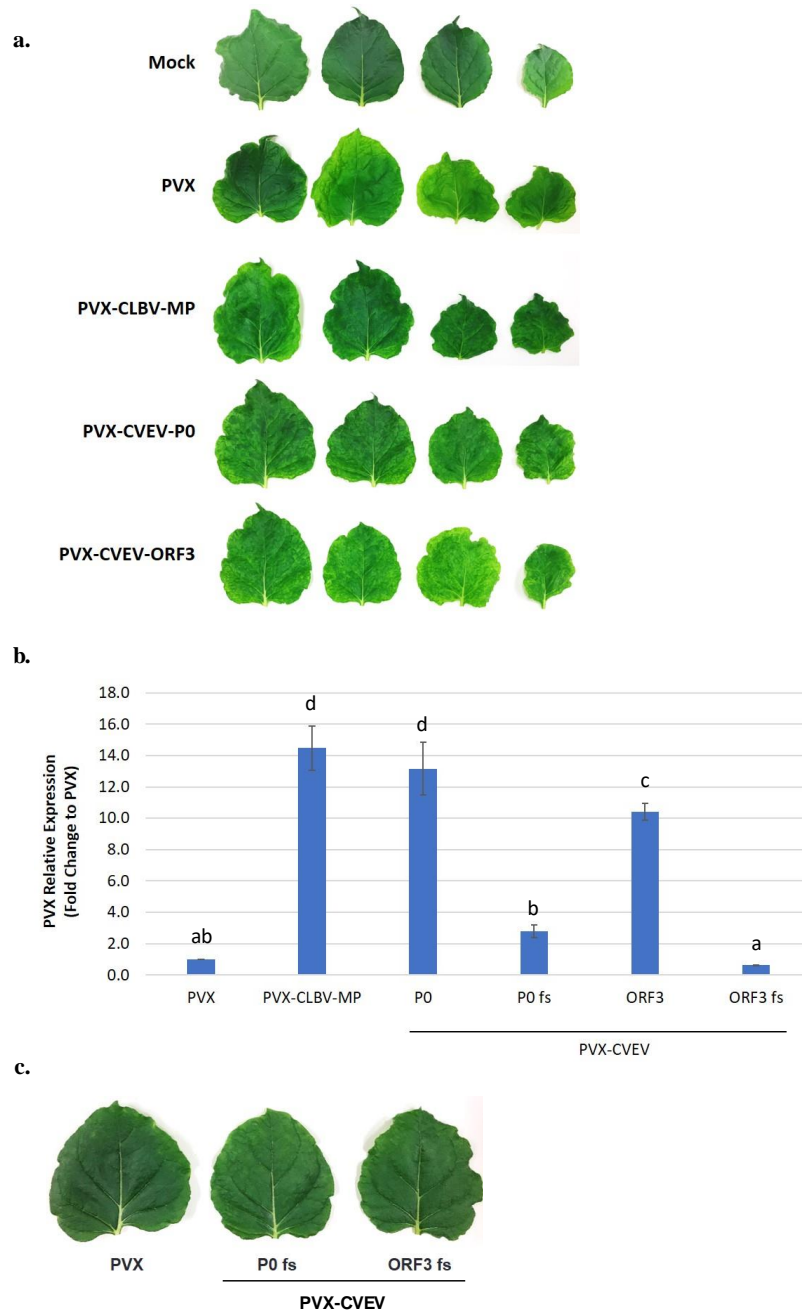
a. Local
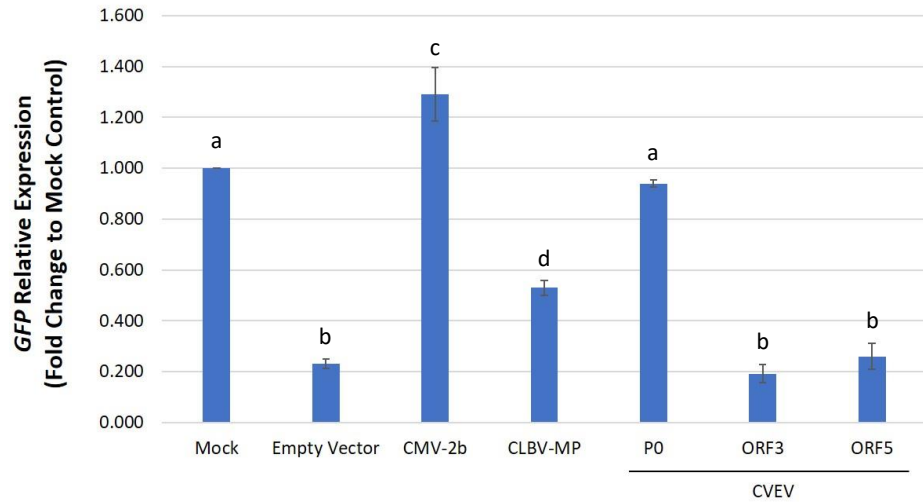
b. Systemic

Figure 4.3 Relative expression analysis of *GFP* mRNA for silencing suppression co-infiltration assay with (a) local and infiltrated leaf tissue collected at 5 dpi and (b) systemic tissue collected at 14 dpi. (Significance level α=0.05) (CMV-2b: cucumber mosaic virus 2b; CLBV-MP: citrus leaf blotch virus movement protein; CVEV: citrus vein enation virus; ORF3: open reading frame 3; ORF5: open reading frame 5)
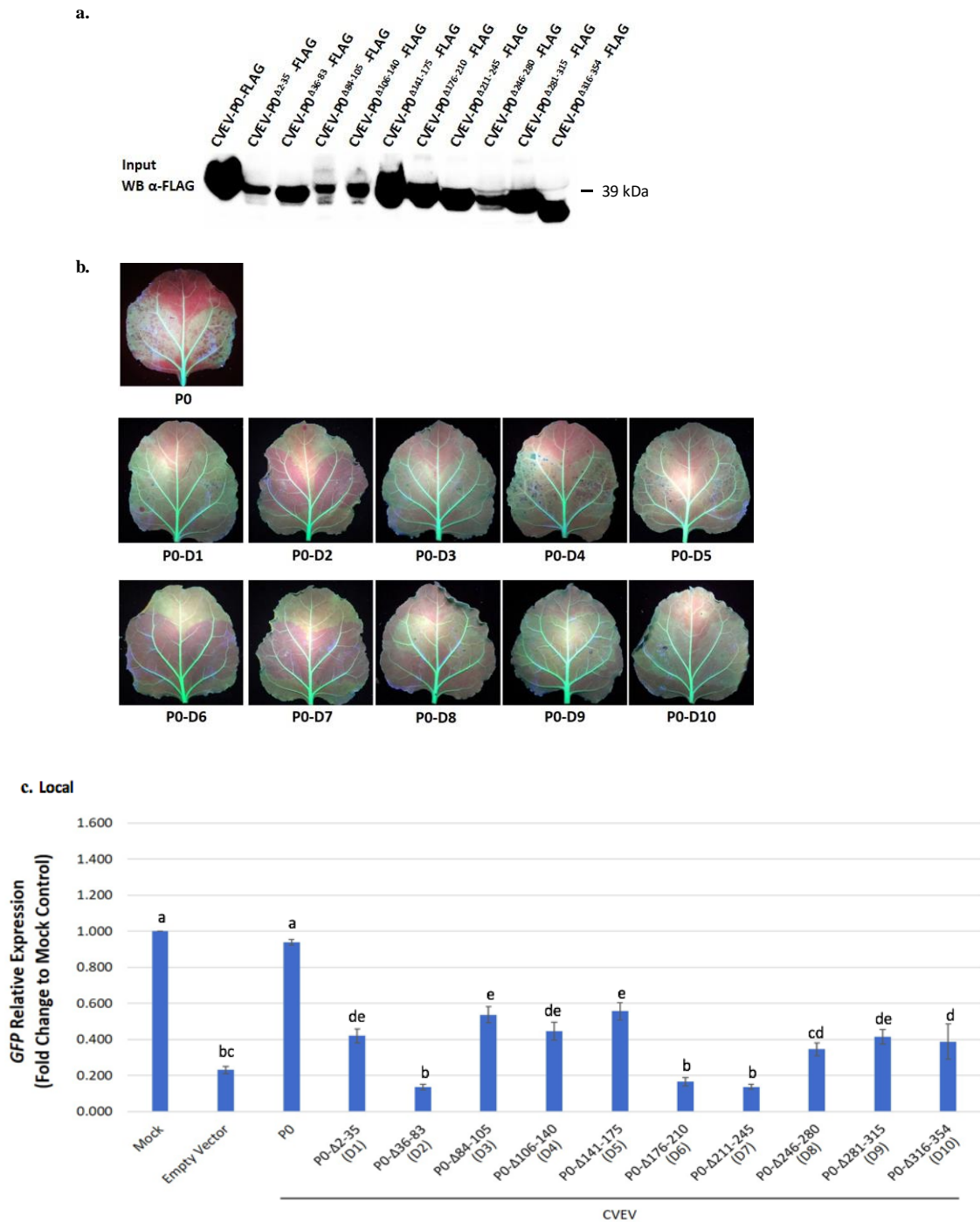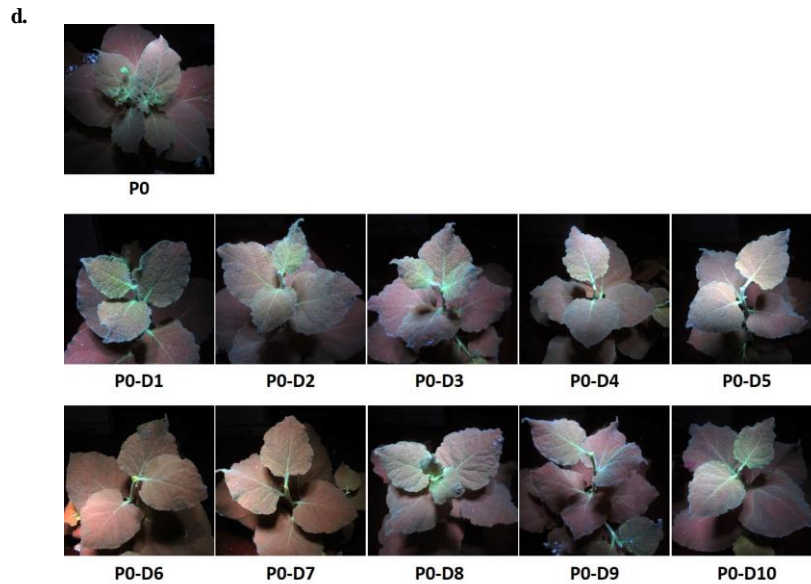
Figure 4.4 Potato virus X assay to test P0 and open reading frame 3 encoded by citrus vein enation virus on the suppression of siRNA-mediated host immunity in *N benthamiana* plants. (a) Leaf symptoms. (b) Relative expression analysis by PVX CP RT-qPCR (Significance level α=0.05). (c) Leaf symptoms of frameshifting mutations of P0 and open reading frame 3. (PVX: potato virus x; CLBV-MP: citrus leaf blotch virus movement protein; CVEV: citrus vein enation virus; ORF3: open reading frame 3; fs: frameshifting mutation)

Figure 4.5 RNA silencing suppression co-infiltration assay of citrus vein enation virus P0 and its deletions. (a) Western blot analysis to confirm protein expression. (b) Local silencing suppression observed under UV light at 5 dpi. (c) Relative expression level analysis of *GFP* mRNA level in local tissue by *GFP* RT-qPCR (Significance level α=0.05). (CVEV: citrus vein enation virus; WB: western blot)
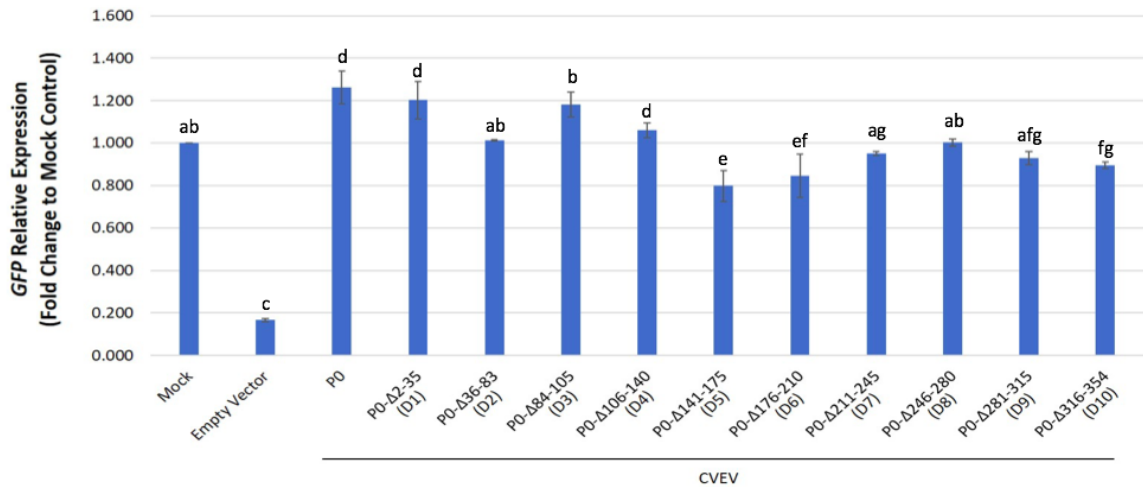
d.

e. Systemic

Figure 4.5 RNA silencing suppression co-infiltration assay of citrus vein enation virus P0 and its deletions (cont'd). (d) Systemic silencing suppression observed under UV light at 14 dpi. (e) Relative expression level analysis of *GFP* mRNA level in systemic tissue by *GFP* RT-qPCR (Significance level α=0.05). (CVEV: citrus vein enation virus)
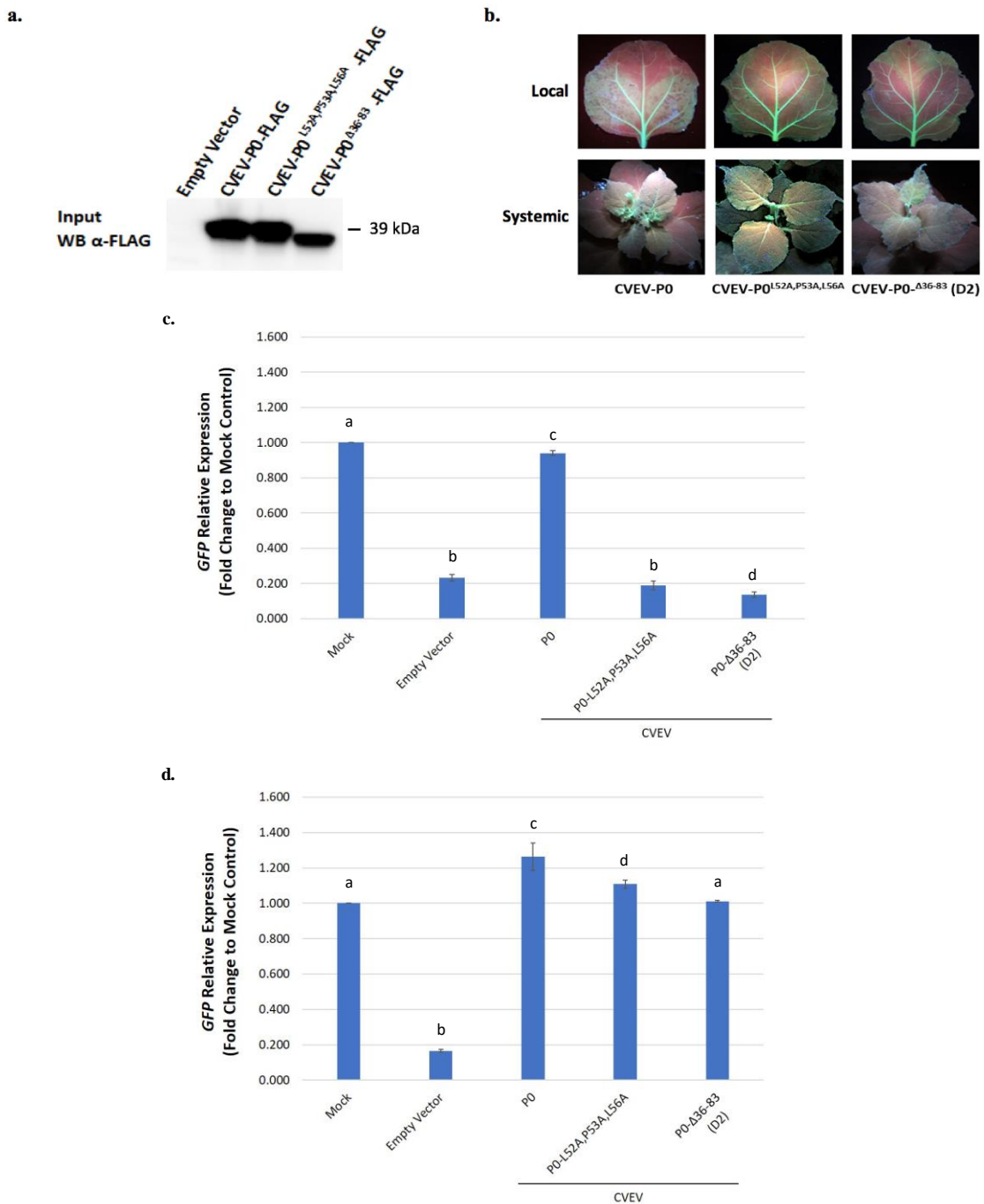
Figure 4.6 RNA silencing suppression co-infiltration assay of citrus vein enation virus P0, $P0^{L52A,P53A,L56A}$ and $P0^{\Delta36-83}$. (a) Western blot analysis to confirm protein expression. (b) Local and systemic silencing suppression observed under UV light at 5 and 14 dpi, respectively. Relative expression level analysis of *GFP* mRNA level (c) in local tissue and (d) in systemic tissue by *GFP* RT-qPCR (Significance level α=0.05). (CVEV: citrus vein enation virus; WB: western blot)
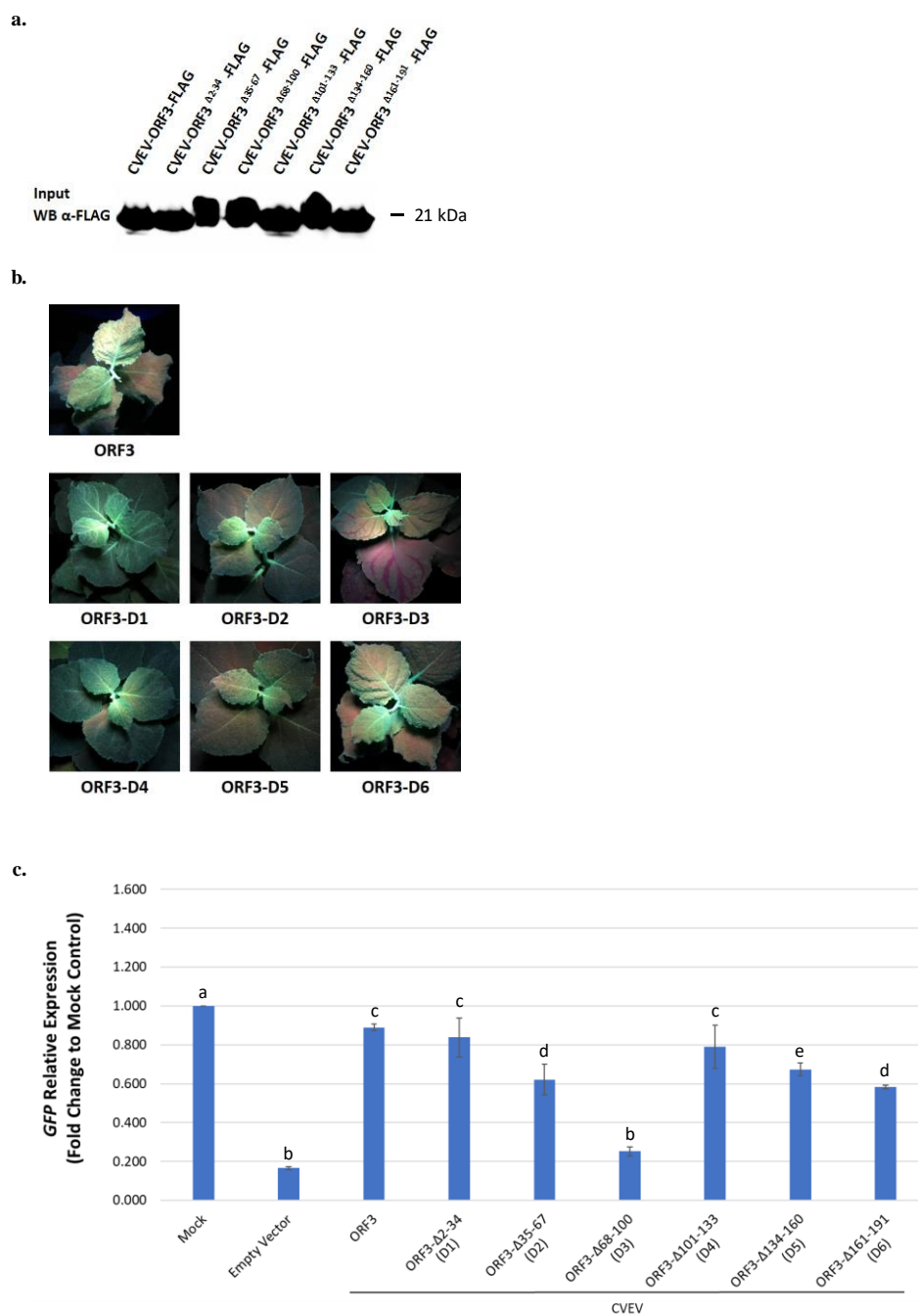
Figure 4.7 RNA silencing suppression co-infiltration assay of citrus vein enation virus open reading frame 3 and its deletions. (a) Western blot analysis to confirm protein expression. (b) Systemic silencing suppression observed under UV light at 14 dpi. (c) Relative expression level analysis of *GFP* mRNA level in systemic tissue by *GFP* RT-qPCR (Significance level α=0.05). (CVEV: citrus vein enation virus; ORF3: open reading frame 3; WB: western blot)

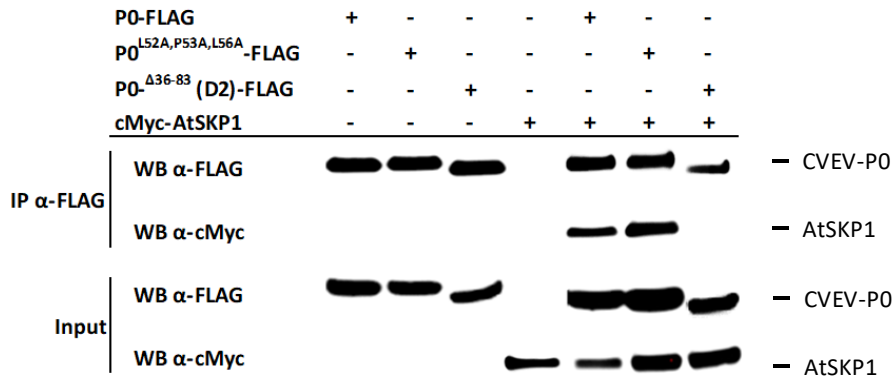|	P0-FLAG	+	-	-	-	+	-	-
	P0^{L52A,P53A,L56A}-FLAG	-	+	-	-	-	+	-
	P0-$^{\Delta36-83}$ (D2)-FLAG	-	-	+	-	-	-	+
	cMyc-AtSKP1	-	-	-	+	+	+	+

IP α-FLAG
- WB α-FLAG — CVEV-P0
- WB α-cMyc — AtSKP1

Input
- WB α-FLAG — CVEV-P0
- WB α-cMyc — AtSKP1

Figure 4.8 Western blot analysis of **c**o-immunoprecipitation of cMyc-AtSKP1 with CVEV-P0-FLAG. The immune-precipitated proteins were examined by western blot analysis. (IP: immunoprecipitation; WB: western blot)
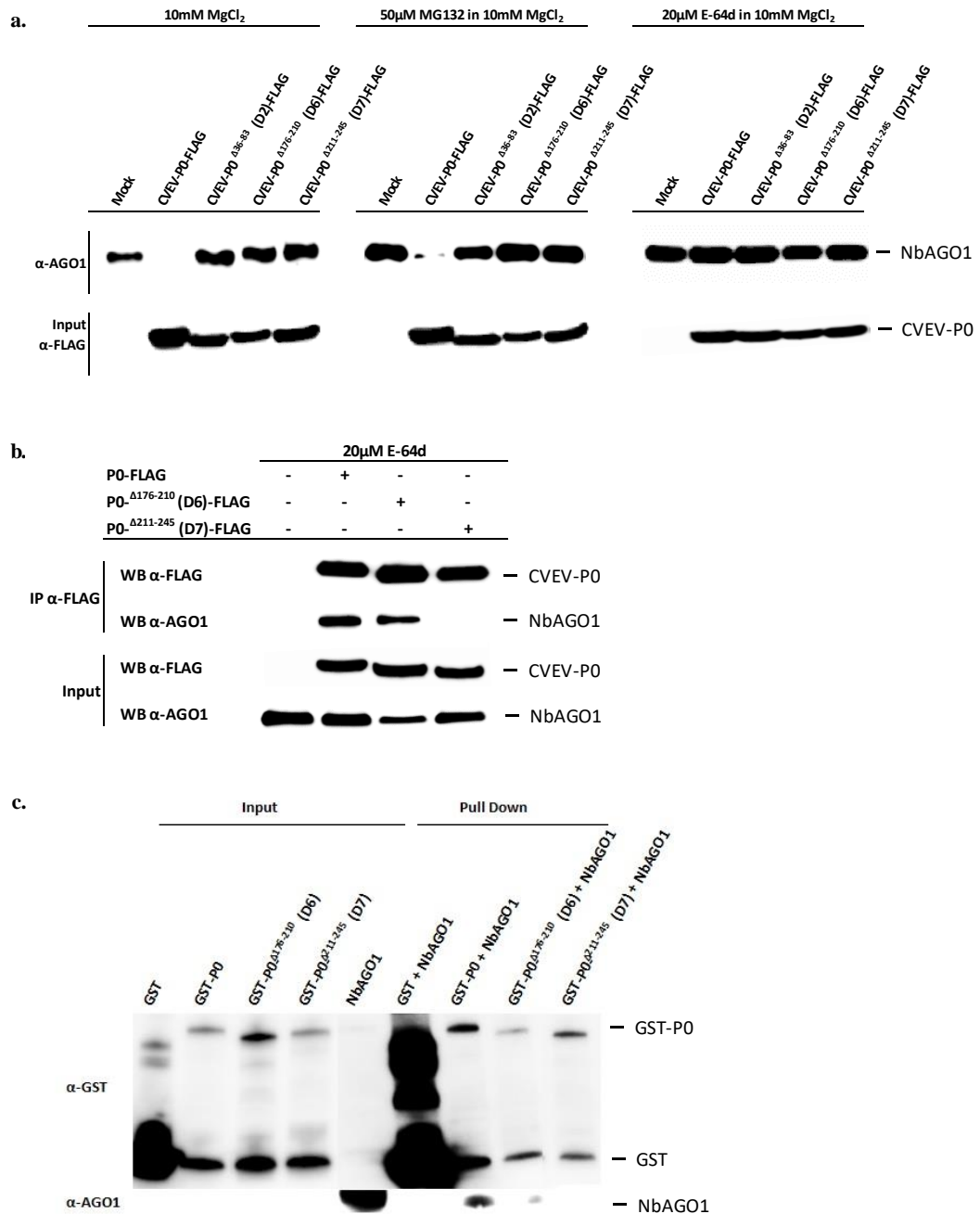
Figure 4.9 Interactions between citrus vein enation virus P0 or its deletions and NbAGO1. Western blot analysis of (a) AGO1 degradation assay treated with 50μM MG132, 20μM E-64d or buffer only (10mM MgCl₂) as controls, (b) co-immunoprecipitation of NbAGO1 with CVEV-P0-FLAG, and (c) pull-down assay of GST-CVEV-P0 and NbAGO1. (CVEV: citrus vein enation virus; IP: immunoprecipitation; WB: western blot)
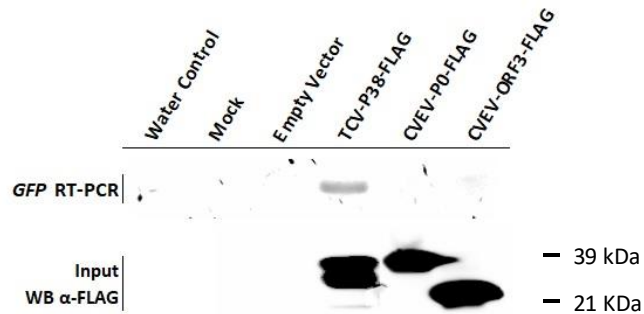
Figure 4.10 RNA immunoprecipitation (RIP) of citrus vein enation virus P0 and open reading frame 3 (ORF3). The agarose gel electrophoresis of *GFP* RT-PCR products is shown in the upper part of the figure. The input of the protein was examined by western blot analysis and is shown in the lower panel. (TCV: turnip crinkle virus; CVEV: citrus vein enation virus; ORF3: open reading frame 3; WB: western blot)
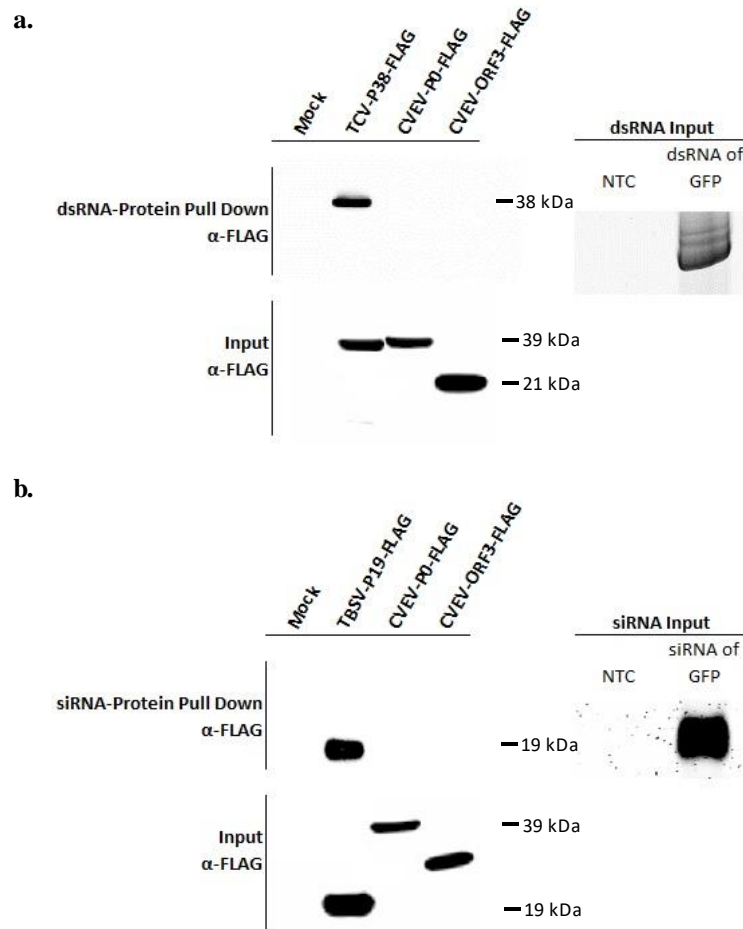
Figure 4.11 RNA-protein pull-down assay to examine citrus vein enation virus P0 and open reading frame 3 RNA binding capability with (a) double-stranded RNA (dsRNA) of *GFP* and (b) small interfering RNA (siRNA). Inputs of dsRNA and siRNA were examined by polyacrylamide gel electrophoresis. (TCV: turnip crinkle virus; CVEV: citrus vein enation virus; TBSV: tomato bushy stunt virus; ORF3: open reading frame 3; WB: western blot)

Mock   **CVEV P0**

Figure 4.12 Robust hypersensitive response (HR)-like cell death triggered by P0 of citrus vein enation virus at 2 dpi in *N. benthamiana*.

Table 4.1 List of primers and probes used in this study.

No.	Name	Primer Sequence	Purpose of use
Cloning			
1	VSR_CVEV-ORF3/5-F	CACCATGGTGAGTCGCAATCAAAGACGAAG	Viral gene cloning- pEarleyGate vectors
2	VSR_CVEV-ORF3-R	TTTGGGCAGTCGCGTTTCCAGGCGAAAGA	Viral gene cloning- pEarleyGate vectors
3	VSR_CVEV-ORF5-R	CCGCCAGGAAAATCGAGAGGGTTTATCCTC	Viral gene cloning- pEarleyGate vectors
4	VSR_CVEV-ORF0-F	CACCATGCCTTGCTACCATGTCATCC	Viral gene cloning- pEarleyGate vectors
5	VSR_CVEV-ORF0-R	AGCCTCGGGTCCGCTACC	Viral gene cloning- pEarleyGate vectors
6	VSR_CLBV-MP-F	CACCATGGCATCCCTGATCAATGTAAG	Viral gene cloning- pEarleyGate vectors
7	VSR_CLBV-MP-R1	CTTGGTCCCAGTGTCACTGGC	Viral gene cloning- pEarleyGate vectors
8	VSR_CLBV-MP-R2	TCACTTGGTCCCAGTGTCACTGG	Viral gene cloning- pEarleyGate vectors
9	VSR_CMV-2b-F	CACCATGGAATTGAACGHRGGYG	Viral gene cloning- pEarleyGate vectors
10	VSR_CMV-2b-R1	RAAMGCACCTTCCGCCCA	Viral gene cloning- pEarleyGate vectors
11	VSR_CMV-2b-R2	TCARAAMGCACCTTCCGCCC	Viral gene cloning- pEarleyGate vectors
12	VSR_GFP-F	CACCATGAGTAAAGGAGAAGAACTTTTCACTGGA	Gene cloning- pEarleyGate vectors
13	VSR_GFP-R1	TTTGTATAGTTCATCCATGCCATGTGTAATCCCA	Gene cloning- pEarleyGate vectors
14	VSR_GFP-R2	TTATTTGTATAGTTCATCCATGCCATGTGTAATCCCA	Gene cloning- pEarleyGate vectors
15	pGR106-CVEV-P0-F	GGCGCGCCATGCCTTGCTACCAT	Viral gene cloning- pGR106 vector
16	pGR106-CVEV-P0-R	GCGGCCGCCTAAGCCTCGG	Viral gene cloning- pGR106 vector
17	pGR106-CVEV-ORF3-F	GGCGCGCCATGGTGAGTCGCAATCAA	Viral gene cloning- pGR106 vector
18	pGR106-CVEV-ORF3-R	GCGGCCGCCTATTTGGGCAGT	Viral gene cloning- pGR106 vector
19	pGR106-CLBV-MP-F	GGCGCGCCATGGCATCCCTG	Viral gene cloning- pGR106 vector
20	pGR106-CLBV-MP-R	GCGGCCGCTCACTTGGTCCCAG	Viral gene cloning- pGR106 vector
21	pGR106-CVEV-P0 fs-F1	AAGAGAAGTGGGCTTGCT	CVEV-P0 frameshifting clone- pGR106 vector
22	pGR106-CVEV-P0 fs-R1	CACCCAGACAGTATGTTC	CVEV-P0 frameshifting clone- pGR106 vector
23	pGR106-CVEV-P0 fs-F2	cTGAGCGGCCGCGTCGACC	CVEV-P0 frameshifting clone- pGR106 vector
24	pGR106-CVEV-P0 fs-R2	AGCCTCGGGTCCGCTACC	CVEV-P0 frameshifting clone- pGR106 vector
25	pGR106-CVEV-ORF3 fs-F	cGGAAGGCGCAGGCTTCTT	CVEV-ORF3 frameshifting clone- pGR106 vector
26	pGR106-CVEV-ORF3 fs-R	ACTGTACTCTCAACTGGGTTATTTTATAC	CVEV-ORF3 frameshifting clone- pGR106 vector
27	pEG1001-CVEV-P0-D1-F	CATGGTGAAGGGGGCGGCC	CVEV-P0 deletion clone- pGR106 vector
28	pEG1001-CVEV-P0-D1-R	TGTCCTACACAGGAGGGAACGCCATGC	CVEV-P0 deletion clone- pGR106 vector
29	pEG1001-CVEV-P0-D2-F	GCCCATCCCAACATAATTAATGAGAGCAAGTAAG	CVEV-P0 deletion clone- pGR106 vector
30	pEG1001-CVEV-P0-D2-R	CCACGCGGGTTCAACATCGTTG	CVEV-P0 deletion clone- pGR106 vector
31	pEG1001-CVEV-P0-D3-F	CAAAGTGAGGGCCTCAAGCGAGACCC	CVEV-P0 deletion clone- pGR106 vector
32	pEG1001-CVEV-P0-D3-R	ATCGGGCTTATCATCCCCCAATCTTACTGGC	CVEV-P0 deletion clone- pGR106 vector
33	pEG1001-CVEV-P0-D4-F	TCGAGCGGCACAAATTCTAAAGTACCAC	CVEV-P0 deletion clone- pGR106 vector
34	pEG1001-CVEV-P0-D4-R	GCAAGTGGCAAGGCAGAATACCAC	CVEV-P0 deletion clone- pGR106 vector
35	pEG1001-CVEV-P0-D5-F	AGCCATGAGCCAACATGGAAGAGAGGTGAATAGC	CVEV-P0 deletion clone- pGR106 vector
36	pEG1001-CVEV-P0-D5-R	TGCTGGCATGAGCTTATTGTTGGGTTGCTTG	CVEV-P0 deletion clone- pGR106 vector
37	pEG1001-CVEV-P0-D-6-F	AGCCCACTTCTCTTCCACCCA	CVEV-P0 deletion clone- pGR106 vector
38	pEG1001-CVEV-P0-D6-R	GGAAAACGCAATCTTATCGTGGATGCT	CVEV-P0 deletion clone- pGR106 vector
39	pEG1001-CVEV-P0-D7-F	AAGCACTTGGCTGTGAGGAGTAACGCCTC	CVEV-P0 deletion clone- pGR106 vector
40	pEG1001-CVEV-P0-D7-R	AGGCTCTTTTGCCTACGAGAACCGTATCTGTCG	CVEV-P0 deletion clone- pGR106 vector
41	pEG1001-CVEV-P0-D8-F	AGTGAGAGAACAATCATCCATATAGCGGTTC	CVEV-P0 deletion clone- pGR106 vector
42	pEG1001-CVEV-P0-D8-R	GAGTATCTTGCCCACTCTTTTGCTGAAC	CVEV-P0 deletion clone- pGR106 vector
43	pEG1001-CVEV-P0-D9-F	GCCACCCTCAGGAATTTCAGGCCAAGG	CVEV-P0 deletion clone- pGR106 vector
44	pEG1001-CVEV-P0-D9-R	GATGGTGAGGGTGATATTGAGAATCCCCCTGCTC	CVEV-P0 deletion clone- pGR106 vector
45	pEG1001-CVEV-P0-D10-F	ATCAGAGAACCAACCAAGATCCTCCTC	CVEV-P0 deletion clone- pGR106 vector
46	pEG1001-CVEV-P0-D10-R	AAGGGTGGGCGCGCCGA	CVEV-P0 deletion clone- pGR106 vector
47	pEG1001-CVEV-ORF3-D1-F	CGAAGACGCAACGCCCCC	CVEV-ORF3 deletion clone- pGR106 vector
48	pEG1001-CVEV-ORF3-D1-R	CATGGTGAAGGGGGCGGC	CVEV-ORF3 deletion clone- pGR106 vector
49	pEG1001-CVEV-ORF3-D2-F	GGTTATCTCACTTTTGGTCC	CVEV-ORF3 deletion clone- pGR106 vector
50	pEG1001-CVEV-ORF3-D2-R	GGAACGTGTGGGGTTGTT	CVEV-ORF3 deletion clone- pGR106 vector
51	pEG1001-CVEV-ORF3-D3-F	TGGAAGGCGCAGGCTTCT	CVEV-ORF3 deletion clone- pGR106 vector
52	pEG1001-CVEV-ORF3-D3-R	CTTGTCGTTGCATTTAAGCCCATAC	CVEV-ORF3 deletion clone- pGR106 vector
53	pEG1001-CVEV-ORF3-D4-F	AAGTTGACCAGTTCGGGG	CVEV-ORF3 deletion clone- pGR106 vector
54	pEG1001-CVEV-ORF3-D4-R	CTGTACTCTCAACTGGGTTATTTTATAC	CVEV-ORF3 deletion clone- pGR106 vector
55	pEG1001-CVEV-ORF3-D5-F	GACCAATTCCGCCTTGCC	CVEV-ORF3 deletion clone- pGR106 vector
56	pEG1001-CVEV-ORF3-D5-R	AAATGAGATAGCCCGGTTG	CVEV-ORF3 deletion clone- pGR106 vector
57	pEG1001-CVEV-ORF3-D6-F	AAGGGTGGGCGCGCCGAC	CVEV-ORF3 deletion clone- pGR106 vector
58	pEG1001-CVEV-ORF3-D6-R	CTCGTTAGAGGAGTTATACATTCTACCGTCACCG	CVEV-ORF3 deletion clone- pGR106 vector
59	pEG1001-CVEV-P0-Fbox-F5	TCT TGC TCT GCT ATG GGG TCA CCC TCG	F box: no substitution
60	pEG1001-CVEV-P0-Fbox-F6	TCT TGC TCT GCT ATG GGG TCA CGC ACG	F box: P67A
61	pEG1001-CVEV-P0-Fbox-R1	GCA CAT AAT AGG ACG TAG GGA AGC GCC ACG	F box: no substitution
62	pEG1001-CVEV-P0-Fbox-R2	GCA CAT AAA GCG ACG TAG GGA AGC GCC A	F box: L56A
63	pEG1001-CVEV-P0-Fbox-R3	GCA CAT AAT AGG ACG TAA GCA GCC GCC ACG	F box: L52A and P53A
64	pEG1001-CVEV-P0-Fbox-R4	GCA CAT AAA GCG ACG TAA GCA GCC GC	F box: L52A, P53A, L56A

Table 4.1 List of primers and probes used in this study (cont'd).

No.	Name	Primer Sequence	Purpose of use
65	TOPO-ASK1-F	CACCATGTCTGCGAAGAAGATTGTGTTGAAGAG	Cloning ot Arabidopsis ASK1/SKP1
66	TOPO-ASK1-R	TCATTCAAAAGCCCATTGGTTCTCTCTGCG	Cloning ot Arabidopsis ASK1/SKP1
67	Flexi-CVEV-P0-F	GATGGCGATCGCCATGCCTTGCTACCATGTCATCC	GST pull-down assay; P0 fused with GST at N-terminal
68	Flexi-CVEV-P0-R	GTGAGTTTAAACCTAAGCCTCGGGTCCGCTAC	GST pull-down assay; P0 fused with GST at N-terminal
69	TnT-NbAGO1-1-F	GAATTCACGCGTATGGTGCGGAAGAAGAGGACTG	NbAGO1 cloning- pCMVTnT vector
70	TnT-NbAGO1-1-R	CCGCCCCGGGTCAACAATAAAACATAACCCTCTTAAC	NbAGO1 cloning- pCMVTnT vector
71	VSR_TCV-P38-F	CACCATGGAAAATGATCCTAGAGTCCGGAAGTTC	Viral gene cloning- pEarleyGate vectors
72	VSR_TCV-P38-R	AATTCTGAGTGCTTGCCATTTACCCTTTGGC	Viral gene cloning- pEarleyGate vectors
73	VSR_TBSV-P19-F	CACCATGGAACGAGCTATACAAGGAAACGAC	Viral gene cloning- pEarleyGate vectors
74	VSR_TBSV-P19-R	CTCGCTTTCTTTTTCGAAGGTCTCAGTACCTTC	Viral gene cloning- pEarleyGate vectors
75	GFP-F-full gene	AAGGATCCATGGTAGATCTGACTAGTAAAGGAGAAG	Cloning GFP gene for northern blot probe production
76	GFP-R-full gene	ATCTCGAGTCACACGTGGTGGTGGTGGTGGT	Cloning GFP gene for northern blot probe production

DIG-Labeled DNA Probe

No.	Name	Primer Sequence	Purpose of use
77	U6 Probe	AGGGGCCATGCTAATCTTCTC /Dig_N/	Small RNA loading control DIG-labeled probe

RT-qPCR / RT-PCR Assays

No.	Name	Primer Sequence	Purpose of use
78	GFP-F	ACGGCATCAAAGCCAACTTC	GFP RT-qPCR
79	GFP-R	GCACGCCGCCGTCTT	GFP RT-qPCR
80	GFP Probe	/FAM/ CCCGCCACAACAT /NFQ/	GFP RT-qPCR, TaqMan™ MGB probe, Applied Biosystems™
81	PVX CP F	GGCCAGGGCACAATCCA	PVX RT-qPCR assay
82	PVX CP R	GACCTCGAGTGACAGCTGCAT	PVX RT-qPCR assay
83	PVX CP Probe	/FAM/ CGACTTTGCCAGCCTA /NFQ/	PVX RT-qPCR assay, TaqMan™ MGB probe, Applied Biosystems™
84	NbPP2A F	CCACTCGGTGGTGGAGAAA	NbPP2A RT-qPCR assay
85	NbPP2A R	CATCAGGGTCTTCAGCTAGCTCTA	NbPP2A RT-qPCR assay
86	NbPP2A Probe	CCATTCGCCCTAGTTT	NbPP2A RT-qPCR assay, TaqMan™ MGB probe, Applied Biosystems™
87	mgfp5 FWD	GGCCAACACTTGTCACTACT	GFP RT-PCR primer for RIP assay
88	mgfp5 REV	GGTCTTGAAGTTGGCTTTGATG	GFP RT-PCR primer for RIP assay

Table 4.2 List of plasmids, constructs, and bacterial strains used in this study.

Plasmids or Strains	Description	Source / Reference
Plasmids		
pEarleyGate100	pEG100; a Gateway binary vector with cauliflower mosaic virus *35S* promoter, Kan[R]	Earley et al.
pEarleyGate100::*GFP*	pEG100 carrying *GFP* , Kan[R]	This study
pEarleyGate100::*CMV2b*	pEG100 carrying *CMV2b* , Kan[R]	This study
pEarleyGate100::*CLBV-MP*	pEG100 carrying *CLBV-MP* , Kan[R]	This study
pEarleyGate100::*CVEV-P0*	pEG100 carrying *CVEV-P0* , Kan[R]	This study
pEarleyGate100::*CVEV-ORF3*	pEG100 carrying *CVEV-ORF3* , Kan[R]	This study
pEarleyGate100::*CVEV-ORF5*	pEG100 carrying *CVEV-ORF5* , Kan[R]	This study
pEarleyGate1001	pEG1001; modified from pEG100 by adding *Flag* at the downstream of cloning site, Kan[R]	This study
pEarleyGate1001::*GFP*	pEG1001 carrying *GFP* tagged with *Flag* at C-terminal, Kan[R]	This study
pEarleyGate1001::*CMV2b*	pEG1001 carrying *CMV2b* tagged with *Flag* at C-terminal, Kan[R]	This study
pEarleyGate1001::*CLBV-MP*	pEG1001 carrying *CLBV-MP* tagged with *Flag* at C-terminal, Kan[R]	This study
pEarleyGate1001::*CVEV-P0*	pEG1001 carrying *CVEV-P0* tagged with *Flag* at C-terminal, Kan[R]	This study
pEarleyGate1001::*CVEV-ORF3*	pEG1001 carrying *CVEV-ORF3* tagged with *Flag* at C-terminal, Kan[R]	This study
pEarleyGate1001::*CVEV-ORF5*	pEG1001 carrying *CVEV-ORF5* tagged with *Flag* at C-terminal, Kan[R]	This study
pGR106	A binary and infectious vector carrying the Potato virus X genome, Kan[R]	Jones et al.
pGR106::*CLBV-MP*	pGR106 carrying *CLBV-MP* , Kan[R]	This study
pGR106::*CVEV-P0*	pGR106 carrying *CVEV-P0* , Kan[R]	This study
pGR106::*CVEV-ORF3*	pGR106 carrying *CVEV-ORF3* , Kan[R]	This study
pGR106::*CTLV-P0* -frameshift	pGR106 carrying *CVEV-P0* with framshifting, Kan[R]	This study
pGR106::*CTLV-ORF3* -frameshift	pGR106 carrying *CVEV-ORF3* with framshifting, Kan[R]	This study
pEarleyGate1001::*CVEV-P0* -D1	pEG1001 carrying *CVEV-P0* with deletion from 2 to 35 amino acid, Kan[R]	This study
pEarleyGate1001::*CVEV-P0* -D2	pEG1001 carrying *CVEV-P0* with deletion from 36 to 83 amino acid, Kan[R]	This study
pEarleyGate1001::*CVEV-P0* -D3	pEG1001 carrying *CVEV-P0* with deletion from 84 to 105 amino acid, Kan[R]	This study
pEarleyGate1001::*CVEV-P0* -D4	pEG1001 carrying *CVEV-P0* with deletion from 106 to 140 amino acid, Kan[R]	This study
pEarleyGate1001::*CVEV-P0* -D5	pEG1001 carrying *CVEV-P0* with deletion from 141 to 175 amino acid, Kan[R]	This study
pEarleyGate1001::*CVEV-P0* -D6	pEG1001 carrying *CVEV-P0* with deletion from 176 to 210 amino acid, Kan[R]	This study
pEarleyGate1001::*CVEV-P0* -D7	pEG1001 carrying *CVEV-P0* with deletion from 211 to 245 amino acid, Kan[R]	This study
pEarleyGate1001::*CVEV-P0* -D8	pEG1001 carrying *CVEV-P0* with deletion from 246 to 280 amino acid, Kan[R]	This study
pEarleyGate1001::*CVEV-P0* -D9	pEG1001 carrying *CVEV-P0* with deletion from 281 to 315 amino acid, Kan[R]	This study
pEarleyGate1001::*CVEV-P0* -D10	pEG1001 carrying *CVEV-P0* with deletion from 316 to 354 amino acid, Kan[R]	This study

Abbreviations: [R]: Resistance Gene; Kan: kanamycin; Amp: ampicillin; Gen: gentamycin; Tet: tetracycline.

Table 4.2 List of plasmids, constructs, and bacterial strains used in this study (cont'd).

Plasmids or Strains	Description	Source / Reference
Plasmids		
pEarleyGate1001::*CVEV-ORF3*-D1	pEG1001 carrying *CVEV-ORF3* with deletion from 2 to 34 amino acid, Kan^R	This study
pEarleyGate1001::*CVEV-ORF3*-D2	pEG1001 carrying *CVEV-ORF3* with deletion from 35 to 67 amino acid, Kan^R	This study
pEarleyGate1001::*CVEV-ORF3*-D3	pEG1001 carrying *CVEV-ORF3* with deletion from 68 to 100 amino acid, Kan^R	This study
pEarleyGate1001::*CVEV-ORF3*-D4	pEG1001 carrying *CVEV-ORF3* with deletion from 101 to 133 amino acid, Kan^R	This study
pEarleyGate1001::*CVEV-ORF3*-D5	pEG1001 carrying *CVEV-ORF3* with deletion from 134 to 160 amino acid, Kan^R	This study
pEarleyGate1001::*CVEV-ORF3*-D6	pEG1001 carrying *CVEV-ORF3* with deletion from 161 to 191 amino acid, Kan^R	This study
pEarleyGate100::*CVEV-P0*^{L52A,P53A,L56A}	pEG100 carrying *CVEV-P0*^{L52A,P53A,L56A} tagged with *Flag* at C-terminal, Kan^R	This study
pEarleyGate1001::*CVEV-P0*^{L52A,P53A,L56A}	pEG1001 carrying *CVEV-P0*^{L52A,P53A,L56A} tagged with *Flag* at C-terminal, Kan^R	This study
pEarleyGate1001::*TCV-P38*	pEG1001 carrying *TCV-P38* tagged with *Flag* at C-terminal, Kan^R	This study
pEarleyGate1001::*TBSV-P19*	pEG1001 carrying *TBSV-P19* tagged with *Flag* at C-terminal, Kan^R	This study
pEarleyGate203	pEG203; a Gateway binary vector with cauliflower mosaic virus *35S* promoter and *cMyc*, Kan^R	Earley et al.
pEarleyGate203::*AtSKP1*	pEG203 carriying *AtSKP1* gene tagged with *cMyc* at N-terminal, Kan^R	This study
pFN2K	pFN2K (GST) Flexi® Vector, contains a T7 promoter for bacterial protein expression, Kan^R	Promega
pFN2K::*CVEV-P0*	pFN2K (GST) carrying *CVEV-P0* tagged with glutathione-S-transferase (GST) at N-terminal, Kan^R	This study
pFN2K::*CVEV-P0*-D6	pFN2K (GST) carrying *CVEV-P0*-D6 tagged with glutathione-S-transferase (GST) at N-terminal, Kan^R	This study
pFN2K::*CVEV-P0*-D7	pFN2K (GST) carrying *CVEV-P0*-D7 tagged with glutathione-S-transferase (GST) at N-terminal, Kan^R	This study
pCMVTnT	pCMVTnT™, contains SP6 and T7 promoter for convenient expression of cloned gene, Amp^R	Promega
pCMVTnT-NbAGO1	pCMVTnT™ carrying *NbAGO1* for in vitro protein synthesis, Amp^R	This study
pGEMT-Easy::*T7-GFP*	pGEM®-T Easy carrying *GFP*, upstream with T7 promoter, Amp^R	This study
pGEMT-Easy::*GFP-T7*	pGEM®-T Easy carrying *GFP*, downstream with T7 promoter, Amp^R	This study
Bacterial Strains		
Escherichia coli NEB® 5-alpha	*fhuA2 Δ(argF-lacZ)U169 phoA glnV44 Φ80Δ (lacZ)M15 gyrA96 recA1 relA1 endA1 thi-1 hsdR17*	New England Biolabs
Escherichia coli TOP10	F- *mcrA* Δ(*mrr-hsdRMS-mcrBC*) φ80*lacZ* ΔM15 Δ*lac* X74 *rec* A1 *ara* D139 Δ(*araleu*)7697 *gal* U *gal* K *rps* L (Str`) *endA1 nupG*	Thermal Fisher Scientific
Escherichia coli BL21(DE3)pLysS	F−, *omp* T, *hsd* S$_B$ (r$_B$−, m$_B$−), *dcm*, *gal*, λ(DE3), pLysS, Cm^r	Promega
Agrobacterium tumefaciens GV3101 (pMP90)	Rif^R, Gen^R	Wroblewski et al.
Agrobacterium tumefaciens GV3101 (pMP90::pSOUP)	Rif^R, Gen^R, Tet^R	This study

Abbreviations: ^{R}: Resistance Gene; Kan: kanamycin; Amp: ampicillin; Gen: gentamycin; Tet: tetracycline.

Table 4.3 Antibodies used in this study.

Antibody	Host	Dilution	Note
Monoclonal ANTI-FLAG® M2 antibody	mouse	1:2000	Sigma-Aldrich®, Cat# F3165
Monoclonal Myc-Tag antibody	rabbit	1:1000	Cell Signaling Technology®, Cat# 71D10
Monoclonal GST (B-14) antibody	mouse	1:500	Santa Cruz Biotechnology®, Cat# sc-138
Polyclonal AGO1 antibody	rabbit	1:5000	Agrisera, Cat# AS09527
Anti-mouse IgG, HRP-linked antibody	horse	1:5000	Cell Signaling Technology®, Cat# 7076
Anti-rabbit IgG, HRP-linked antibody	goat	1:5000	Cell Signaling Technology®, Cat# 7074

Table 4.4 Silencing suppression rate of co-infiltration assay of citrus vein enation virus coat protein and movement protein.

Constructs	No. of Plants Infiltrated	No. of Plants Silencing Suppressed	
		Locally	Systemically
pEG100-GFP + pEG100	40	0 **(0%)**	0 **(0%)**
pEG100-GFP + pEG100-CMV-2b	40	40 **(100%)**	40 **(100%)**
pEG100-GFP + pEG100-CLBV-MP	39	16 **(41%)**	6 **(15%)**
pEG100-GFP + pEG100-CVEV-P0	24	23 **(96%)**	23 **(96%)**
pEG100-GFP + pEG100-CVEV-ORF3	12	0 **(0%)**	4 **(33%)**
pEG100-GFP + pEG100-CVEV-ORF5	12	0 **(0%)**	0 **(0%)**

Abbreviations: CMV-2b: cucumber mosaic virus 2b; CLBV: citrus leaf blotch virus; CVEV: citrus vein enation virus; ORF3: open reading frame 3; ORF5: open reading frame 5

Table 4.5 List of potential citrus vein enation virus P0-associated proteins identified by UPLC/Q-TOF-MS in *N. benthamiana*. S phase kinase-associated protein 1, cullin 1 and proteins associated with ubiquitination are highlighted in grey.

N. benthamiana Accession No.	Best Match in *Arabidopsis thaliana*	Protein Name / Description	No. of Observed Peptides	emPAI	Mascot Score	Sequence Coverage
NbS00030810g0011.1	AT2G43160.1	ENTH/VHS family protein	25	15.30	816.58	28.91
NbS00000030g0010.1	AT2G43160.4	ENTH/VHS family protein	25	15.07	785.66	27.53
NbS00035989g0001.1	AT5G11580.1	Regulator of chromosome condensation (RCC1) family protein	20	14.85	937.47	35.57
NbS00015059g0009.1	AT1G75950.1	S phase kinase-associated protein 1	11	13.25	147.74	50.98
NbS00014373g0001.1	AT1G75950.1	S phase kinase-associated protein 1	12	12.90	212.49	54.19
NbS00024298g0005.1	AT1G75950.1	S phase kinase-associated protein 1	10	10.94	152.21	50.98
NbS00037725g0008.1	AT1G75950.1	S phase kinase-associated protein 1	12	10.79	113.13	54.19
NbS00041237g0007.1	AT3G12110.1	Actin-11	12	6.74	519.45	42.22
NbS00031412g0004.1	AT3G12110.1	Actin-11	13	6.74	514.87	42.52
NbS00005284g0009.1	AT1G75950.1	S phase kinase-associated protein 1	9	5.11	192.55	50.00
NbS00022532g0009.1	AT3G20320.1	Trigalactosyldiacylglycerol2	13	3.77	216.11	44.33
NbS00031961g0001.1	AT1G12310.1	Calcium-binding EF-hand family protein	8	3.39	90.78	55.21
NbS00016397g0010.1	AT4G33090.1	Aminopeptidase M1	27	3.30	374.16	42.82
NbS00041732g0004.1	AT4G02570.4	Cullin 1	25	3.26	209.67	33.69
NbS00001653g0010.1	AT1G04080.1	Tetratricopeptide repeat (TPR)-like superfamily protein	16	3.22	314.47	28.90
NbS00045823g0014.1	AT2G28900.1	Outer plastid envelope protein 16-1	3	3.22	40.11	33.76
NbS00019252g0009.1	AT3G20320.1	Trigalactosyldiacylglycerol2	6	3.13	48.09	28.72
NbS00014695g0014.1	AT4G02990.1	Mitochondrial transcription termination factor family protein	13	3.03	131.78	35.53
NbS00022640g0007.1	AT4G02570.4	Cullin 1	25	2.91	201.55	34.39
NbS00060849g0001.1	AT5G19350.2	RNA-binding (RRM/RBD/RNP motifs) family protein	5	2.83	41.06	37.93
NbS00007213g0011.1	AT3G44110.1	DNAJ homologue 3	9	2.73	211.65	26.25
NbS00017354g0008.1	AT1G04080.1	Tetratricopeptide repeat (TPR)-like superfamily protein	15	2.59	200.04	30.28
NbS00027424g0009.1	AT1G09620.1	ATP binding; leucine-tRNA ligases; aminoacyl-tRNA ligases; nucleotide binding	29	2.37	221.67	37.29
NbS00036157g0005.1	AT4G02570.4	Cullin 1	24	2.16	150.49	29.34
NbS00034783g0004.1	AT5G12020.1	HSP17.6	3	2.16	81.67	26.28
NbC26128793g0002.1	AT2G37170.1	Plasma membrane intrinsic protein 2	2	2.16	10.64	40.00
NbS00027195g0012.1	AT5G20570.2	RING-box 1	2	2.16	6.52	23.53
NbS00009244g0020.1	AT1G51730.1	Ubiquitin-conjugating enzyme family protein	4	1.93	32.07	22.58
NbS00003962g0002.1	AT5G13560.1	Structural maintenance of chromosomes protein	5	1.78	36.70	37.33
NbS00003320g0019.1	AT1G75350.1	Ribosomal protein L31	4	1.78	41.93	43.41

Table 4.5 List of potential citrus vein enation virus P0-associated proteins identified by UPLC/Q-TOF-MS in *N. benthamiana* (cont'd). S phase kinase-associated protein 1, cullin 1 and proteins associated with ubiquitination are highlighted in grey.

N. benthamiana Accession No.	Best Match in *Arabidopsis thaliana*	Protein Name / Description	No. of Observed Peptides	emPAI	Mascot Score	Sequence Coverage
NbS00001649g0018.1	AT5G12020.1	HSP17.6	3	1.78	81.81	25.79
NbS00010354g0016.1	AT1G72660.3	P-loop containing nucleoside triphosphate hydrolases superfamily protein	9	1.72	60.99	36.36
NbS00025239g0009.1	AT4G35100.2	Plasma membrane intrinsic protein 3	3	1.68	41.29	18.45
NbS00000471g0009.1	AT2G05100.1	Photosystem II light harvesting complex gene 2.1	4	1.68	48.74	18.94
NbS00008003g0012.1	AT3G18480.1	CCAAT-displacement protein alternatively spliced product	22	1.67	160.88	34.92
NbS00003962g0006.1	AT5G13560.1	Structural maintenance of chromosomes protein	7	1.61	69.95	31.98
NbS00049664g0004.1	AT5G62670.1	H(+)-ATPase 11	4	1.61	34.12	21.61
NbS00002437g0006.1	AT2G32240.1	Early endosome antigen	38	1.55	283.14	38.41
NbS00003508g0016.1	AT3G13330.1	Proteasome activating protein 200	34	1.26	530.40	25.06
NbS00029456g0006.1	AT2G37170.1	Plasma membrane intrinsic protein 2	3	1.25	33.29	12.18
NbS00024537g0009.1	AT5G19350.2	RNA-binding (RRM/RBD/RNP motifs) family protein	4	1.25	42.49	28.57
NbS00003506g0011.1	AT4G24100.1	Protein kinase superfamily protein	14	1.22	82.96	30.03
NbS00019118g0008.1	AT5G20490.1	Myosin family protein with DiI domain	31	1.21	355.07	25.45
NbS00006964g0008.1	AT5G62670.1	H(+)-ATPase 11	13	1.19	94.72	20.80
NbS00019145g0009.1	AT3G23990.1	Heat shock protein 60	13	1.15	105.97	26.93
NbS00010073g0014.1	AT3G66654.2	Cyclophilin-like peptidyl-prolyl cis-trans isomerase family protein	5	1.15	26.67	23.75
NbS00004550g0007.1	AT5G20490.1	Myosin family protein with DiI domain	29	1.12	341.67	24.33
NbS00031411g0009.1	AT4G02570.4	Cullin 1	15	1.10	126.51	20.26
NbS00035598g0008.1	AT1G26480.1	General regulatory factor 12	5	1.09	73.78	20.28
NbS00002044g0005.1	AT1G61520.3	Photosystem I light harvesting complex gene 3	3	1.03	8.90	13.55

Table 4.6 List of potential citrus vein enation virus open reading frame 3 (ORF3)-associated proteins identified by UPLC/Q-TOF-MS in *N. benthamiana*.

N. benthamiana Accession No.	Best Match in *Arabidopsis thaliana*	Protein Name / Description	No. of Observed Peptides	emPAI	Mascot Score	Sequence Coverage
NbS00035989g0001.1	AT5G11580.1	Regulator of chromosome condensation (RCC1) family protein	21	24.12	382.18	29.98
NbS00026081g0008.1	AT5G65220.1	Ribosomal L29 family protein	10	18.31	205.88	34.13
NbS00006458g0003.1	AT4G14960.2	Tubulin/FtsZ family protein	12	5.21	259.91	34.80
NbS00052711g0007.1	AT1G05190.1	Ribosomal protein L6 family	13	5.16	82.64	40.53
NbS00017301g0008.1	AT3G09630.1	Ribosomal protein L4/L1 family	13	4.41	154.38	38.02
NbS00016397g0010.1	AT4G33090.1	Aminopeptidase M1	28	4.21	339.22	42.82
NbS00022532g0009.1	AT3G20320.1	Trigalactosyldiacylglycerol2	14	4.18	149.22	36.60
NbS00002437g0006.1	AT2G32240.1	Early endosome antigen	58	3.49	383.33	49.92
NbS00012499g0004.1	AT5G02610.1	Ribosomal L29 family protein	4	3.22	35.77	30.08
NbS00006821g0002.1	AT1G56190.1	Phosphoglycerate kinase family protein	16	3.08	198.39	42.13
NbS00024868g0008.1	AT2G44120.1	Ribosomal protein L30/L7 family protein	12	2.98	47.64	42.50
NbS00016827g0001.1	AT3G44890.1	Ribosomal protein L9	8	2.88	71.35	38.54
NbS00024093g0010.1	AT3G16780.1	Ribosomal protein L19e family protein	6	2.83	26.69	30.93
NbS00007385g0004.1	AT1G30230.1	Glutathione S-transferase, C-terminal-like; Translation elongation factor EF1B/ribosomal protein S6	6	2.73	34.38	37.44
NbS00012928g0003.1	AT2G01250.1	Ribosomal protein L30/L7 family protein	12	2.73	43.69	42.50
NbS00002188g0022.1	AT1G74060.1	Ribosomal protein L6 family protein	8	2.59	43.29	33.48
NbS00012784g0015.1	AT4G35090.1	Catalase 2	13	2.49	127.59	37.76
NbS00019252g0009.1	AT3G20320.1	Trigalactosyldiacylglycerol2	5	2.46	41.82	24.10
NbS00043955g0003.1	AT1G30230.2	Glutathione S-transferase, C-terminal-like;Translation elongation factor EF1B/ribosomal protein S6	7	2.38	36.25	39.02
NbS00010354g0016.1	AT1G72660.3	P-loop containing nucleoside triphosphate hydrolases superfamily protein	9	2.33	62.23	32.92
NbS00003552g0008.1	AT3G18480.1	CCAAT-displacement protein alternatively spliced product	27	2.28	132.99	35.66
NbS00030810g0011.1	AT2G43160.1	ENTH/VHS family protein	12	2.28	102.88	18.99
NbS00006116g0019.1	AT4G35090.1	Catalase 2	14	2.26	127.08	37.63
NbS00013388g0010.1	AT3G18610.1	Nucleolin like 2	14	2.24	239.46	29.86
NbS00018918g0016.1	AT1G61580.1	R-protein L3 B	11	2.16	85.26	22.37
NbS00045823g0014.1	AT2G28900.1	Outer plastid envelope protein 16-1	3	2.16	16.44	26.11
NbS00038860g0017.1	AT1G02840.3	RNA-binding (RRM/RBD/RNP motifs) family protein	9	2.16	56.19	26.04
NbS00010967g0020.1	AT2G33800.1	Ribosomal protein S5 family protein	7	2.16	92.40	32.66
NbS00039797g0003.1	AT3G09630.1	Ribosomal protein L4/L1 family	10	2.05	93.84	26.04
NbS00038051g0004.1	AT4G14960.2	Tubulin/FtsZ family protein	8	2.05	180.55	24.75
NbS00004706g0011.1	AT3G18480.1	CCAAT-displacement protein alternatively spliced product	15	1.99	51.04	26.40
NbS00002408g0006.1	AT5G48760.2	Ribosomal protein L13 family protein	5	1.98	21.73	25.24
NbS00005651g0008.1	AT1G09640.1	Translation elongation factor EF1B, gamma chain	11	1.97	70.52	26.17
NbS00000030g0010.1	AT2G43160.4	ENTH/VHS family protein	12	1.96	92.08	18.14

Table 4.6 List of potential citrus vein enation virus open reading frame 3 (ORF3)-associated proteins identified by UPLC/Q-TOF-MS in *N. benthamiana* (cont'd).

N. benthamiana Accession No.	Best Match in *Arabidopsis thaliana*	Protein Name / Description	No. of Observed Peptides	emPAI	Mascot Score	Sequence Coverage
NbS00022677g0027.1	AT3G16780.1	Ribosomal protein L19e family protein	6	1.93	22.24	33.96
NbS00008464g0006.1	AT5G12110.1	Glutathione S-transferase, C-terminal-like;Translation elongation factor EF1B/ribosomal protein S6	6	1.89	38.49	33.19
NbS00029619g0005.1	AT2G27710.4	60S acidic ribosomal protein family	4	1.85	34.51	28.19
NbS00003508g0016.1	AT3G13330.1	Proteasome activating protein 200	35	1.73	301.12	25.65
NbS00016385g0017.1	AT3G18480.1	CCAAT-displacement protein alternatively spliced product	21	1.65	69.43	29.06
NbS00022823g0015.1	AT2G39800.4	delta1-pyrroline-5-carboxylate synthase 1	19	1.65	103.28	32.74
NbS00030134g0011.1	AT5G09880.1	Splicing factor, CC1-like	7	1.63	69.66	18.73
NbS00003962g0006.1	AT5G13560.1	Structural maintenance of chromosomes protein	8	1.61	67.16	34.59
NbS00037512g0009.1	AT5G19510.1	Translation elongation factor EF1B/ribosomal protein S6 family protein	6	1.51	35.84	33.19
NbS00012048g0003.1	AT3G14600.1	Ribosomal protein L18ae/LX family protein	4	1.51	33.09	20.22
NbS00030956g0015.1	AT1G51730.1	Ubiquitin-conjugating enzyme family protein	4	1.51	20.43	28.16
NbS00009244g0020.1	AT1G51730.1	Ubiquitin-conjugating enzyme family protein	4	1.51	22.76	29.44
NbS00019252g0008.1	AT3G20320.1	Trigalactosyldiacylglycerol2	7	1.51	63.15	27.15
NbS00007372g0013.1	AT5G60390.3	GTP binding Elongation factor Tu family protein	11	1.45	132.32	26.52
NbC25340200g0001.1	AT3G48870.2	HSP93-III	4	1.42	21.99	34.90
NbS00023515g0003.1	AT3G62870.1	Ribosomal protein L7Ae/L30e/S12e/Gadd45 family protein	6	1.31	43.98	20.54
NbS00002820g0009.1	AT3G14600.1	Ribosomal protein L18ae/LX family protein	4	1.25	39.33	18.75
NbS00041476g0008.1	AT1G18270.1	Ketose-bisphosphate aldolase class-II family protein	28	1.21	147.19	22.19
NbS00002899g0003.1	AT1G04430.2	S-adenosyl-L-methionine-dependent methyltransferases superfamily protein	12	1.19	86.72	23.30
NbS00057730g0003.1	AT3G27160.1	Ribosomal protein S21 family protein	2	1.15	5.89	15.61
NbS00027424g0009.1	AT1G09620.1	ATP binding; leucine-tRNA ligases; aminoacyl-tRNA ligases; nucleotide binding	19	1.11	122.55	23.22
NbS00026041g0013.1	AT1G02840.3	RNA-binding (RRM/RBD/RNP motifs) family protein	8	1.09	54.84	21.99
NbS00023116g0002.1	AT1G05320.3	Myosin heavy chain, embryonic smooth protein	31	1.07	186.40	25.88
NbS00001653g0010.1	AT1G04080.1	Tetratricopeptide repeat (TPR)-like superfamily protein	10	1.00	63.41	19.78

GENERAL CONCLUSION

A comprehensive study of two citrus viruses, citrus tatter leaf virus (CTLV) and citrus vein enation virus (CVEV), was presented in this dissertation. First, the full genome sequences of all CTLV and CVEV isolates preserved at Citrus Clonal Protection Program (CCPP) were characterized. The sequences of CCPP isolates and the data available on NCBI GenBank were further studied for their identity, phylogenetic relationship and evolutionary between different isolates. In the meantime, the detection assays were developed within the most conserved region according to their genome-wise sequence analysis. Furthermore, the viral suppressors of RNA silencing (VSRs) were also identified for both viruses in this dissertation and showed that CTLV and CVEV use VSRs to suppress host antiviral RNA silencing, however, by using different mechanisms and targeting at different components within the pathway.

The present study provides in-depth information of CTLV and CVEV in genomic, phylogenetic, diagnostic and virus-host interaction and also touches the base of pathogenicity which can further lead to the development of disease management strategies in nearly future. Meanwhile, the detection assays developed in present studies have already been implemented to the diagnostic system of CCPP to prevent outbreaks and manage the spread of these two viruses by distributing clean plant materials. Therefore, we believe this dissertation provides information in several aspects on two citrus viruses which further benefits and contributes to academia, the high-value germplasm program as well as the multi-billion citrus industry. Moreover, the approach used in this study will be applied to

CCPP as a role model for studying and characterizing the newly discovered virus and its disease and further leading to the development of a detection assay and management programs in a timely manner.